DANMARKS OG GRØNLANDS GEOLOGISKE UNDERSØGELSE RAPPORT 2007/42

Chemostratigraphy and mineral-chemical fingerprinting

Heno Formation, Danish North Sea

Rikke Weibel & Christian Knudsen

GEOLOGICAL SURVEY OF DENMARK AND GREENLAND
MINISTRY OF THE ENVIRONMENT

G E U S

DANMARKS OG GRØNLANDS GEOLOGISKE UNDERSØGELSE RAPPORT 2007/42

Chemostratigraphy and mineral-chemical fingerprinting

Heno Formation, Danish North Sea

Rikke Weibel & Christian Knudsen

Released 01.09.2012

GEOLOGICAL SURVEY OF DENMARK AND GREENLAND
MINISTRY OF THE ENVIRONMENT

GEUS

Abstract

This report describes the findings of a geochemical and mineral-chemistry project on the Upper Jurassic sediments from the Danish sector of the North Sea conducted by GEUS for Conoco Phillips, the operator on the Hejre licence. The project was carried out in the period 1st April 2006 to 28th February 2007.

A total of 615 geochemical analyses (264 on core samples and 351 on cuttings samples) and 30 zircon geochronology analyses are performed on the Upper Jurassic sediments in the wells, Diamant-1, Gert-1, Gert-2, Gert-4, Gwen-2, Hejre-1, Hejre-2, Jeppe-1 and Rita-1 in the Danish North Sea sector. Major elements are generally analysed by XRF (X-ray fluorescence) and trace elements by ICP-MS (inductively coupled plasma - mass spectrometry). Multivariate analysis has proven to be an important tool for evaluation of the geochemical data and is used for comparison between different members and formations. U-Pb zircon geochronology is performed by Laser ablation - inductively coupled plasma - mass spectrometry (LA-ICP-MS).

Multivariate analysis shows that the Farsund Formation is significantly different to the Lola Formation and to the Heno Formation. Consequently, a mudstone sample can with 95% certainty be assigned to the Lola Formation or Farsund Formation. The Farsund Formation contains higher amounts of V; and smaller amounts of Zr, MgO, K_2O and Rb than the Lola Formation. Possibly these differences are related to the Farsund Formation being deposited more distal in the basin than the Lola Formation.

The Ravn and Gert Members can be distinguished from each other by multivariate analysis, though overlapping values do occur. Practically this means that a distinction between the Gert and Ravn Members is possible, but it takes more analysed samples (probably 15 non-calcite-cemented samples). Cross plots show that the Gert and Ravn Members are separated by different amounts of TiO_2, Nb, K_2O, Rb, Th, REE and Cr. Gert Member typically contains varying amounts of TiO_2, K_2O, Rb, Cr and Zr, and has lower Th / TiO_2 (and REE / TiO_2) and Nb / TiO_2 ratios. Some samples have similar contents to the Ravn Member and Lola and Farsund Formations, however, peak amounts are higher for the Gert Member than for the other member or formations. Several possible explanations can account for the observed differences between the Ravn and Gert Members. Less altered material could have been brought into the system during deposition of the Gert Member, whereas intensively altered material dominated during deposition of the Ravn Member. Different source areas could have been exposed during deposition of the Gert Member than when the Ravn Member was deposited. The higher peak amounts of Cr and Ti found in the Gert Member could origin from recycled Carboniferous material. Influence from a local volcanic source, which supplied high amounts of K-feldspar, can be observed in the area of the Hejre-2 and Jeppe-1 wells. The depositional environment may also have played a major role in the variation of Mg, as the Ravn Member in the more distal placed wells generally has a much higher MgO content than the Ravn Member from the wells characterised by shoreface conglomerate. The relatively higher Na_2O and P_2O_5 contents in the Ravn Member compared to the Gert Member could also reflect depositional differences, as the Gert Member was deposited in a back-barrier environment and the Ravn Member had an upper to lower shoreface depositional environment. However, the differences could also be related to variation in the detrital mineral assemblage, as Na_2O might be incorporated in plagioclase, and P_2O_5 might be associated with apatite instead or marine authigenic phosphates.

Multivariate analysis shows that the Gert Member and the Lower Gert Member in the Hejre-2 well fits almost equally well with the Gert and Ravn Members, and that some of the same samples are outliers in both models. The Lower sandstone unit in the Hejre-2 well may belong to the Gert Member. However, additional non-calcite-cemented samples are necessary in order to make a final decision. Multivariate analysis has shown that even though the possible Gert Member in Rita-1 seems different to the Gert Member in other wells its variation is within the variability of the Gert Member even though this was only based on the three Gert wells. The Rita-1 well could be more influenced by a local source both during deposition of the Gert Member and the Ravn Member. This source may occasionally have delivered fluxes that even reached the position of the Gert-4 well.

Future investigations ought to combine diagenetic, petrographic and geochemical data, which could lead to establishment of a tool for predicting reservoir properties from the geochemical composition.

Contents

Extended summary 7

Introduction 13

Geological background 15

Jurassic Danish Central Graben 15
Heno Formation 18
Geochemical analyses 21
U-Pb zircon geochronology by Laser ablation - inductively coupled plasma - mass spectrometry (LA-ICP-MS) 22
Garnet chemistry by Computer controlled scanning electron microscopy (CCSEM) 23

Material 25

Geochemical results and discussion 27

Artefacts 27
Major and trace elements 30
Gert Member, Heno Formation 36
Lola Formation 37
Ravn Member, Heno Formation 37
Farsund Formation 39
Geochemical variation between different formations and members 40
Gert Member, Heno Formation 40
Ravn Member, Heno Formation 44
Lola Formation 47
Farsund Formation 49
Geochemical variation between wells 51

Zircon geochronology 53

Garnet geochemistry 59

Conclusions 61

Recommendations 65

Acknowledgements 67

References 69

Appendix 1A.	Core samples
Appendix 1B.	Cuttings samples
Appendix 2.	Geochemical logs from Hejre-2, Gert-1, Gert-2, Gert-4, Gwen-2 and Rita-1
Appendix 3.	Multivariate analysis
Appendix 4.	Selected cross plots
Appendix 5.	Zircon geochronology (zircon ages for each sample)
Appendix 6.	Garnet geochemistry

Extended summary

This report describes the findings of a geochemical and mineral-chemistry project on the Upper Jurassic sediments from the Danish sector of the North Sea conducted by GEUS for Conoco Phillips, the operator on the Hejre licence. The project has been carried out in the period 1st April 2006 to 28th February 2007.

An integrated study investigating chemostratigraphic variation and provenance of the Upper Jurassic Heno Formation in the Danish North Sea was conducted by combining bulk rock chemistry and zircon age data in an attempt to solve the following objectives:

- Correlation of Heno Formation sandstones units laterally between different wells.
- Evaluation of the possibility of a vertical distinction between the Ravn and Gert Members in each well, and eventual subdivision of the Gert Member.
- Determination of the lower sandstone units (below Gert Member in Hejre-2) affiliation to the Gert Member or other Jurassic sandstone unit in the area.
- Determination of the extent and type of carbonate cement in sandstone units.
- Correlation of mudstone intervals between different wells.

Chemostratigraphic studies have not previously been published on Danish Jurassic sediments, even though some Jurassic intervals are almost barren of fossils and therefore obvious to attempt non-biostratigraphic methods. However, few proprietary chemostratigraphic studies on Upper Jurassic sediments in the north-eastern part of the Danish Central Graben have been performed by GEUS (Christian Knudsen, personal communication 2006).

The tectonic stationary conditions of the Early Jurassic with deposition of offshore uniform mudstones changed in the earliest Middle Jurassic with the regional uplift related to the doming of the central North Sea and the Ringkøbing–Fyn High (Andsbjerg et al. 2001). Due to extensive and continued uplift a highly erosive unconformity formed in the North Sea, on the Ringkøbing–Fyn High and in the Fennoscandian Border Zone (Andsbjerg et al. 2001; Nielsen 2003). Older sandstones were exposed and eroded and re-deposited in accommodation space generated by incipient rift-related subsidence in the Danish Central Graben (Andsbjerg et al. 2001). The rift-related subsidence ceased or slowed down in the late Kimmeridgian resulting in a decrease in accommodation space generation, which, combined with a possible increase in sediment supply, caused the progradation of shallow marine sands of the Heno Formation in the north-western parts of the Danish Central Graben (Andsbjerg et al. 2001). Sands with their source in the Mid North Sea High, prograded towards the east on to the Heno Plateau, while sands from the Mandal High prograded towards the west on to the Gertrud Plateau and in the Feda Graben (Johannessen & Andsbjerg 1993; Johannessen et al. 1996; Andsbjerg et al. 2001; Johannessen 2003). The Heno Formation has been redefined by Michelsen et al. (2003). The classical shoreface sandstone previously defined as the Heno Formation or Heno Sand is now referred to the Ravn Member (Michelsen et al. 2003) and the back-barrier and shoreface sediments previously described as the 'basal sandstone unit' (Johannessen et al. 1996) or Basal Sand are now referred to the Gert Member (Michelsen et al. 2003). According to Johannessen (2003) the Heno Formation is roughly equivalent to the Fulmar Formation in the UK sector and has many similarities with the 'Heno equivalent' and the Ula Formation of the Norwegian sector. The Lola Formation, an offshore mudstone, underlies the Gert Member and wedges in between the Gert and Ravn Members. The Farsund Formation, another offshore mudstone overlies the Ravn Member.

In all 615 geochemical analyses (264 on core samples and 351 on cuttings samples) and 30 zircon geochronology analyses have been performed on the Upper Jurassic sediments in the following wells in the Danish North Sea sector: Diamant-1, Gert-1, Gert-2, Gert-4, Gwen-2, Hejre-1, Hejre-2, Jeppe-1 and Rita-1. Additionally 2 zircon geochronology analyses were performed on Precambrian samples from P-1 (Mid North Sea High) and Ugle-1 (Ringkøbing–Fyn High). Major elements were generally analysed by XRF (X-ray fluorescence) and trace elements by ICP-MS (inductively coupled plasma - mass spectrometry). U-Pb zircon geochronology was performed by Laser ablation - inductively coupled plasma - mass spectrometry (LA-ICP-MS).

The way cuttings samples are generated will give rise to pollution by several elements, which may reflect the drilling mud composition instead of the rock formation they represent. Consequently, Ba, Sr, Fe, Cr, Mn and Cu cannot be applied from cuttings samples. In some cuttings samples barite may actually constitute the majority of the sample. Never the less, these cuttings samples seem to reflect the geochemical composition of the cores better than cuttings samples with much lower barite contents. Geochemical application of cuttings will depend on the treatment of the cuttings samples.

Core samples give the most distinctive results, which leads to the following conclusions:

Mudstone intervals (Lola and Farsund Formations) can be distinguished geochemically from each other and can therefore be correlated from well to well.
Multivariate analysis (Appendix 3) has shown that the Farsund Formation is significantly different to the Lola Formation and to the Heno Formation. Consequently, a mudstone sample can with 95% certainty be assigned to the Lola Formation or Farsund Formation. Cross plots have shown that Lola and Farsund Formations are distinguished from the sandstones of the Heno Formation by a higher content of Ni, Cu, Zn, V, Na_2O and P_2O_5 and a lower Zr content. The Farsund Formation contains higher amounts of V; and smaller amounts of Zr, MgO, K_2O and Rb than the Lola Formation. Possibly these differences are related to the Farsund Formation being deposited more distal in the basin than the Lola Formation.

The Heno Formation sandstone intervals (Ravn and Gert Members) can be distinguished geochemically from each other, though several samples have to be analysed.
Multivariate analysis (Appendix 3) has shown that the Ravn and Gert Members can be distinguished from each other, though overlapping values do occur. Practically, this means that a distinction between the Gert and Ravn Members is possible, but it takes more analysed samples (probably 15 non-calcite-cemented samples). Cross plots have shown that the Gert and Ravn Members are separatable by different amounts of TiO_2, Nb, K_2O, Rb, Th, REE and Cr. Gert Member typically contains varying amounts of TiO_2, K_2O, Rb, Cr and Zr, and has lower Th / TiO_2 (and REE / TiO_2) and Nb / TiO_2 ratios. Some samples have similar contents to Ravn Member and Lola and Farsund Formations, however, peak amounts are higher for Gert Member than for the other formations or member.

Several possible explanations can account for the observed differences between the Ravn and Gert Members:

1. <u>Less altered material brought into the system during deposition of the Gert Member, whereas intensively altered material dominated during deposition of the Ravn Member.</u>

   Cr is probably located in chrome spinel, which is a stable heavy mineral, though not as stable as zircon and rutile. The relatively low Nb / TiO_2 ratio suggests that much of the titanium is present in other Ti-bearing minerals than rutile. The Gert Member therefore seems to be characterised by material coming from relatively fresh source rock and material from more altered source rocks. The Gert Member is deposited during transgression in a back-barrier and marine shoreface environment (Johannessen et al., 1996; Johannessen 2003). During transgression relatively unaltered or less altered material might occasionally have been brought into the system possibly during storm episodes.

   The zircon content seems to be as high in the Ravn Member as in the Gert Member. However, the content of titanium and chromium is much lower in the Ravn Member compared with the Gert Member. The Nb / TiO_2 ratio is relatively high, which may indicate that titanium is primarily located in rutile and Fe-Ti oxides. The Ravn Member is also characterised by abundant oversized quartz and quartzite clasts. Combined, this shows a dominance of very stable minerals suggesting that the material originated from a considerably altered source rock. The alteration could have taken place on the surrounding highs (Mandal High, Mid North Sea High), but may also have continued under temporal deposition during its transport to the final place of deposition.

2. <u>Source area differences</u>

   Where other source areas exposed during deposition of the Gert Member?:
   Another possible explanation for the relatively higher chrominun content in the Gert Member could be that an alternative source area was exposed during deposition of the Gert Member. High chrome spinel has been reported from Early Carboniferous sandstones in the Danish North Sea sector (Spathopoulos et al. 2000) and Late Carboniferous sandstones from the southern North Sea (Morton et al. 2001) and both are interpreted as having their source on the Ringkøbing–Fyn High or recycled sediments originally with this high as their source. The Gert Member could have been deposited with greater influence of recycled sedimentary material, which originally came from the Ringkøbing–Fyn High.

   The Ravn Member can also be differentiated from the Gert Member by higher amounts of Na_2O and P_2O_5 though with the Diamant-1 well as an exception. P_2O_5 might be present in heavy minerals as apatite, monazite or in marine authigenic phosphate minerals. The most obvious origins of sodium are halite, clay minerals and plaigoclase. Halite seems less likely as sodium generally occurs in similar amounts in core samples and in washed and dried cuttings samples. Plagioclase might occur in increased amounts together with oversized quartz clasts in the Ravn Member. The geochemical differences between the Ravn Member and the Gert could therefore relect a difference in the major source areas.

Local volcanic source:

The higher K_2O / Al_2O_3, Rb / K_2O and Ga / K_2O ratios in the Gert Member in the Hejre-2 well and in the Ravn Member in the Jeppe-1 well indicate the influence of a local potassium-rich source, probably K-feldspar. The pre-Jurassic volcanoclastic conglomerate in the Hejre-2 well has equally high K_2O / Al_2O_3, Rb / K_2O and Ga / K_2O ratios and seems to be related to an alkaline volcanism. Lower – Middle Jurasssic alkaline volcanism is known from the Egensund sub-Basin (Furnes et al. 1982). Possibly an alkaline volcanic event could have occurred at the same time close to the Hejre wells. This alkaline volcanic source supplied K-feldspar rich materials during deposition of the Gert Member and continued supplying during deposition of the Ravn Member, at the time when the Hejre-2 area was covered by the Gert Member.

3. Depositional differences

The Ravn Member in the most distal wells (Gert-4, Gert-2 and Rita-1) are characterised by higher amounts of MgO than the Ravn Member in wells dominated by shoreface conglomerate. Clay minerals deposited in a highly saline environment would be surrounded by highly saline pore fluids, and the high cation exchange capacity of clays could possibly lead to clays being richer in MgO in a distale marine environment than in the beach deposit. Abundant bioturbation by various borrowing organisms show that perfect conditions for formation of glauconite were present. Therefore glauconite may have formed *in situ* and may have incorporated Mg, Fe and K in various amounts depending on their availability. During subsequent diagenesis the glauconite may have been replaced by chlorite and eventually increased the amount of Mg incorporated in the clay. The presence of MgO might eventually be defined by a combination of depositional environment and source area.

Variation in the MgO content in the Ravn Member and the Lola Formation seem to have a strong relation to the depositional environment and may be used for tracing and timing the transgression.

The Lower sandstone unit in the Hejre-2 well may belong to the Gert Member. However, additional non-calcite-cemented samples are necessary in order to make a final decision.
Multivariate analysis shows that the Gert Member and the Lower Gert Member in Hejre-2 fits almost equally well with the Gert and Ravn Members, and that some of the same samples are outliers in both models. Several samples (calcite cemented) have to be removed from the data set before multivariate analysis is performed. This resulted in too few samples for a reliable comparison of the lower sandstone unit in Hejre-2 with the other sandstone units. The geochemical logs for all the Gert Member successions, including those from the Hejre-2 and Rita-1 wells, are characterised by very high variations in Cr, Zr and TiO_2 contents. So from this point of view the Gert Member and the Lower Gert Member in Hejre-2 seem to appear similar to other Gert Member successions.

The Gert Member is most likely also represented in the Rita-1 well.
The possible Gert Member in the Rita-1 well generally has a more straightforward correlation between Cr, Zr and TiO_2 than other Gert Member samples, which have a greater scatter. The REE content seems to be much higher in the Rita-1 wells and some samples from the Gert-4 well than in other Gert Member samples. The Rita-1 well could be more influenced by a local source, which occasionally delivered fluxes that even reached the Gert-4 well area. The source might be similar to the monazite-rich source on the Mid North Sea High described by Spatholoupos et al. (2000). Multivariate analysis has shown that even though the possible Gert Member in the Rita-1 well seems different to the Gert Member in other wells its variation is within the variability of the Gert Member even though this was only based on the three Gert wells.

Calcite is the most common carbonate cement
Carbonate cement occurs frequently in both the Gert and Ravn Members. The most common carbonate type is calcite containing minor amounts of Mg and Mn. Rare dolomite and ankerite cemented samples have been found.

Future investigations ought to combine diagenetic and geochemical data, which could lead to establishment of a tool for predicting reservoir properties from the geochemical composition.

Introduction

A number of different non-biostratigraphic tools have been developed for dating and correlating biostratigraphically barren strata, including heavy mineral distribution and heavy mineral chemistry (Basu & Molinaroli 1989), isotopic composition (Dirk Frei, personal communication 2006) and bulk rock geochemistry (Pearce & Jarvis 1995). When these techniques are combined they can lead to construction of an integrated stratigraphic framework, whereas employed individually they may not be particularly beneficial. Heavy minerals are sensitive indicators of sediment provenance, sediment-transport history and post-depositional alteration. The source rock available defines the heavy minerals present and in which quatitives. Sorting depending on transport media and hydrodynamics, and changes in hydraulic conditions during sedimentation may change the original heavy mineral assemblage. These effects, together with weathering during temporal deposition and after final deposition and diagenesis, may overprint the original provenance signature (Morton & Hallsworth 1999).

Chemostratigraphy or chemical stratigraphy involves the geochemical characterisation and correlation of strata by using major and trace element geochemistry (Pearce et al. 1999). Chemostratigraphy has been introduced as a substitution for biostratigraphy in barren sequences or as a supplementary technique for improved stratigraphic resolution (Ehrenberg & Siring 1992; Preston et al. 1998; Peace et al. 1999; Ratcliffe et al. 2004). Preston et al. (1998) demonstrate that chemostratigraphy can be applied on sandstone sequences and stress the importance of differentiating between those elements associated with diagenetic activity and those more immobile. For example, during feldspar dissolution the concentration of Ca, Na, K, Pb, Rb, Sr and certain REEs can be modified considerably. Therefore Preston et al. (1998) apply immobile elements such as Al, Ti, Zr, Nb and Cr for the construction of reservoir-scale inter-well correlations.

The Jurassic in the Danish North Sea and Greenland has been intensively investigated over many years. The latest is a detailed review publication by Surlyk & Ineson (2003). Despite detailed investigations chemostratigraphic studies have not previously been applied on Danish Jurassic sediments, even though some Jurassic intervals are almost barren of fossils and therefore obvious contenders for non-biostratigraphic methods. Recently, a few proprietary chemostratigraphic studies have been carried out by GEUS (Christian Knudsen, personal communication 2006).

This report describes results from an integrated study investigating chemostratigraphic variation and provenance of the Upper Jurassic Heno Formation in the Danish North Sea by combining bulk rock chemistry, heavy mineral assemblage, garnet chemistry and zircon age data in an attempt of solving the following objectives:

- Correlation of Heno Formation sandstones units laterally between different wells.
- Evaluation of the possibility of vertical distinction between the sandstones of the Gert and Ravn Members in each wells, and eventual subdivision of the Gert Member.
- Determination of the sandstone unit below the Gert Member in the Hejre-2 well and its affiliation to the Gert Member or other Jurassic sandstone units in the area.
- Determination of the extent and type of carbonate cementation in the sandstone units.
- Correlation of mudstone intervals between different wells.

The present report describes the findings in a project conducted by GEUS for Conoco Phillips, the operator on the Hejre licence. The project has been carried out in the period 1st April 2006 to 28th February 2007. In all 132 geochemical analyses and 6 zircon geochronological analyses have been performed on material from the Hejre wells and the Gwen-2 well for Conoco Phllips. The 483 geochemical records and 26 zircon geochronological analyses that form the basis for the present study are part of the GEUS North Sea geochemical database.

Geological background

Jurassic Danish Central Graben

The Danish Central Graben formed as a result of plate reorganisation in the Late Carboniferous – Early Permian time and has since undergone a complex history of differential subsidence (Japsen et al. 2003; Fig. 1). In the Early Jurassic tectonic stationary period a marine shelf covered the Central Graben and thick laterally uniform sequences of homogeneous mudstones were deposited under the influence of eustatic (sea level) changes (Andsbjerg et al. 2001; Nielsen 2003). These conditions changed in the earliest Middle Jurassic with the regional uplift related to the doming of the central North Sea and the Ringkøbing–Fyn High (Andsbjerg et al. 2001). Due to extensive and continued uplift a highly erosive unconformity formed on the Ringkøbing–Fyn High in the North Sea and in the Fennoscandian Border Zone (Andsbjerg et al. 2001; Nielsen 2003). Older sandstones were exposed and eroded and re-deposited in the accommodation space generated by incipient rift-related subsidence in the Danish Central Graben (Andsbjerg et al. 2001). The regional uplift and subsequent rifting caused the development of grabens and half-grabens, which determined the depositional style and thus the distribution of the Middle and Upper Jurassic sediments.

Early Middle Jurrasic (**Aalenian–Bajocian)** deposits are confined mainly to fault-controlled grabens (i.e. Tail End Graben). In the northern part of the Danish Central Graben the Bryne Formation is dominated by flood plain deposits, in which up to 10 m thick correlatable channel sandstones are embedded in thick floodplain mudstones. Coastal plain environment prevailed in the southern part, therefore the deposits were characterised by thinner channel sandstones embedded in thick lacustrine mudstones with thin interbedded marine mudstones (Andsbjerg et al. 2001).

In Late Middle Jurassic (**Bathonian–Callovian**) time lagoonal and shoreface deposits backstepped up the flanking ramps of the deep areas of the Danish Central Graben (Andsbjerg et al. 2001). Braided-river deposits dominated on the ramps dipping towards the deep basins and interbedded fluvial and estuarine deposits were formed towards the centre of the basin.

During the **Callovian–Oxfordian** regional transgression the coastal plains were drowned as a responds to sea-level rise and basin expansion (Andsbjerg et al. 2001). In the Søgne Basin the Callovian Lulu Formation is characterised by coarsening-upward successions representing shoreface units prograding towards the west and south-west (Andsbjerg 2003; Michelsen et al. 2003). Regionally extensive coal beds (up to 4 m thick) were deposited on a coastal plain during relative sea-level rise (Petersen & Andsbjerg 1996; Andsbjerg et al. 2001). The coarsening-upward succession started with these coal beds and continued with shoreface and beach sandstones and was completed with a transgressive conglomerate (Andsbjerg et al. 2001). Along the western margin of the Søgne Basin and the Tail End Graben, the successions are dominated by back barrier deposits, consisting of sandstones with tidal influence (Michelsen et al. 2003). In the southern Danish Central Graben, the transgressive succession is dominated by lagoonal and lacustrine mudstones of the Middle Graben Shale Formation (Andsbjerg et al. 2001). The coastal plains of this area, dominated by lagoons and coastal swamps, also gave rise to abundant coals beds at the base of the transgressive succession.

Upper Jurassic (**Oxfordian–Kimmeridgian**) time was characterised by differential subsidence and transgression. During the Oxfordian a high rate of subsidence along the main faults of the Danish Central Graben created accumulation space for 900 m thick marine mudstones of the Lola Formation (Andsbjerg et al. 2001). Turbidite sands, forming units only a few metres thick, were deposited in the axial parts of the basin, and locally marginal marine sands accumulated on the hanging-wall slope (Andsbjerg & Dybkjær 2003).

The rift-related subsidence ceased or slowed down in **late Kimmeridgian** resulting in a decrease in accommodation space generation, which, combined with a possible increase in sediment supply, caused the progradation of shallow marine sands of the Heno Formation in the north-western parts of the Danish Central Graben (Andsbjerg et al. 2001). Sands with their source in the Mid North Sea High, prograded towards the east onto the Heno Plateau, while sands from the Mandal High prograded towards the west onto the Gertrud Plateau (on Fig. 1 the area of the Gertrud Graben) and into the Feda Graben (Johannessen & Andsbjerg 1993; Johannessen et al. 1996; Andsbjerg et al. 2001; Johannessen 2003). According to Andsbjerg et al. (2001) the Ringkøbing–Fyn High was the main source for the Norwegian-Danish Basin, and local turbidite sands in the Danish Central Graben.

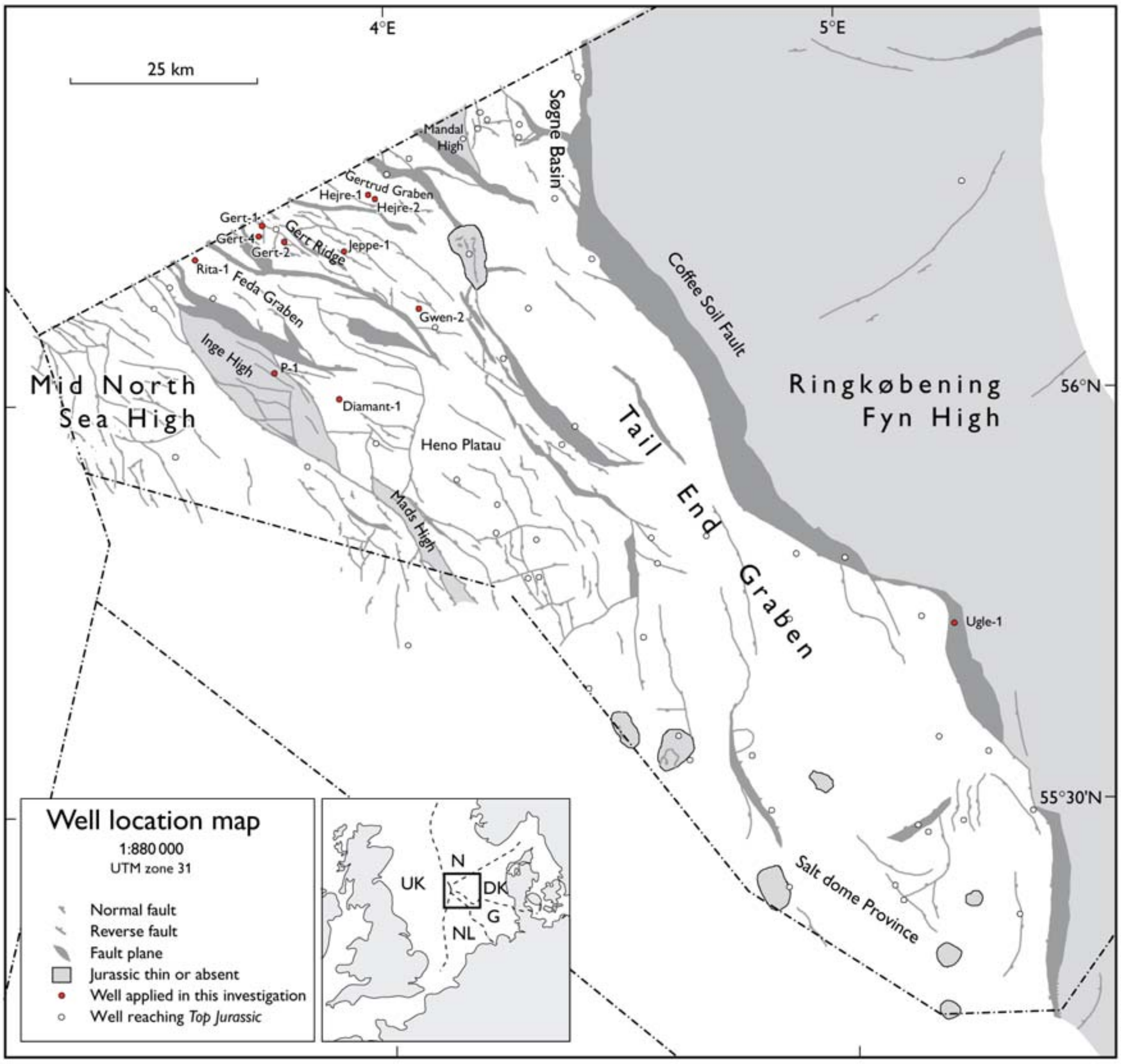

Figure 1. *Wells reaching the Jurassic in the Danish sector of the North Sea are indicated with white dots. Wells used for this investigation are marked with red dots. Modified after Japsen et al. 2003.*

Heno Formation

The Heno Formation has been redefined by Michelsen et al. (2003). The classical shoreface sandstone previously defined as the Heno Formation or Heno Sand is now referred to the Ravn Member (Michelsen et al. 2003) and the back-barrier and shoreface sediments previously described as the 'basal sandstone unit' (Johannessen et al. 1996) or Basal Sand are now referred to the Gert Member (Michelsen et al. 2003). According to Johannessen (2003) the Heno Formation is roughly equivalent to the Fulmar Formation in the UK sector and has many similarities with the 'Heno equivalent' and the Ula Formation of the Norwegian sector (Fig. 2).

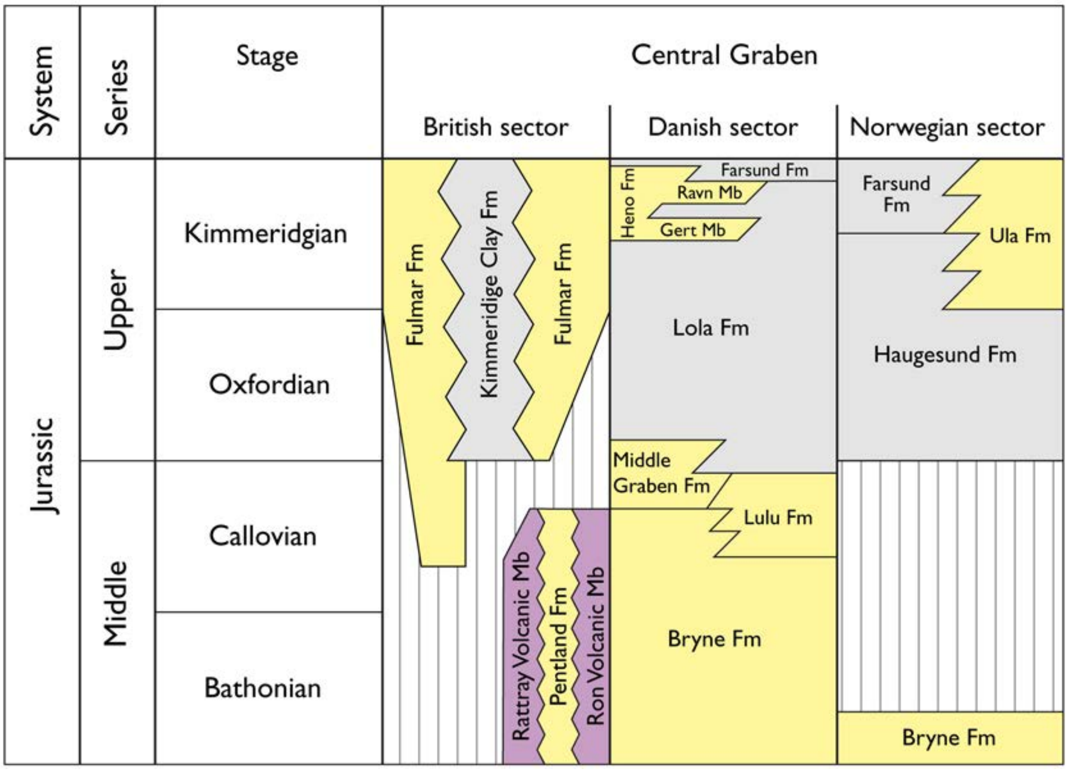

Figure 2. *Stratigraphic scheme showing the Middle and Upper Jurassic formations in different sectors of the North Sea. Note that the Lola Formation may intersects the two members (Ravn Member and Gert Member) of the Heno Formation. Sandstones are yellow, mudstones are grey and volcanic units are purple. Hiatus is marked by vertical lines. Modified after Michelsen et al. 2003.*

The Gert Member comprises interbedded fine-grained sandstones and claystones with thin coal beds (Johannessen 2003). The sandstone intervals are intensively bioturbated and affected by water-escape structures. Rootlets and coal fragments are common. Claystone intervals contain only a few dinoflagellae cysts, whereas terrestrially derived organic particles such as black wood fragments, cuticles, spores and pollen are common. A back-barrier depositional environment was suggested for these deposits (Johannessen 2003). Coarsening-upwards successions were interpreted as prograding mouth bars near the bayhead shoreline. Fining-upwards successions started with active channel fill by migrating mega-ripples or bars, succeeded by passive channel fill of siltstones and claystones and capped by thin coal beds representing the final abandonment of the channel (Johannessen 2003). The transgressive back-barrier sediments are typically overlain by sandstones, interpreted as back-stepping shoreface sand deposited during marine transgression (Johannessen 2003).

The clastic supply to the Feda Graben was delivered partly from the Inge High, which at that time was part of the Mid North Sea High, and partly from the Gertrud Plateau, which at this time had experienced a footwall uplift resulting in an enlarged source area including the Mandal High (Johannessen et al. 1996; Fig. 1 and 3). Carboniferous spores and pollen in the Gert Member in the Gert-1 well indicate a local Carboniferous sediment source, possibly in the area of the nearby Gert-2 well (Carboniferous sandstones cored in Gert-2), situated on the up-thrown side of the fault between Gert-1 and Gert-2 wells (Johannessen et al. 1996; Johannessen 2003). The Gert Member is overlain by offshore mudstones (the Lola Formation) deposited during the continued transgression (Johannessen et al. 1996). At this time the Gertrud Plateau was submerged and the clastic source area was farther away now at the Mandal High and the Mid North Sea High (Johannessen et al. 1996).

The Gert Member is encountered in the lowermost part of the Upper Jurassic in the Feda Graben and on the Gertrud Plateau. In the investigated wells, the Gert Member is represented in the Gert-1, Gert-2, Gert-4 Jeppe-1, Diamant-1, Hejre-1 and Hejre-2 wells, and possibly in the Rita-well (Fig. 1).

The overlying Ravn Member appears with fine- to medium-grained sand in coarsening-upward successions. The Ravn Member either succeeds the Gert Member or the offshore claystone, the Lola Formation, wedges in between these sandstone members. Intensive bioturbation obliterates the primary sedimentary structures. Relative abundances of dinoflagellate cysts are high and organic matter is dominated by wood fragments (Johannessen 2003). Bioturbated sandstones are interpreted as having been deposited by storm generated currents that transported sand from the beach to the middle and lower shoreface (Johannessen 2003). Poorly preserved cross-lamination indicates that traction currents operated over the sea floor giving rise to migrating small-scale ripples (Johannessen 2003). Scattered, out-sized quartz clasts were possibly deposited on scour surfaces by storm currents that swept across the sea floor; and the clasts were subsequently dispersed in the sediment by burrowing (Johannessen et al. 2003). On the Gertrud Plateau and the northern part of the Heno Plateau the coarsening-upwards successions are abruptly overlain by conglomerates. The conglomerates are mostly matrix supported, and contain quartz and quarzite clasts (diameter of 0.5-2 cm) and a matrix of fine- to medium-grained sandstone with pyrite, coal fragments and bivalve shells (Johannessen 2003). As the conglomerates overlie coarsening-upward shoreface sandstones and are overlain by fining-upward middle shoreface sandstones they are interpreted as transgression lags on a ravinement (erosion) surface and represents amalgamated sequence boundaries (Johannessen et al. 1996; Johannessen 2003). The conglomerates could either represent storm events on the beach or shoreface, or reworked fluvial deposits formed during maximum regression (Johannessen 2003). On the southern part of the Heno Plateau the equivalent to the conglomerate is an abrupt change from clay to sand-dominated deposits, which is interpreted as formed during maximum flooding episodes (Johannessen 2003). Clastic supply was delivered from the Mandal High and the Inge High to the Feda Graben and Gertrud Plateau (Johannessen et al. 1996). The Ravn Member is abruptly overlain by offshore mudstones – the Farsund Formation on the plateau areas, whereas in the basin areas the Ravn Member fines gradually upward to the Farsund Formation (Johannessen et al. 1996). The abrupt facies change on the plateau areas reflects an abrupt increase in water depth or is a result of a sudden cessation of sediment supply from nearby sand source areas (Mandal High and Inge High) due to complete drowning of these local highs (Johannessen et al. 1996).

The Ravn Member has been encountered in the Upper Jurassic on the Gertrud Plateau, the Heno plateau and the Feda Graben. In the investigated wells, the Ravn Member is represented in the Gert-2, Gert-4, Jeppe-1, Gwen-2, Diamant-1, Hejre-1, Hejre-2 and Rita-1 wells (Fig. 1).

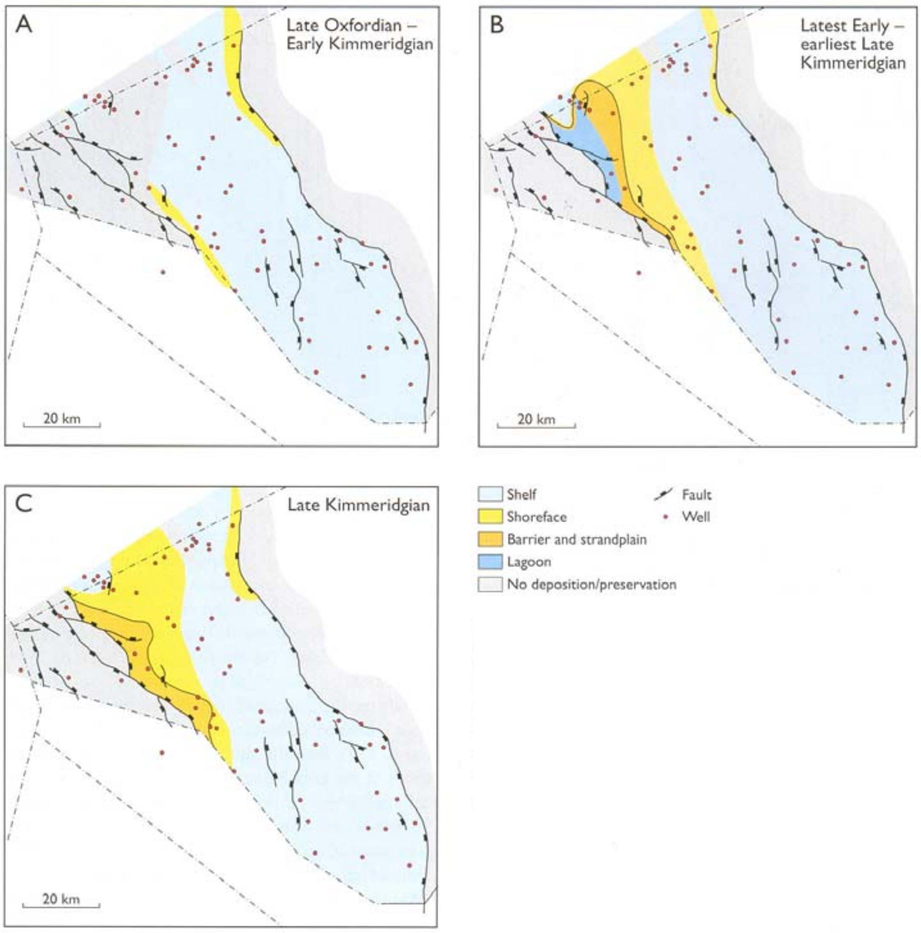

Figure 3. *Paleogeographic maps for Late Oxfordian – Late Kimmeridgian (Late Jurassic). (A) Transgression continued across the northern Heno Plateau, the Gertrud Plateau and the Feda Graben areas. (B) After a major regression marginal and shallow marine conditions dominated the plateau areas. (C) Subsequently, renewed transgression resulted in a westwards shift of the coastline and extension to the west of paralic and marginal marine conditions. After Andsbjerg & Dybkjær (2003).*

Methods

Geochemical analyses

Geochemical samples were taken, when possible, from both cuttings and cores in the same well. The cuttings samples were taken directly from the washed and dried cuttings. Magnetic or electrostatic removal of foreign material was avoided as it led to preferential removal of certain minerals (i.e. rock fragments and mica). The only exception was manual removal of hessian and large flakes of green paint using a pair of tweezers. Core samples were generally taken as plugs, which were trimmed in order to minimise possible contamination.

The main elements were measured by X-ray fluorescence (XRF) or atomic absorption spectrometry (AAS) whereas most trace elements and REEs were measured by inductively coupled plasma - mass spectrometry (ICP-MS). For detailed information see Table 1.

Methods used for analysing the different elements	
Method	Elements
XRF	Si, Ti, Al, Fe, Mn, Mg, Ca, K, P Ba, Ce, Cr, La, Nb, Ni, Rb, Sr, V, Y, Zn, Zr
ICP-MS	Ba, Ce, Co, Cr, Cs, Cu, Dy, Er, Eu, Ga, Gd, Hf, Ho, La, Lu, Mn, Nb, Nd, Ni, Pb, Pr, Rb, Sc, Sm, Sr ,Ta, Tb, Th, Ti, Tm, U, V, Y, Yb, Zn, Zr
AAS	Na, Cu
Loss on ignition	volatiles

Table 1. *Methods used for analysing the different elements.*

XRF

Samples were machine crushed in a tungsten carbide mortar. Contents of organic matter and volatiles were analysed by ignition (1 hour at 1000°C) of the powdered samples. Glass discs were prepared by fusing 0.75 g of ignited powder with 5.25 g sodium tetraborate for 1–1½ hours in Pt/Au crucibles over gas burners before it was poured into a Pt/Au mould (Kystol & Larsen 1999). The fusion method was chosen to ensure that refractive minerals, such as zircon and chrome spinel, were brought into solution when the glass disc was dissolved for the subsequent ICP-MS analysis. The glass discs were analysed with a Phillips PW 1606 wavelength dispersive multichannel XRF spectrometer equipped with a Rh-anode X-ray tube operating at 50 kV and 50 mA. Recommended detection limits for the main elements were in general twice the precision (= trueness), which was one standard deviation based on experimentally repeated analysis over time of a set of international standards (Kystol & Larsen 1999). The recommended detection limits for the main elements (Si, Ti, Al, Fe, Mn, Mg, Ca, Na, K and P) varied from 0.01 wt% for P_2O_5 to 0.3 wt% for SiO_2 (Kystol & Larsen 1999 for more detailed information). Trace elements (V, Cr, Ni, Zn, Rb, Sr and Nb with the exception of Ba and Y) were determined on reconnaissance basis at the >50 ppm level (Kystol & Larsen 1999). Values for Mo and Sn were only informative.

ICP-MS
A piece of the glass disc was dissolved in a mixture of HCl and HNO_3 (in the ratio 3:1). The solutions were dried and dissolved again in HNO_3 three times. Finally the solutions were diluted and sprayed, with a Meinhard nebuliser, into the argon carrier gas and analysed by the Perkin Elmer 6100 DRC quadrupole inductively coupled plasma – mass spectrometer (ICP-MS). Detection limits vary with sample type and elements analysed, from < 100 ppb to < 1 ppt (Frei & Kystol 2004). Routine analyses of international standards and in-house standards have demonstrated that the analytical precision and the accuracy are better than 5 % for the majority of elements analysed (Dirk Frei, personal communication 2006).

Europium results in the cuttings are obscured by interference from Ba, due to BaO generated in the ICP-MS instrument, which has a mass equivalent to the main Eu isotope analysed. Due to extremely high amounts of barite in cuttings samples correction of BaO interference on Eu was not possible. Eu in core samples can be used. Zn has interference from Ba^{2+} and usually this can be corrected. However, the extremely high barite content and probably especially the S content change the ionisation of the plasma so the usual correction factor is incorrect for the cuttings samples with high barite content. Consequently, XRF results for Zn have been applied in stead.

XRF of Ba and Sr at extremely high concentrations are better than ICP-MS data and consequently XRF data for these elements have been applied for correction for barite in drilling mud.

AAS
Crushed samples (0.25–0.5 g) were dissolved in hydrofluoric acid, evaporated to dryness and re-dissolved in a hydrochloric-potassium chloride solution (Kystol & Larsen 1999). These solutions were analysed for Na and Cu on a Perkin Elmer PE2280 atomic absorption spectrometer (AAS). Recommended detection limits are 0.08 wt% for Na_2O and 5 ppm for Cu (Kystol & Larsen 1999).

U-Pb zircon geochronology by Laser ablation - inductively coupled plasma - mass spectrometry (LA-ICP-MS)

Machine crushing in a tungsten carbide mortar took place in several steps, each followed by removal of the fine fraction. Heavy mineral concentrates were achieved by washing and panning the fine fraction. Zircon grains were hand-picked with a preparation needle from the heavy mineral concentrates and mounted in epoxy.

The samples were placed in a helium-flushed cell of the ICP-MS and sub-micron particles were ablated from the surface using a NewWave Research®/Merchantek® UP213 laser ablation unit that is equipped with a frequency quintupled ND-YAG laser (Frei et al. 2006). Laser-emitting wavelength was 213 nm with pulse duration of 5 ± 2 % RSD (Frei et al. 2006). The laser pulse repetition rate was 10 Hz and the nominal energy output 44 %, corresponding to a laser fluency of 8 J/cm^2 (Frei et al. 2006). The laser ablation microprobe uses a focused spot (30 µm in diameter) and an ablation time of 35 s, which results in ablated masses of zircon of approximately 150–300 ng (Scherstein *in press*). The ablated particles were transferred in a carrier gas via a Tygon® tube into the GEUS' Element2 (ThermoFinnigan®, Bremen) single-collector double focusing magnetic sector ICP-MS, which is equipped with a fast field regulator for increased scanning speed. The total acquisition time for each analysis was 90 s of which the first 30 s were used to determine the gas blank (Frei et al. 2006).

The instrument was tuned to give large, stable signals for ^{206}Pb and ^{238}U peaks, low background count rates for ^{207}Pb and low oxide production rates for example: $^{238}U^{16}O$ / ^{238}U < 2.5 % (Frei et al. 2006). ^{202}Hg, $^{204}(Pb + Hg)$, ^{206}Pb, ^{207}Pb, ^{208}Pb, ^{232}Th, ^{235}U and ^{238}U intensities were determined through peak jumping using electrostatic scanning in low resolution mode and with the magnet resting at ^{202}Hg. Each peak was determined at four slightly different masses and integrated sampling and a settling time of 1 ms for each isotope. ^{202}Hg was measured in order to monitor the interference of ^{202}Hg on ^{204}Pb, using a ^{202}Hg / ^{204}Hg ratio of 4.36 (Dirk Frei, personal communication 2006). The instrumental mass bias on ^{207}Pb / ^{206}Pb ratios during ablation was corrected using the NIST SRM 612 glass reference material. The laser induced elemental fractionation and the instrumental mass bias on measured isotopic ratios were corrected through standard-sample bracketing using the GJ-1 zircon (Jackson et al. 2004; Scherstein *in press*). Six measurements of the standard started and ended each session, and three measurements of the standard were performed for every10th zircon measurement. The raw data is corrected for instrumental mass bias and laser-induced U-Pb fractionation through normalisation to the GJ-1 zircon using the program GLITTER. Data presentation was performed by ISOPLOT (Ludwig 1997) and 'Age-Display' (Sircombe 2004).

Garnet chemistry by Computer controlled scanning electron microscopy (CCSEM)

Machine crushing of samples took place in several steps similar to the first part of the zircon separation process. Heavy minerals were concentrated by heavy liquid separation using bromoform, followed by embedment in epoxy in 5 mm diameter plastic vials. The vials were cut in half and mounted in epoxy blocks for subsequent grinding and polishing (Dirk Frei, personal communication 2006). Polished thin sections were experimentally prepared of Hejre-2 as a supplement to the heavy mineral concentrates. Polished blocks and polished thin section were carbon coated prior to analysis performed on a Phillips XL 40 scanning electron microscope (SEM) equipped with a ThermoNoran Voyager 2.7 energy dispersive X-ray analysis (EDX) system. The electron beam was generated by a tungsten filament operating at 17 kV and 50–60 µA. The number of measured grains varied from 500–1500. X-ray data were corrected for atomic number, absorption or fluorescence effects by the Proza correction scheme prior to semi-quantitative, standard-less calculation of elemental concentrations (Dirk Frei personal communication 2006). Data reduction was performed on a spreadsheet calculation program developed by GEUS (Laursen 1997; Sørensen 1998).

Material

The material used in this study consists of cores from known depths in eleven wells and a selection of cuttings from known depth intervals in the same wells. The number of core samples and cuttings samples from each well studied is presented in Table 2 and the location of the wells is indicated on Fig. 1.

Number of samples analysed by different methods in each well used in this investigation				
Well	Geochemical analysis		Geochronology by zircons	Garnet geo-chemistry
	Core samples	Cuttings	Core samples	Core samples
Diamant-1	17	20	3	3
Gert-1	30	48	6	6
Gert-2	14	22	6	6
Gert-4	52	66	6	6
Gwen-2	*32*	*22*		
Jeppe-1	40	27	3	3
Hejre-1	-	*21*		
Hejre-2	*26*	*31*	*6*	*6*
Rita-1	51	94		
P-1	1		1	
Ugle-1	1		1	
In total 01-02-2007	264	351	32	30

Table 2. *The number of sample types from eleven wells from the Danish sector of the North Sea.All samples are part of the GEUS North Sea database, except those marked in italic, which have been performed for Conoco Phillips.*

Geochemical results and discussion

All raw analytical results are presented on the enclosed CD ROM. Appendix 1A and 1B gives an overview of all investigated samples in each well.

In general the ICP-MS method is more accurate for trace elements than XRF, therefore ICP results are generally chosen instead of XRF results, when results are available from both methods. However, Eu is excluded in cuttings due to difficulties with correction of high barium content. Ba is a major element in many cuttings samples and the XRF values are better and accordingly used in this presentation.

Artefacts

The way cuttings samples are produced will give rise to pollution by several elements, which may reflect the drilling mud composition instead of the sedimentary rock. Barite is a common constituent in the drilling mud and therefore common in cuttings samples. Cuttings samples have been corrected for their barite contents.

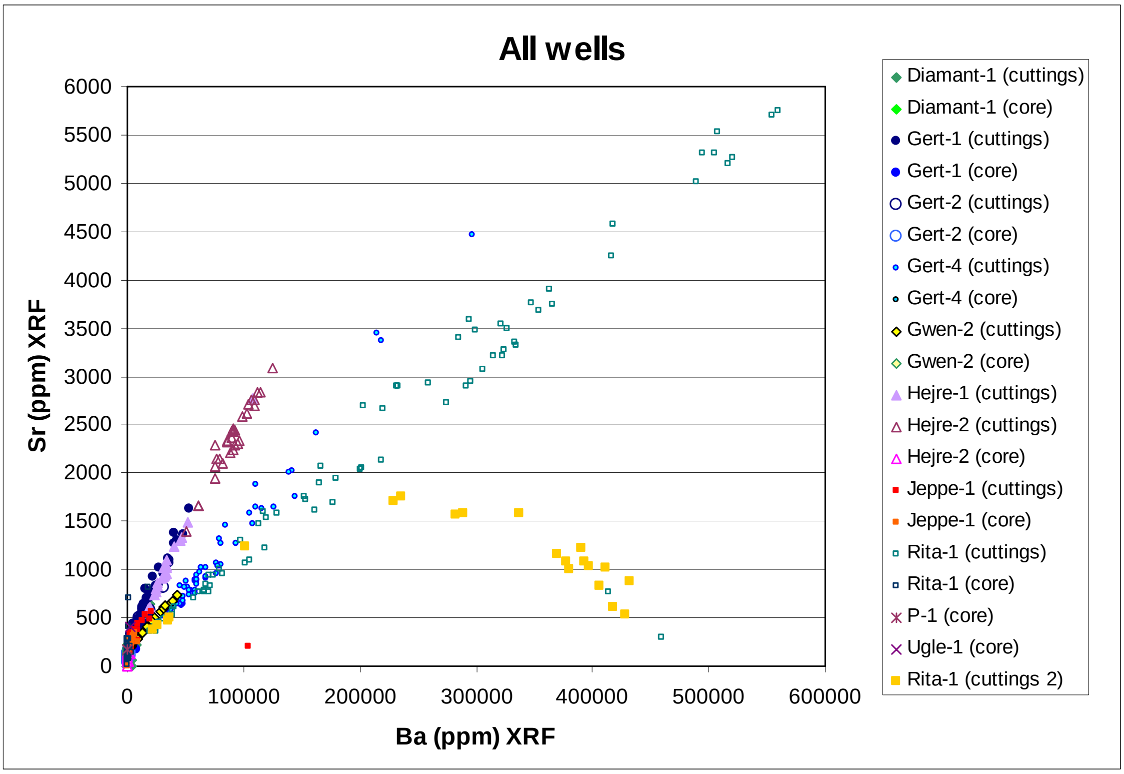

Figure 4. *Sr (ppm) XRF versus Ba (ppm) XRF on cuttings samples and core samples in all wells. The Sr/Ba ratio seems to fingerprint different mud types. Similar barite types have been used in Hejre-1, Hejre-2 and Gert-1 and are different to the barite types used in Gert-4 and Rita-1. In Rita-1 another barite type seems to have been used for the lower part of the well (cuttings 2), which is distinctive from the upper part of the well.*

Cuttings samples show rather large contents of Ba from barite (Fig. 4), in some cuttings barite actually constitutes the greater part of the sample. Different Sr/Ba ratios between Hejre-1, Hejre-2, Gert-1 and Gert-4, Rita-1 indicate that barite from various sources has been used during drilling. Cuttings samples from the lower part of Rita-1 (Rita-1 cuttings 2 on Fig. 4) separate themselves from other results, possibly as a result of dilution with barite from another source.

Steel chips are a common impurity in cuttings. These steel chips may, depending on their origin, contain additives such as C, Si, Mn, Ni, Cr, Cu and V. The relationship between Fe_2O_3 and the trace metals Cr, and to some extend Mn, in some Rita-1 samples (Figs. 5 and 6) indicates that Cr, and possibly Mn, in cuttings from Rita-1 may originate from the steel chips. The extremely high Cr content in Gert-1 and Gert-2 cuttings samples most likely comes from high-Cr steel chips mixed with low-Cr steel chips and therefore without correlation to the iron content. Ni has a positive correlation with Fe_2O_3 for all wells in both core and cuttings samples. In a similar way V shows a positive correlation with Fe_2O_3 in some wells in both cuttings and core samples. As core samples contain no steel chips these positive relations are not artificial.

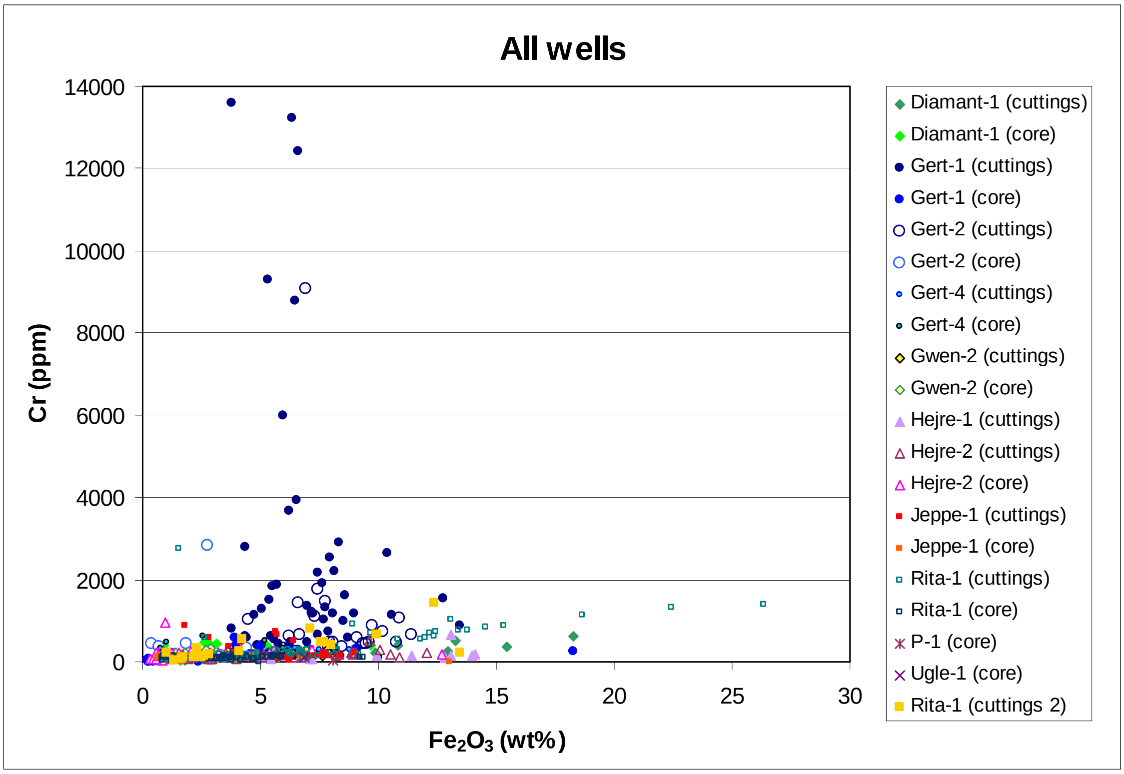

Figure 5. *Cr (ppm) versus Fe_2O_3 (wt%). Iron has a positive correlation with Cr in Rita-1 cuttings suggesting the presence of steel chips. Gert-1 cuttings have extremely high Cr content indicating the presence of high-Cr steel ships.*

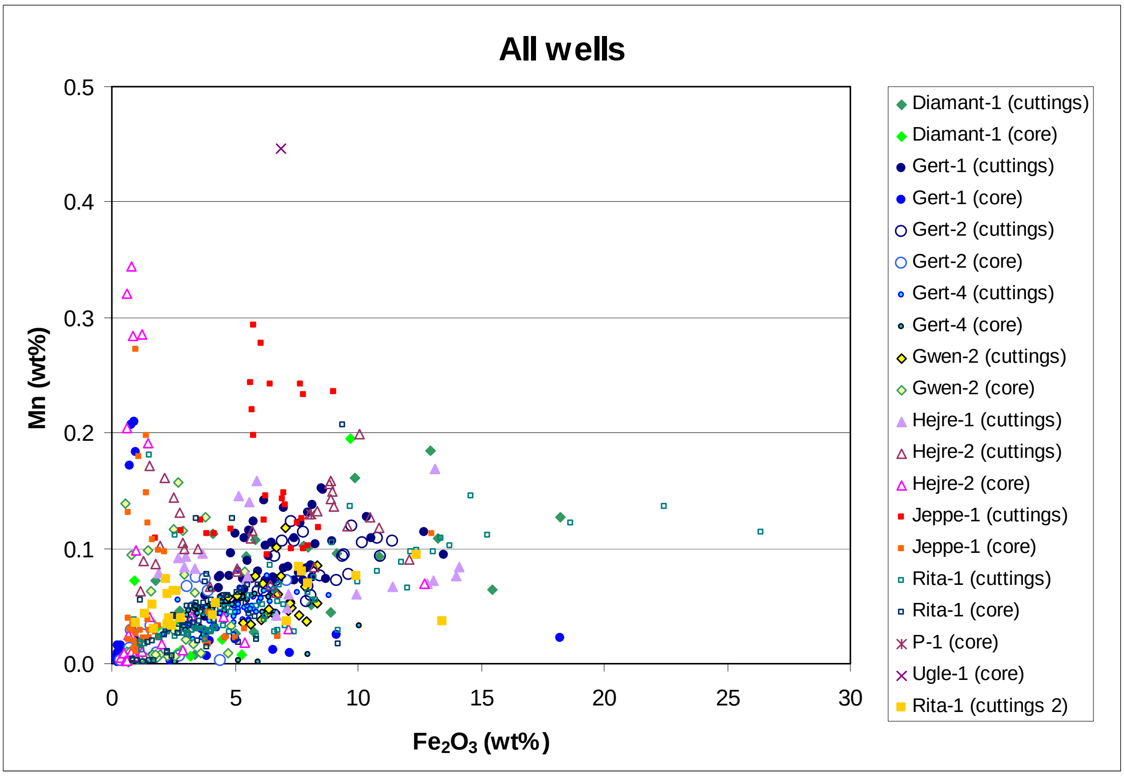

Figure 6. *Mn (wt%) versus Fe_2O_3 (wt%). Iron has a positive correlation with manganese in Rita-1 indicating the presence of steel chips in the cuttings from this particular well.*

Flakes of green paint are found in several cuttings (especially in the Diamant-1 well). Copper phthalo-cyanin, chromium oxide, copper oxide and copper carbonate are common pigments in green paint. The highest Cu values are measured in cuttings in the Diamant-1 well and must consequently be considered an artifact.

During preparation all samples were crushed in tungsten carbide mortars, and may consequently have taken up minor amounts of impurities. Tungsten carbide is known to contain considerable amounts of Co and Ta.

Major and trace elements

Selected major elements showing clear correlations are presented in the following.

Volatiles show various relations with other elements in different formations and different wells. Decreasing amounts of SiO_2 is correlated to increasing amounts of volatiles, probably reflecting a facies relationship (mudstones containing higher amounts crystal-bound water and of organic material than sandstones). In some wells (Jeppe-1 and Diamant-1) the volatiles seem to be related to CaO, i.e. reflecting the degree of calcite cement.

The negative correlation between Al_2O_3 and SiO_2 in Fig. 7 is found in all wells and indicates a dilution effect, high amount of SiO_2 (possibly as quartz) in the sediment result in lower amounts of Al_2O_3 (possibly as clay and feldspar). Outliers are mainly due to relatively calcite-rich samples from the Farsund Formation (in the Diamant-1and Rita-1 wells) or the pre-Jurassic sediments. Relatively high amounts of alumina could be caused by pollution by Al of core samples wrapped in aluminium-foil.

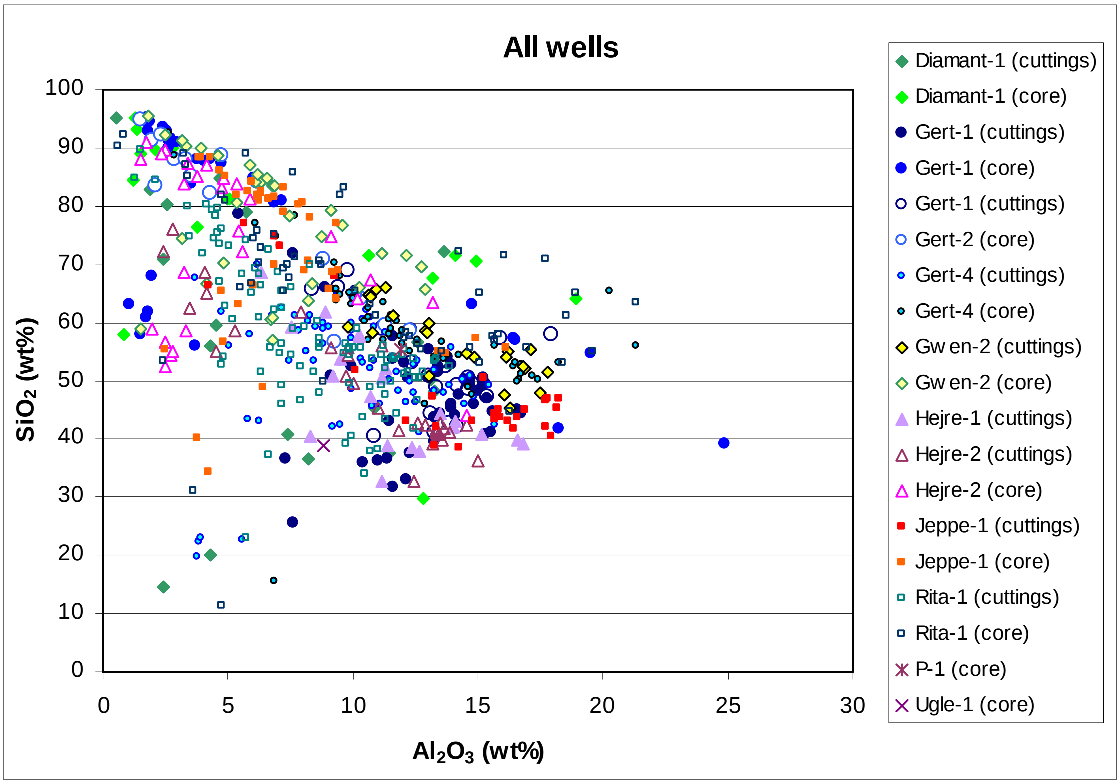

Figure 7. *Graph showing general negative correlation between SiO_2 (wt%) and Al_2O_3 (wt%).*

All wells show a more or less distinct negative correlation between CaO and SiO_2, which also reflects a dilution effect. High SiO_2 contents probably indicate quartz-rich intervals in the successions, whereas low SiO_2 contents reflect intervals with clay and carbonates.

Al_2O_3 and K_2O show positive correlation with two different trends (Fig. 8). These two trends are also found in the K_2O / Rb ratio (Fig. 9). In sediments, aluminium and potassium are typically situated in clay minerals, mica and K-feldspar. K-feldspar will typically have a much higher K_2O / Al_2O_3 ratio than clay and mica, though both may vary depending on actual composition. The highest K_2O / Al_2O_3 ratio in Fig. 8 probably reflects higher K-feldspar content in Hejre-1 and Hejre-2 samples than in the other wells. The lower K_2O / Al_2O_3 trend reflects clay and mica of mixed composition, as MgO also shows a positive correlation with Al_2O_3 in most wells. When the wells are subdivided into members and formations more information is revealed. The Gert Member from the Hejre wells and the pre-Jurassic sample from the Hejre-2 well have similar K_2O / Al_2O_3 ratios, which are distinctly different to Gert Member in other wells and Farsund Formation in Hejre 1 and 2 and other wells (Fig. 8). The Ravn Member in the Jeppe-1 well has an K_2O / Al_2O_3 ratio which lies between the main group of wells and the Hejre wells. This indicates that a local source might have supplied the Hejre-1 and Hejre-2 wells and possibly to a smaller degree to Jeppe-1. There seem to be no difference between upper and lower part of the cored sand (Gert Member) in the Hejre-2 well.

Another possibility could be diagenetic alterations in favour of K-feldspar and consequently authigenic precipitation of K-feldspar (and dissolution of albite). However, the strong relation between the composition of the Heno sandstone units in the Hejre wells and the pre-Jurassic sediment in the Hejre-2 well indicate that source rock differences are of major importance. Consequently, Al_2O_3 and K_2O are difficult to use for distinguishing between different formations and members and for correlation between wells.

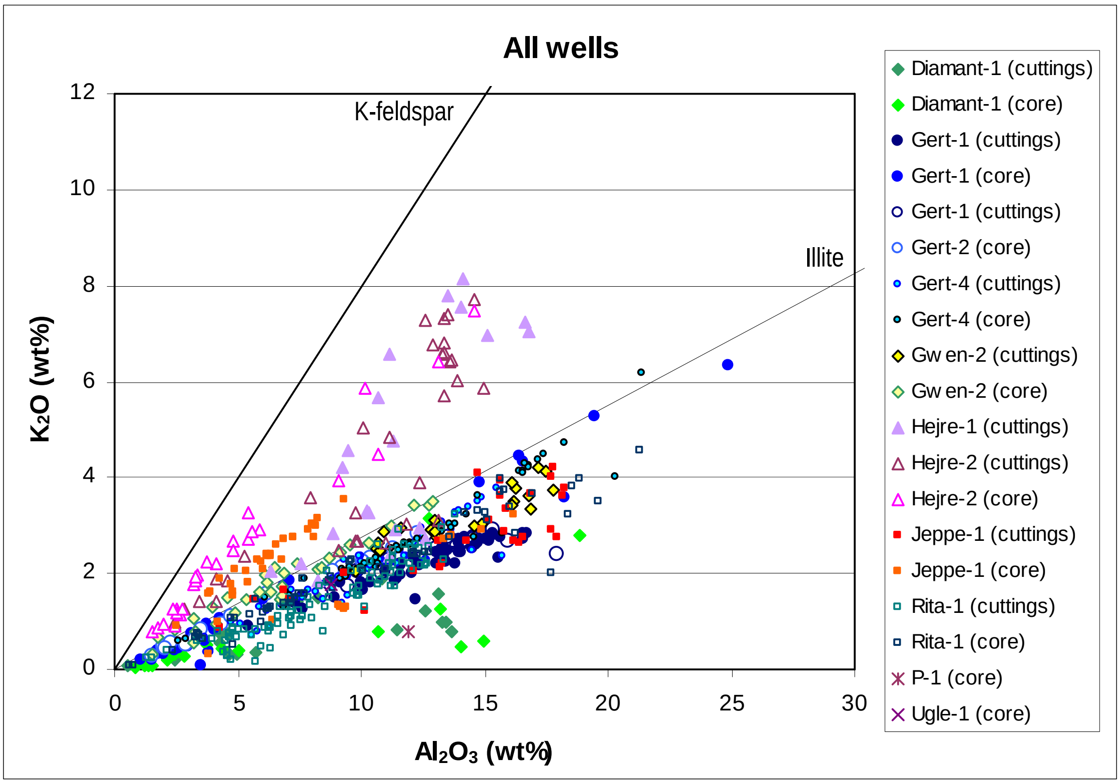

Figure 8. *Graph showing positive correlation between K_2O (wt%) and Al_2O_3 (wt%). Note the high K_2O / Al_2O_3 ratios in the Hejre samples. Jeppe-1 core samples are also characterised by elevated K_2O / Al_2O_3.*

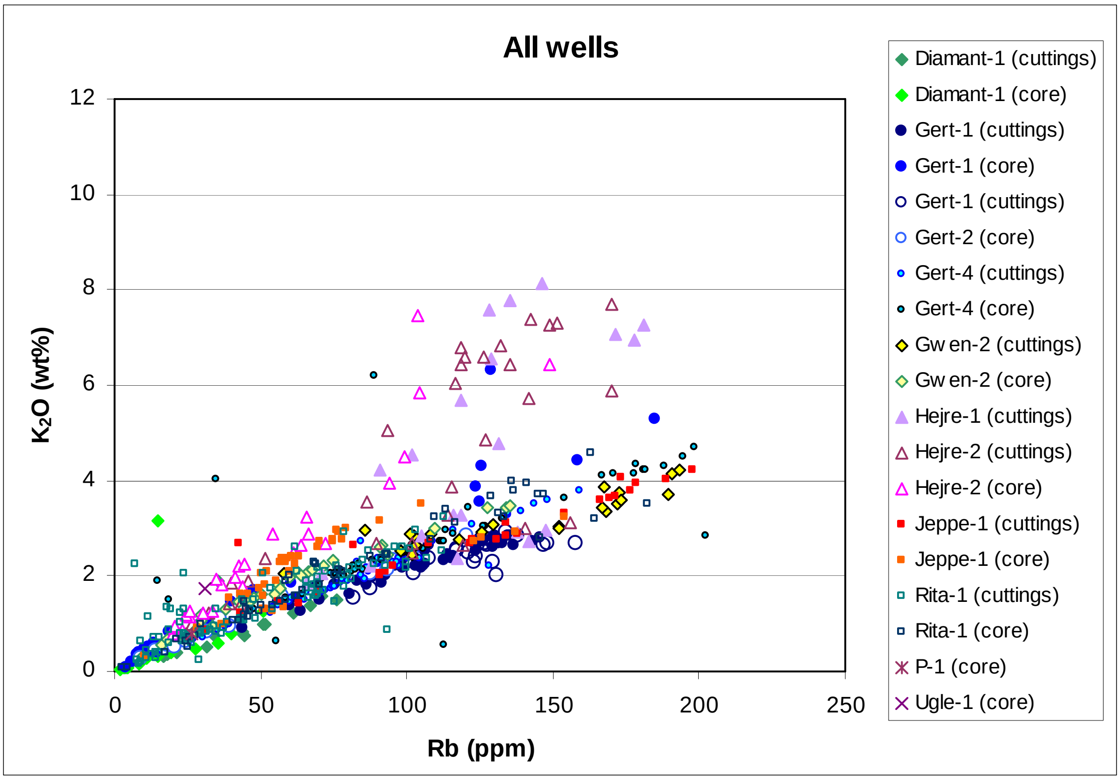

Figure 9. *Graph showing positive correlation between K_2O (wt%) and Rb (ppm) with similar trends as in the K_2O versus Al_2O_3 graph (Fig. 8).*

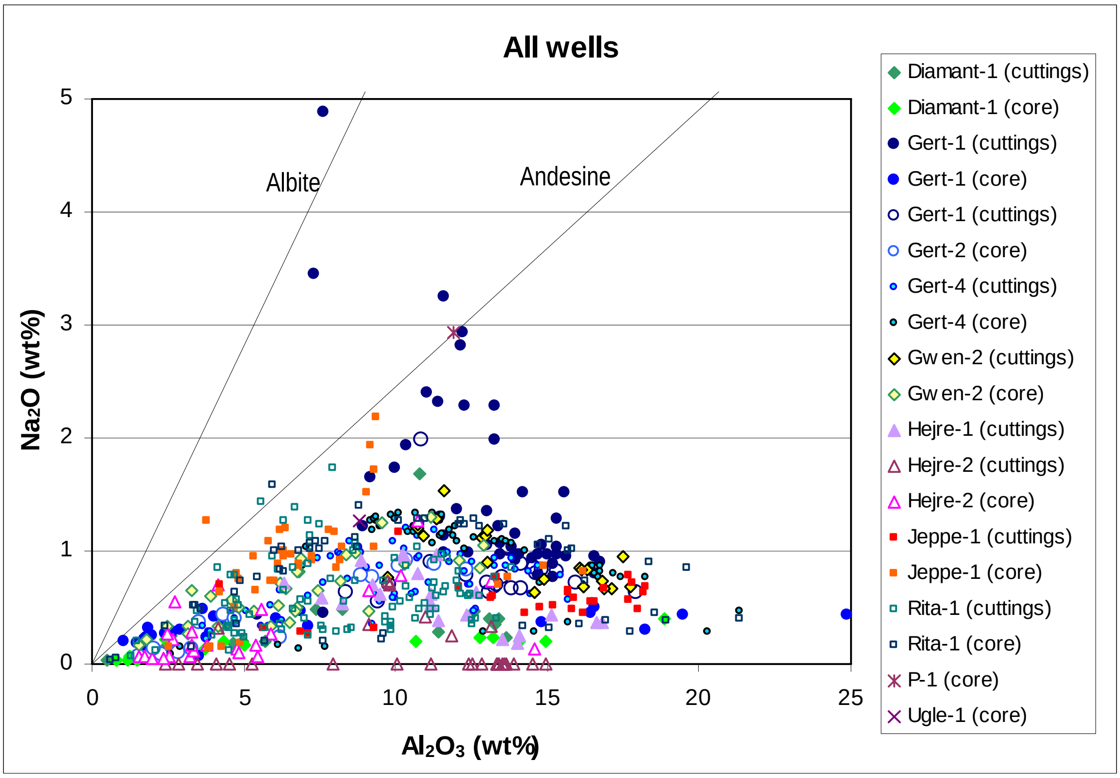

Figure 10. *Graph showing positive correlation between Na_2O (wt%) and Al_2O_3 (wt%) up to approximately 10 % Al_2O_3. Higher amounts Al_2O_3 show a negative correlation with Na_2O.*

Al_2O_3 and Na_2O show a positive correlation up to approximately 10 wt% Al_2O_3; higher amounts of Al_2O_3 and Na_2O show a negative correlation (Fig. 10). This indicates that the Na_2O content is low in very clay-rich samples with high Al_2O_3 contents. Therefore sodium is more likely related to feldspar than to clay minerals. However, caution must be taken when evaluating Na contents as there is a potential risk that Na from brine may still be present in the core.

Al_2O_3 and TiO_2 show overall positive correlations with trends varying among the different wells (Fig. 11). The correlation suggests location of TiO_2 in specific minerals. The main Ti-bearing minerals are ilmenite, amphiblole, pyroxene and biotite, and the differences may be due to distinctly different proportions of these minerals in the sediments. However, basic volcanic material also holds high contents of Ti and a TiO_2 / Al_2O_3 ratio of ca. 1/10 may indicate an influx or reworking of volcanic materials as in the Gert Member in Hejre-1 and Hejre-2 wells.

The sandy part of the Gert Member in Gert-4 and some cuttings samples from the Gert Member in Rita-1 show high TiO_2/Al_2O_3 ratios in a trend more or less oblique to the overall trend, which might be related to the presence of heavy minerals (ilmenite and rutile).

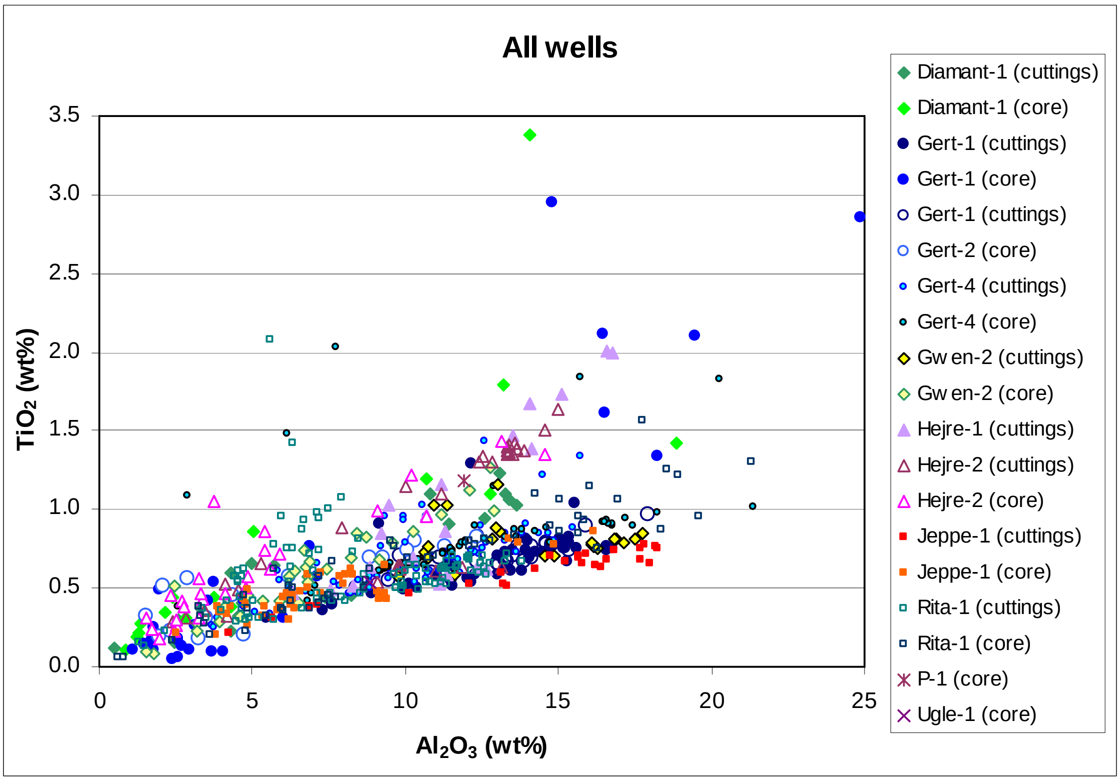

Figure 11. *Graph showing positive correlation between TiO_2 (wt%) and Al_2O_3 (wt%) in all wells. Note the varying TiO_2 / Al_2O_3 ratios.*

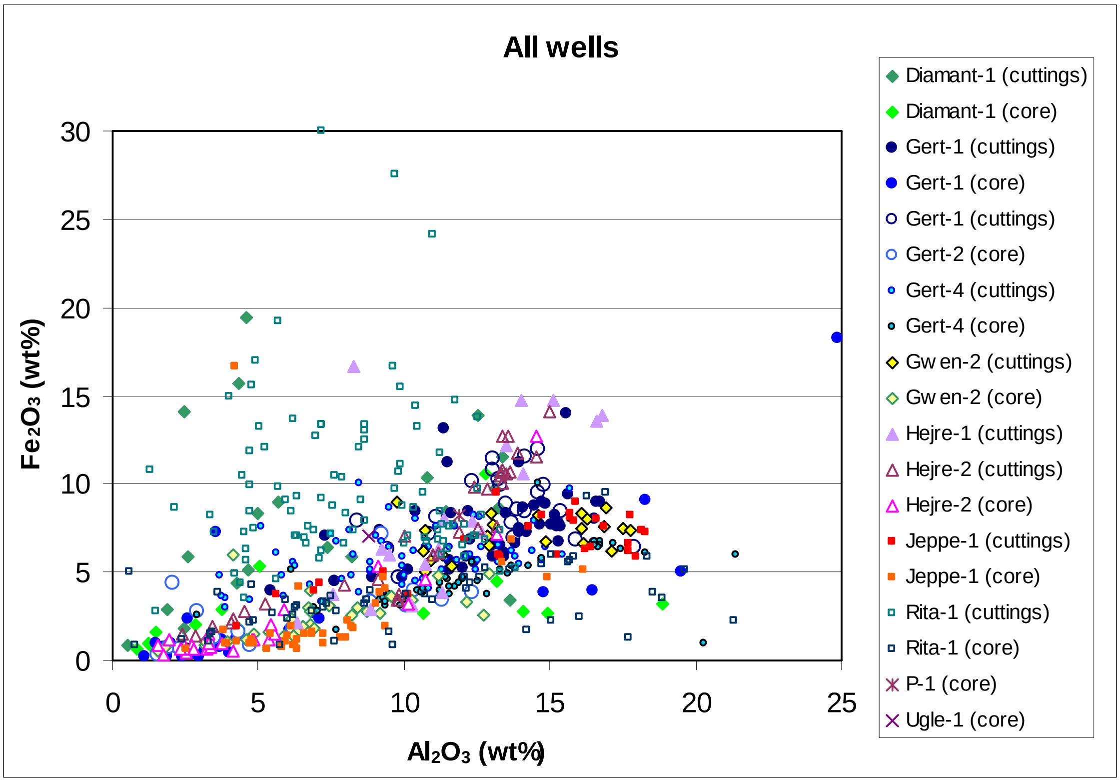

Figure 12. *Graph showing a general positive correlation between Fe_2O_3 (wt%) and Al_2O_3 (wt%).*

Most wells, with the exception of Rita-1, show a positive correlation between Al_2O_3 and Fe_2O_3, which indicates the presence of iron in clay minerals (Fig. 12). The very high Fe_2O_3 content (> 10 wt%) are related to pyrite cemented sandstones from cores and steel chips from cuttings.

Some elements are strongly associated with one another due to their occurrence in similar minerals. Zirconium typically occurs in zircon grains, which also contain trace elements as U, Th, Pb and Hf. Hafnia is a rare trace element, which commonly and almost exclusively occurs in zircons, and therefore Hf is strongly associated with Zr (Fig. 13). In a similar way all REE and Y seem to occur in almost the same ratios in all samples, indicating that they are present in the same minerals (Fig. 13). Ce (and other REE and Y) show a positive correlation with Al_2O_3 (Fig. 14). The REE and Y may be incorporated in clay minerals or might occur in minerals associated with clay minerals, which could be authigenic phosphate minerals. Ce and Lu show an almost exponential correlation, which indicate that the light REE are slightly increased relative to the heavy REE.

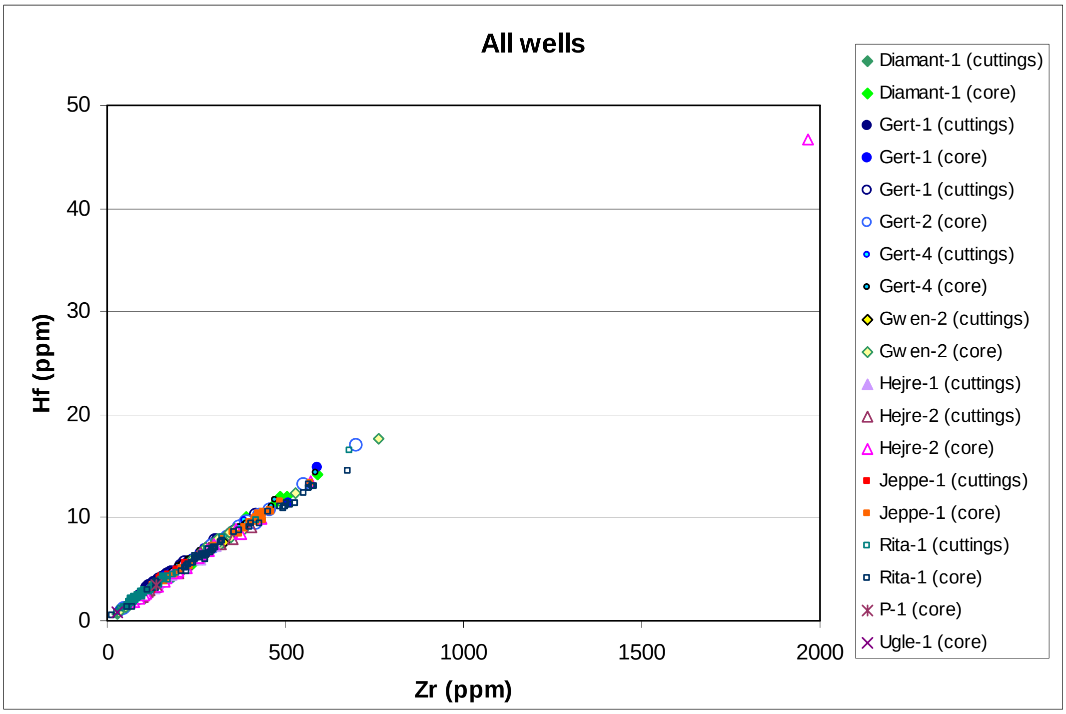

Figure 13. *Graph showing perfect positive correlation between Zr (ppm) and Hf (ppm).*

Hf is closely similar to Zr, and the Zr / Hf ratio in most rocks in the World varies within fairly narrow limits around 35–45. In accordance with this, the analysed sediments have an average Zr / Hf of 40.2 ± 2.4 (1s), i.e. a very tight correlation as seen in Fig. 13, which illustrates the high quality of the analyses.

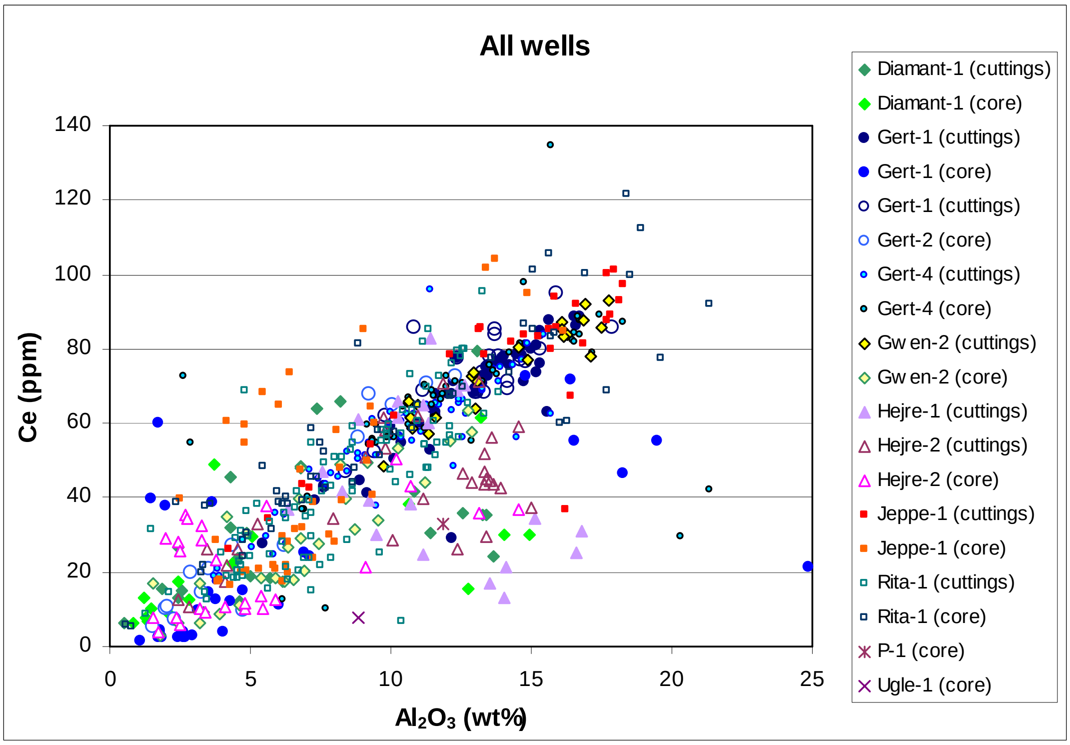

Figure 14. *Graph showing an overall positive correlation between Ce (ppm) and Al_2O_3 (wt%). Other REE and Y have similar trends as Ce.*

Geochemical variation with burial depth

The geochemical variation with depth of burial is presented for selected elements for the Hejre-2, Gert-1, Gert-2, Gert-4, Gwen-2 and Rita-1 wells in Appendix 2. The chemical results of cuttings samples may be almost similar to the core samples, as in the Gert-4 well; or show almost systematic differences to core samples, as is seen in the Rita-1 well (Appendix 2). The cuttings samples may also be completely different to the core samples as observed in the Gwen-2 well (Appendix 2). In some cuttings samples there can be a tendency to preserve clay chips rather than sand grains. Consequently, elements which typically occur in clays or are associated with clay minerals, will be over-represented, whereas elements that are typically related to the sand fraction will be underestimated. This variation between wells is probably related to the quality of the cuttings samples.

Gert Member, Heno Formation

The lithology of the Gert Member is alternating claystone and sandstone beds, which has resulted in equally alternating chemical content. The best core representations of Gert Member occur in Hejre-2, Gert-1, Gert-4 and Diamant-1. The lowermost Jurassic sediments in Rita-1 may belong to the Gert Member, but it could also be part of the Bryne Formation (Peter Johannessen, personal communication 2006). Questions have also been arised whether the lowermost part of the Hejre-2 core is a part of the Gert Member or should be distinguished from the Gert Member. Three Upper Jurassic sand intervals have been encountered in Hejre-2. The middle sand interval is coarsening upwards, which is usually characteristic of the Ravn Member. However, the lithology and sedimentary structures indicate that the lowermost and the middle sand layers are both part of the Gert Member (Peter Johannessen, personal communication during Core workshop 2006). The subdivision of the Gert Member into two sand intervals in Hejre-2 is caused by an internal flooding surface, which also occurs in the Gert Member in other wells. In order to focus on this problem these samples have been separated into two groups: 'Gert Member? Rita-1' or 'Possible Gert Member in Rita-1' and 'Lower Gert Member' in Hejre-2.

Cuttings samples represent a larger part of the sediment and therefore show more homogenised results compared with core samples. The Gert Member has an overall upward-increasing SiO_2 content and simultaneously a constant or weakly decreasing Al_2O_3 content in the Hejre-2, Diamant-1, Gert-1 and Gert-4 wells, which have the best coverage of the Gert Member. A high SiO_2 content reflects the sand-dominated intervals, whereas a relatively high Al_2O_3 content reflects more clayey intervals. Several elements, such as TiO_2, K_2O, P_2O_5 and Rb, seem to correlate with the Al_2O_3 content. Fe_2O_3, MnO and MgO show similar relations to the Al_2O_3 content in some wells. Core samples from Gert-1 and Gert-4 show clearly that relatively high contents of several elements (Al, Ti, K, P, Rb, Fe, Mn, Mg, Na, P, V, Co, Ni, Cu, Nb, Cs, Y, La, Ce (and other REE), Th and U) are related to clay-rich core samples. Besides clays, feldspar can also contribute with Al_2O_3, K_2O, Na_2O and CaO, the latter being considerably influenced by carbonate cements and therefore not particularly useable to distinguish between clay and feldspar.

The Gert Member in the Gert-1, Gert-2, Gert-4 and Rita-1 wells has lower Na_2O contents when compared with those in the Ravn Member, and the Lola and Farsund Formations. A similar trend cannot definitely be confirmed for the Hejre wells. The Gert Member (in the Hejre-2, Jeppe-1, Gert-4 and Rita-1 wells) has a relatively low MgO content compared with the Ravn Member, and the Lola and Farsund Formations. Few samples with relatively high MgO contents in the Gert Member seem to be related to clay-rich core samples.

The highest TiO_2, content is found in the Gert Member in the Gert-1, Gert-4, Diamant-1 and Rita-1 wells, whereas the Ravn Member, and the Lola and Farsund Formations typically have a lower content. Zr shows an overall decrease upwards in the Gert Member, although this trend is difficult to see due to large variations. Usually the Zr content increases with increasing SiO_2 content, but when the purity of the sample reaches 70–80 % SiO_2 the Zr content begins to decrease with increasing SiO_2 (Appendix 4).

The large variation within the Gert Member makes if difficult to define geochemical trends. A few elements (V, Ni, Cr, Y, Ce, La and all REE), though, show a tendency of upward-decreasing amount until reaching the marine transgressive surface of erosion or the flooding surface defined by Johannessen (2003).

Lola Formation

The lithology of the Lola Formation appears more homogeneous than that of the Gert Member and therefore the chemical results show less fluctuations and more distinct trends. The Gert-4 and Rita-1 wells have the best core representation of the Lola Formation.

Wells with a thick sequence of Lola Formation (Gert-1, Gert-4, and Rita-1) show first an upward-decreasing SiO_2 trend followed by an upward-increasing SiO_2 content. Minimum SiO_2 content is located at the maximum flooding surface defined by Johannessen (2003). The Al_2O_3 content shows a different trend with two maxima, first at the same maximum flooding surface (Johannessen 2003) as SiO_2 and another at the flooding surface just above the Gert Member in the Gert-1 well, whereas in the Gert-4 well it is at a possibly not earlier recognised flooding surface. K_2O, Rb, Fe_2O_3, Cs, La, Ce (and then all REE), Th and to some extend TiO_2, Nb and Y, generally correlate with the Al_2O_3 content in the Lola Formation.

The lower part of the Lola Formation in Gert-4 shows an interval of increasing MgO content until stabilising at the typical level. Similar trends can be observed in the Rita-1 well and possibly in the Gert-1 and Hejre-2 wells. The upward-increasing MgO content in the lower part of the Lola Formation in the Gert-4 well follows an increasing content of Al_2O_3. However, the similar upward-increasing MgO content in the Gert-1 and Rita-1 wells is accompanied with, respectively, decreasing or stabile Al_2O_3 content. The MgO content in the lower Lola Formation in the Rita-1 well is accompanied with increasing CaO content.

Ravn Member, Heno Formation

The lithology of the Ravn Member appears almost as homogeneous as that of the Lola Formation, but is more silty or sandy. The Gwen-2 and Jeppe-1 wells have the best core-coverage of the Ravn Member, but the Rita-1 and Gert-4 wells also have several core samples in the Ravn Member.

Core samples from the Rita-1 and Gert-4 wells show that the Ravn Member has an upward-increasing SiO_2 trend followed by an upward-decreasing SiO_2 content. Maximum SiO_2 content is located at the sequence boundary and the coinciding marine transgressive surface of erosion defined by Johannessen (2003). The Gwen-2 and Jeppe-1 wells show only an upward-increasing content before the flooding surface. The Al_2O_3 content follows the SiO_2 content with the highest amount of Al_2O_3 at lowest SiO_2 content and visa versa. Several elements (K, Rb, Ti, Fe, Mg, Na, P, V, Ni, Cu, Nb, Cs, Zr, Y, La, Ce (and other REE), Th and U) seem to follow the aluminium trend, as they increase when SiO_2 decreases. Co, Sc and Cr are the exceptions, as the first two seem to follow the trend of SiO_2, whereas chromium seems to be independent of the SiO_2 content. Very generally the Cr content seems to decrease in core samples from the Gert Member, through the Lola Formation and the Ravn Member until reaching its minimum in overlying Farsund Formation. Cuttings samples show occasionally extremely high peak values, which must have been caused by pollution probably by steel chips. The dilution effect of SiO_2 is so strong that any other element in the Jeppe-1 and Gwen-2 wells, K, Rb, Ti, Fe, Mg, Na, P, V, Ni, Cu, Nb, Cs, Zr, Y, La, Ce (and other REE), Th and U generally correlates negatively with the SiO_2 content in the Ravn Formation. This dilution effect could be a consequence of abundant quartz or quartzite oversized clasts in the Ravn Member in the Jeppe-1 and Gwen-2 wells. The chromium content in core samples is much more scattered in the Jeppe-1 and Gwen-2 wells than in Gert-4, Rita-1 and Diamant-1. Cuttings samples from the Ravn Member in the Hejre-1 and Hejre-2 wells seem to have similar behaviour as in the Jeppe-1 and Gwen-2 wells, but low sample coverage makes verification difficult.

The zirconium content is associated with the SiO_2 content in most wells (Rita-1, Gert-4, Gert-2, Diamant-1 and possibly Gert-1). The Zr content increases upwards until the flooding surface in the Gert-2, Gert-1 and Diamant-1 wells. The Rita-1 and Gert-4 wells also have an interval of upward-decreasing Zr content from the boundary sequence before reaching the flooding surface. TiO_2 and Nb have completely opposite trends, as they follow the Al_2O_3 content. Jeppe-1 and Gwen-2 have a completely different trend, with Zr following Al_2O_3 and TiO_2.

The P_2O_5 content in cores seems to be lowest in the middle of the Ravn Member and increases upwards and downwards towards top and base. This can best be observed in the Gwen-2 well and is supported data from the Gert-2, Gert-4 and Rita-1 wells. Thus P_2O_5 seems to increase towards the maximum flooding surfaces defined by Johannessen (2003). Variations in P_2O_5 content within the Ravn Member could be influenced by the depositional environment, as the highest content is present in the offshore claystones (Farsund Formations and to a lesser extend the Lola Formation).

Carbonate cemented samples appear to be more common in the Ravn Member than in the Gert Member. The low background CaO (and MnO) content follows elements as Al_2O_3, K_2O, TiO_2, Fe_2O_3, and MgO, and probably indicates the amount of CaO located in clays minerals. The relatively high CaO peaks (> 10 %) probably represent carbonate cemented samples. Calcite cement in the Jeppe-1 and Diamant-1 wells is characterised by a small content of MnO, and one sample in the Rita-1 well by a high MgO content suggesting that dolomite might also be present.

Halite is a common mineral precipitating in the core samples as the pore water is dried out. The cuttings are washed and dried samples and consequently most of the halite in the cuttings would have been washed away. The fine relation in Na_2O content between cuttings and cores indicate that halite is not a major problem in core samples. Instead sodium is probably bound in the clay minerals or feldspar. The Na_2O content shows a maximum in the lower part of the Ravn Member in the Gert-4, Rita-1, Gwen-2, Jeppe-1 wells and most likely also in the Hejre-1, Hejre-2 and Gert-2 wells. The Na_2O maximum coincides with the coarsest grain-size in the Ravn Member. These oversized clasts are strongly dominated by quartz and quartzites, but feldspar has also been identified. Therefore the maximum in sodium content could be related to this source of oversized clasts. Cuttings samples from the Gert-1 well show a Na_2O maximum in the Lola Formation instead. A dominance of clay minerals could be responsible for this maximum.

Clay minerals deposited in a highly saline environment would be surrounded by highly saline pore fluids, and the high cation exchange capacity of clays could possibly lead to clays being richer in Na_2O in a marine deposit (Ravn Member and Lola Formation) than in a brackish deposit (Gert Member).

Farsund Formation

Core samples of the Farsund Formation are only present in the Rita-1 and Jeppe-1 wells. The Farsund Formation consists of homogeneous claystone. But again core samples show a larger variation than cuttings due to the homogenising effect of the cuttings.

The Farsund Formation has a lower SiO_2 content than the other formations. The Al_2O_3 content is generally higher due to the higher clay content; one exception being the gamma ray minimum in the Rita-1 well close to the core in the Farsund Formation. K_2O, Rb, TiO_2, Nb, La, Ce (and all other REE) and partly V and U follows the alumina trend. The gamma ray minimum in Rita-1 in the Farsund Formation is associated with only a small increase in CaO, MgO, P_2O_3 and partly TiO_2. One core sample from this level shows a high content of dolomite. Core samples from the Jeppe-1 well show the presence of calcite cemented samples instead.

The Farsund Formation seems to have the highest U content of all the formations, though clay-rich samples of Gert Member and occasionally Lola Formation may have equally high U contents. The high U content could be related to organic matter and thus reflects the depositional environment. The high phosphorus content in the Farsund Formation might be related to marine phosphate minerals or organic matter.

Geochemical variation between different formations and members

Comparison between cuttings samples and core samples showed that some wells have relatively good intra-well correlations, some with systematic variations and some without any correlation at all (see previous section: Geochemical variation with burial depth). Consequently, the differentiation of the different members and formations was based on core samples for the purpose of this report. A similar differentiation should be possible for cuttings samples of the best quality.

Averages of selected oxides and elements in core samples																	
Well	Formation / member	TiO_2	MgO*	Fe_2O_3	K_2O	Na_2O	P_2O_5	Nb	Rb	Zr	Cr	Ni	Cu	Zn	V	Th	La
JE1	Farsund	0.54	1.31	5.50	1.75	1.24	0.24	13	76	155	79	70	86	16	167	7	38
RI1	Farsund	0.86	1.60	6.79	3.18	0.83	0.21	19	164	132	128	121	78	7	155	12	44
RI1	Lola	0.83	2.77	5.12	2.81	1.18	0.15	23	109	254	109	69	67	8	93	11	59
GE4	Lola	0.84	2.98	5.40	3.30	0.99	0.14	23	136	239	106	68	66	13	108	11	39
GE4	Ravn	0.65	2.30	3.60	2.12	1.24	0.14	19	80	375	111	38	46	8	55	9	29
GE2	Ravn	0.61	1.45	3.15	1.81	0.66	0.11	18	75	357	110	37	28	5	53	8	26
RI1	Ravn	0.46	2.15	2.88	1.39	0.92	0.14	14	53	208	91	30	44	6	40	6	24
GW2	Ravn	0.58	0.58	2.33	1.81	0.65	0.06	12	60	263	160	24	41	2	46	4	15
JE1	Ravn	0.45	0.32	1.25	2.31	0.81	0.08	11	62	392	130	13	33	3	28	4	18
DI1	Ravn	0.30	0.27	1.40	0.22	0.10	0.09	7	9	186	101	13	31	1	24	2	8
GE1	Gert	0.55	0.22	1.88	1.25	0.30	0.03	9	42	192	126	26	18	2	52	3	25
GE2	Gert	0.37	0.13	1.63	0.79	0.19	0.03	9	27	292	332	28	22	0	23	2	7
HE2	Gert	0.54	0.25	1.72	2.26	0.24	0.08	7	53	176	152	19	37	10	49	2	10
DI1	Gert	1.86	0.56	3.13	0.93	0.21	0.04	22	41	376	316	50	49	6	208	7	39
GE4	Gert	1.38	0.70	3.60	2.51	0.24	0.06	24	75	342	366	57	55	6	116	8	8
HE2	Gert Lower	0.60	0.18	1.46	2.15	0.37	0.04	9	44	526	256	19	24	50	49	3	12
RI1	Gert ?	0.87	0.51	2.55	2.37	0.27	0.04	29	82	416	126	27	37	1	76	9	32

Table 3. *Averages of selected oxides and elements in core samples. GE1 = Gert-1, GE2 = Gert-2, GE4 = Gert-4, GW2 = Gwen-2, JE1 = Jeppe-1, DI1 = Diamant-1, RI1 = Rita-1, HE2 = Hejre-2. * Dolomite cemented samples have not been used for the average.*

Gert Member, Heno Formation

Gert Member is characterised by:

- Low – high TiO_2 and Nb contents
- High Cr content
- Low – high Zr content
- Medium – high K_2O content, low – high Rb content
- Low MgO content
- Low Na_2O and P_2O_5 contents
- Low Ni, Cu, Zn, V contents
- Low Th (and REE) contents

Multivariate analysis has shown (Appendix 3) that Gert and Ravn Members, both of the Heno Formation, can be distinguished from each other, though overlapping values do occur. Consequently, more samples (probably 15 samples) are required in order to conclude whether a sandstone unit belongs to the Ravn Member or the Gert Member. The Heno Formation is significant different to the Farsund Formation and can be distinguished from the Lola Formation, though again with some overlapping values.

Cross plots (Appendix 4), geochemical logs (Appendix 2) and average composition (Table 3) show that the Heno Formation sandstones are distinguishable from the clay-dominated Lola and Farsund Formations by a higher content of Zr and a lower Ni, Cu, Zn, V, Na_2O and P_2O_5 contents. The Gert and Ravn Members are separated by different amounts of MgO, Na_2O, P_2O_5, TiO_2, Nb, Th, REE and Cr. The Gert Member typically contains varying amounts of TiO_2, Nb, K_2O, Rb, Cr and Zr. Some samples from the Gert Member have similar contents to those in the Ravn Member and the Lola and Farsund Formations. However, peak amounts of Cr and TiO_2 are higher in the Gert Member than for the other formations or member (Figs. 15 and 16). Chromium commonly occurs in the relatively stable heavy mineral chrome spinel (Pearce et al. 1999) and in volcanic lithoclasts (Garcia et al. 2004). Chrome spinel is a stable heavy mineral, though not as stable as zircon and rutile. Titanium can be mobilised, but tends to do so only on a local scale (Weibel & Friis 2004). Ti is therefore, together with elements such as Al, Zr, Nb and Cr, typically applied for chemostratigraphical investigations (Preston et al. 1998). Nb typically occurs together with TiO_2 in rutile and other Ti-minerals; however, TiO_2 can also be present in other minerals, for example feldspars, mafic silicates and clay minerals. The relatively low Nb / TiO_2 ratio suggests that much of the titanium is present in other Ti-bearing minerals than rutile, thus less stable minerals. The Gert Member could therefore be characterised by several small episodes of material deposition from both relatively fresh source rocks and from more altered source rocks. Gert Member is deposited during transgression in a back-barrier and marine shoreface environment (Johannessen et al. 1996; Johannessen 2003). During transgression relatively unaltered or less altered material might occasionally have been brought into the system possibly during storm episodes.

A high chrome spinel content has been reported from Early Carboniferous sandstones in the Danish North Sea sector (Spathopoulos et al. 2000) and Late Carboniferous sandstones from the southern North Sea (Morton et al. 2001) and both are interpreted as having a source on the Ringkøbing–Fyn High or recycled sediments with their original source form this high. Another explanation of the occasional higher Cr and Ti contents in the Gert Member compared to the Ravn Member could be another local source supplying recycled Carboniferous material originally originating from the Ringkøbing–Fyn High. Pre-Jurassic rocks form the Hejre-2 well and Permian rocks from the Diamant-1 and Gert-1 wells plot with an even lower Nb / TiO_2 ratio than that of the Gert Member. This could indicate that source material from areas where these sediments where exposed might have contributed with material to the Gert Member.

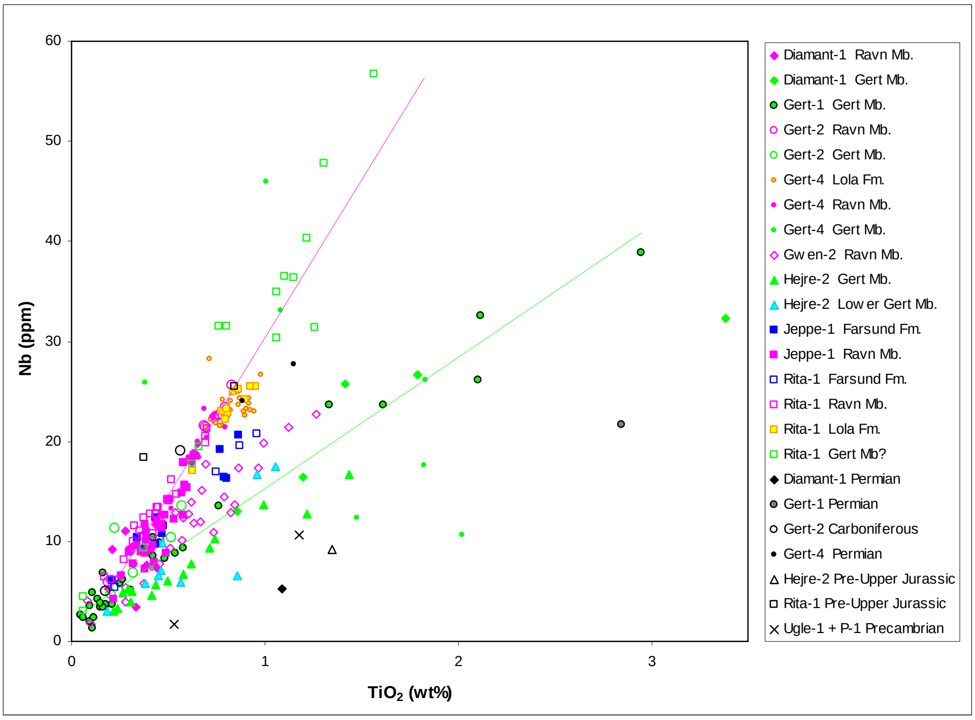

Figure 15. *Graph showing positive correlation between Nb (ppm) and TiO_2 (wt%) in core samples with different ratios for the Gert and Ravn Members (Gert Member from the Rita-1 well, though, being different).*

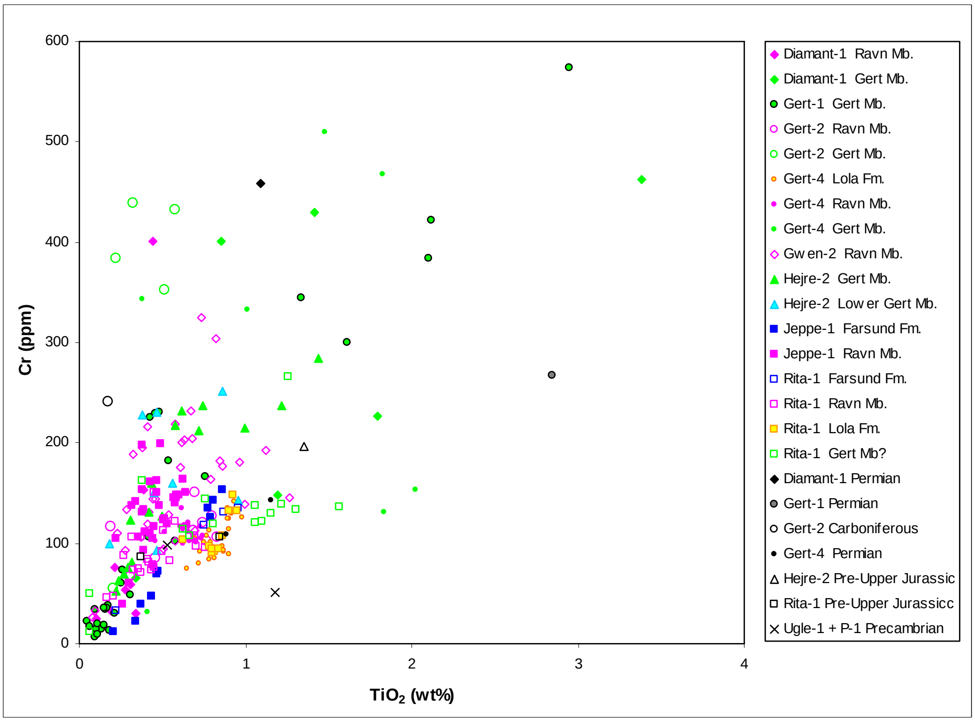

Figure 16. *Graph showing generally the highest amounts of TiO_2 (wt%) and Cr (ppm) in the Gert Member core samples and lower than those of the Ravn Member (the Ravn Member in the Gwen-2 well seems to be an exception).*

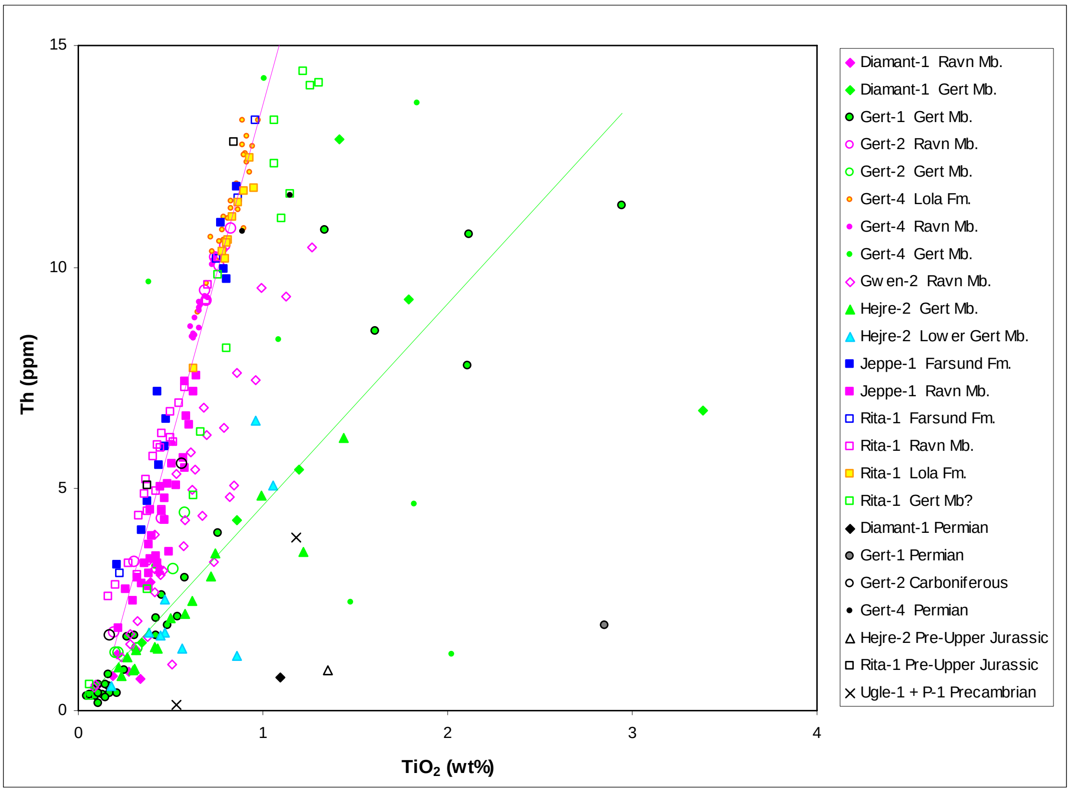

Figure 17. *Graph showing positive correlations between Th (ppm) and TiO_2 (wt%) in core samples with different ratios for the Gert and Ravn Members (the Gert Member from the Rita-1 well seems to be an exception).*

Multivariate analysis (Appendix 3) shows that the Gert Member and the Lower Gert Member in the Hejre-2 well fits almost equally well with the Gert and Ravn Members, and that some of the same samples are outliers in both models. The geochemical logs for all Gert Members, including the Hejre-2 and Rita-1 wells (Appendix 2), are characterised by very high variations in Cr, Zr and TiO_2 contents. So, from this point of view, the Gert Member and the Lower Gert Member in Hejre-2 appear to be similar to the Gert Members in other wells.

The Gert Member in most wells seems to have a lower Th / TiO_2 ratio (and also lower REE / TiO_2 ratio) than the Ravn Member (Fig. 17). Th typically occurs in heavy minerals (Friis et al. 2007) such as monazite and will therefore generally behave similar to the REE. The possible Gert Member in the Rita-1 well and some samples in the Gert-4 well (and possibly the Gert-2 well) have a higher ratio, similar to that of the Ravn Member. The possible Gert Member in Rita-1 also has a more straightforward correlation between Cr, Zr and TiO_2 than the other Gert Member samples, which has a greater scatter. The Rita-1 well could be dominated by a local source, which occasionally delivered fluxes that even reached the area of the Gert-4 and Gert-2 wells. The source might be similar to the monazite-rich source on the Mid North Sea High described by Spatholoupos et al. (2000). Multivariate analysis has shown that even though the possible Gert Member in Rita-1 seems different to the Gert Member in other wells its variation is within the model of the Gert Member even though this was only based on the three Gert wells.

Ravn Member, Heno Formation

Ravn Member is characterised by:

- Low – high Zr content
- Low Cr content
- Low TiO_2 and Nb contents
- Medium K_2O and Rb contents (except Diamant-1)
- Medium MgO content
- Low – medium Na_2O and P_2O_5 contents
- Low Ni, Cu, Zn, V contents
- Low – medium Th (and REE) contents

The Gert and Ravn Members can be separated by multivariate analysis (Appendix 3), though several samples (probably 15 samples) are needed to conclude whether a sandstone unit belongs to Ravn Member or Gert Member, as overlapping values occur.

The zircon content seems to be as high for the Ravn Member as for the Gert Member. However, the content of titanium and chromium is much lower in the Ravn Member compared to the Gert Member (Fig. 16, Appendix 2, Table 3). The Nb / TiO_2 ratio is relatively high, which might indicate that titanium is primarily located in rutile and Fe-Ti oxides (Fig. 15). The Ravn Member is also characterised by abundant oversized quartz and quartzite clasts. Combined, this shows a dominance of very stable minerals suggesting that the material had its origin in an intensively altered source rock. The alteration could have taken place on the surrounding highs (Mandal High, Mid North Sea High), but it may also have continued under temporal deposition during its transportation to the final place of deposition.

Another possible explanation for the differences between the Gert and Ravn Members could be differing main source areas as already mentioned under the discussion of the Gert Member. The Ravn Member typically has rather high Th / TiO_2 and Nb / TiO_2 ratios and higher contents of Th, La and other REE than the Gert Member (Figs. 15, 17 and Table 3). Spatholoupos et al. (2000) describes a monazite-rich source on the Mid North Sea High. Such a source could have become more prominent during deposition of the Ravn Member and may have supplied more regionally to the basin, whereas during deposition of the Gert Member its influence may have been more local.

The Ravn Member is differentiated from the Gert Member by higher amounts of MgO, Na_2O and P_2O_5 (Figs. 18 and 19), though with Diamant-1 as the exception. P_2O_5 may be pesent in detrital heavy minerals, as apatite or monazite, but couldalso be part of authigenic marine phosphate minerals or even in organic matter.

During the lower part of deposition of the Lola Formation the amount of MgO increases in several wells and continues on this level throughout deposition of the Ravn Member (Appendix 2). The Gert Member has the lowest magnesium content. The Ravn Member seems to de divided into two groups with different MgO / Al_2O_3 ratios (Fig. 18), one following the trend of the Lola Formation (Ravn Member in Rita-1, Gert-4 and partly Gert-2) and another closer to the Gert Member (Jeppe-1, Diamant-1, Gwen-2 and partly Gert-2). The division of Ravn Member into two groups is possibly related to depositional environment and grain-size differences, as the Gwen-2 and Jeppe-1 wells are dominated by oversized clasts. Magnesium occurs in the sediments as clays, glauconite and heavy minerals, some of which are stable and others very unstable. Glauconite or minerals resembling chlorite are observed quite frequently in the sediments. Liberation of magnesium from unstable minerals has probably occurred during diagenesis; rare dolomite precipitation is evidence for this. Chloritisation of glauconite is another possible diagenetic alteration that could be expected. To what degree the mobilisation of Mg is local (within a member) or regional is difficult to know and can only be evaluated by diagenetic investigation. The increased Mg content could reflect more magnesium brought into the depositional system, i.e. more Mg-rich material reached the final area of deposition or the depositional environment favoured incorporation of Mg in glauconite and chlorite, or a combination of both.

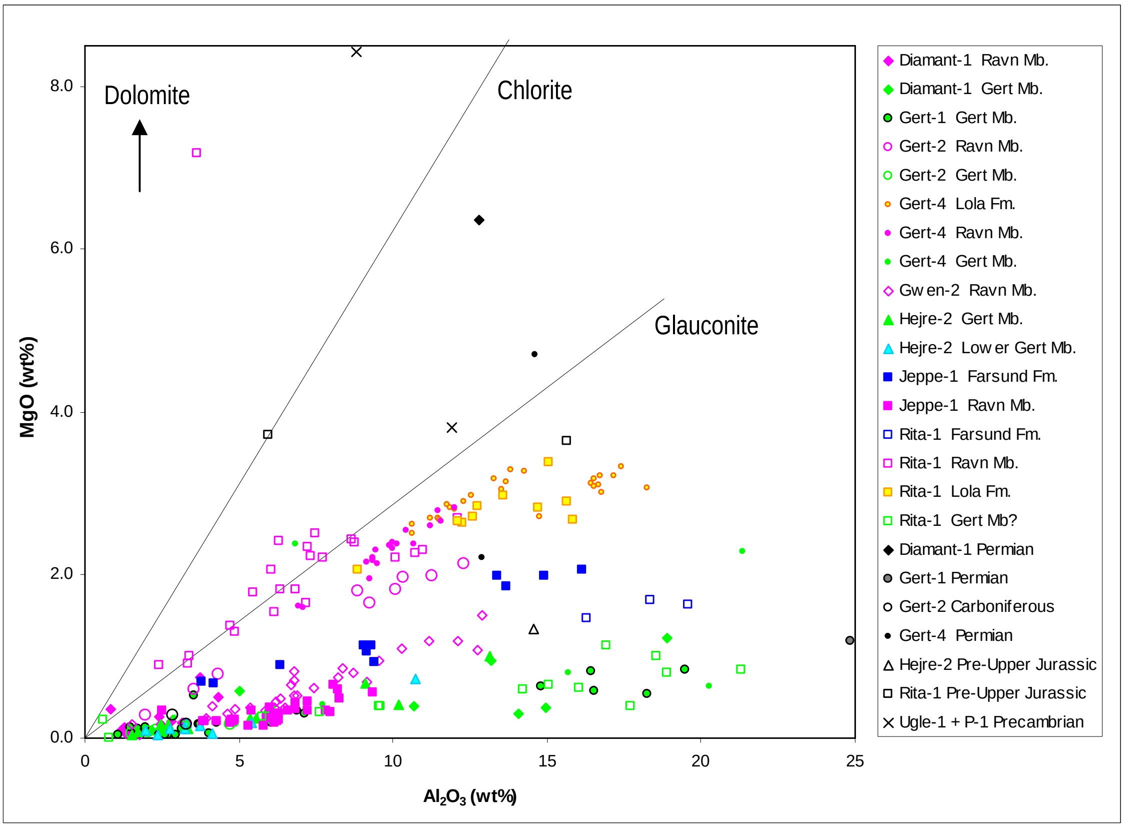

Figure 18. *Graph showing positive correlations between MgO (wt%) and Al_2O_3 (wt%) in core samples. Note the subdivision of the Ravn Member into two groups with different ratios. The Ravn Member in the Jeppe-1, Diamant-1 and Gwen-2 wells have a low ratio MgO / Al_2O_3. The sediment in these wells was deposited in a shoreface environment. The Ravn Member in the Rita-1, Gert-2 and Gert-4 wells has a higher MgO / Al_2O_3 ratio. The sediments in these wells were deposited farther out in the middle to upper shoreface which explains their stronger affinity to the Lola Formation. Consequently the subdivision of Ravn Member seems to be related to to depositional environment. Chlorite and glauconite chemical composition are examples and may vary more than indicated by the lines in the graph.*

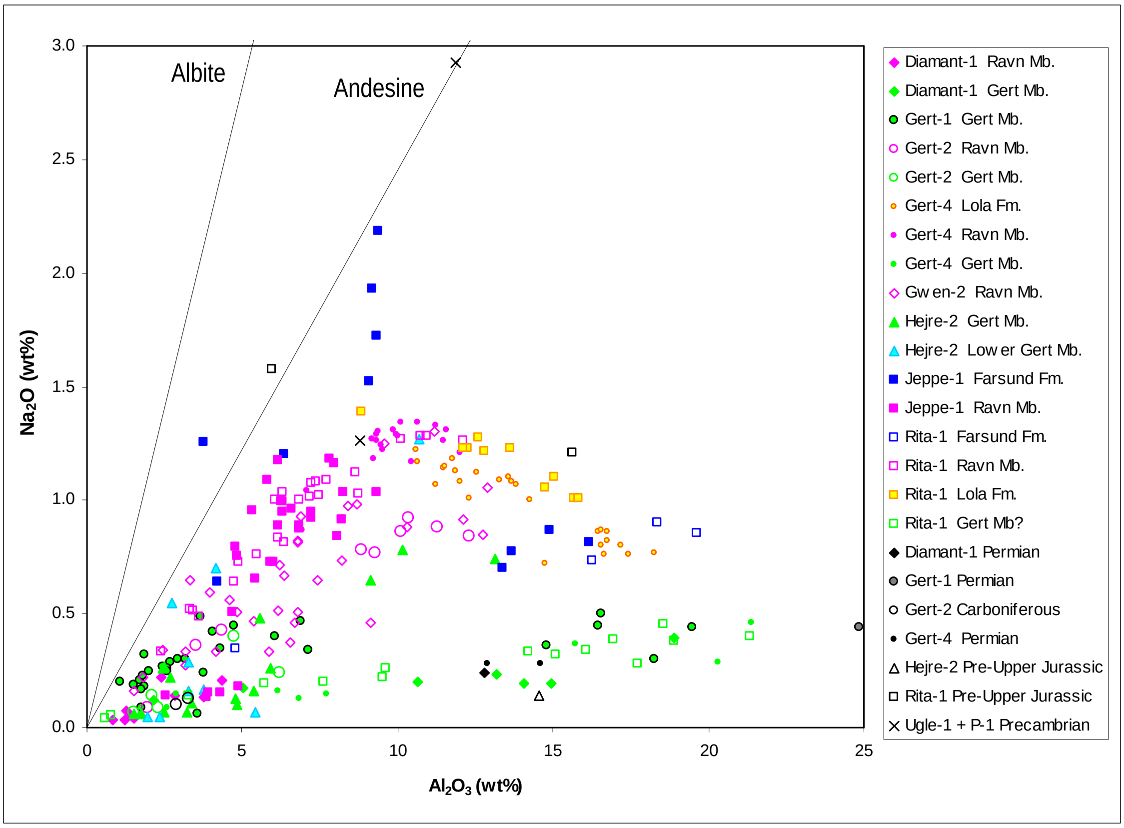

Figure 19. *Graph showing positive correlations between Na_2O (wt%) and Al_2O_3 (wt%) in core samples of the Heno Formation. But the graph shows more than that. The Ravn Member generally has higher sodium content than Gert Member and the Lola Formation shows a negative correlation between Na_2O and Al_2O_3. The negative correlation of the Lola Formation suggests that sodium is located in other minerals than for the Heno Formation, possibly clay minerals.*

The most obvious origins of sodium are halite, clay minerals and plaigoclase. Halite seems less likely as sodium generally occurs in similar amounts in core samples and in washed and dried cuttings samples (Appendix 2). Plagioclase might occur in increased amounts together with oversized quartz clasts in the Ravn Member, but sodium maximum also occurs in the Lola Formation with no oversized clasts (Fig. 19; Appendix 2). Therefore sodium might reflect a combination of clay minerals and plagioclase. The Ravn Member was deposited in a marine shoreface environment, whereas the Gert Member was deposited in a back-barrier and marine shoreface environment (Johannessen et al., 1996, Johannessen, 2003). Consequently, the salinity of the pore water would have been higher in the environment of the Ravn Member than in the more brackish environment of the Gert Member. Clay minerals deposited in a highly saline environment would be surrounded by highly saline pore fluids, and the high cation exchange capacity of clays could possibly lead to clays being richer in Na_2O and MgO in a marine shoreface deposit than in a brackish deposit. Abundant bioturbation by various borrowing organisms show that perfect conditions for formation of glauconite were present. Therefore glauconite may have formed *in situ* and may have incorporated various ions depending on their availability. The presence of MgO might eventually be defined by a combination of depositional environment and source area.

Variation in the MgO content in the Ravn Member and the Lola Formation seem to have a strong relation to the depositional environment and may be used for tracing and timing the transgression.

Lola Formation

The Lola Formation is characterised by:

- Medium Zr content
- Low Cr content
- Medium TiO_2 and Nb contents
- High K_2O content, medium – high Rb content
- Highest MgO content
- High Na_2O content and medium P_2O_5 content
- Medium Ni, Cu, Zn, V contents
- High Th (and REE) contents

Multivariate analysis (Appendix 3) shows that the Lola Formation is significantly different from the Farsund Formation and Gert Member. The Lola Formation shows a clear difference to the Ravn Member, although a few samples close to the boundary between the Ravn Member and the Lola Formation are undistinguishable.

Cross plots (Appendix 4) and geochemical logs (Appendix 2) show that the offshore claystones of the Lola and Farsund Formations are distinguished from the Heno Formation sandstones by a higher content of Ni, Cu, Zn, V, Na_2O and P_2O_5 and a lower Zr content. The Lola Formation contains higher amounts of Zr, MgO, K_2O and Rb; and smaller amounts of V, U and P_2O_5 than the Farsund Formation.

During the early part of the deposition of Lola Formation the amount of MgO increases in several wells and the MgO content continues on this level trough deposition of Ravn Member (Appendix 2). This is very clear from the geochemical logs of Gert-4 and Rita-1 (Appendix 2). The core samples especially show that the amount of magnesium (and aluminium) is much higher in the Lola Formation than in other formations. The possible reason for the higher magnesium content has been discussed previously under the Ravn Member.

The Lola Formation commonly occurs with different ratios than in the Gert and Ravn Members (for example Figs. 19 and 20, Appendix 4) indicating that major mineralogical difference are present. Since the Lola Formation is an offshore claystone it is possibly much more dominated by clay minerals, whereas the sandstone units probably contain less clays and relatively more feldspar, mica and heavy minerals.

Zr shows a fine positive correlation with SiO_2 in the Lola and Farsund Formations; this is evident from both core samples and cuttings samples (Appendix 4). As these formations consist of claystones a small increase in the amount of sand and silt fraction would lead to an increase in both SiO_2 and Zr. For the sand-dominated Gert and Ravn Members the picture is a little more complicated. In some wells the Zr content increase with the SiO_2 content, but in others there seems to be a negative correlation (Appendix 4). The negative correlation is probably partly due to sorting effects, as the negative trend is particular pronounced in the Ravn Member in the

Gwen-2, Rita-1 and Jeppe-1 wells, which generally contain rather coarse-grained quartz and quartzite clasts, as well as the Gert-1 and Gert-2 wells.

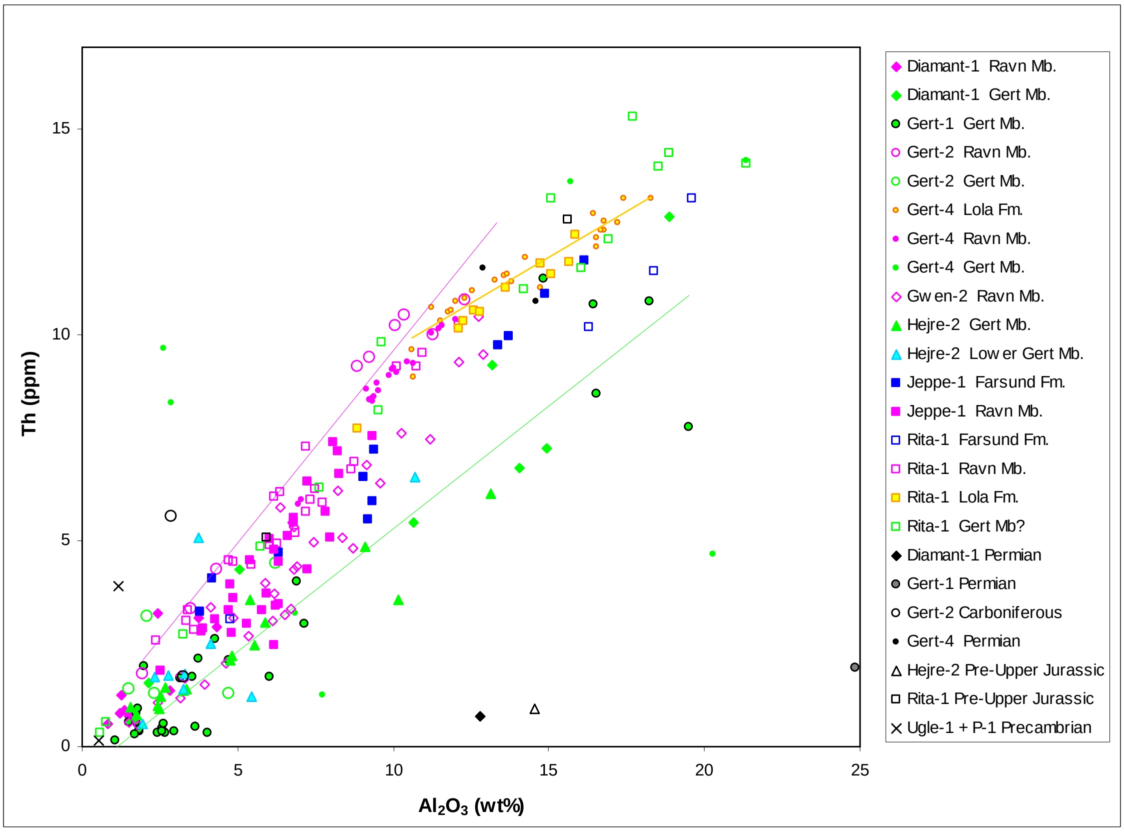

Figure 20. *Graph showing positive correlations between Th (ppm) and Al_2O_3 (wt%) in core samples of the Heno Formation. The Ravn Member generally has a higher Th content than the Gert Member. The Lola Formation has another ratio than that of the Heno Formation, suggesting mineralogical differences.*

Farsund Formation

Farsund Formation is characterised by:

- Low Zr content
- Low Cr content
- Low - medium TiO_2 content, low Nb content
- Medium K_2O and Rb contents
- Medium – high MgO content
- High Na_2O and P_2O_5 contents
- Medium Ni, Cu, Zn contents
- High V and U contents
- High Th (and REE) contents

Multivariate analysis shows that the Farsund Formation is significantly different to the Lola Formation, Gert and Ravn Members (Appendix 3). Cross plots (Appendix 4), geochemical logs (Appendix 2) and average composition (Table 3) show that the Lola and Farsund Formations are distinguished from the Heno Formation sandstones by higher contents of Ni, Cu, Zn, V, Na_2O and P_2O_5 and lower Zr contents. The Farsund Formation contains higher amounts of V and U, and smaller amounts of Zr, MgO, K_2O and Rb than the Lola Formation.

The Farsund Formation is characterised by high U, V and P_2O_5 contents (Fig. 21 and 22). Uranium may be related to organic matter and P_2O_5 might be present as marine authigenic phosphate minerals. Vanadium may be present in detrital heavy minerals (Friis et al. 2007; Weibel & Friis 2004). During oxidising conditions vanadium and uranium are likely to be mobilised, whereas during reducing conditions they would be stable (Weibel & Friis 2004). Offshore claystones as the Lola and Farsund Formations contain abundant organic matter. The Heno Formation contains several coal fragments, besides abundant pyrite and siderite. All this is evidence for reducing conditions, which probably was present immediately after deposition and continued during diagenesis.

In the Farsund Formation both cuttings and core samples show that the uranium content is not influenced by the zirconium or REE contents at all (Appendix 4), therefore the U is most likely related to the organic matter. Core samples from the more sand-dominated Heno Formation show that the uranium content generally increases with the zirconium content (Appendix 4), indicating that heavy minerals contribute with much of the uranium present in the sands. The Lola Formation shows a negative correlation between uranium and zirconium, which is a response to decreasing zirconium with increasing aluminium. This probably reflects less zircon grains in the most clay-rich part of the Lola Formation where uranium is related to organic matter instead of heavy minerals.

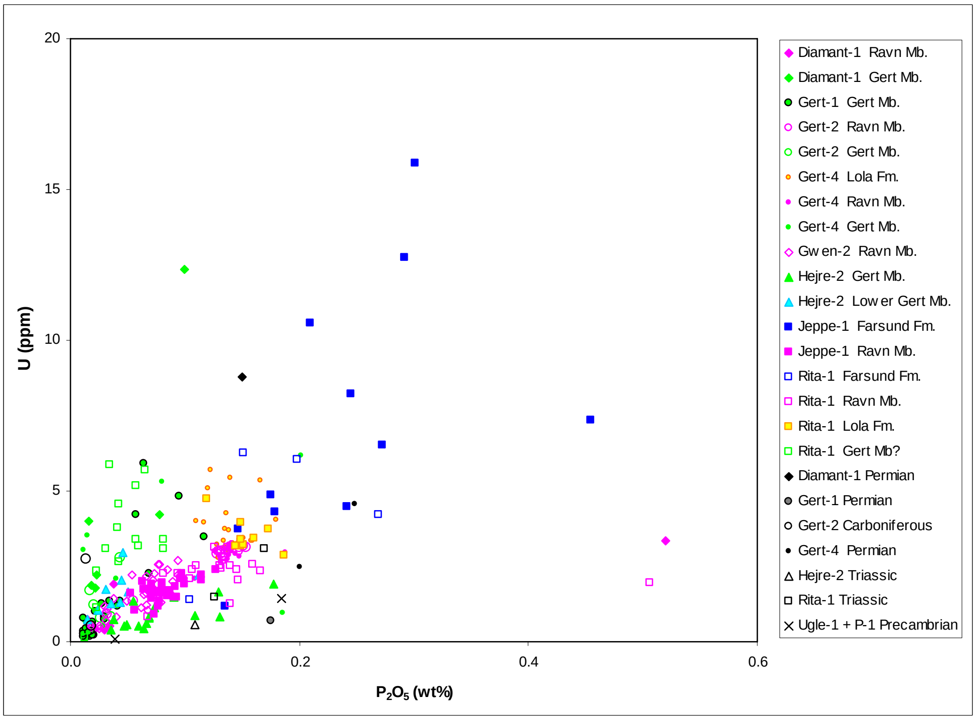

Figure 21. *Graph showing large variations in the U (ppm) and P_2O_5 (wt%) content in core samples. The Farsund Formation has generally the largest content of both U and P_2O_5 compared with the Lola and Heno Formations.*

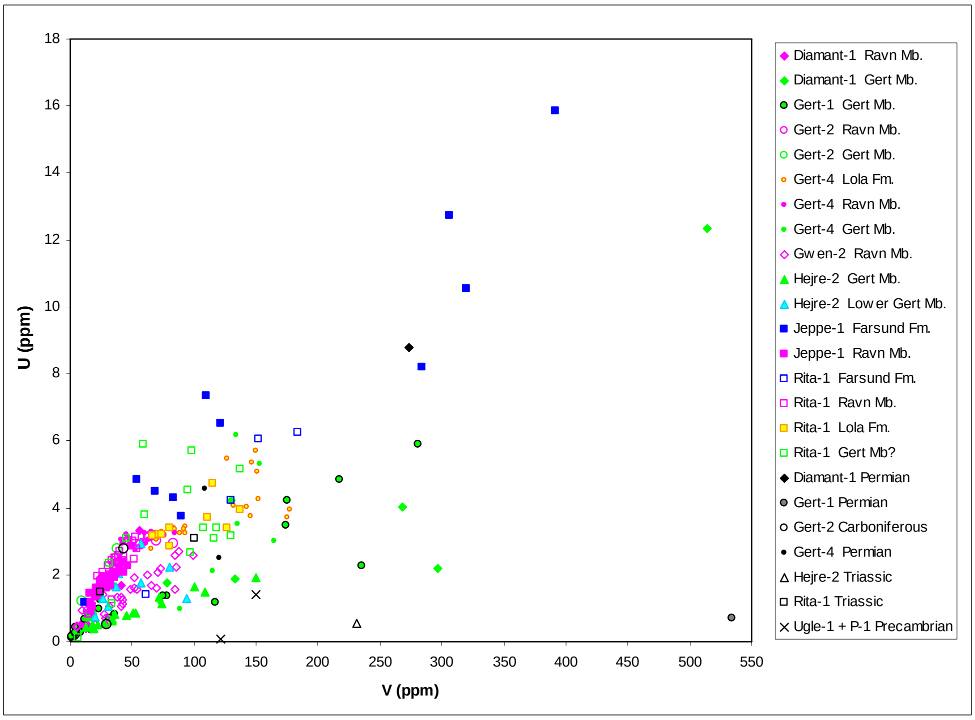

Figure 22. *Graph showing general positive correlation between U (ppm) and V (ppm) in core samples. The Farsund Formation has generally the highest content of both U and V. The Gert Member generally has a lower U / V ratio than the Ravn Member, with the Gert Member from the Rita-1 well and some Gert-4 well samples as exceptions.*

Geochemical variation between wells

Some geochemical variations show stronger affinity to the site of the well (i.e. location in the basin during deposition of the sediments) than to its appropriate member or formation. These geochemical variations are typically related to local source areas.

One of the most distinctive features is the variation in K_2O / Al_2O_3 ratios between wells and independently of member and formation (Fig. 23). The Gert Member in the Hejre-2 well has the highest K_2O / Al_2O_3 ratio with the pre-Jurassic volcanoclastic conglomerate as an end point. The Ravn Member in the Jeppe-1 well also has a rather high K_2O / Al_2O_3 ratio. The ratio between K_2O and Al_2O_3 can indicate whether clays or feldspar are the main contributing factor. The K_2O / Al_2O_3 ratios in the Hejre-2 and Jeppe-1 wells indicate that K-feldspar must be an important mineral component in the Hejre-2 and Jeppe-1 wells. K-feldspar must have been supplied by a local source close to Hejre-2. The source was most likely an alkaline volcanic source, which also supplied material to the underlying volcanoclastic conglomerate in the Hejre-2 well. Furnes et al. (1982) have described a Lower – Middle Jurassic alkaline volcanic event in the Egersund sub-Basin in the Norwegian North Sea Sector. Similar volcanic events may have occurred closer to the Hejre-2 well. During this period of regional uplift in the North Sea related to the doming of the central North Sea and the Ringkøbing–Fyn High (Andsbjerg et al. 2001) which lead to volcanic event several places in the North Sea basin.

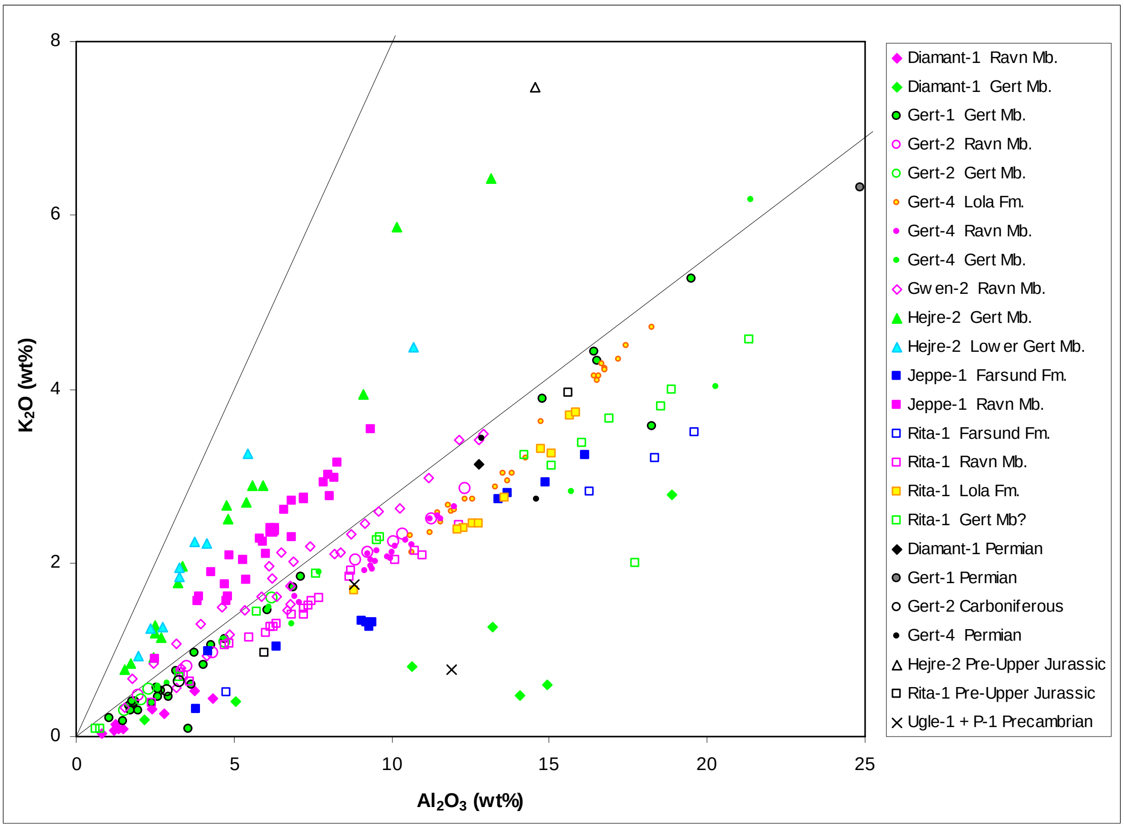

Figure 23. *Graph showing positive correlations between K_2O (wt%) and Al_2O_3 (wt%) in core samples of the Heno Formation. The Gert Member in the Hejre-2 well, followed by the Ravn Member in the Jeppe-1 well, has the highest ratios, indicating that K-feldspar is an important mineral in these sediments. The increased K_2O content is found locally close to the Hejre-2 area, where a volcanoclastic conglomerate is found underlying the Gert Member.*

As mentioned earlier during discussion of the Gert Member, the possible Gert Member in the Rita-1 well is distinguishable from the other Gert Members by having a more straightforward correlation between Cr, Zr and TiO_2 and a generally higher content of Th and REE. The Rita-1 well could be more influenced by a local source, which occasionally delivered fluxes that even reached as far north-east as the site of the Gert-4 and Gert-2 wells. The source might be similar to the monazite-rich source on the Mid North Sea High described by Spatholoupos et al. (2000).

Zircon geochronology

The ^{238}U / ^{206}Pb and ^{235}U / ^{207}Pb systems are two geochronometers that give concordant dates if the mineral dated has remained closed to U and Pb after formation (Fonneland et al. 2004). When zircon grains with such concordant ages are plotted graphically they define a curve, which is termed the concordia. If the zircon grains have experienced lead loss, the two U / Pb ages will not plot on the concordia, consequently they are discordant. Discordant zircon grains are defined as zircon with difference between the two U / Pb age estimates as: 0.9 < (^{238}U / ^{206}Pb) / (^{235}U / ^{207}Pb) > 1.1 (the concordance criteria is 90-110 %). When the ^{207}Pb / ^{206}Pb ratio for each zircon is plotted against the ^{238}U / ^{206}Pb ratio in principal all zircon data will lie on or close to a concordia (Appendix 5). Discordant zircon data may have several origins. Zircons may have experienced ancient lead loss during metamorphism or recent lead loss during diagenetic influences. Discordant zircons, though, may also occur due to measurement difficulties or errors (i.e. poorly defined background). Small zircon grains lead to several difficulties during preparation and measurement. Picking and mounting is extremely difficult and some small grains may even jump out of the mould during laser ablation. Common lead contamination of zircons may occur on the surface and along cracks in the grains. In order to avoid common lead on the surface the first part of the measurement is typically disregarded. For small grains this can be difficult as some are penetrated to obtain a stable measurement. Younger rims on zircon grains are also a common phenomenon. This problem can easily be dealt with in large zircons, where measurements from the centre are chosen, whereas in small grains it is more difficult. In all, results on small zircon grains lead to larger standard deviations on age estimates than larger grains and more discordant results. The sedimentary samples from the Heno and the Lola Formation are characterised by small zircon grains.

Zircon is chemically and physically stable and not liable to destruction during the sedimentary cycle unless it has become metamict through radiation damage to its crystal structure (Morton et al. 2001). Zircons form predominantly in felsic-intermediate igneous rocks (such as granite) and high-grade (granulite facies) metamorphic rocks, and thus records the ages of major crust-forming events (Morton et al. 2001). The ability to date single zircon gains has revolutionised provenance studies since these methods allow relatively rapid acquisition of data that constrain the geological history of sediment source regions (Morton et al. 2005). LA-ICP-MS is particularly promising as it combines low cost and extraordinary speed with suitable accuracy and precision (Frei et al. 2006).

The zircon age distribution in a sediment reflects the age distribution of the source rocks where their relative abundance is a function of how common zircon is in each source rock, the abundance of each source rock in the source area and fractionation from transport. Transport and diagenesis have the largest impact on metamict zircons and on old zircon which have been exposed to radiation damage (Hallsworth et al. 2000). All these factors influence the zircon age distribution in a sediment, which cannot simply be inverted to represent the relative source contributions (Scherstein *in press*). Nevertheless, the likelihood of identifying an age component in a sample is a function of its relative presence in the population and the size of the sample (i.e. number of dated zircon grains). The more zircon grains that are analysed in any given sample, the more likely is it that all the age components present are identified (Fig. 24; Scherstein *in press*). This relationship can be described as

$$P = (1-f)^n \qquad (1)$$

where P is the probability for finding a single component in the population, f is the relative abundance of any given component in the population and n is the number of dated grains (Dodson et al. 1988; Scherstein *in press*). However, 117 grains have to be dated for a 95% confidence level that all components present are identified in a worst-case population (Fig. 24; Scherstein *in press*). Generally, we aim for 100 grains or more when possible, but a number of samples yielded considerably fewer grains, or even no grains in three cases (GE1-492140, UG1-305275, P1-349168).

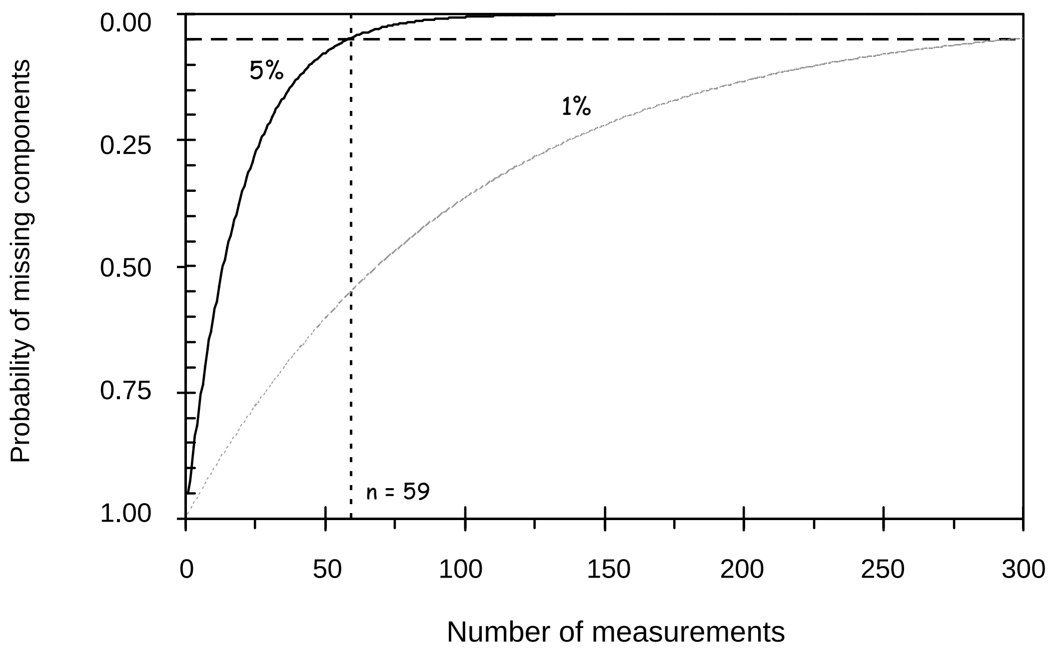

Figure 24. *The likelihood of missing a component present as a function of the number of dated grains and the frequency of the component in a detrital zircon sample (equation 1). For a 95% confidence (P = 0.05) of identifying all components in a sample (horizontal dashed line), a 5% component abundance requires at least 59 grains to be dated, while a 1% component abundance requires 298 grains to be dated. After Scherstein (in press).*

The zircon age distributions obtained in the present study are shown for all samples in Appendix 5 and some examples are shown in Fig. 25 and 26. Unfortunately no zircon grains were found in Precambrian samples from P-1 and from Ugle-1. Combined relative probability diagrams and histograms showing zircon age distribution are based on ^{207}Pb / ^{206}Pb ages when the age is larger than 600 Ma, but on ^{206}Pb / ^{238}U ages when less than 600 Ma, due to the low accumulation of ^{207}Pb in younger zircons.

Zircon in samples form the Ravn Member, Gert Member and Lola Formation show the same overall pattern with a strong Proterozoic population (1700–900 Ma), a Caledonian aged population (500–400 Ma), a possible Variscan aged population (350–310 Ma) and a small indication of an Archaean component (2900–2800 Ma, 2700–2600 Ma). The wide range of zircon ages reflects a combination of several sources probably recycled several times and mixed by ocean floor currents (Fig. 25 and 26).

Upper Cretaceous sandstones from the Norwegian Sea contain Archaean zircon grains which have been related to an East Greenlandic source (Fonneland et al. 2004). The presence of small numbers of Archaean zircon in Carboniferous sediments in the Pennine Basin has been interpreted as sediment being partly sourced from ancient rocks, such as those of Greenland or from the Appalachian–Labrador–Newfoundland area (Hallsworth et al. 2000). Archaean zircon found in the Late Jurassic Bjorøy Formation in south-western Norway have been interpreted as far-transported and re-deposited detritus from the Svecofennian (1800–2000 Ma) and Archaean domains of the Baltic Shield (Knudsen & Fossen 2001).Therefore the Archaean zircon might have had its original source in either East Greenland or the Baltic Shield and may have experienced several events of sedimentary recyling.

The Proterozoic group of zircon grains has ages between 900 and 1700 Ma, which coincides with the Sveconorwegian orogenesis. The southern part of the Fennoscandian Shield has bedrock ages of 1660–1480 Ma, 1400–1130 Ma, 1000–900 Ma (Stephens et al., 1994; Bingen et al., 2005). The Fennoscandian Shield has also been interpreted as the most likely source of zircon with these ages (Hallsworth et al. 2000; Knudsen & Fossen 2001). The Norwegian-derived detrital zircon grains show a narrow pattern with age maxima between 1000 and 1600 Ma reflecting the Swegonorwegian orogenesis (Middle Proterozoic) and the Early Proterozoic Gothian orogensis (Fonneland et al. 2004). The Upper Triassic continental red-bed deposits (Lunde Formation) in the North Sea Rift areas have a zircon age-distribution with significant peaks at 390–440 Ma (Caledonian) and a higher peak at 870–1100 Ma (Sveconorwegian) and no zircon ages between 1750–2730 Ma (Knudsen 2001). The Lunde Formation is interpreted as a sequence directly derived from the south-west margin of Norway, or alternatively re-deposited post- Middle-Devonian sediments (Knudsen 2000). The Statfjord Formation of the Brent Oilfield and of the Gullfaks Oilfield is characterised by Archaean (2700–2850 Ma) and Caledonian (380–460 Ma) zircon ages, which have their source in the East Shetland Platform where uplifted Proterozoic metasediments were intruded by Caledonian granites or represents recycled Triassic sediments from this terrane (Morton et al. 1996; Knudsen 2001). The dominance of Proterozoic zircon ages in the Heno Formation indicates that they had their source in the Fennoscandian Shield, and that this was the major source area.

The Caledonian fold belt extends from Ireland and Scotland north-east ward through Scandinavia. The Caledonian fold belt forms the major part of Middle and Northern Norway, but is less dominant in Southern Norway (Bingen et al. 2005). An External Caledonian Belt can be traced from the eastern North Sea to Poland (Katzung 2001). In the Danish North Sea sector micro-granite was encountered in Per-1, which is situated 10 km north-west of Ugle-1 (Katzung 2001). Age determinations (^{40}Ar / ^{39}Ar and K / Ar) point to a 2400 Ma age with a strong Caledonian overprint at about 435 Ma (Katzung 2001). A similar low-grade overprint of, respectively, 436 Ma and 415 Ma can be found in laminated schists in P-1 and muscovite-biotite augen gneiss in Q-1, located 40 km south-south-east of P-1 (Katzung 2001).The Caledonian fold belt in Norway, Scotland or possibly Mid North Sea High and Rinkøbing–Fyn High could therefore have supplied zircons of Caledonian age. Zircons with Caledonian ages in the Heno Formation could possibly have their origin in the Fennoscandian Shield.

The occurrence of 600 Ma zircon ages cannot directly be related to a source area. The British Isles, however, have records of granitic magnetism at 870 Ma, 740 Ma and 600 Ma (Rogers et al. 1998; Rogers et al. 2001). From this area zircon grains of Caledonian ages could also be expected. The westernmost well, Gert-4, has the relatively highest content of Caledonian ages and 600 Ma zircon grains (Fig. 25), and both peaks decrease towards the east. This could be an indication of a western source for both the Caledonian and 600 Ma zircon ages. Possibly repeated recycling of sediments could have brought this material to the depositional area of the Feda Graben.

Hallsworth et al. (2000) found a zircon age spectrum with Variscan age (323–357 Ma) in Carboniferous sediments in the Pennine Basin and interpreted these zircon ages as inherited from the Variscan belt. The European Variscan Belt includes south-western Ireland, southern British Isles, large parts of Germany and several other European countries of greater distance to the North Sea area. In the Danish North Sea area it is also difficult to identify a possible Variscan source, and though sediment transport from the south (even though including several episodes of recycling the sediments) seems a bit doubtful it might be the only possible explanation, especially as the Variscan influence seems more pronounced in the southernmost placed well – Diamant-1 (Fig. 26).

Applying the intensities in the frequency diagrams is difficult, as the likelihood of finding all ages present is depending on the number of zircon grains analysed. Therefore the dominance of zircon with Proterozoic ages (1700–900 Ma) and lack of concordant zircons with Archaean and Caledonian age in the pre-Jurasssic volcanoclastic conglomerate in the Hejre-2 well ought to be investigated more in order to find out if there is a source difference (possibly a strong influence from the Swedish part of the Fennoscandian) or merely too few grain analysed. In a similar way the Permian sample from the Gert-4 well ought to be investigated more in order to find out if the presence of Proterozoic, Caledonian and Archaean zircon ages and lack of Variscan ages is evidence of a major influence from the Norwegian part of the Fennoscandian or again is due to a non-representative sample (too few grains).

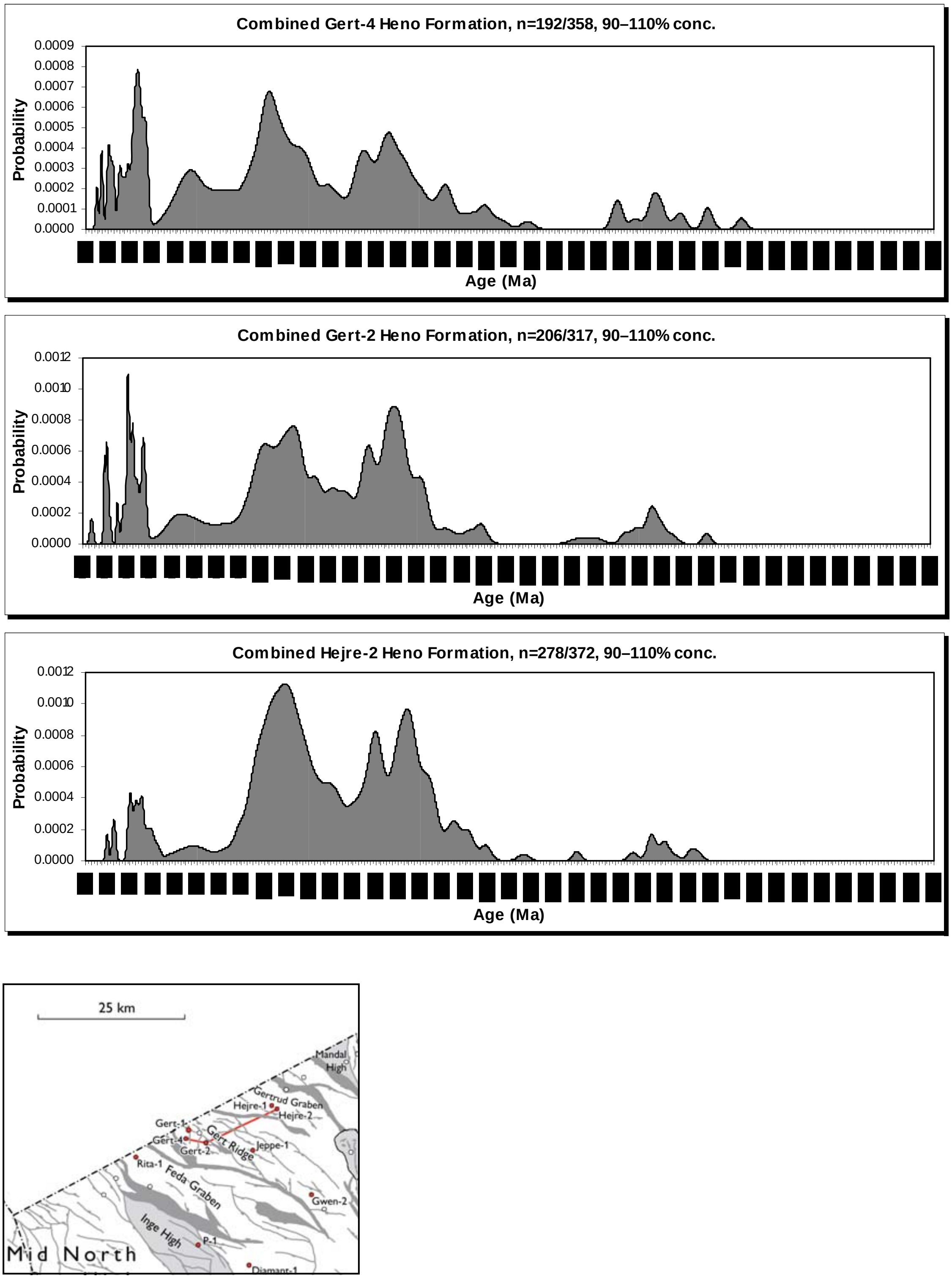

Figure 25. *Combined zircon age data for all samples from the Heno Formation in the Gert-4, Gert-2 and Hejre-2 well, respectively, plotted in relative probability diagrams. Note the simultaneously decrease in the Caledonian and 600–700 Ma zircon ages as the location of the wells becomes more eastern. Zircon ages are based on ^{207}Pb / ^{206}Pb ages when older than 600 Ma, otherwise on ^{206}Pb / ^{238}U ages.*

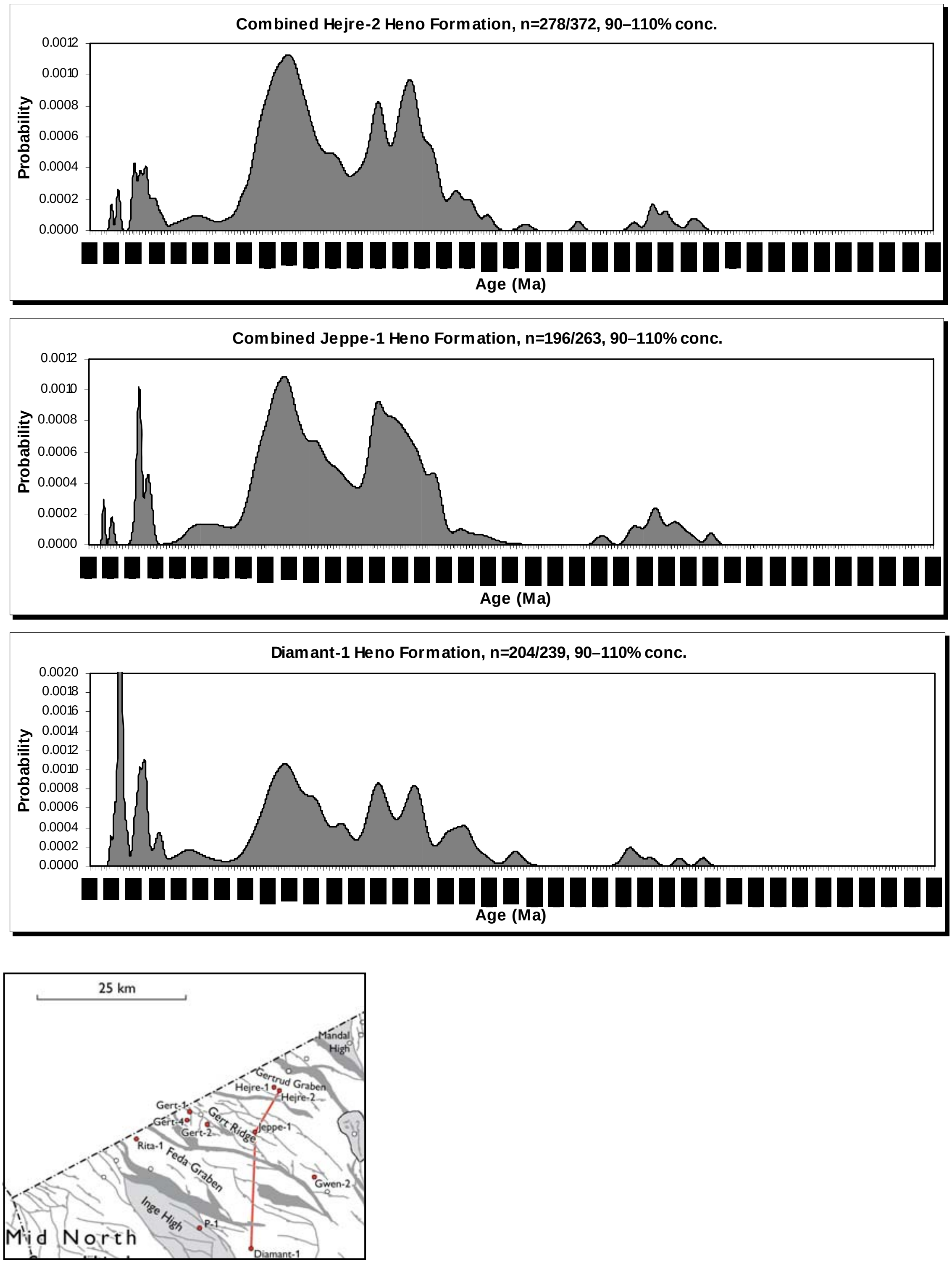

Figure 26. *Combined zircon ages data for all samples from the Heno Formation in the Hejre-2, Jeppe-1 and Diamant-1 wells, respectively, plotted in relative probability diagrams. Note the increase in the Variscan zircon ages as the location of the wells becomes more southern. Zircon ages are based on ^{207}Pb / ^{206}Pb ages when older than 600 Ma, otherwise on ^{206}Pb / ^{238}U ages.*

Garnet geochemistry

Garnet has proved to be very useful for provenance studies as garnets have a mineralogical and chemical diversity which reflects different source rocks. Garnets are abundant in sediments due to a relatively high physical and chemical stability. However, garnets begin dissolution at burial depth below 3600 m (Morton et al. 1999). The burial depth of the investigated samples varies from 3800 m in the Diamant-1 well to 5400 m in the Hejre-2 well. Consequently, only small amounts of garnet could be expected in these samples. By applying the CCSEM method to heavy mineral concentrates few garnets where detected and chemically analysed (Appendix 6). Besides garnets being rare in the investigated samples, authigenic heavy minerals (pyrite) also disturbed the CCSEM analyses as they occurred in such massive amounts that even 2000 analysed grains where insufficient. Therefore application of thin section for CCSEM analysis was tested additional to the traditionally heavy mineral concentrate. Preliminary investigations of garnet chemistry in large thin section (Appendix 6) showed that this might be something worth pursuing. As partly dissolved garnet may not survive the treatment in the laboratory in order to concentrate the heavy minerals fraction. These partly altered garnets may on the other hand be identified in thin sections by the use of the CCSEM method.

Conclusions

Geochemical investigations cannot stand alone, but are a very useful tool for achieving more information about the sediments. So far the evaluation of the geochemical data obtained on the Upper Jurassic sediments in the northern part of the Danish North Sea area has lead to the following results:

Geochemical differentiation of the formations:

- The Farsund Formation is significantly different from the Lola Formation and the Heno Formation.

- The Lola Formation can be differentiated from the Gert and Ravn Members, though a few overlapping values do occur at the border between the Lola Formation and the Ravn Member in the most distal wells.

- The Gert and Ravn Members can be separated geochemically, though overlapping values do occur.

- The Gert Member (core samples) and lower Gert Member (core samples) in the Hejre-2 well have similar occurrences as the Gert Member in other wells. Multivariate analysis, though, shows similarities to both the Gert and Ravn Members in other wells.

- The possible Gert Member (core samples) in the Rita-1 well fits well with the multivariate analysis model of the Gert Member (core samples) based on the three Gert wells. The possible Gert Member in Rita-1, though, has not been compared with the Bryne Formation. In case it actually belongs to the Bryne Formation, then some samples in Gert-4 might also be Bryne Formation, as they tend to group together. As these Gert-4 samples were included in the multivariate analysis model of Gert Member, the possible Gert Member in Rita-1 would not be distinguishable from the Gert Member model. Establishment of a geochemical model for the Bryne Formation would be necessary in order to make a final conclusion.

Origin of geochemical differences:

- The Heno Formation sandstones (core samples) are distinguished from the clay-dominated Lola and Farsund Formations by a higher content of Zr and a lower Th, V, U, Ni, Cu, Zn, Na_2O and P_2O_5 content. The higher amounts of Th, V, U, Na_2O and P_2O_5 in the Farsund and Lola Formations are probably related to the depositional environment.

- Gert Member (core samples) is characterised by varying amounts of TiO_2, Nb, K_2O, Rb, Cr and Zr, but typically with the highest maximum amounts of Cr and Ti. One explanation could be that another source area was dominant during deposition of the Gert Member successions and supplied material relatively rich in Cr and Ti. Another possible explanation could be that the Gert Member was characterised by several small episodes of material deposition from relatively fresh source rocks, therefore containing a higher amount of less stable minerals. The Gert Member is deposited during a transgression in a back-barrier and marine shoreface environment and during this transgression relatively unaltered or less altered material might occasionally have been brought into the system possibly during storm episodes.

- Ravn Member (core samples) has a similar content of zircons as the Gert Member, but a lower content of titanium and chromium and higher sodium and phosphorus content. The relatively high Nb / TiO_2 ratio might indicate that titanium is located primarily in rutile and Fe-Ti oxides. This combined with abundant oversized quartz and quartzite clast shows a dominance of very stable minerals, suggesting that the material has its origin in an intensively altered source rock. The alteration could have taken place on the surrounding highs (Mandal High, Mid North Sea High), or alternatively it might have taken place during temporal deposition during its transport to the final place of deposition. Another possible explanation could be that during deposition of the Ravn Member another source area was dominant than during deposition of the Gert Member giving rise to a geochemically different compositions. The high Na_2O content in Ravn Member could origin from a higher plagioclase content; and the high P_2O_5 could be related to another heavy mineral assemblage (for example dominated by apatite and monazite), which both are factors that could reflect that different source areas dominated during deposition of Ravn Member than during Gert Member.

- Parts of the Ravn Member (core samples) are differentiated from the Gert Member (core samples) by higher amounts of MgO. Magnesium (and phosphorus) could reflect the depositional environment. P_2O_5 might be present as marine authigenic phosphate minerals. Magnesium might be incorporated in clays, especially glauconite.

Local source area:

- The area of the Hejre and Jeppe-1 wells is influenced by a high K_2O / Al_2O_3 and high K_2O / Rb source rock, which probably is similar to the source rock of the underlying volcanoclastic conglomerate in the Hejre-2 well. This source rock (rich in K-feldspar) dominates especially in the Gert Member in the Hejre wells, but its influence gradually decreases and is lower in the Ravn Member (cuttings in Hejre wells) possibly due to intermixing with other sources. However, still during deposition of the Ravn Member in the Jeppe-1 well this source affects the sediments, even though its influence is less than in the Gert Member in the Hejre-2 well.

Zircon geochronology:

- Zircon samples from the Heno Formation (Gert and Ravn Members) and Lola Formation show the same overall pattern with a strong and wide Proterozoic population (1700–900 Ma), a Caledonian aged population (500–400 Ma), a possible Variscan aged population (350–310 Ma) and a small indication of an Archaean component (2900–2800, 2700–2600). The wide range of zircon ages reflects a combination of several sources possibly mixed by ocean floor currents and several episodes of sediment recycling. The Fennoscandian Shield and the Mid North Sea–Ringkøbing–Fyn Highs are the most likely source areas, as well as erosion and re-deposition of sediments derived here from.

- The Variscan aged zircon grains could reflect an influence from a southern source, which through several episodes of sediment recycling were brought to the depositional area.

- The simultaneously increase in the Caledonian and 600 Ma zircon age populations in the westernmost well could possibly reflect material originally derived from the British Isles, through repeated recycling in the sedimentary cycle.

Future investigations:

- More work will have to be done on the cuttings samples before it is possible to use them for separation of the different formations and members. Cuttings samples from some wells (for example the Gert-2 well) are so homogenised that they are very difficult to use. On the other hand cuttings from the Rita-1 and Gert-4 wells seem to carry more information, even though their barite content was extremely high.

- The geochemical results ought to be combined with petrographical investigations, which could lead to establishment of a tool for predicting reservoir properties from geochemical composition.

Recommendations

Zircon geochronology was performed on samples from the Hejre-2 well and from wells to the west (Gert-1, Gert-2, Gert-4) or south (Jeppe-1, Diamant-1) of Hejre-2. The Heno Formation in the Hejre-2 well may have had a northern source area. In order to evaluate other possible source areas it would be constructive to investigate the zircon geochronology of wells from the Norwegian sector.

XRD and petrographic investigations could verify if the assumptions of magnesium incorporation in clays (glauconite) and sodium incorporation in feldspars and clays are correct; and if phosphor is related to detrital or authigenic marine phosphates.

The geochemical results ought to be combined with diagenetic investigations, which could lead to establishment of a tool for predicting reservoir properties from geochemical composition.

Acknowledgements

Several people contributed to this project without their help the project could not have been carried out. Eva Melskens draw some of the figures; Per Ekelund Andersen extracted selected logs from the database; Bjørn Have Christensen brought all the cores and cuttings samples from the core store in Rødovre to the core laboratory at Øster Voldgade; Hans Jørgen Lorentzen plugged all the core samples; Marga Jørgensen helped with the numbering; Karen Henriksen and Erik Nielsen prepared all the samples for analyses, Jørgen Kystol analysed the samples by XRF and ICP-MS. Ingerlise Knudsen separated the heavy minerals for CCSEM analyses; Daniel, Rasmus, Mathilde, Pelle and Charlotte separated the zircons by washing and manually picking; Hanne Lambert impregnated and polished the zircon samples and the heavy mineral concentrates; Jørgen Kystol provided the CCSEM analyses of the heavy minerals; Susanne Schmid performed CCSEM analyses of thin sections; Dirk Frei took SEM photographs before analysing all zircon samples by ICP-MS; Anders Scherstén and Dirk Frei assisted during zircon-data processing; Per Rosenberg introduced and helped with the multivariate analysis; Karen Dybkjær and Peter Johannessen participated in inspiring discussions; Peter Johannessen read the preliminary version of the report and for constructive comments; Stuart Watt corrected the English and ensured the GEUS report format.

References

Andsbjerg, J. 2003: Sedimentology and sequence stratigraphy of the Bryne and Lulu Formations, Middle Jurassic, northern Danish Central Graben. In: Ineson, J. R. & Surlyk, F. (eds.): The Jurassic of Denmark and Greenland. Geological Survey of Denmark and Greenland Bulletin **1**, 301–347.

Andsbjerg, J. & Dybkjær, K. 2003: Sequence stratigraphy of the Jurassic of the Danish Central Graben. In: Ineson, J. R. & Surlyk, F. (eds.): The Jurassic of Denmark and Greenland. Geological Survey of Denmark and Greenland Bulletin **1**, 265–300.

Andsbjerg, J. Nielsen, L. H., Johannessen, P. N. & Dybkjær, K. 2001: Divergent development of two neighbouring basins following the Jurassic North Sea doming event: the Danish Central Graben and the Norwegian – Danish Basin. In: Martinsen, O. J. and Dreyer, T. (eds.): Sedimentary Environments Offshore Norway - Palaeozoic to Recent. Norwegian Petroleum Society (NPF) Special Publication **10**, 175–197.

Basu, A. & Molinaroli, E. 1989: Provenance characteristics of detrital opaque Fe-Ti oxide minerals. Journal of Sedimentary Petrology **59**, 922–934.

Bingen, B., Skår, Ø, Marker, M., Sigmond, E. M. O., Nordgulen, Ø., Ragnhildstveit, J., Mansfeld, J., Tucker, R. D. & Loégeois, J. P. 2005: Timing of continental building in the Sveconorwegian orogen, SW Scandinavia. Norwegian Journal of Geology **85**, 87–116.

Dodson, M.H., Compston, W., Williams, I.S. & Wilson, J.F. 1988: A search for ancient detrital zircons in Zimbabwean sediments. Journal of the Geological Society of London **145**, 977–983.

Ehrenberg, S. N. & Siring, E. 1992: Use of bulk chemical analyses in stratigraphic correlation of sandstones: an example from the Statfjord Nord Field, Norwegian Continental Shelf. Journal of Sedimentary Petrology **62**, 318–330.

Fonneland, H. C., Lien, T., Martinsen, O. J., Pedersen, R. B & Kosler, J. 2004: Detrital zircon ages: a key to understanding the deposition of deep marine sandstones in the Norwegian Sea. Sedimentary Geology **164**, 147–159.

Frei D., Hollis J.A., Gerdes A., Harlov D., Karlsson C., Vasquez P., Franz G., Johansson L. & Knudsen C. 2006: Advanced in-situ geochronological and trace element microanalysis by laser ablation techniques. Geological Survey of Denmark and Greenland Bulletin **10**, 25–28.

Frei, D. & Kystol, J. 2004: Inductively coupled plasma mass spectrometry (ICP-MS) Laboratory. http://www.geus.dk/departments/geol-mapping/projects/spectrometry-dk.htm

Friis, H., Poulsen, M. L., Svendsen, J. B. & Hamberg, L., 2007: Discrimination of density flow deposits using elemental geochemistry – implications for subtle provenance differentiation in a narrow submarine canyon, Palaeogene, Danish North Sea. Marine and Petroleum Geology **24**, 221-235.

Furnes, H., Elvsborg, A. & Malm, O. A. 1982: Lower and Middle Jurassic alkaline magnetism in the Egersund sub-Basin, North Sea. Marine Geology **46**, 53–69.

Garcia, D., Ravenne, C., Maréchal, B. & Moutte, J. 2004: Geochemical variability induced by entrainment sorting: quantified signals for provenance analysis. Sedimentary Geology **171**, 113–128.

Hallsworth, C. R., Morton, A. C., Claoué-Long, J. & Fanning, C. M. 2000: Carboniferous sand provenance in the Pennine Basin, UK: constraints form heavy minerals and detrital zircon age data. Sedimentary Geology **157**, 147–185.

Jackson, S., Pearson, N.J., Griffin, W.L. & Belousova, E.A. 2004: The application of laser ablation – inductively coupled plasma – mass spectrometry to in situ U-Pb zircon geochronology. Chemical Geology **211**, 47–69.

Japsen, P., Britze, P. & Andersen, C. 2003: Upper Jurassic – Lower Cretaceous of the Danish Central Graben: structural framework and nomenclature. Geological Survey of Denmark and Greenland Bulletin **1**, 233–246.

Johannessen, P. N. 2003: Sedimentology and sequence stratigraphy of paralic and shallow marine Upper Jurassic sandstones in the northern Danish Central Graben. In: Ineson, J. R. & Surlyk, F. (eds.): The Jurassic of Denmark and Greenland. Geological Survey of Denmark and Greenland Bulletin **1**, 367–402.

Johannessen, P.N. & Andsbjerg, J. 1993: Middle to Late Jurassic basin evolution and sandstone reservoir distribution in the Danish Central Trough, North Sea. Marine and Petroleum Geology **13**, 755–770.

Johannessen, P. N., Dybkjær, K. & Rasmussen, E. S. 1996: Sequence stratigraphy of Upper Jurassic reservoir sandstones in the northern part of the Danish Central Trough, North Sea. Marine and Petroleum Geology **13**, 755–770.

Katzung, G. 2001: The Caledonides at the southern margin of the East European Craton. Neues Jahrbuch für Geologie und Paläontologie **222** (1/2), 3–53.

Knudsen, T. -L. 2001: Contrasting provenance of Triassic / Jurassic sediments in North Sea Rift: a single zircon (SIMS), Sm–Nd and trace element study. Chemical Geology **171**, 273-293.

Knudsen, T. L. & Fossen, H. 2001: The Late Jurassic Bjorøy Formation: a provenance indicator for offshore sediments derived from SW Norway as based on single zircon (SIMS) data. Norwegian Journal of Geology **81**, 283–292.

Kystol, J. & Larsen, L. M. 1999: Analytical procedures in the rock geochemical laboratory of the Geological Survey of Denmark and Greenland. Geology of Greenland Survey Bulletin **184**, 59–62.

Laursen, K. 1997: Advanced scanning electron microscope analysis at GEUS. Danmarks og Grønlands Geologiske Undersøgelse Rapport **1997/1**.

Ludwig, K. R. 1997: ISOPLOT – a plotting and regression program for radiogenic isotope data, version 2.95. U. S. Geological Survey, Open-File Report 91-445.

Michelsen, O. Nielsen, L. H, Johannessen, P. N., Andsbjerg, J. and Surlyk, F. 2003: Jurasssic lithostratigraphy and stratigraphic development onshore and offshore Denmark. In: Ineson, J. R. & Surlyk, F. (eds.): The Jurassic of Denmark and Greenland. Geological Survey of Denmark and Greenland Bulletin **1**, 147–216.

Morton, A. C. & Hallsworth, C. R. 1999: Process controlling the composition of heavy mineral assemblages in sandstones. Sedimentary Geology **124**, 3–29.

Morton, A. C., Claoue-Long, J. C. & Berge, C. 1996: SHRIMP constraints on sediment provenance and transport history in the Mesozoic Statfjord Formation, North Sea. Journal of the Geological Society London **153**, 915-929.

Morton, A. C., Claoué-Long, J. C. & Hallsworth, C. R. 2001: Zircon age and heavy mineral constraints on provenance of North Sea Carboniferous sandstones. Marine and Petroleum Geology **18**, 319–337.

Morton, A. C., Whitham, A. G. & Fanning, C. M. 2005: Provenance of Late Cretaceous to Paleocene submarine fan sandstones in the Norwegian Sea: integration of heavy mineral, mineral chemical and zircon age data. Sedimentary Geology **82**, 3–28.

Nielsen, L. H. 2003: Late Triassic – Jurassic development of the Danish Basin and the Fennoscandian Borde Zone, southern Scandinavia. In: Ineson, J. R. & Surlyk, F. (eds.): The Jurassic of Denmark and Greenland. Geological Survey of Denmark and Greenland Bulletin **1**, 459–526.

Pearce, T. J., Besley, B. M., Wray, D. S. & Wright, D. K. 1999: Chemostratigraphy: a method to improve interwell correlation in barren sequences – a case study using onshore Duckmantian/Stephanian sequences (West Midlands, U.K.). Sedimentary Geology **124**, 197–220.

Pearce, T. J. & Jarvis. I. 1995: High-resolution chemostratigraphy of Quaternary distal turbidites: a case study of new methods for the analysis and correlation of barren sequences. In: Dunay, R. E. & Hailwood, E. A. (eds.): Non-biostratigraphical Methods of Dating and Correlation. Geological Society of Special Publication **89**, 107–143.

Preston, J, Hartley, A, Hole, M, Buck, S., Bond, J, Mange, M & Still, J. 1998: Integrated whole-rock trace element geochemistry and heavy mineral chemistry studies: aid to the correlation of continental red-bed reservoirs in the Beryl Field, UK North Sea. Petroleum Geology **4**, 7–16.

Petersen; H. I. & Andsbjerg, J. 1996: Organic facies development within Middle Jurassic coal seams, Danish Central Graben, and evidence for relative sea-level control on peat accumulation in a coastal plain environment. Sedimentary Geology **106**, 259–277.

Ratcliffe, K. T., Wright, A. M., Hallsworth, C., Morton, A., Zaitlin, B. A., Potocki, D. and Wray, D. S. 2004: An example of alternative correlation techniques in a low-accummodation setting, non-marine hydrocarbon system: The (Lower Cretaceous) Mannville Basal Quartz succession of southern Alberta. AAPG Bulletin **88**, 1419–1432.

Rogers, G., Hyslop, E. K., Strachan, R. A. & Holdsworth, R. E. 1998: The structural setting and U-Pb geochronology of Knoydartian pegmatites in W Inverness-shire; evidence for Neoproterozoic tectonothermal events in the Moine of NW Scotland. Journal of the Geological Society of London **155**, 685–696.

Rogers, G., Kinny, P. D., Strachan, R. A., Friend, C. R. L. & Paterson, B. A. 2001: U-Pb geochronology of the Fort Angus granite neiss; constraints on the timing of Neoprterozoic and Palaeozoic tectonothermal events in the NW Highlands of Scotland. Journal of the Geological Society of London **158**, 7–14.

Scherstein, A. *in press*: Provenance of West Greenland Cretaceous and Paleocene sandstones based on U-Pb dating of detrital zircon. Geological Survey of Denmark and Greenland Bulletin.

Sircombe, K. N. 2004: AGEDISPLAY: an EXCEL workbook to evaluate and display univariate geochronological data using binned frequency histograms and probability density distributions. Computer and Geoscience **30**, 21–31.

Sørensen, H. S. 1998: Computer controlled scanning electron microscopy (CCSEM) of heavy minerals. Danmarks og Grønlands Geologiske Undersøgelse Rapport **1998/74**.

Spathopoulos, F., Doubleday, P. A. & Hallsworth, C. R. 2000: Structural and depositional controls on the distribution of the Upper Jurassic shallow marine sandstones in the Fife and Angus fields area, Quadrants 31 & 39, UK Central North Sea. Marine and Petroleum Geology **17**, 1053–1082.

Stephens, M. S., Wahlgren, C. H. & Weihed, P. 1994: Major tectonic units in the bedrock of Sweden. Geological Survey of Sweden (Map).

Surlyk, F. & Ineson, J. R. 2003: The Jurassic of Denmark and Greenland: key elements in the reconstruction of the North Atlantic Jurassic rift system. In: Ineson, J. R. & Surlyk, F. (eds.): The Jurassic of Denmark and Greenland. Geological Survey of Denmark and Greenland Bulletin **1**, 9–20.

Weibel, R. & Friis, H. 2004: Opaque minerals as keys for distinguishing oxidising and reducing diagenetic conditions in the Lower Triassic Bunter Sandstone, North German Basin. Sedimentary Geology, **169**, 129–149.

Appendix 1. Core samples

Chemostratigraphy and mineral-chemical fingerprinting, Heno Formation, Danish North Sea

Well	Plug No.	ID	Depth (′) top of box	+ Depth (″)	Depth (m)	Cores	Formation/ Member	Environment	Lithology	XRF	Zircon	Garnet
Diamant-1	51	DI1-382808	12559	4	3828.08	1	Ravn Mb	Middle-upper shoreface	Fine-grained sand	x		
	52	DI1-382965	12564	8	3829.71	1	Ravn Mb	Beach	Coarse-grained sand	x	z	g
	53	DI1-383220	12572.5	10	3832.20	1	Ravn Mb	Beach	Coarse-grained sand	x		
	54	DI1-383309	12575	9	3833.09	1	Ravn Mb	Middle-upper shoreface	Fine-grained sand with clay	x		
	55	DI1-383482	12581	5	3834.82	1	Ravn Mb	Middle-upper shoreface	Fine-grained sand with clay	x		
	56	DI1-383596	12585	2	3835.96	1	Ravn Mb	Barrier inlet	Conglomerate	x		
	57	DI1-383797	12591	9	3837.97	1	Gert Mb	Wash over fan?	Sand	x		
	58	DI1-383837	12593	1	3838.37	1	Gert Mb	Lagoon sediments?	Clayey sand	x		
	59	DI1-383908	12595	5	3839.08	1	Gert Mb	Wash over fan	Sand	x		
	60	DI1-384152	12603	5	3841.52	1	Gert Mb	Wash over fan	Sand	x		
	61	DI1-384447	12613	1	3844.47	1	Gert Mb	Shoreface or lagoon?	Sand	x		
	62	DI1-384565	12617	0	3845.66	1	Gert Mb	Shoreface or lagoon?	Sand	x	z	g
	63	DI1-385938	12662	0	3859.38	2	Gert Mb	Lagoon sediments??	Clay	x		
	66	DI1-387350	12708	3	3873.47	2	Perm		Volcanic conglomerate?	x	z	g
	67	DI1-383106	12569	1	3831.06	1	Ravn Mb	Middle-upper shoreface	Coarse-grained sand	x		
	68	DI1-383959	12597	1	3839.59	1	Gert Mb	Back-barrier sediment	Clayey sand	x		
	69	DI1-383510	12582	4	3835.10	1	Ravn Mb	Middle-upper shoreface	Conglomerate	x		

Appendix 1. Core samples

Chemostratigraphy and mineral-chemical fingerprinting, Heno Formation, Danish North Sea

Well	Plug No.	ID	Depth (') top of box	+ Depth (")	Depth (m)	Cores	Formation/ Member	Environment	Lithology	XRF	Zircon	Garnet
Gert-1	1	GE1- 491975	16140	10	4919.73	2	Gert Mb	Back-barrier	Sand	x		
	2	GE1- 492140	16146	5	4921.43	2	Gert Mb	Back-barrier	Sand	x	z	g
	3	GE1-492250	16150	0	4922.52	2	Gert Mb	Back-barrier	Sand	x		
	4	GE1-492415	16155	4	4924.15	2	Gert Mb	Back-barrier	Sand	x		
	5	GE1-492575	16160	7	4925.75	2	Gert Mb	Back-barrier	Sand	x		
	6	GE1-492820	16168	8	4928.21	2	Gert Mb	Beach or Upper Shoreface	Sand	x	z	g
	7	GE1-492880	16170	7	4928.79	3	Gert Mb	Back-barrier	Sand	x		
	8	GE1-493025	16175	4	4930.24	3	Gert Mb	Back-barrier	Clayey sand	x		
	9	GE1-493200	16181	1	4931.99	3	Gert Mb	Back-barrier	Sand	x		
	10	GE1-493430	16188	9	4934.33	3	Gert Mb	Back-barrier	Sand with carbonate vein	x		
	11	GE1-493705	16197	9	4937.07	3	Gert Mb	Rootlets in wash-over fan	Sand	x	z	g
	12	GE1-493880	16203	6	4938.83	3	Gert Mb	Back-barrier	Sand	x		
	13	GE1-493955	16205	10	4939.54	3	Gert Mb	Lagoon sediment	Claystone	x		
	14	GE1-494130	16211	7	4941.29	3	Gert Mb	Top of tidal inlet chanal fill	Claystone	x		
	15	GE1-494255	16215	8	4942.54	3	Gert Mb	Bottom of tidal inlet chanal fill	Sand	x		
	16	GE1-494430	16221	5	4944.29	4	Gert Mb	Back-barrier	Sand	x	z	g
	17	GE1-494630	16228	1	4946.32	4	Gert Mb	Back-barrier	Sand	x		
	18	GE1-495030	16241	1	4950.28	4	Gert Mb	Back-barrier	Sand	x		
	19	GE1-495155	16245	3	4951.55	4	Gert Mb	?	Claystone (shell debris)	x		
	20	GE1-495330	16251	0	4953.30	5	Gert Mb	Lagoon sediment	Claystone with slumping	x		
	21	GE1-495425	16254	1	4954.24	5	Gert Mb	Wash-over fan	Sand (gravegange)	x		
	22	GE1-495655	16261	8	4956.56	5	Gert Mb	Back-barrier	Clayey sand	x		
	23	GE1-495765	16265	3	4957.65	5	Gert Mb	Rootlets in wash-over fan	Sand	x		
	24	GE1-495805	16266	6	4958.03	5	Gert Mb	Back-barrier	Sand	x		
	25	GE1-495980	16272	5	4959.83	5	Gert Mb	Back-barrier	Sand	x		
	26	GE1-496475	16288	6	4964.73	6	Gert Mb	Back-barrier	Clay/sand	x		
	27	GE1-496770	16298	2	4967.68	6	Gert Mb	Back-barrier	Sand	x		
	28	GE1-496870	16301	7	4968.72	6	Gert Mb	Back-barrier	Claystone	x		
	29	GE1-496955	16304	4	4969.56	6	Gert Mb	Back-barrier	Sand	x	z	g

Well	Plug No.	ID	Depth (′) top of box	+ Depth (″)	Depth (m)	Cores	Formation/ Member	Environment	Lithology	XRF	Zircon	Garnet
	30	GE1-497325	16316	5	4973.24	6	Gert Mb	Back-barrier	Sand (cupper minerals)	x		
	31	GE1-498165	16343	11	4981.63	7	Permian		Volcanic material	x	z	g

Appendix 1. Core samples

Chemostratigraphy and mineral-chemical fingerprinting, Heno Formation, Danish North Sea

Well	Plug No.	ID	Depth (′) top of box	+ Depth (″)	Depth (m)	Cores	Formation/ Member	Environment	Lithology	XRF	Zircon	Garnet
Gert-2	35	GE2-481775	15806	3	4817.75	1	Ravn Mb	Below sequence boundary	Sand	x	z	g
	36	GE2-482100	15816	11	4821.00	1	Ravn Mb	Middle-upper shoreface	Sand	x		
	37	GE2-482170	15819	3	4821.71	1	Ravn Mb	Middle-upper shoreface	Sand	x		
	38	GE2-482450	15828	4	4824.48	1	Ravn Mb	Middle-upper shoreface	Clay / sand	x		
	39	GE2-482675	15835	9	4826.74	1	Ravn Mb	Middle-upper shoreface	Sand	x	z	g
	40	GE2-482940	15844	5	4829.38	1	Ravn Mb	Lower shoreface	Sand	x		
	41	GE2-483155	15851	6	4831.54	1	Ravn Mb	Lower shoreface	Sand	x		
	42	GE2-483245	15854	6	4832.45	1	Ravn Mb	Lower shoreface	Sand	x		
	43	GE2-483485	15862	5	4834.86	1	Ravn Mb	Lower shoreface	Sand	x	z	g
	44	GE2-486835	15972	3	4868.34	2	Gert Mb	Back-barreir sediments	Sand	x	z	g
	45	GE2-487050	15979	3	4870.48	2	Gert Mb	Back-barreir sediments	Sand	x		
	46	GE2-487190	15983	10	4871.87	2	Gert Mb	Back-barreir sediments	Sand	x		
	47	GE2-487320	15988	2	4873.19	2	Gert Mb	Shore face (below MTSE)	Sand	x	z	g
	48	GE2-487335	15988	8	4873.35	2	Gert Mb	Back-barrier (below MTSE)	Claystone	x		
	49	GE2-490595	16095	8	4905.96	6	Carbon		Clay / sand	x		
	50	GE2-493940	16205	5	4939.41	9	Carbon		Coarse-grained sandstone	x	z	g

Appendix 1. Core samples

Chemostratigraphy and mineral-chemical fingerprinting, Heno Formation, Danish North Sea

Well	Plug No.	ID	Depth (′) top of box	+ Depth (″)	Depth (m)	Cores	Formation/ Member	Environment	Lithology	XRF	Zircon	Garnet
Gert-4	70	GE4-579135	19000	5	5791.33	1	Ravn Mb	Lower shoreface	Clayey sand	x	z	g
	71	GE4-579355	19007	8	5793.54	1	Ravn Mb	Lower shoreface	Clayey sand	x		
	72	GE4-579640	19017	1	5796.41	1	Ravn Mb	Lower shoreface	Clayey sand	x		
	73	GE4-579930	19026	7	5799.30	1	Ravn Mb	Lower shoreface	Clayey sand	x		
	74	GE4-580185	19034	11	5801.84	1	Ravn Mb	Lower shoreface	Clayey sand	x		
	75	GE4-580500	19045	4	5805.02	1	Ravn Mb	Lower shoreface	Oversize clasts in clayey sand	x		
	76	GE4-580765	19054	0	5807.66	1	Ravn Mb	Lower shoreface	Oversize clasts in clayey sand	x		
	77	GE4-580910	19058	8	5809.08	1	Ravn Mb	Lower shoreface	Oversize clasts in clayey sand	x		
	78	GE4-581140	19066	3	5811.39	2	Ravn Mb	Lower shoreface	Oversize clasts in clayey sand	x		
	79	GE4-581330	19072	6	5813.30	2	Ravn Mb	Lower shoreface	Oversize clasts in clayey sand	x		
	80	GE4-581490	19077	10	5814.92	2	Ravn Mb	Lower shoreface	Oversize clasts in clayey sand	x		
	81	GE4-581600	19081	5	5816.02	2	Ravn Mb	Lower shoreface	Oversize clasts in clayey sand	x		
	82	GE4-581915	19091	8	5819.14	2	Ravn Mb	Lower shoreface	Oversize clasts in clayey sand	x		
	83	GE4-582245	19102	6	5822.44	2	Ravn Mb	Lower shoreface	Oversize clasts in clayey sand	x		
	84	GE4-582395	19107	5	5823.94	2	Ravn Mb	Lower shoreface	Oversize clasts in clayey sand	x		
	85	GE4-582645	19115	8	5826.46	2	Ravn Mb	Lower shoreface	Oversize clasts in clayey sand	x		
	86	GE4-582795	19120	6	5827.93	2	Ravn Mb	Lower shoreface	Oversize clasts in clayey sand	x		
	87	GE4-583010	19127	7	5830.09	2	Ravn Mb	Lower shoreface	Oversize clasts in clayey sand	x		
	88	GE4-583340	19138	5	5833.39	2	Ravn Mb	Lower shoreface	Oversize clasts in clayey sand	x	z	g
	89	GE4-583495	19143	7	5834.96	2	Lola Fm	Offshore claystone	Clayey silt	x		
	90	GE4-583700	19150	4	5837.02	3	Lola Fm	Offshore claystone	Clayey silt	x		
	91	GE4-584040	19161	4	5840.37	3	Lola Fm	Offshore claystone	Oversize clasts in clayey sand	x		
	92	GE4-584230	19167	7	5842.28	3	Lola Fm	Offshore claystone	Clayey sand?	x		
	93	GE4-584415	19173	8	5844.13	3	Lola Fm	Offshore claystone	Clayey silt	x		
	94	GE4-584755	19184	10	5847.54	3	Lola Fm	Offshore claystone	Clayey silt	x		
	95	GE4-584930	19190	8	5849.32	3	Lola Fm	Offshore claystone	Clayey silt	x		
	96	GE4-585250	19201	2	5852.52	3	Lola Fm	Offshore claystone	Clayey silt	x		
	97	GE4-585470	19208	4	5854.70	3	Lola Fm	Offshore claystone	Oversize clasts in clayey sand	x		
	98	GE4-585525	19210	2	5855.26	3	Lola Fm	Offshore claystone	Oversize clasts in clayey sand	x		

Well	Plug No.	ID	Depth (′) top of box	+ Depth (″)	Depth (m)	Cores	Formation/ Member	Environment	Lithology	XRF	Zircon	Garnet
	99	GE4-585880	19221	9	5858.79	3	Lola Fm	Offshore claystone	Clayey silt	x		
	100	GE4-586125	19229	9	5861.23	3	Lola Fm	Offshore claystone	Clayey silt	x		
	101	GE4-586265	19234	5	5862.65	3	Lola Fm	Offshore claystone	Clayey silt	x		
	102	GE4-586520	19242	10	5865.22	4	Lola Fm	Offshore claystone	Clayey silt	x	z	g
	103	GE4-586660	19247	4	5866.59	4	Lola Fm	Offshore claystone	Clayey silt	x		
	104	GE4-587040	19259	10	5870.40	4	Lola Fm	Offshore claystone	Clay with concretions	x		
	105	GE4-587190	19264	8	5871.87	4	Lola Fm	Offshore claystone	Clay with concretions	x		
	106	GE4-587425	19272	6	5874.26	4	Lola Fm	Offshore claystone	Clay	x		
	107	GE4-587650	19279	9	5876.47	4	Lola Fm	Offshore claystone	Clay	x		
	108	GE4-587880	19287	5	5878.80	4	Lola Fm	Offshore claystone	Clay	x		
	109	GE4-588105	19294	9	5881.04	4	Lola Fm	Offshore claystone	Clay	x		
	110	GE4-588380	19303	10	5883.81	4	Lola Fm	Offshore claystone	Clay	x		
	111	GE4-588655	19312	9	5886.53	4	Lola Fm	Offshore claystone	Clay	x		
	112	GE4-588925	19321	8	5889.24	4	Lola Fm	Offshore claystone	Clay	x		
	113	GE4-586425	19339	8	5894.73	4	Lola Fm	Offshore claystone	Clay	x		
	114	GE4-604450	19831	1	6044.51	5	Gert Mb	Back-barrier sediments	SAND	x	z	g
	115	GE4-604580	19835	4	6045.81	5	Gert Mb	Back-barrier sediments	Claystone	x		
	116	GE4-606225	19889	3	6062.24	6	Gert Mb	Back-barrier sediments	SAND	x		
	117	GE4-606330	19892	8	6063.28	6	Gert Mb	Back-barrier sediments	SAND	x		
	118	GE4-606445	19896	6	6064.45	6	Gert Mb	Back-barrier sediments	SAND	x		
	119	GE4-606520	19898	11	6065.19	6	Gert Mb	Back-barrier sediments	Conglomerate	x	z	g
	120	GE4-606560	19900	3	6065.60	6	Gert Mb	Back-barrier sediments	Claystone	x		
	121	GE4-606760	19906	9	6067.58	6	Gert Mb	Back-barrier sediments	Claystone	x		
	122	GE4-607585	19933	10	6075.83	7	Permian			x	z	g

Appendix 1. Core samples

Chemostratigraphy and mineral-chemical fingerprinting, Heno Formation, Danish North Sea

Well	Plug No.	ID	Depth (') top of box	+ Depth (")	Depth (m)	Cores	Formation/ Member	Environment	Lithology	XRF	Zircon	Garnet
Gwen-2	180	GW2-423730	13901	11	4237.30	1	Ravn Mb	Lower-middle shoreface	Sand (bioturbated)	x		
	181	GW2-423908	13907	9	4239.08	1	Ravn Mb	Lower-middle shoreface	Clay and sand lamina	x		
	182	GW2-424076	13913	3	4240.76	1	Ravn Mb	Middle-upper shoreface	Sand and clay lamina	x		
	183	GW2-424266	13919	6	4242.66	1	Ravn Mb	Middle-upper shoreface	Sand with shell fragmets	x		
	184	GW2-424457	13925	9	4244.57	1	Ravn Mb	Middle-upper shoreface	Sand with shell fragmets	x		
	185	GW2-424541	13928	6	4245.41	1	Ravn Mb	Middle-upper shoreface	Sand with shell and coal frag.	x		
	186	GW2-424693	13933	6	4246.93	1	Ravn Mb	Middle-upper shoreface	Sand with shell and coal frag.	x		
	187	GW2-424856	13938	10	4248.56	1	Ravn Mb	Middle-upper shoreface	Sand with clay lamina	x		
	188	GW2-425090	13946	5	4250.87	1	Ravn Mb	Beach	Sand with oversize clasts	x		
	189	GW2-425250	13951	10	4252.52	1	Ravn Mb	Middle-upper shoreface	Sand and clay lamina	x		
	190	GW2-425480	13959	3	4254.78	1	Ravn Mb	Middle-upper shoreface	Homogeneous sand	x		
	191	GW2-425650	13964	9	4256.46	2	Ravn Mb	Beach	Sand with oversize clasts	x		
	192	GW2-425850	13971	4	4258.46	2	Ravn Mb	Middle-upper shoreface	Sand and clay lamina	x		
	193	GW2-426070	13978	6	4260.65	2	Ravn Mb	Top para sequence	Sand and clay lamina	x		
	194	GW2-426250	13984	6	4262.48	2	Ravn Mb	Middle-upper shoreface	Sand and clay lamina	x		
	195	GW2-426400	13989	6	4264.00	2	Ravn Mb	Middle-upper shoreface	Sand and clay lamina	x		
	196	GW2-426480	13992	3	4264.84	2	Ravn Mb	Middle-upper shoreface	Sand with shell and coal frag.	x		
	197	GW2-426650	13997	9	4266.51	2	Ravn Mb	Middle-upper shoreface	Sand with coal fragmets	x		
	198	GW2-426820	14003	3	4268.19	2	Ravn Mb	Middle-upper shoreface	Sand with thin clay lamina	x		
	199	GW2-427040	14010	6	4270.40	2	Ravn Mb	Middle-upper shoreface	Clayey with sand	x		
	200	GW2-427150	14017	4	4272.48	2	Ravn Mb	Middle-upper shoreface	Sand with thin clay lamina	x		
	201	GW2-427370	14021	4	4273.70	2	Ravn Mb	Middle-upper shoreface	Sand with thin clay lamina	x		
	202	GW2-427500	14025	6	4274.97	3	Ravn Mb	Middle-upper shoreface	Clay with sand lamina	x		
	203	GW2-427680	14031	6	4276.80	3	Ravn Mb	Middle-upper shoreface	Sand (bioturbated)	x		
	204	GW2-427890	14038	3	4278.86	3	Ravn Mb	Middle-upper shoreface	Sand (bioturbated)	x		
	205	GW2-428080	14044	8	4280.81	3	Ravn Mb	Middle-upper shoreface	Sand (bioturbated)	x		
	206	GW2-428270	14050	10	4282.69	3	Ravn Mb	Middle-upper shoreface	Sand (bioturbated)	x		
	207	GW2-428470	14057	4	4284.68	3	Ravn Mb	Middle-upper shoreface	Sand (bioturbated)	x		
	208	GW2-428660	14063	6	4286.55	3	Ravn Mb	Middle-upper shoreface	Sand (bioturbated)	x		

Well	Plug No.	ID	Depth (′) top of box	+ Depth (″)	Depth (m)	Cores	Formation/ Member	Environment	Lithology	XRF	Zircon	Garnet
	209	GW2-428840	14069	6	4288.38	3	Ravn Mb	Middle-upper shoreface	Sand (bioturbated)	x		
	210	GW2-429010	14075	3	4290.14	3	Ravn Mb	Middle-upper shoreface	Sand (bioturbated)	x		
	211	GW2-429270	14083	9	4292.73	3	Ravn Mb	Middle-upper shoreface	Sand (bioturbated)	x		

Appendix 1. Core samples

Chemostratigraphy and mineral-chemical fingerprinting, Heno Formation, Danish North Sea

Well	Plug No.	ID	Depth (′) top of box	+ Depth (″)	Depth (m)	Cores	Formation/Member	Environment	Lithology	XRF	Zircon	Garnet
Hejre-2	220	HE2-537822	5378	22	5378.22	1	Gert Mb (Upper)		Sandstone	x		
	221	HE2-537944	5379	44	5379.44	1	Gert Mb (Upper)		Sandstone	x	z	g
	222	HE2-538070	5380	70	5380.70	1	Gert Mb (Upper)		Homogeneous sandstone	x		
	223	HE2-538140	5381	40	5381.40	1	Gert Mb (Upper)		Calcite-cementered sandstone	x	z	g
	224	HE2-538191	5381	91	5381.91	1	Gert Mb (Upper)		Sandstone with thin claylamina	x		
	225	HE2-538285	5382	85	5382.85	1	Gert Mb (Upper)		Calcite-cementered sandstone	x		
	226	HE2-538375	5383	75	5383.75	1	Gert Mb (Upper)		Sandstone with thin claylamina	x		
	227	HE2-538490	5384	90	5384.90	1	Gert Mb (Upper)		Sandstone	x		
	228	HE2-538558	5385	58	5385.58	1	Gert Mb (Upper)		Homogeneous sandstone	x		
	229	HE2-538657	5386	57	5386.57	1	Gert Mb (Upper)		Calcite-cementered sandstone	x		
	230	HE2-538735	5387	35	5387.35	1	Gert Mb (Upper)		Sandstone with thin claylamina	x		
	231	HE2-538895	5388	95	5388.95	1	Gert Mb (Upper)		Calcite-cementered sandstone	x		
	232	HE2-538986	5389	86	5389.86	1	Gert Mb (Upper)		Sandstone with clay lamina	x	z	g
	233	HE2-539098	5390	98	5390.98	1	Gert Mb (Upper)		Sandstone with clay lamina	x		
	234	HE2-539186	5391	86	5391.86	1	Gert Mb (Upper)		Sandstone with clay lamina	x		
	235	HE2-539256	5392	56	5392.56	1	Gert Mb (Lower) ?		Sandstone with clay lamina	x		
	236	HE2-539395	5393	95	5393.95	1	Gert Mb (Lower) ?		Sandstone with clay lamina	x		
	237	HE2-539498	5394	98	5394.98	1	Gert Mb (Lower) ?		Calcite-cementered sandstone	x	z	g
	238	HE2-539560	5395	60	5395.60	1	Gert Mb (Lower) ?		Homogeneous sandstone	x		
	239	HE2-539685	5396	85	5396.85	1	Gert Mb (Lower) ?		Homogeneous sandstone	x		
	240	HE2-539748	5397	48	5397.48	1	Gert Mb (Lower) ?		Homogeneous sandstone	x		
	241	HE2-539825	5398	25	5398.25	1	Gert Mb (Lower) ?		Homogeneous sandstone	x		
	242	HE2-539957	5399	57	5399.57	1	Gert Mb (Lower) ?		Homogeneous sandstone	x	z	g
	243	HE2-540045	5400	45	5400.45	1	Gert Mb (Lower) ?		Homogeneous sandstone	x		
	244	HE2-540125	5401	25	5401.25	1	Gert Mb (Lower) ?		Calcite-cementered sandstone	x		
	245	HE2-540232	5402	32	5402.32	1	Pre-Upper Jurassic		Volcanic conglomerate	x	z	g

Appendix 1. Core samples

Chemostratigraphy and mineral-chemical fingerprinting, Heno Formation, Danish North Sea

Well	Plug No.	ID	Depth (') top of box	+ Depth (")	Depth (m)	Cores	Formation / Member	Environment	Lithology	XRF	Zircon	Garnet
Jeppe-1	130	JE1-440145	4401.22	23	4401.45	1	Farsund Fm	Offshore claystone	Claystone with thin sand layers	x		
	131	JE1-440305	4403.05	50	4403.55	1	Farsund Fm	Offshore claystone	Interbeded sand layer	x		
	132	JE1-440600	4405.9	10	4406.00	1	Farsund Fm	Offshore claystone	Claystone with thin sand layers	x		
	133	JE1-440820	4408.2	10	4408.30	1	Farsund Fm	Offshore claystone	Slumped interbeded sand	x		
	134	JE1-441078	4410.78	45	4411.23	1	Farsund Fm	Offshore claystone	Claystone with thin sand layers	x		
	135	JE1-441253	4412.53	20	4412.73	1	Farsund Fm	Offshore claystone	Coarse-grained sand	x		
	136	JE1-441420	4414.2		4414.20	1	Farsund Fm	Offshore claystone	Claystone	x		
	137	JE1-441530	4415.3		4415.30	1	Farsund Fm	Offshore claystone	Interbeded sand layer	x		
	138	JE1-441770	4417.7		4417.70	1	Farsund Fm	Offshore claystone	Claystone with thin sand layers	x		
	139	JE1-441862	4418.57	5	4418.62	1	Farsund Fm	Offshore claystone	Interbeded sand layer	x		
	140	JE1-441922	4418.57	65	4419.22	1	Farsund Fm	Offshore claystone	Claystone	x		
	141	JE1-493720	4937.2		4937.20	2	Ravn Mb	Middle shoreface	Sandstone	x		
	142	JE1-493930	4939.3		4939.30	2	Ravn Mb	Middle shoreface	Sandstone	x	z	g
	143	JE1-494053	4940.53	55	4941.08	2	Ravn Mb	Middle shoreface	Sandstone	x		
	144	JE1-494202	4942.02		4942.02	2	Ravn Mb	Middle shoreface	Conglomerate	x		
	145	JE1-494374	4943.74		4943.74	2	Ravn Mb	Middle shoreface	Conglomerate	x		
	146	JE1-494581	4945.81		4945.81	2	Ravn Mb	Middle shoreface	Conglomerate	x		
	147	JE1-494757	4947.35	22	4947.57	2	Ravn Mb	Middle shoreface	Conglomerate	x		
	148	JE1-494940	4949.4		4949.40	2	Ravn Mb	Middle shoreface	Sandstone	x		
	149	JE1-495075	4950.75		4950.75	2	Ravn Mb	Middle shoreface	Sandstone	x		
	150	JE1-495315	4953.15		4953.15	2	Ravn Mb	Middle shoreface	Sandstone	x		
	151	JE1-495523	4955.23		4955.23	3	Ravn Mb	Middle shoreface	Sandstone	x		
	152	JE1-495757	4957.57		4957.57	3	Ravn Mb	Middle shoreface	Sandstone	x		
	153	JE1-495880	4958.8		4958.80	3	Ravn Mb	Middle shoreface	Sandstone	x		
	154	JE1-496172	4961.72		4961.72	3	Ravn Mb	Middle shoreface	Sandstone	x		
	155	JE1-496308	4963.08		4963.08	3	Ravn Mb	Middle shoreface	Sandstone	x		
	156	JE1-496520	4965.2		4965.20	3	Ravn Mb	Middle shoreface	Sandstone	x		
	157	JE1-496715	4967.15		4967.15	3	Ravn Mb	Middle shoreface	Sandstone	x		
	158	JE1-496912	4969.12		4969.12	3	Ravn Mb	Middle shoreface	Sandstone	x		

Well	Plug No.	ID	Depth (′) top of box	+ Depth (″)	Depth (m)	Cores	Formation / Member	Environment	Lithology	XRF	Zircon	Garnet
	159	JE1-497183	4971.83		4971.83	3	Ravn Mb	Middle shoreface	Sandstone	x	z	g
	160	JE1-497315	4973.15		4973.15	4	Ravn Mb	Middle shoreface	Sandstone	x		
	161	JE1-497505	4975.05		4975.05	4	Ravn Mb	Middle shoreface	Sandstone	x		
	162	JE1-497740	4977.40		4977.40	4	Ravn Mb	Middle shoreface	Sandstone	x		
	163	JE1-497930	4979.30		4979.30	4	Ravn Mb	Middle shoreface	Sandstone	x		
	164	JE1-498110	4981.10		4981.10	4	Ravn Mb	Middle shoreface??	Sandstone	x		
	165	JE1-498300	4983.00		4983.00	4	Ravn Mb	Lower shoreface??	Sandstone	x		
	166	JE1-498495	4984.95		4984.95	4	Ravn Mb	Lower shoreface	Sandstone	x		
	167	JE1-498726	4987.26		4990.91	4	Ravn Mb	Lower shoreface	Sandstone	x		
	168	JE1-499041	4990.41	50	4990.91	4	Ravn Mb	Lower shoreface	Sandstone	x		
	169	JE1-499900	4991.02		4991.02	4	Ravn Mb	Lower shoreface	Sandstone	x	z	g

Appendix 1. Core samples

Chemostratigraphy and mineral-chemical fingerprinting, Heno Formation, Danish North Sea

Well	Plug No.	ID	Depth (') top of box	+ Depth (")	Depth (m)	Cores	Formation/Member	Environ-ment	Lithology	XRF	Zircon	Garnet
Rita-1	258	RI1-391599	12847	9	3915.99	1	Farsund Fm		Claystone			
	259	RI1-391737	12852	3	3917.37	1	Farsund Fm		Claystone			
	260	RI1-391693	12850	10	3916.93	1	Farsund Fm		Claystone			
	261	RI1-391848	12855	11	3918.48	1	Farsund Fm		Claystone			
	262	RI1-452712	14852	9	4527.12	2	Ravn Mb		Sandy mudstone, bioturbated			
	263	RI1-452872	14858	0	4528.72	2	Ravn Mb		Sandy mudstone, bioturbated			
	264	RI1-453050	14863	10	4530.50	2	Ravn Mb		Sandy mudstone, bioturbated			
	265	RI1-453230	14869	9	4532.30	2	Ravn Mb		Sandy mudstone, bioturbated			
	266	RI1-453360	14874	0	4533.60	2	Ravn Mb		Sandy mudstone, bioturbated			
	267	RI1-453558	14880	6	4535.58	2	Ravn Mb		Sandy mudstone, bioturbated			
	268	RI1-453730	14886	2	4537.30	2	Ravn Mb		Sandy mudstone, bioturbated			
	269	RI1-453913	14892	2	4539.13	2	Ravn Mb		Sandy mudstone, bioturbated			
	270	RI1-454099	14898	3	4540.99	2	Ravn Mb		Sandy mudstone, bioturbated			
	271	RI1-454254	14903	4	4542.54	3	Ravn Mb		Sandy mudstone, bioturbated			
	272	RI1-454416	14908	8	4544.16	3	Ravn Mb		Weakly laminated sand and mud			
	273	RI1-454589	14914	4	4545.89	3	Ravn Mb		Sandstone with over-size clasts			
	274	RI1-454736	14919	2	4547.36	3	Ravn Mb		Sandstone with over-size clasts			
	275	RI1-454988	14927	5	4549.88	3	Ravn Mb		Sandstone, bioturbated			
	276	RI1-455049	14929	5	4550.49	3	Ravn Mb		Sandstone, bioturbated			
	277	RI1-455259	14936	4	4552.59	3	Ravn Mb		Muddy sandstone			
	278	RI1-455445	14942	5	4554.45	3	Ravn Mb		Sandy mudstone, bioturbated			
	279	RI1-455671	14949	10	4556.71	3	Ravn Mb		Sandy mudstone, bioturbated			
	280	RI1-455856	14955	11	4558.56	3	Ravn Mb		Sandy mudstone, bioturbated			
	281	RI1-456044	14962	1	4560.44	3	Ravn Mb		Sandy mudstone, bioturbated			
	282	RI1-456202	14967	3	4562.02	4	Lola Fm		Claystone, homogenous			
	283	RI1-456382	14973	2	4563.82	4	Lola Fm		Claystone, homogenous			
	284	RI1-456565	14979	2	4565.65	4	Lola Fm		Claystone, homogenous			
	285	RI1-456740	14984	11	4567.40	4	Lola Fm		Claystone, homogenous			
	286	RI1-453835	14989	7	4568.83	4	Lola Fm		Claystone, homogenous			

Well	Plug No.	ID	Depth (′) top of box	+ Depth (″)	Depth (m)	Cores	Formation/Member	Environ-ment	Lithology	XRF	Zircon	Garnet
	287	RI1-457048	14995	0	4570.48	4	Lola Fm		Claystone, homogenous			
	288	RI1-457246	15001	6	4572.46	4	Lola Fm		Claystone, homogenous			
	289	RI1-457413	15007	0	4574.13	4	Lola Fm		Claystone, homogenous			
	290	RI1-457578	15012	5	4575.78	4	Lola Fm		Carbonate cemented claystone			
	291	RI1-457779	15019	0	4577.79	4	Lola Fm		Claystone, homogenous			
	292	RI1-465023	15256	8	4650.23	5	Gert Mb?		Coarse-grained sandstone, coal frag.			
	293	RI1-465155	15261	0	4651.55	5	Gert Mb?		Claystone, homogeneous			
	294	RI1-465394	15268	10	4653.94	5	Gert Mb?		Medium-grained sandstone, coal frag.			
	295	RI1-465511	15272	8	4655.11	5	Gert Mb?		Laminated clay			
	296	RI1-465681	15278	3	4656.81	5	Gert Mb?		Pyrite cemented conglomerate			
	297	RI1-465869	15284	5	4658.69	5	Gert Mb?		Claystone, homogenous			
	298	RI1-466006	15288	11	4660.06	5	Gert Mb?		Mixed sand and clay lamina			
	299	RI1-466164	15294	1	4661.64	5	Gert Mb?		Claystone, homogenous			
	300	RI1-466413	15302	3	4664.13	6	Gert Mb?		Siltstone - fine-grained sandstone			
	301	RI1-466608	15308	8	4666.08	6	Gert Mb?		Laminated siltstone with sand lamina			
	302	RI1-466651	15310	1	4666.51	6	Gert Mb?		Mixed sand and clay			
	303	RI1-466877	15317	6	4668.77	6	Gert Mb?		Siltstone - fine-grained sandstone			
	304	RI1-467030	15322	6	4670.30	6	Gert Mb?		Clay matrix with cemented sandstone frag.			
	305	RI1-467312	15331	9	4673.12	6	Gert Mb?		Mixed sand and clay lamina			
	306	RI1-467375	15333	10	4673.75	6	Gert Mb?		Siltstone - fine-grained sandstone			
	307	RI1-470736	15444	1	4707.36	8	Pre-Upper Jurassic		Green claystone, homogeneous			
	308	RI1-470903	15449	7	4709.03	8	Pre-Upper Jurassic		White sandstone			
	310	RI1-454442	14909	6	4544.42	3	Ravn Mb		Matrix-supported conglomerate			
	311	RI1-454518	14912	0	4545.18	3	Ravn Mb		Matrix-supported conglomerate			
	312	RI1-454960	14926	6	4549.60	3	Ravn Mb		Calcite-cemented sandstone			

Appendix 1. Core samples

Chemostratigraphy and mineral-chemical fingerprinting, Heno Formation, Danish North Sea

Well	Plug No.	ID	Depth (') top of box	+ Depth (")	Depth (m)	Cores	Formation/Member	Environment	Lithology	XRF	Zircon	Garnet
Ugle-1	250	UG1-305275	3052	75	3052.75	2	Precambrium			x	z	

Well	Plug No.	ID	Depth (') top of box	+ Depth (")	Depth (m)	Cores	Formation/Member	Environment	Lithology	XRF	Zircon	Garnet
P-1	255	P1-349168	11454	50	3491.68	5	Precambrium			x	z	

Appendix 1B. Cuttings samples

Chemostratigraphy and mineral-chemical fingerprinting, Heno Formation, Danish North Sea

Well	No	ID	Depth (′) top	Depth (′) bottom	Depth (m)	Formation/Member
Diamant-1	1	DI1-3808cu	12490	12500	3808	Farsund Fm
	2	DI1-3815cu	12510	12520	3815	Farsund Fm
	3	DI1-3821cu	12530	12540	3821	Farsund Fm
	4	DI1-3827cu	12550	12560	3827	Ravn Mb
	5	DI1-3830cu	12560	12570	3830	Ravn Mb
	6	DI1-3833cu	12570	12580	3833	Ravn Mb
	7	DI1-3836cu	12580	12590	3836	Gert Mb
	8	DI1-3839cu	12590	12600	3839	Gert Mb
	9	DI1-3842cu	12600	12610	3842	Gert Mb
	10	DI1-3845cu	12610	12620	3845	Gert Mb
	11	DI1-3848cu	12620	12630	3848	Gert Mb
	12	DI1-3851cu	12630	12640	3851	Gert Mb
	13	DI1-3854cu	12640	12650	3854	Gert Mb
	14	DI1-3857cu	12650	12660	3857	Gert Mb
	15	DI1-3860cu	12660	12670	3860	Gert Mb
	16	DI1-3863cu	12670	12680	3863	Gert Mb
	17	DI1-3866cu	12680	12690	3866	Gert Mb?
	18	DI1-3869cu	12690	12700	3869	Perm
	19	DI1-3878cu	12710	12720	3876	Perm
	20	DI1-3882cu	12730	12740	3882	Perm

Appendix 1B. Cuttings samples

Chemostratigraphy and mineral-chemical fingerprinting, Heno Formation, Danish North Sea

Well	No	ID	Depth (′) top	Depth (′) bottom	Depth (m)	Formation/Member
Gert-1	1	GE1- 4678cu	15460	15470	4713.73	Farsund Fm
	2	GE1- 4684cu	15480	15490	4719.83	Farsund Fm
	3	GE1- 4690cu	15500	15510	4725.92	Farsund Fm
	4	GE1- 4696cu	15520	15530	4732.02	Ravn Mb
	5	GE1- 4702cu	15540	15550	4738.12	Ravn Mb
	6	GE1- 4708cu	15560	15570	4744.21	Ravn Mb
	7	GE1- 4714cu	15580	15590	4750.31	Ravn Mb
	8	GE1- 4720cu	15600	15610	4756.40	Ravn Mb
	9	GE1- 4727cu	15620	15630	4762.50	Ravn Mb
	10	GE1- 4733cu	15640	15650	4768.60	Ravn Mb
	11	GE1- 4739cu	15660	15670	4774.69	Ravn Mb
	12	GE1- 4745cu	15680	15690	4780.79	Ravn Mb
	13	GE1- 4751cu	15700	15710	4786.88	Ravn Mb
	14	GE1- 4757cu	15720	15730	4792.98	Ravn Mb
	15	GE1- 4763cu	15740	15750	4799.08	Ravn Mb
	16	GE1- 4769cu	15760	15770	4805.17	Lola Fm
	17	GE1- 4775cu	15780	15790	4811.27	Lola Fm
	18	GE1- 4781cu	15800	15810	4817.36	Lola Fm
	19	GE1- 4787cu	15820	15830	4823.46	Lola Fm
	20	GE1- 4793cu	15840	15850	4829.56	Lola Fm
	21	GE1- 4799cu	15860	15870	4835.65	Lola Fm
	22	GE1- 4805cu	15880	15890	4841.75	Lola Fm
	23	GE1- 4811cu	15900	15910	4847.84	Lola Fm
	24	GE1- 4817cu	15920	15930	4853.94	Lola Fm
	25	GE1- 4823cu	15940	15950	4860.04	Lola Fm
	26	GE1- 4829cu	15960	15970	4866.13	Lola Fm
	27	GE1- 4835cu	15980	15990	4872.23	Lola Fm.
	28	GE1- 4841cu	16000	16010	4878.32	Lola Fm
	29	GE1- 4845cu	16010	16020	4881.37	Lola Fm

Well	No	ID	Depth (′) top	Depth (′) bottom	Depth (m)	Formation/Member
	30	GE1- 4851cu	16030	16040	4887.47	Gert Mb
	31	GE1- 4857cu	16050	16060	4893.56	Gert Mb
	32	GE1- 4863cu	16070	16080	4899.66	Gert Mb
	33	GE1- 4866cu	16080	16090	4902.71	Gert Mb
	34	GE1- 4872cu	16100	16110	4908.80	Gert Mb
	35	GE1- 4878cu	16120	16130	4914.90	Gert Mb
	36	GE1- 4884cu	16140	16150	4921.00	Gert Mb
	37	GE1- 4890cu	16160	16170	4927.09	Gert Mb
	38	GE1- 4896cu	16180	16190	4933.19	Gert Mb
	39	GE1- 4902cu	16200	16210	4939.28	Gert Mb
	40	GE1- 4908cu	16220	16230	4945.38	Gert Mb
	41	GE1- 4914cu	16240	16250	4951.48	Gert Mb
	42	GE1- 4920cu	16260	16270	4957.57	Gert Mb
	43	GE1- 4926cu	16280	16290	4963.67	Gert Mb
	44	GE1- 4932cu	16300	16310	4969.76	Gert Mb
	45	GE1- 4938cu	16320	16330	4975.86	Permian
	46	GE1- 4944cu	16340	16350	4981.96	Permian
	47	GE1- 4950cu	16360	16370	4988.05	Permian
	48	GE1- 4956cu	16380	16390	4994.15	Permian

Appendix 1B. Cuttings samples

Chemostratigraphy and mineral-chemical fingerprinting, Heno Formation, Danish North Sea

Well	No	ID	Depth (′) top	Depth (′) bottom	Depth (m)	Formation/Member
Gert-4	1	GE4-5698cu	18690	18700	5698	Farsund Fm
	2	GE4-5710cu	18730	18740	5710	Farsund Fm
	3	GE4-5717cu	18750	18760	5717	Farsund Fm
	4	GE4-5723cu	18770	18780	5723	Farsund Fm
	5	GE4-5729cu	18790	18800	5729	Farsund Fm
	6	GE4-5735cu	18810	18820	5735	Farsund Fm
	7	GE4-5741cu	18830	18840	5741	Farsund Fm
	8	GE4-5747cu	18850	18860	5747	Farsund Fm
	9	GE4-5753cu	18870	18880	5753	Ravn Mb
	10	GE4-5759cu	18890	18900	5759	Ravn Mb
	11	GE4-5765cu	18910	18920	5765	Ravn Mb
	12	GE4-5771cu	18930	18940	5771	Ravn Mb
	13	GE4-5777cu	18950	18960	5777	Ravn Mb
	14	GE4-5787cu	18980	18990	5787	Ravn Mb
	15	GE4-5793cu	19000	19010	5793	Ravn Mb
	16	GE4-5799cu	19020	19030	5799	Ravn Mb
	17	GE4-5805cu	19040	19050	5805	Ravn Mb?
	18	GE4-5811cu	19060	19070	5811	Ravn Mb?
	19	GE4-5817cu	19080	19090	5817	Ravn Mb?
	20	GE4-5823cu	19100	19110	5823	Ravn Mb?
	21	GE4-5829cu	19120	19130	5829	Ravn Mb?
	22	GE4-5835cu	19140	19150	5835	Lola Fm
	23	GE4-5841cu	19160	19170	5841	Lola Fm
	24	GE4-5848cu	19180	19190	5848	Lola Fm
	25	GE4-5854cu	19200	19210	5854	Lola Fm
	26	GE4-5860cu	19220	19230	5860	Lola Fm
	27	GE4-5866cu	19240	19250	5866	Lola Fm
	28	GE4-5872cu	19260	19270	5872	Lola Fm
	29	GE4-5878cu	19280	19290	5878	Lola Fm

Well	No	ID	Depth (′) top	Depth (′) bottom	Depth (m)	Formation/Member
	30	GE4-5884cu	19300	19310	5884	Lola Fm
	31	GE4-5890cu	19320	19330	5890	Lola Fm
	32	GE4-5896cu	19340	19350	5896	Lola Fm
	33	GE4-5902cu	19360	19370	5902	Lola Fm
	34	GE4-5909cu	19380	19390	5909	Lola Fm
	35	GE4-5915cu	19400	19410	5915	Lola Fm
	36	GE4-5921cu	19420	19430	5921	Lola Fm
	37	GE4-5927cu	19440	19450	5927	Lola Fm
	38	GE4-5933cu	19460	19470	5933	Lola Fm
	39	GE4-5936cu	19470	19480	5936	Lola Fm
	40	GE4-5942cu	19490	19500	5942	Lola Fm
	41	GE4-5948cu	19510	19520	5948	Lola Fm
	42	GE4-5954cu	19530	19540	5954	Lola Fm
	43	GE4-5960cu	19550	19560	5960	Lola Fm
	44	GE4-5966cu	19570	19580	5966	Lola Fm
	45	GE4-5973cu	19590	19600	5973	Lola Fm
	46	GE4-5979cu	19610	19620	5979	Lola Fm
	47	GE4-5985cu	19630	19640	5985	Lola Fm
	48	GE4-5991cu	19650	19660	5991	Lola Fm
	49	GE4-5997cu	19670	19680	5997	Gert Mb?
	50	GE4-6003cu	19690	19700	6003	Gert Mb
	51	GE4-6009cu	19710	19720	6009	Gert Mb
	52	GE4-6015cu	19730	19740	6015	Gert Mb
	53	GE4-6021cu	19750	19760	6021	Gert Mb
	54	GE4-6027cu	19770	19780	6027	Gert Mb
	55	GE4-6034cu	19790	19800	6034	Gert Mb
	56	GE4-6040cu	19810	19820	6040	Gert Mb
	57	GE4-6046cu	19830	19840	6046	Gert Mb
	58	GE4-6052cu	19850	19860	6052	Gert Mb
	59	GE4-6058cu	19870	19880	6058	Gert Mb
	60	GE4-6064cu	19890	19900	6064	Gert Mb
	61	GE4-6070cu	19910	19920	6070	Gert Mb
	62	GE4-6076cu	19930	19940	6076	Perm?

Well	No	ID	Depth (′) top	Depth (′) bottom	Depth (m)	Formation/Member
	63	GE4-6082cu	19950	19960	6082	Perm?
	64	GE4-6088cu	19970	19980	6088	Perm?
	65	GE4-6094cu	19990	20000	6094	Perm?
	66	GE4-6101cu	20010	20020	6101	Perm?

Appendix 1B. Cuttings samples

Chemostratigraphy and mineral-chemical fingerprinting, Heno Formation, Danish North Sea

Well	No	ID	Depth (′) top	Depth (′) bottom	Depth (m)	Formation/Member
Gwen-2	1	GW2- 4176cu	13800	13810	4207.76	Farsund Fm
	2	GW2- 4182cu	13820	13830	4213.86	Farsund Fm
	3	GW2- 4188cu	13840	13850	4219.96	Ravn Mb
	4	GW2- 4194cu	13860	13870	4226.05	Ravn Mb
	5	GW2- 4200cu	13890	13890	4233.67	Ravn Mb
	6	GW2- 4206cu	13900	13910	4238.24	Ravn Mb
	7	GW2- 4225cu	13960	13970	4256.53	Ravn Mb
	8	GW2- 4228cu	13970	13980	4259.58	Ravn Mb
	9	GW2- 4243cu	14020	14030	4274.82	Ravn Mb
	10	GW2- 4246cu	14030	14040	4277.87	Ravn Mb
	11	GW2- 4252cu	14050	14060	4283.96	Ravn Mb
	12	GW2- 4261cu	14080	14090	4293.11	Lola Fm
	13	GW2- 4267cu	14100	14110	4299.20	Lola Fm
	14	GW2- 4273cu	14120	14130	4305.30	Lola Fm
	15	GW2- 4279cu	14140	14150	4311.40	Lola Fm
	16	GW2- 4285cu	14160	14170	4317.49	Lola Fm
	17	GW2- 4291cu	14180	14190	4323.59	Lola Fm
	18	GW2- 4297cu	14200	14210	4329.68	Lola Fm
	19	GW2- 4303cu	14220	14230	4335.78	Lola Fm
	20	GW2- 4309cu	14240	14250	4341.88	Lola Fm
	21	GW2- 4315cu	14260	14270	4347.97	Lola Fm
	22	GW2- 4321cu	14280	14290	4354.07	Triassic

Appendix 1B. Cuttings samples

Chemostratigraphy and mineral-chemical fingerprinting, Heno Formation, Danish North Sea

Well	No	ID	Depth (m) top interval	Depth (m) bottom interval	Depth (m)	Formation/Member
Hejre-1	1	HE1-5071cu	5069	5072	5071	Farsund Fm
	2	HE1-5077cu	5075	5078	5077	Farsund Fm
	3	HE1-5083cu	5081	5084	5083	Farsund Fm
	4	HE1-5089cu	5087	5090	5089	Farsund Fm
	5	HE1-5098cu	5096	5099	5098	Ravn Mb
	6	HE1-5104cu	5102	5105	5104	Ravn Mb
	7	HE1-5107cu	5105	5108	5107	Ravn Mb
	8	HE1-5110cu	5108	5111	5110	Ravn Mb
	9	HE1-5113cu	5111	5114	5113	Lola Fm?
	10	HE1-5116cu	5114	5117	5116	Lola Fm?
	11	HE1-5119cu	5117	5120	5119	Gert Mb?
	12	HE1-5123cu	5120	5126	5123	Gert Mb?
	13	HE1-5136cu	5126	5145	5136	Gert Mb?
	14	HE1-5147cu	5145	5148	5147	Gert Mb?
	15	HE1-5150cu	5148	5151	5150	Carbon?
	16	HE1-5153cu	5151	5154	5153	Carbon?
	17	HE1-5156cu	5154	5157	5156	Carbon?
	18	HE1-5159cu	5157	5160	5159	Carbon?
	19	HE1-5162cu	5160	5163	5162	Carbon?
	20	HE1-5165cu	5163	5166	5165	Carbon?
	21	HE1-5168cu	5166	5169	5168	Carbon?

Appendix 1B. Cuttings samples

Chemostratigraphy and mineral-chemical fingerprinting, Heno Formation, Danish North Sea

Well	No	ID	Depth (m) top interval	Depth (m) bottom interval	Depth (m)	Formation/Member
Hejre-2	1	HE2-5345cu	5343	5346	5345	Farsund Fm
5603/28-5	2	HE2-5351cu	5349	5352	5351	Farsund Fm
	3	HE2-5357cu	5355	5358	5357	Farsund Fm
	4	HE2-5363cu	5361	5364	5363	Ravn Mb
	5	HE2-5366cu	5364	5367	5366	Ravn Mb
	6	HE2-5369cu	5367	5370	5369	Ravn Mb
	7	HE2-5372cu	5370	5373	5372	Lola Fm
	8	HE2-5375cu	5373	5376	5375	Lola Fm
	9	HE2-5378cu	5376	5379	5378	Lola Fm
	10	HE2-5381cu	5379	5382	5381	Gert Mb (Upper)
	11	HE2-5384cu	5382	5385	5384	Gert Mb (Upper)
	12	HE2-5387cu	5385	5388	5387	Gert Mb? (Upper)
	13	HE2-5390cu	5388	5391	5390	Gert Mb (Upper)
	14	HE2-5393cu	5391	5394	5393	Gert Mb (Upper)
	15	HE2-5396cu	5394	5397	5396	Gert Mb (Upper)
	16	HE2-5399cu	5397	5400	5399	Gert Mb (Upper)
	17	HE2-5402cu	5400	5403	5402	Gert Mb Lower
	18	HE2-5405cu	5403	5406	5405	Gert Mb Lower
	19	HE2-5408cu	5406	5409	5408	Gert Mb Lower
	20	HE2-5411cu	5409	5412	5411	Gert Mb Lower
	21	HE2-5414cu	5412	5415	5414	Pre-Upper Jurassic
	22	HE2-5417cu	5415	5418	5417	Pre-Upper Jurassic
	23	HE2-5420cu	5418	5421	5420	Pre-Upper Jurassic
	24	HE2-5423cu	5421	5424	5423	Pre-Upper Jurassic
	25	HE2-5426cu	5424	5427	5426	Pre-Upper Jurassic
	26	HE2-5429cu	5427	5430	5429	Pre-Upper Jurassic
	27	HE2-5432cu	5430	5433	5432	Pre-Upper Jurassic
	28	HE2-5435cu	5433	5436	5435	Pre-Upper Jurassic

Well	No	ID	Depth (m) top interval	Depth (m) bottom interval	Depth (m)	Formation/Member
	29	HE2-5438cu	5436	5439	5438	Pre-Upper Jurassic
	30	HE2-5441cu	5439	5442	5441	Pre-Upper Jurassic
	31	HE2-5444cu	5442	5445	5444	Pre-Upper Jurassic

Appendix 1B.   Cuttings samples

Chemostratigraphy and mineral-chemical fingerprinting, Heno Formation, Danish North Sea

Well	No	ID	Depth (') top	Depth (') bottom	Depth (m)	Formation/Member
Jeppe-1	1	JE1- 4885cu			4885	Farsund Fm
5603/28-3	2	JE1- 4890cu			4890	Farsund Fm
	3	JE1- 4895cu			4895	Farsund Fm
	4	JE1- 4900cu			4900	Farsund Fm
	5	JE1- 4905cu			4905	Farsund Fm
	6	JE1- 4910cu			4910	Farsund Fm
	7	JE1- 4915cu			4915	Farsund Fm
	8	JE1- 4920cu			4920	Farsund Fm
	9	JE1- 4925cu			4925	Farsund Fm
	10	JE1- 4930cu			4930	Farsund Fm
	11	JE1- 4935cu			4935	Farsund Fm
	12	JE1- 4940cu			4940	Ravn Mb
	13	JE1- 4945cu			4945	Ravn Mb
	14	JE1- 4955cu			4955	Ravn Mb
	15	JE1- 4960cu			4960	Ravn Mb
	16	JE1- 4965cu			4965	Ravn Mb
	17	JE1- 4967cu			4967	Ravn Mb
	18	JE1- 4975cu			4975	Ravn Mb
	19	JE1- 4977cu			4977	Ravn Mb
	20	JE1- 4982cu			4982	Ravn Mb
	21	JE1- 4992cu			4992	Ravn Mb
	22	JE1- 4995cu			4995	Ravn Mb
	23	JE1- 5000cu			5000	Ravn Mb
	24	JE1- 5005cu			5005	Gert Mb
	25	JE1- 5010cu			5010	Gert Mb
	26	JE1- 5015cu			5015	Gert Mb
	27	JE1- 5020cu			5020	Gert Mb

Appendix 1B. Cuttings samples

Chemostratigraphy and mineral-chemical fingerprinting, Heno Formation, Danish North Sea

Well	No	ID	Depth (′) top	Depth (′) bottom	Depth (m)	Formation/Member
Rita-1	1	RI1-3796cu	12450	12460	3796	Farsund Fm
	2	RI1-3802cu	12470	12480	3802	Farsund Fm
	3	RI1-3808cu	12490	12500	3808	Farsund Fm
	4	RI1-3815cu	12510	12520	3815	Farsund Fm
	5	RI1-3821cu	12530	12540	3821	Farsund Fm
	6	RI1-3827cu	12550	12560	3827	Farsund Fm
	7	RI1-3833cu	12570	12580	3833	Farsund Fm
	8	RI1-3839cu	12590	12600	3839	Farsund Fm
	9	RI1-3845cu	12610	12620	3845	Farsund Fm
	10	RI1-3851cu	12630	12640	3851	Farsund Fm
	11	RI1-3857cu	12650	12660	3857	Farsund Fm
	12	RI1-3863cu	12670	12680	3863	Farsund Fm
	13	RI1-3869cu	12690	12700	3869	Farsund Fm
	14	RI1-3876cu	12710	12720	3876	Farsund Fm
	15	RI1-3882cu	12730	12740	3882	Farsund Fm
	16	RI1-3888cu	12750	12760	3888	Farsund Fm
	17	RI1-3894cu	12770	12780	3894	Farsund Fm
	18	RI1-3900cu	12790	12800	3900	Farsund Fm
	19	RI1-3906cu	12810	12820	3906	Farsund Fm
	20	RI1-3912cu	12830	12840	3912	Farsund Fm
	21	RI1-3918cu	12850	12860	3918	Farsund Fm
	22	RI1-3924cu	12870	12880	3924	Farsund Fm
	23	RI1-3930cu	12890	12900	3930	Farsund Fm
	24	RI1-3936cu	12910	12920	3936	Farsund Fm
	25	RI1-3943cu	12930	12940	3943	Farsund Fm
	26	RI1-3952cu	12960	12970	3952	Farsund Fm
	27	RI1-3958cu	12980	12990	3958	Farsund Fm
	28	RI1-3964cu	13000	13010	3964	Farsund Fm
	29	RI1-3970cu	13020	13030	3970	Farsund Fm

Well	No	ID	Depth (') top	Depth (') bottom	Depth (m)	Formation/Member
	30	RI1-3976cu	13040	13050	3976	Farsund Fm
	31	RI1-3982cu	13060	13070	3982	Farsund Fm
	32	RI1-3988cu	13080	13090	3988	Farsund Fm
	33	RI1-3994cu	13100	13110	3994	Farsund Fm
	34	RI1-4001cu	13120	13130	4001	Farsund Fm
	35	RI1-4007cu	13140	13150	4007	Farsund Fm
	36	RI1-4013cu	13160	13170	4013	Farsund Fm
	37	RI1-4019cu	13180	13190	4019	Farsund Fm
	38	RI1-4025cu	13200	13210	4025	Farsund Fm
	39	RI1-4031cu	13220	13230	4031	Farsund Fm
	40	RI1-4037cu	13240	13250	4037	Farsund Fm
	41	RI1-4043cu	13260	13270	4043	Farsund Fm
	42	RI1-4049cu	13280	13290	4049	Farsund Fm
	43	RI1-4058cu	13310	13320	4058	Farsund Fm
	44	RI1-4065cu	13330	13340	4065	Farsund Fm
	45	RI1-4071cu	13350	13360	4071	Farsund Fm
	46	RI1-4077cu	13370	13380	4077	Farsund Fm
	47	RI1-4083cu	13390	13400	4083	Farsund Fm
	48	RI1-4089cu	13410	13420	4089	Farsund Fm
	49	RI1-4095cu	13430	13440	4095	Farsund Fm
	50	RI1-4101cu	13450	13460	4101	Farsund Fm
	51	RI1-4107cu	13470	13480	4107	Farsund Fm
	52	RI1-4113cu	13490	13500	4113	Farsund Fm
	53	RI1-4119cu	13510	13520	4119	Farsund Fm
	54	RI1-4125cu	13530	13540	4125	Farsund Fm
	55	RI1-4132cu	13550	13560	4132	Farsund Fm
	56	RI1-4455cu	14610	14620	4455	Farsund Fm
	57	RI1-4473cu	14670	14680	4473	Farsund Fm
	58	RI1-4485cu	14710	14720	4485	Farsund Fm
	59	RI1-4497cu	14750	14760	4497	Farsund Fm
	60	RI1-4503cu	14770	14780	4503	Farsund Fm
	61	RI1-4610cu	14790	14800	4510	Farsund Fm
	62	RI1-4516cu	14810	14820	4516	Farsund Fm

Well	No	ID	Depth (′) top	Depth (′) bottom	Depth (m)	Formation/Member
	63	RI1-4522cu	14830	14840	4522	Ravn Mb
	64	RI1-4528cu	14850	14860	4528	Ravn Mb
	65	RI1-4534cu	14870	14880	4534	Ravn Mb
	66	RI1-4543cu	14900	14910	4543	Ravn Mb
	67	RI1-4549cu	14920	14930	4549	Ravn Mb
	68	RI1-4555cu	14940	14950	4555	Ravn Mb
	69	RI1-4561cu	14960	14970	4561	Ravn Mb
	70	RI1-4570cu	14990	15000	4570	Lola Fm?
	71	RI1-4577cu	15010	15020	4577	Lola Fm?
	72	RI1-4583cu	15030	15040	4583	Lola Fm?
	73	RI1-4589cu	15050	15060	4589	Lola Fm?
	74	RI1-4595cu	15070	15080	4595	Lola Fm?
	75	RI1-4601cu	15090	15100	4601	Lola Fm?
	76	RI1-4607cu	15110	15120	4607	Lola Fm?
	77	RI1-4613cu	15130	15140	4613	Lola Fm?
	78	RI1-4619cu	15150	15160	4619	Lola Fm?
	79	RI1-4625cu	15170	15180	4625	Lola Fm?
	80	RI1-4638cu	15210	15220	4638	Gert Mb?
	81	RI1-4644cu	15230	15240	4644	Gert Mb?
	82	RI1-4650cu	15250	15260	4650	Gert Mb?
	83	RI1-4656cu	15270	15280	4656	Gert Mb?
	84	RI1-4662cu	15290	15300	4662	Gert Mb?
	85	RI1-4668cu	15310	15320	4668	Gert Mb?
	86	RI1-4674cu	15330	15340	4674	Gert Mb?
	87	RI1-4680cu	15350	15360	4680	Gert Mb?
	88	RI1-4686cu	15370	15380	4686	Gert Mb?
	89	RI1-4692cu	15390	15400	4692	Gert Mb?
	90	RI1-4698cu	15410	15420	4698	Pre-Upper Jurassic
	91	RI1-4702cu	15430	15440	4705	Pre-Upper Jurassic
	92	RI1-4711cu	15450	15460	4711	Pre-Upper Jurassic
	93	RI1-4717cu	15470	15480	4717	Pre-Upper Jurassic
	94	RI1-4729cu	15510	15520	4729	Pre-Upper Jurassic

Appendix 2. Geochemical logs of selected wells

Chemostratigraphy and mineral-chemical fingerprinting, Heno Formation, Danish North Sea

The following legend has been used in the selected geochemical logs:

- Farsund Fm (cuttings)
- Farsund Fm (cores)
- Ravn Mb (cuttings)
- Ravn Mb (cores)
- Lola Fm (cuttings)
- Lola Fm (cores)
- Gert Mb (cuttings)
- Gert Mb (cores)
- Gert Mb Lower (cuttings)
- Carboniferous (cores)
- Carboniferous (cuttings)
- Triassic or Pre-Jurassic (cores)
- Triassic or Pre-Jurassic (cuttings)
- Permian (cores)
- Permian (cuttings)

Colour code on the Gamma-ray logs reflects the depositional environment (according to the definition by Johannessen, 2003), green = back-barrier sediments, yellow = middle-upper shoreface sandstone, brown = lower shoreface clayey sandstone.

Cored intervals are marked with bars on the Gamma-ray log (GR); and zircon and garnet samples are indicated next to the bars by either squares or triangles.

Appendix 2. Geochemical logs of selected wells

Chemostratigraphy and mineral-chemical fingerprinting, Heno Formation, Danish North Sea

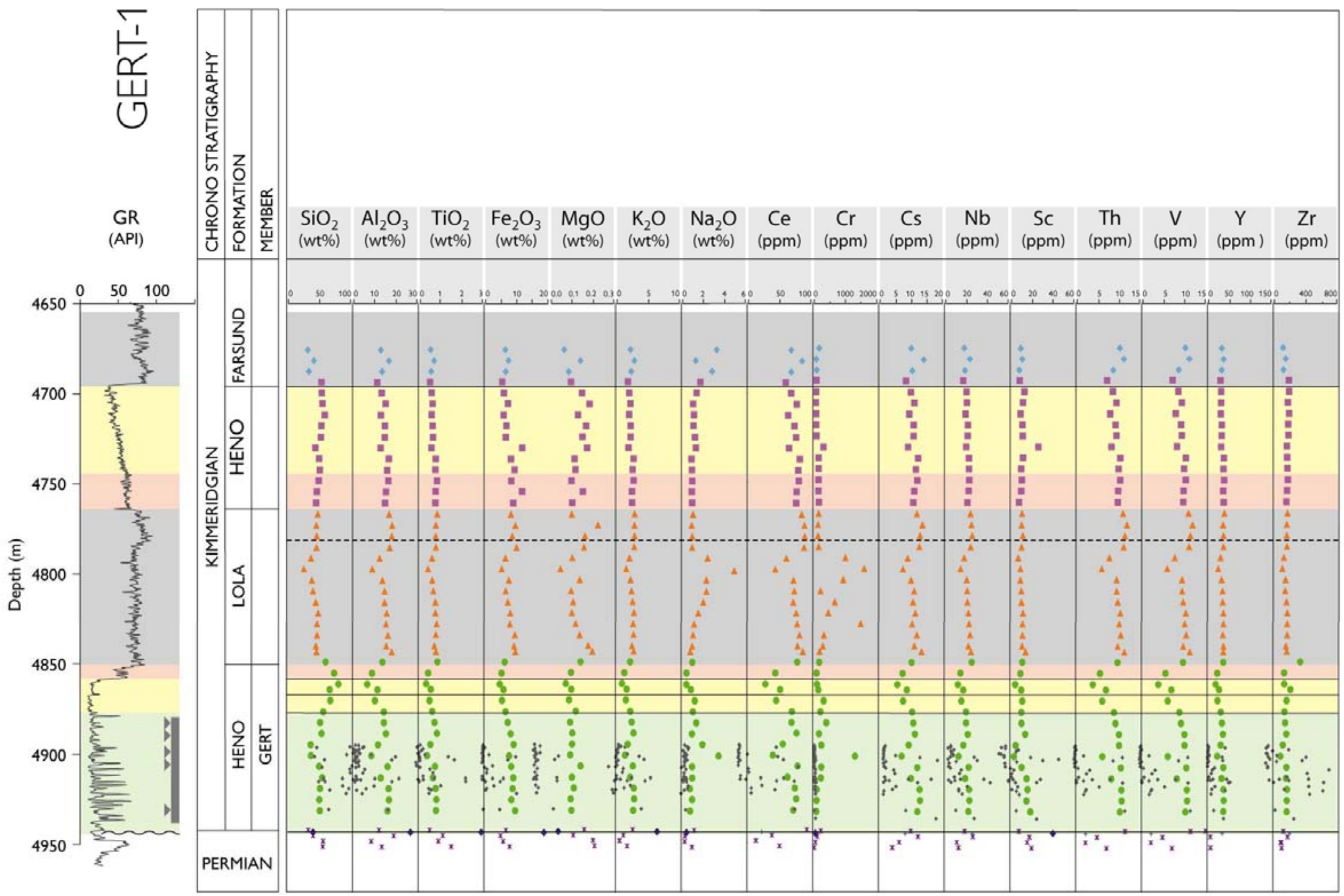

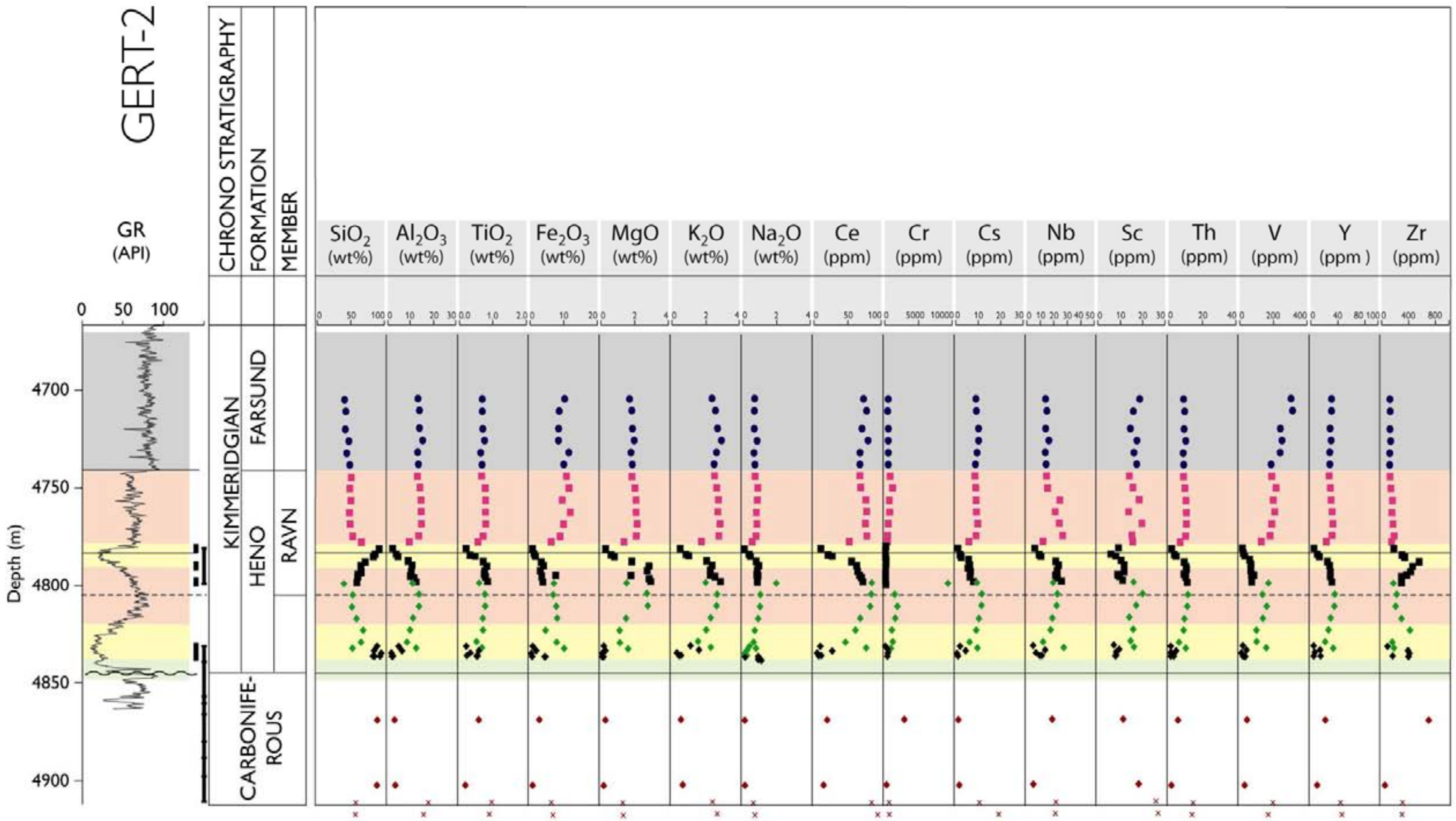
GERT-2
GR (API)
0 50 100
Depth (m)
4700
4750
4800
4850
4900
CHRONO STRATIGRAPHY
FORMATION
MEMBER
KIMMERIDGIAN
FARSUND
HENO
RAVN
CARBONIFE-ROUS
SiO2 (wt%)
Al2O3 (wt%)
TiO2 (wt%)
Fe2O3 (wt%)
MgO (wt%)
K2O (wt%)
Na2O (wt%)
Ce (ppm)
Cr (ppm)
Cs (ppm)
Nb (ppm)
Sc (ppm)
Th (ppm)
V (ppm)
Y (ppm)
Zr (ppm)

Appendix 2. Geochemical logs of selected wells

Chemostratigraphy and mineral-chemical fingerprinting, Heno Formation, Danish North Sea

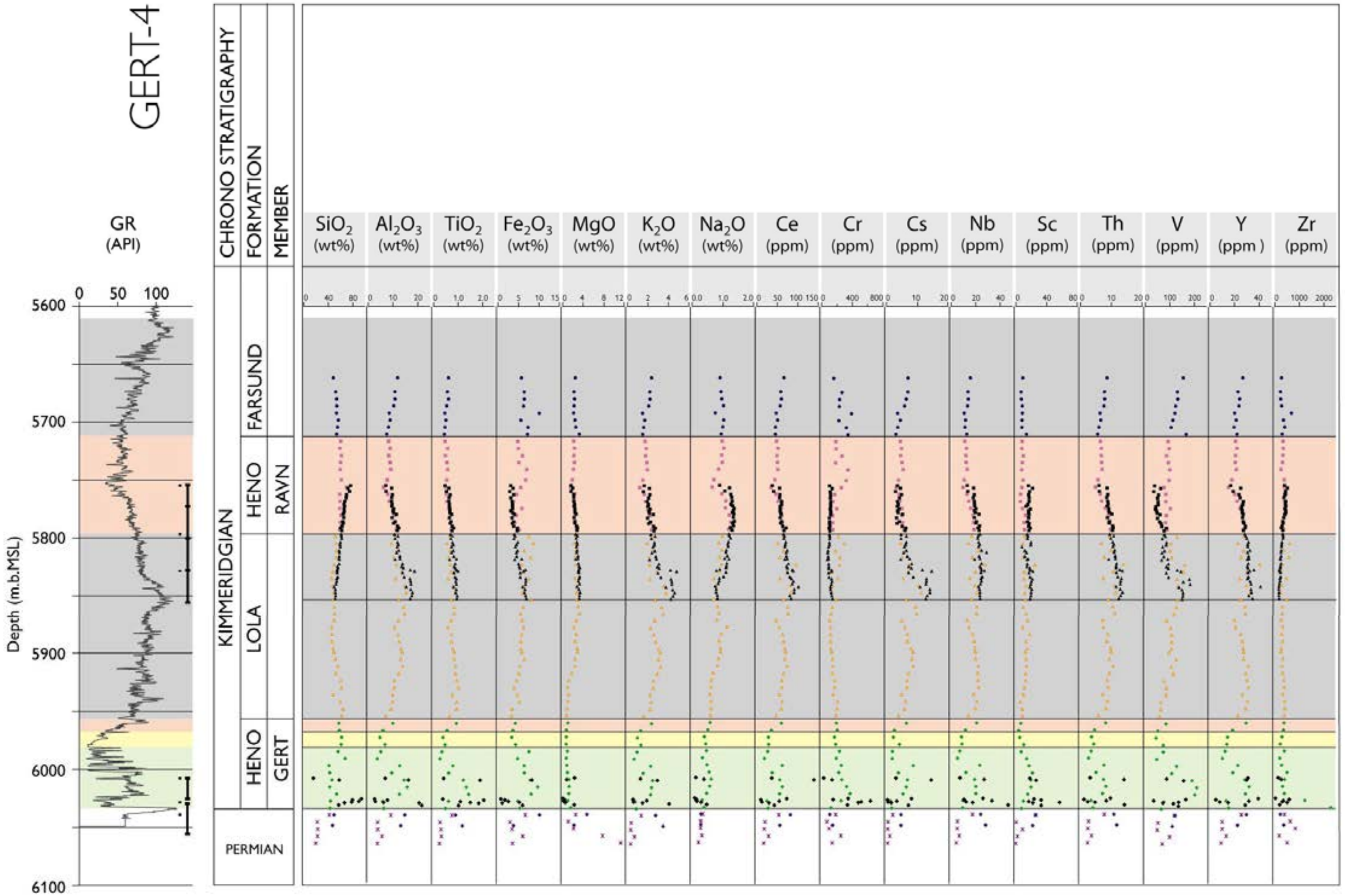

Appendix 2. Geochemical logs of selected wells

Chemostratigraphy and mineral-chemical fingerprinting, Heno Formation, Danish North Sea

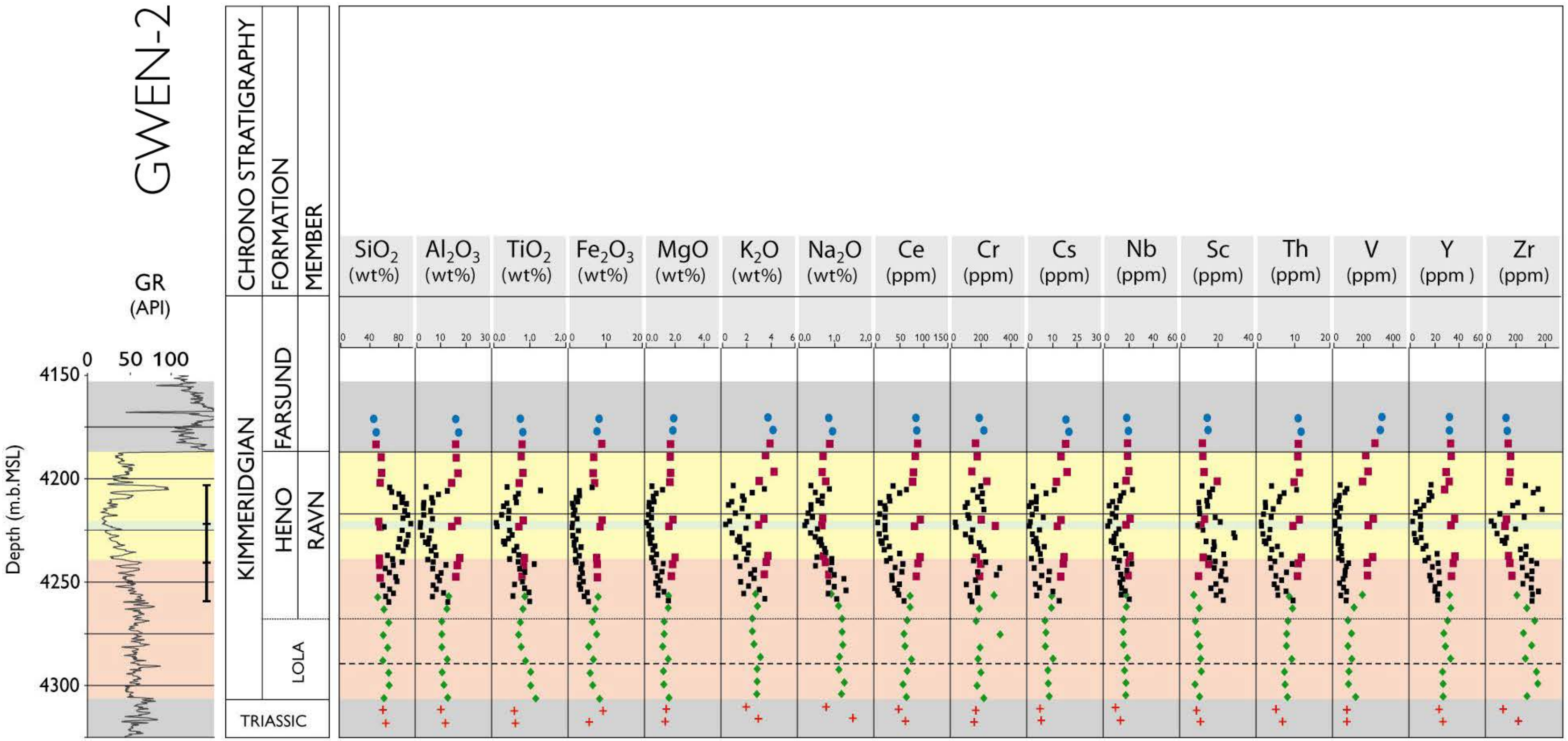

Appendix 2. Geochemical logs of selected wells

Chemostratigraphy and mineral-chemical fingerprinting, Heno Formation, Danish North Sea

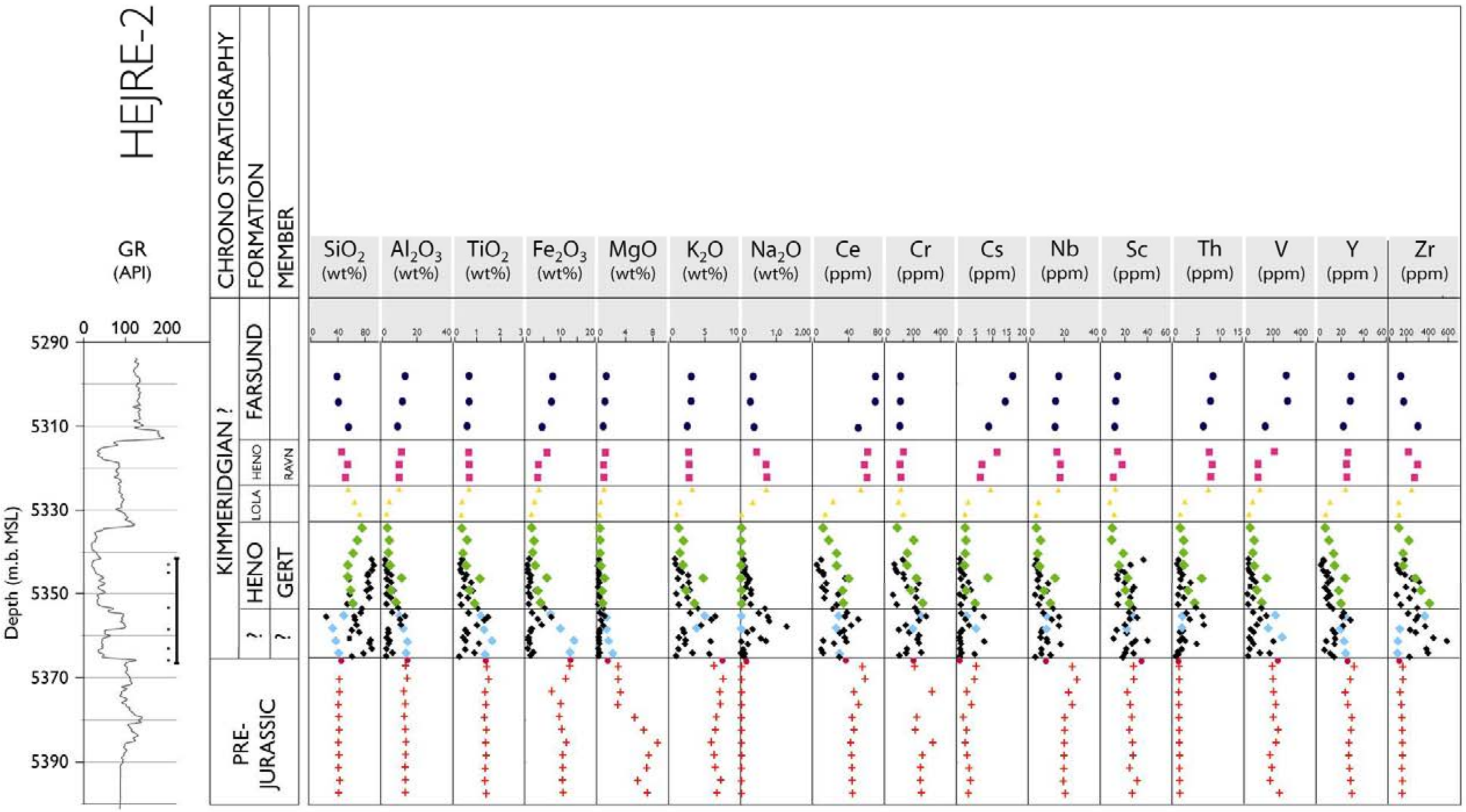

Appendix 2. Geochemical logs of selected wells

Chemostratigraphy and mineral-chemical fingerprinting, Heno Formation, Danish North Sea

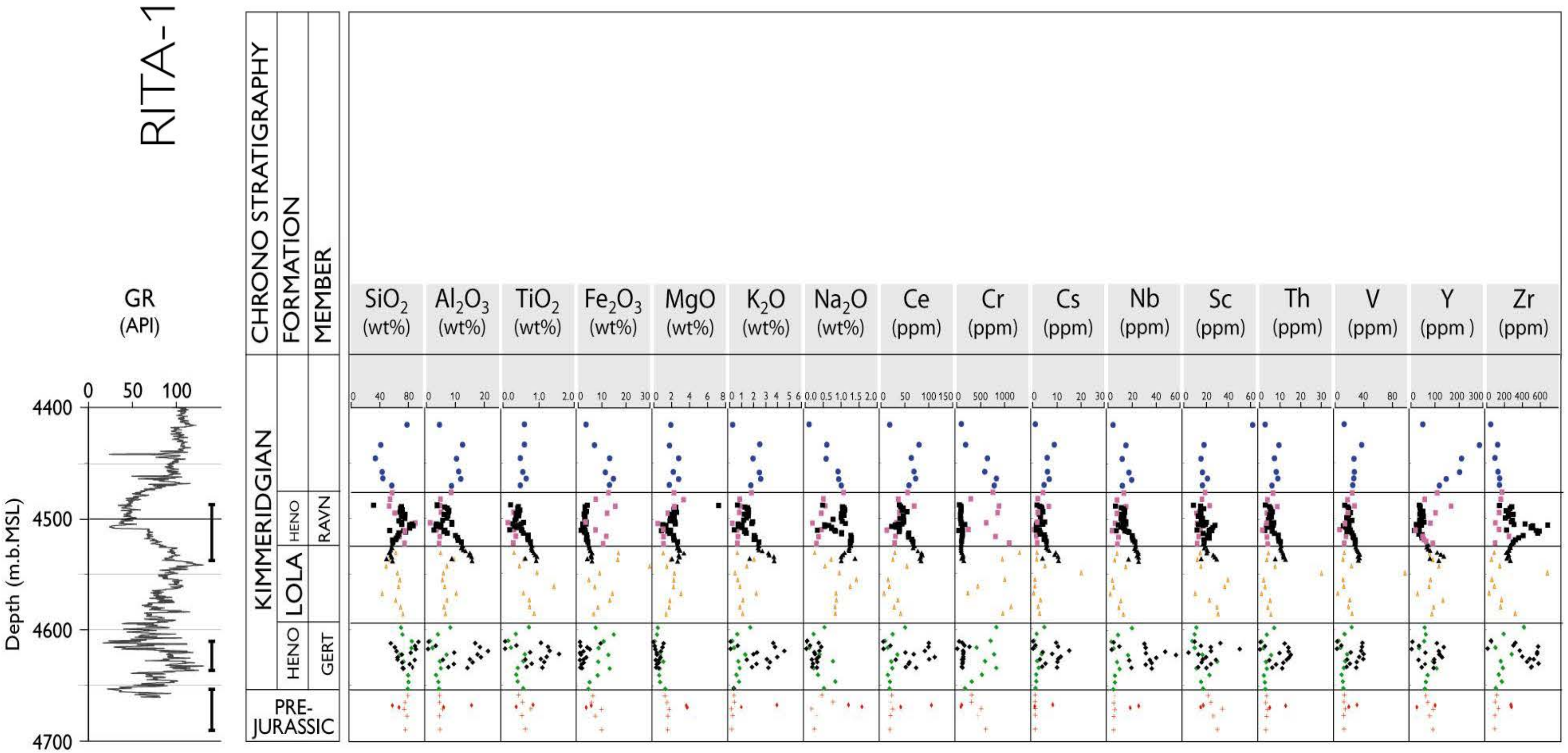

Multivariate analysis of core samples

Preliminary multivariate analyses of core and cuttings samples show that they always group differently even when within the same formation or member. The first multivariate analyses are therefore performed on core samples in order to find out if the different formations and members are distinguishable from each other. All samples with a CaO-content above 10 wt% are excluded from the analyses. CaO, volatiles and phosphorus are not included in the model.

Gert Member

The first Gert Member model is based on data from the three Gert wells. One sample outlier: GE4-604450 is removed from the model. The Ravn Member data from all investigated wells is projected on the Gert Member model and show a fine separation of the two dataset (Fig. 1). Only a few Ravn Member samples lie within the limit of the Gert model (GE2-481775, DI1-383596, DI1-383797, GW2-424856, GW2-425087, GW2-425250, GW2-425478, GW2-425846, GW2-426400, JE1-493720, JE1-494202, JE1-494374). Separation of the Ravn data set from the Gert model seems to be based mainly on higher Na_2O, MnO, Al_2O_3, K_2O, MgO, Rb, Cs and lower content of Ni, Cu and SiO_2 (Fig. 2).

The Heno Formation in Hejre-2 is divided into three sand layers, the pronounced Lower Gert Member (the lowermost cored sand layer), Gert Member (the middle cored sand layer) and Ravn Member (the uppermost not-cored sand layer). Each of the cored sand layers are compared with the Gert Member model based on the three Gert wells. The Gert Member in Hejre-2 fits well with the model of the Gert Member based on the three Gert wells (Fig. 3). Three outliers from this model are the deepest samples of the Hejre-2 Gert Member (in the middle sand layer). The lower Gert Member sand layer in Hejre-2 resembles the Gert Member model based on the Gert wells (Fig. 4), but there are too few non-calcite-cemented samples for a thorough comparison. The Lower Gert Member in Hejre-2 has no samples, which lie within the Ravn Member model.

The lower sand layer, i.e. the possible Gert Member in Rita-1, has been compared with the Gert Member model based on the three Gert wells. Generally Gert Member in Rita-1 fits well with the Gert Member model (Fig. 5). Some outliers, though, occur (RI1-465155, RI1-465681, RI1-467030) which may mainly be due to an increased Na_2O content. The Gert Member in Rita-1 is significantly different from the Ravn Member.

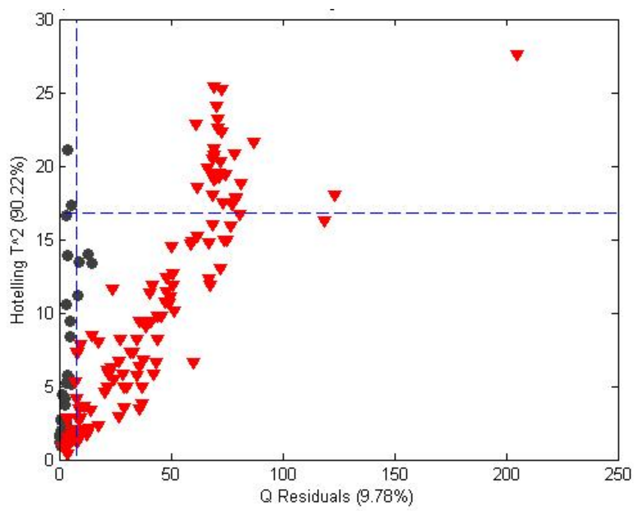

Figure 1. *Ravn Member data (red triangles) projected on the Gert Member model which was based on the three Gert wells (black dots). Hotelling T^2 and Q residuals show a well defined model. Dashed lines show the 95 % confidence limit. A few Ravn Member samples lie within the Gert Member model.*

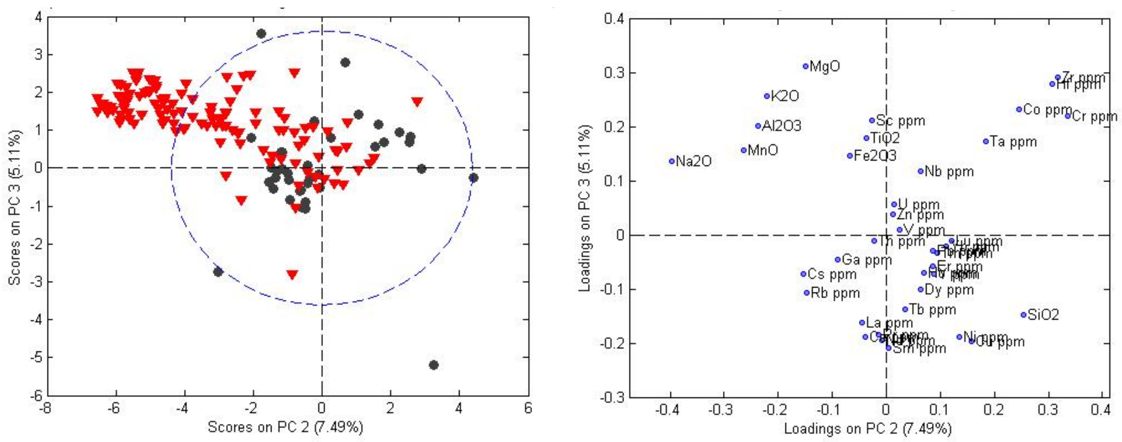

Figure 2. *Ravn Member data (red triangles) projected on the Gert Member model that was based on the three Gert wells (black dots). Scores and loadings from principal components 1 and 2.*

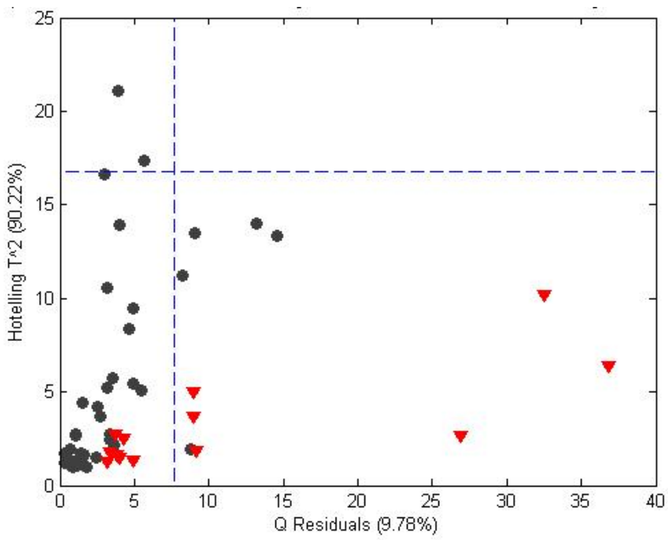

Figure 3. *Gert Member in Hejre-2 (red triangles) projected on the Gert Member model that was based on the three Gert wells (black dots). Hotelling T^2 and Q residuals show a well defined model. Dashed lines show the 95 % confidence limit. The Gert Member in Hejre-2 has several samples within the Gert Member model, but also three outliers.*

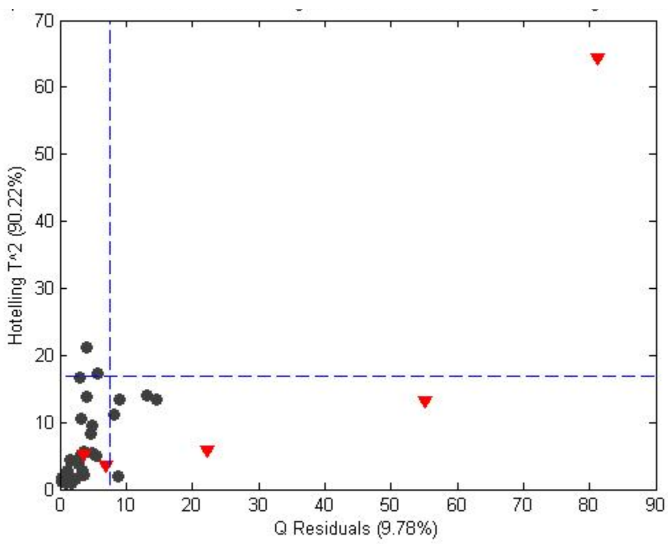

Figure 4. *Lower Gert Member in Hejre-2 (red triangles) projected on the Gert Member model that was based on the three Gert wells (black dots). Hotelling T^2 and Q residuals show a well defined model. Dashed lines show the 95 % confidence limit.*

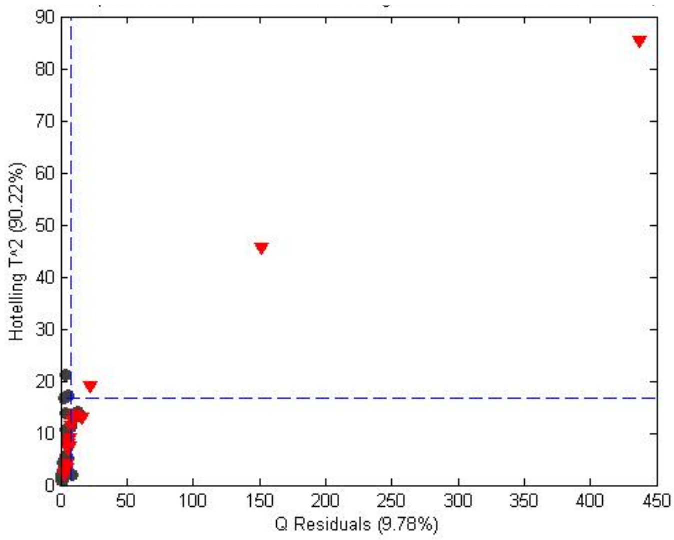

Figure 5. *The possible Gert Member in Rita-1 (red triangles) projected on the Gert Member model that was based on the three Gert wells (black dots). Hotelling T^2 and Q residuals show a well defined model. Dashed lines show the 95 % confidence limit.*

Ravn Member

The Ravn Member model is based on all Ravn Member samples from all the investigated wells. The following outliers were removed from the model: DI1-383482, DI1-383510. Gert Member data from the three Gert wells were projected on the Ravn model and shows a fairly good separation (Fig. 6). Few Gert samples lie within the limits of the Ravn model: GE1-492575, GE1-493705, GE1-495425, GE1-495805, GE1-496770, GE2-486835. Separation of the Gert Member data set based on the three Gert wells from the Ravn model based on all wells occurs on several parameters (loadings) and as such is difficult to show by comparing principal components. Gert data is characterised by higher Cs, TiO_2, V, Cr and Rb and lower Zr and Hf than the Ravn Member model (Fig. 7). Pb seems to be higher and Sc lower for Gert Member data than for the Ravn Member model.

The Gert Member from the Hejre-2 well compared with the Ravn Member shows some outliers, three of which are similar to the outliers when the Gert Member in the Hejre-2 well is compared with the Gert Member model that is based on the three Gert wells (Fig. 8). These samples include the four deepest samples and the top sample in Gert Member in the Hejre-2 well (HE2-537822, HE2-538986, HE2-539098, HE2-539186, HE2-539256). The Gert Member in the Hejre-2 well can therefore geochemically be related to both the Gert and Ravn Member.

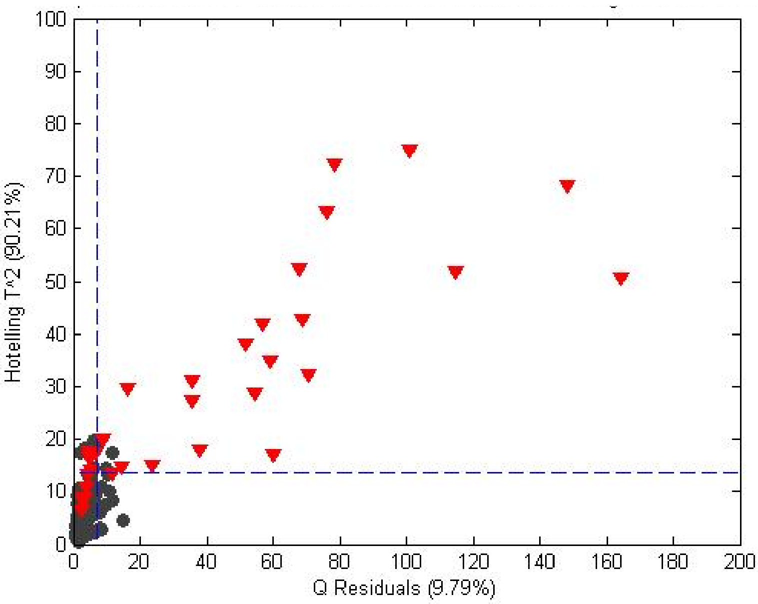

Figure 6. *Gert Member from the Gert wells (red triangles) projected on the Ravn Member model (black dots). Hotelling T^2 and Q residuals show a well defined model. Dashed lines show the 95 % confidence limit.*

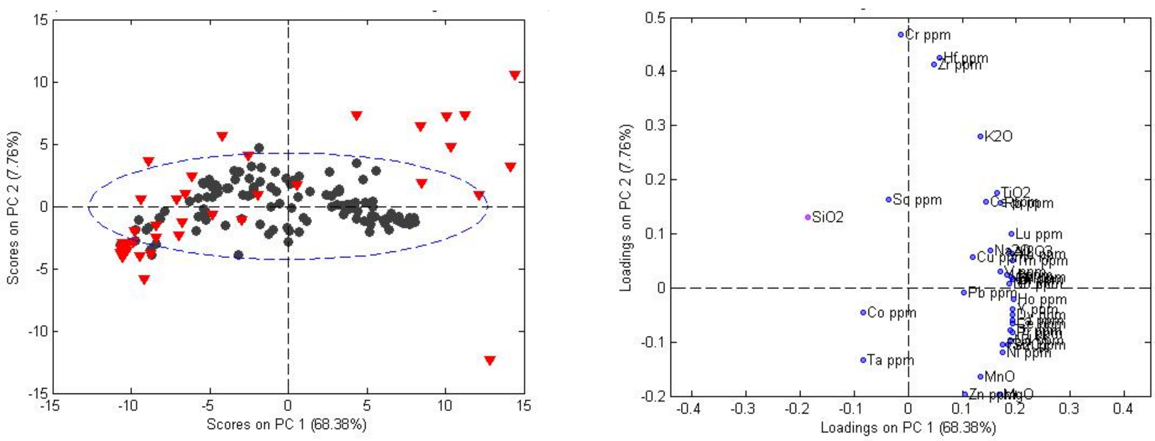

Figure 7. *Gert Member (red triangles) projected on the Ravn Member model (black dots). Scores and loadings from principal components 1 and 2.*

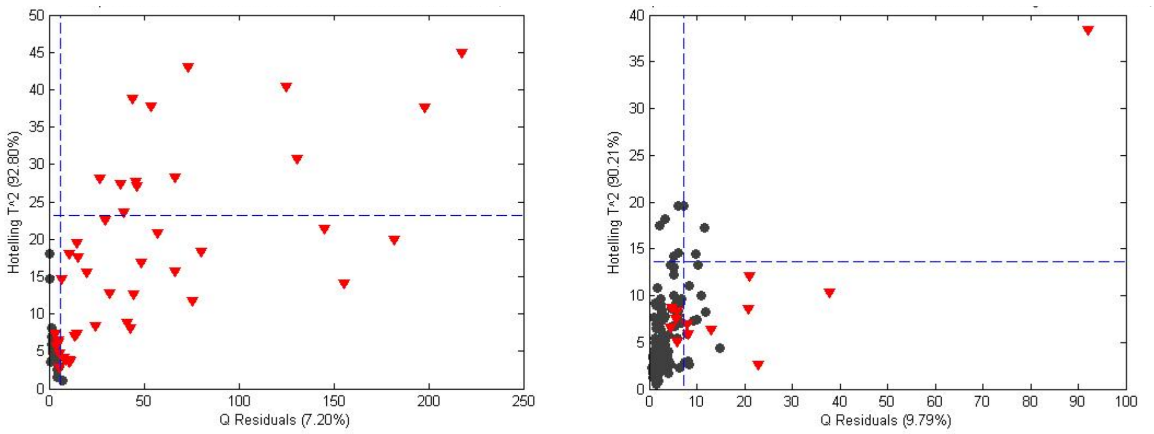

Figure 8. *Gert Member in the Hejre-2 well (red triangles) projected on the Ravn Member model (black dots). Hotelling T^2 and Q residuals show a well defined model. Dashed lines show the 95 % confidence limit.*

Lola Formation

The Farsund Formation data projected on the Lola Formation model are significant different (Fig. 9).

The Ravn Member data projected on the Lola Formation model show a clear differentiation (Fig. 10). The Ravn Member samples, which lie within the Lola Formation model include: GE4-582795 and RI1-456044, which are located close to the boundary between the Ravn Member and the Lola Formation. The Ravn Member is differentiated from the Lola Formation by having a higher content of SiO_2, Zr, Hf and a lower content of REE (Fig. 11).

The Gert Member from the three Gert wells is differentiated significantly from Lola Formation (Fig. 12) mainly by having higher SiO_2, Zr, Hf, Na_2O, Cr, TiO_2, Nb, Sc and lower REE and MnO contents. The Gert Member in the Hejre-2 well is also differentiated significantly from the Lola Formation by some of the similar elements as Gert Member from the three Gert wells (Fig. 12). Gert Member in Hejre-2 has higher SiO_2, Zr, Hf, Cr, TiO_2, Th and lower REE contents. The Lower Gert Member in the Hejre-2 well is also different to Lola Formation on the exact same elements as the Gert Member in the Hejre-2 well. The possible Gert Member in Rita-1 is also significantly different to the Lola Formation (Fig. 13). Gert Member in Rita-1 differentiates itself from the Lola Formation on same parameters as the Gert Member in the Hejre-2 well. Gert Member in Rita-1 has higher contents of SiO_2, Zr, Hf, TiO_2, Na_2O and lower REE and Mn.

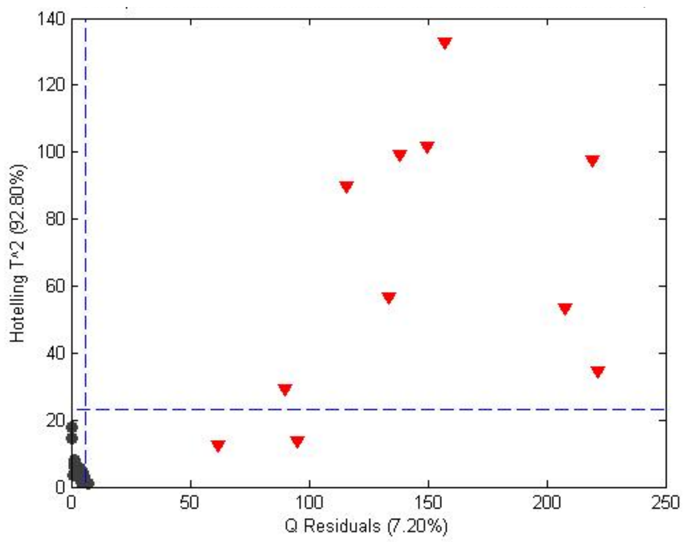

Figure 9. *The Farsund Formation data (red triangles) projected on the Lola Formation model (black dots). Hotelling T^2 and Q residuals show significantly different models. Dashed lines show the 95 % confidence limit.*

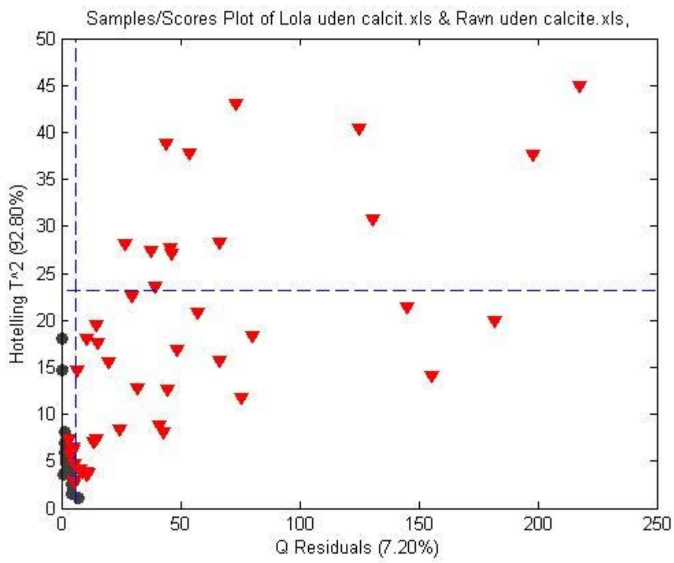

Figure 10. *Ravn Member data (red triangles) projected on the Lola Formation model (black dots). Hotelling T^2 and Q residuals show significantly different models. Dashed lines show the 95 % confidence limit. Note than Ravn Member samples are out of scale.*

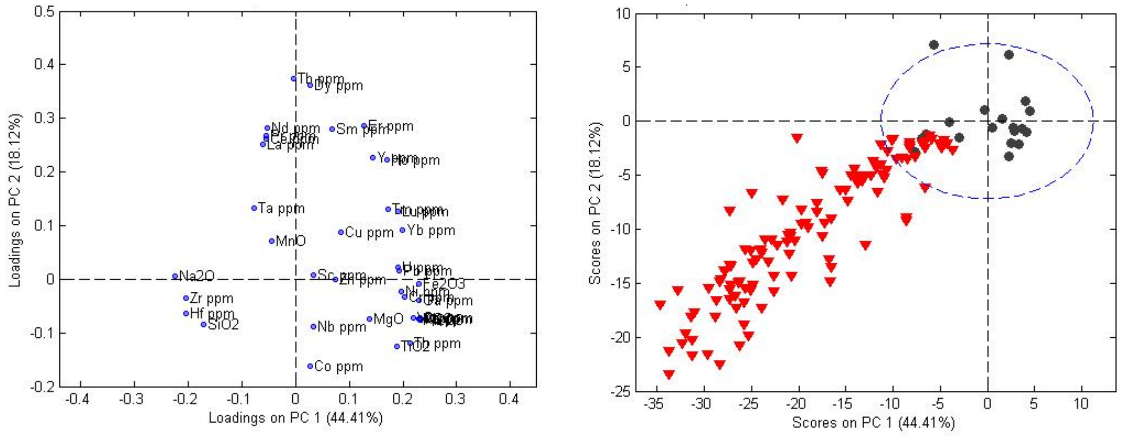

Figure 11. *Ravn Member data (red triangles) projected on the Lola Formation model (black dots). Scores and loadings from principal components 1 and 2.*

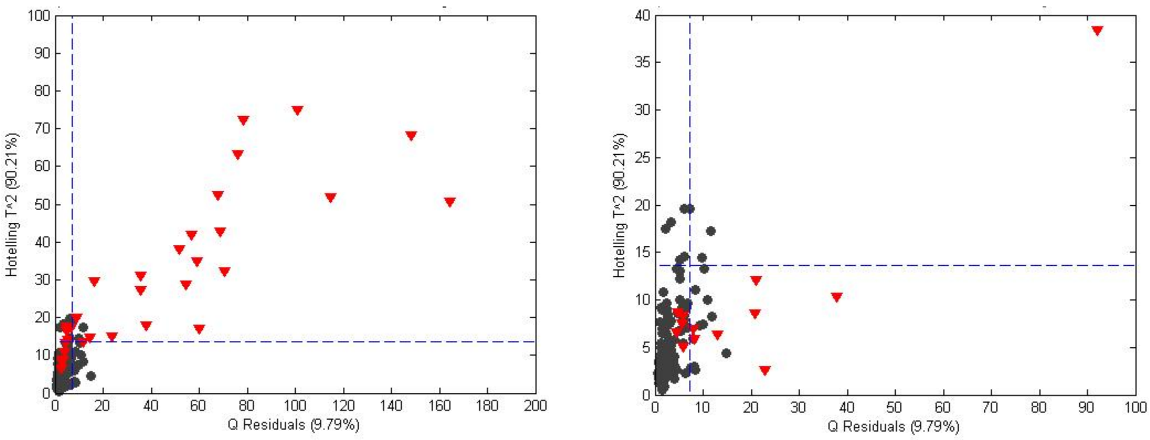

Figure 12. *Left: Gert Member data from the three Gert wells (red triangles) projected on Lola Formation model (black dots). Right: Gert Member data from the Hejre-2 well (red triangles) projected on the Lola Formation model (black dots). Hotelling T^2 and Q residuals show significantly different models. Dashed lines show the 95 % confidence limit.*

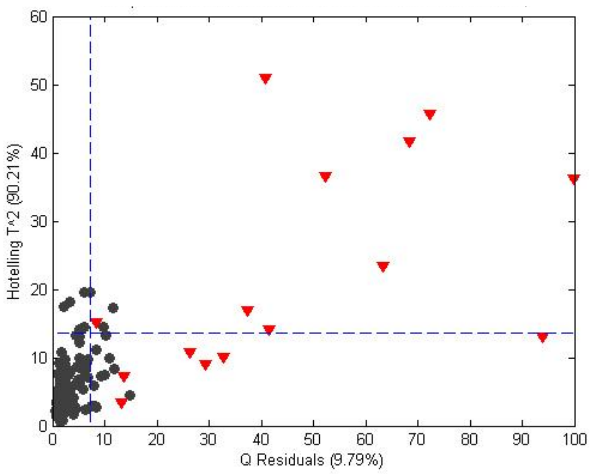

Figure 13. *The possible Gert Member in Rita-1 (red triangles) projected on Lola Formation model (black dots). Hotelling T^2 and Q residuals show significantly different models. Dashed lines show the 95 % confidence limit.*

Farsund Formation

The Lola Formation data projected on the Farsund Formation model show that Lola and Farsund formations are significantly different (Fig. 14). The Farsund Formation model, though, is based on only a few samples and therefore reflects a smaller degree of variation. Lola Formation seems to have a higher content of REE, Th, Cs, Ga, Rb, Nb and Al_2O_3 than Farsund Formation (Fig. 15).

The Ravn Member samples are significant different to the Farsund Formation samples (Fig. 16). The Ravn Member tends to have higher SiO_2, Zr, Hf, Na_2O and lower Ni, Fe_2O_3, Cu, Zn (Fig. 17).

All Gert Member samples are significantly different to the Farsund Model (Fig. 18). The Gert Member is differentiable from the Farsund Formation by having higher SiO_2, Zr, Hf, Na_2O and lower U, V, Ni, Zn, Fe_2O_3, Cu (Fig. 19).

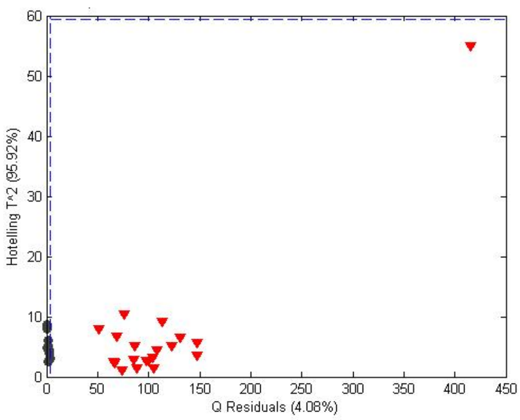

Figure 14. *Lola Formation data (red triangles) projected on the Farsund Formation (black dots). Hotelling T^2 and Q residuals show significantly different models. Dashed lines show the 95 % confidence limit.*

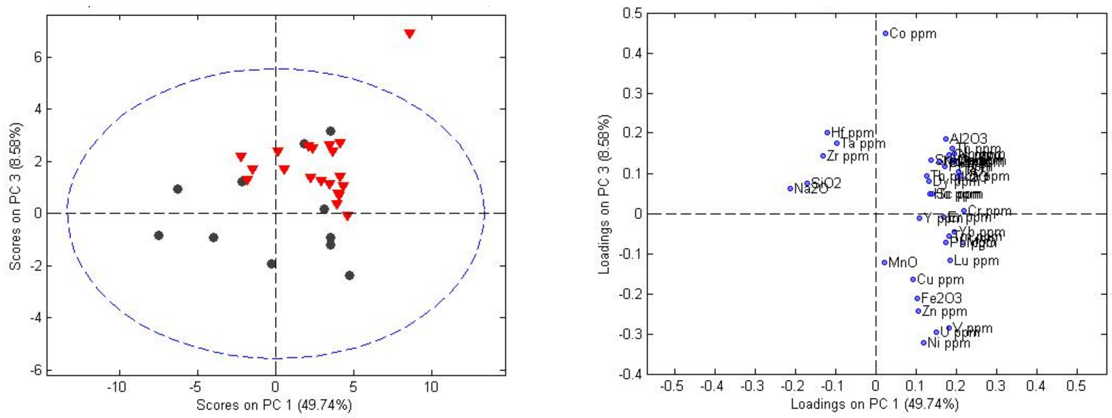

Figure 15. *Lola Formation data (red triangles) projected on the Farsund Formation (black dots). Scores and loadings from principal components 1 and 3.*

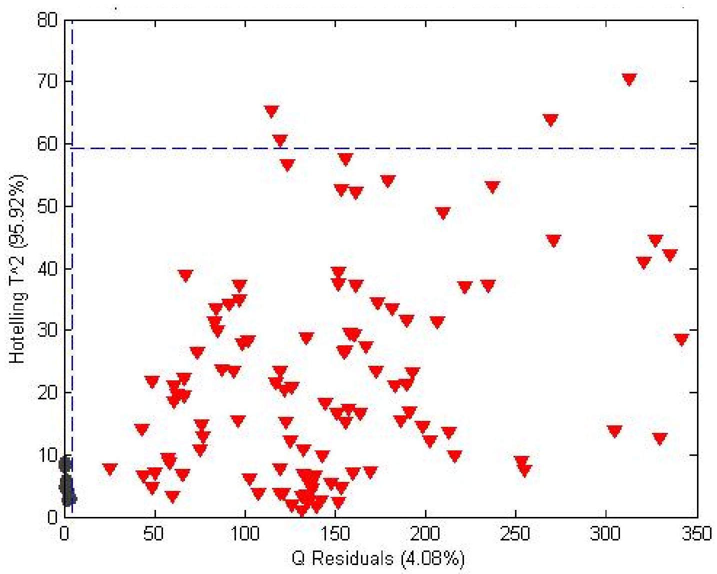

Figure 16. *Ravn Member data (red triangles) projected on the Farsund Formation model (black dots). Hotelling T^2 and Q residuals show significantly different models. Dashed lines show the 95 % confidence limit.*

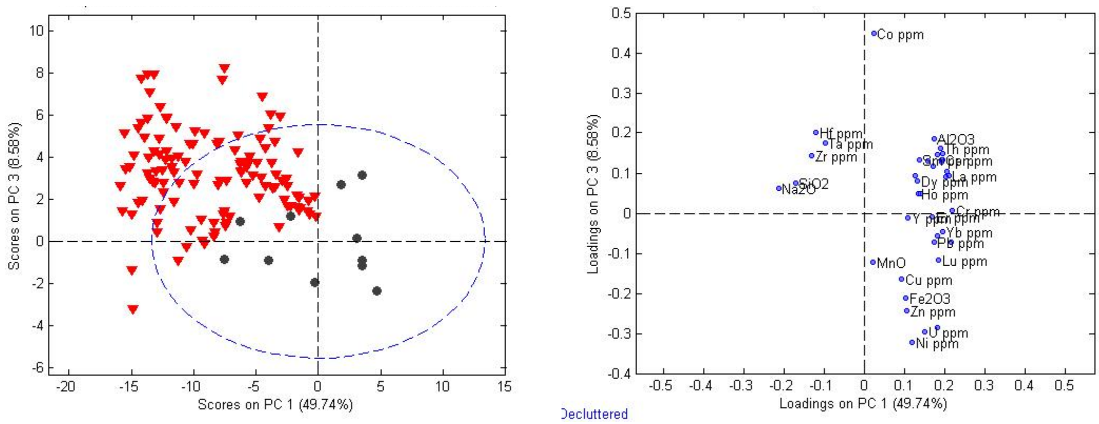

Figure 17. *Ravn Member data (red triangles) projected on the Farsund Formation model (black dots). Scores and loadings from principal components 1 and 3.*

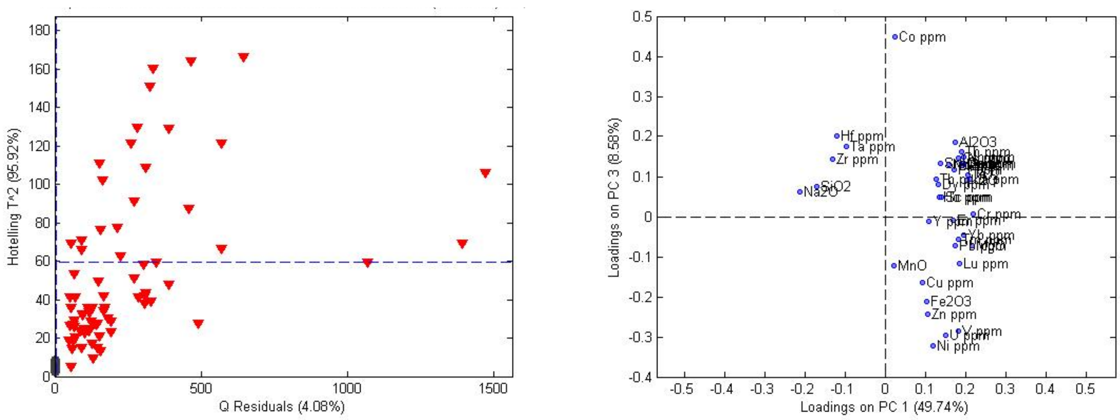

Figure 18. *Gert Member data from all the investigated wells (red triangles) projected on the Farsund Formation model (black dots). Hotelling T^2 and Q residuals show significantly different models. Dashed lines show the 95 % confidence limit.*

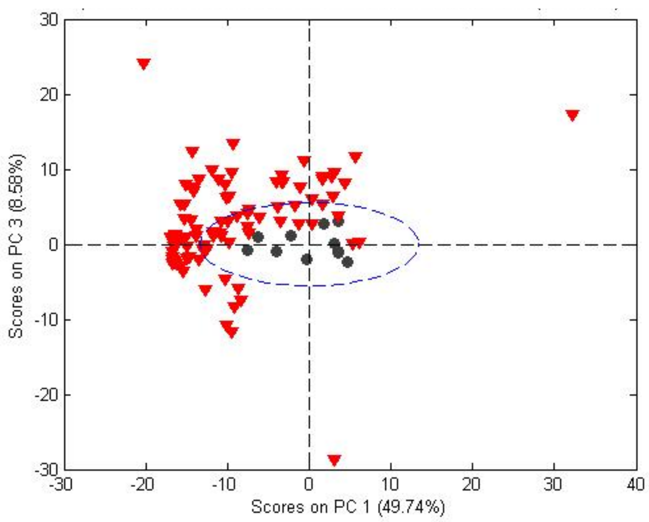

Figure 19. *Gert Member data from all the investigated wells (red triangles) projected on the Farsund Formation model (black dots). Scores and loadings from principal components 1 and 3.*

Appendix 4. Selected cross plots

Chemostratigraphy and mineral-chemical fingerprinting, Heno Formation, Danish North Sea

All cross plots are paired with cuttings samples and core samples separately. In the first part of the Appendix all major element and several trace elements have been plotted against Al_2O_3. In the last part of the Appendix selected elements has been plotted against Zr, TiO_2 and Th. The legend in the two graphs below applies to all the graphs in Appendix 4.

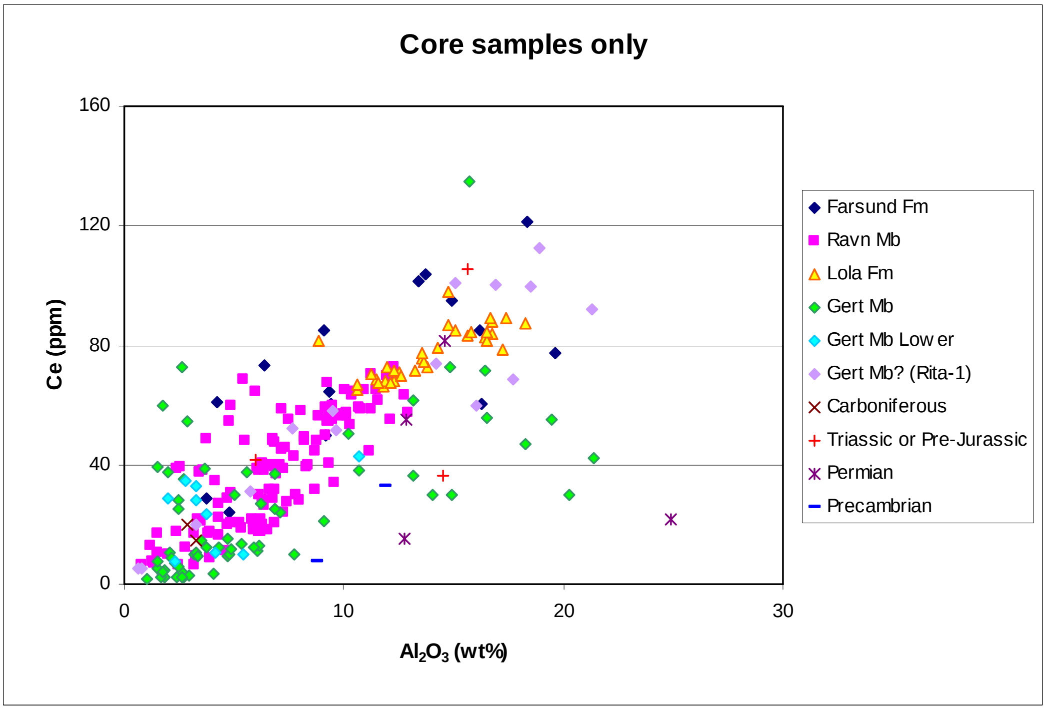

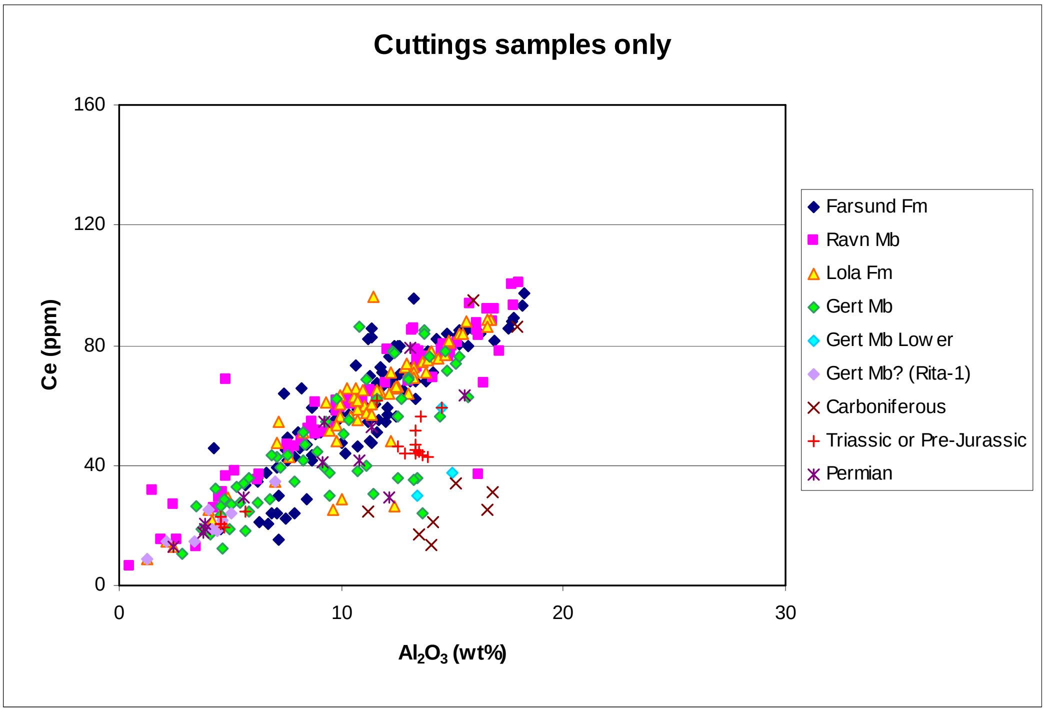

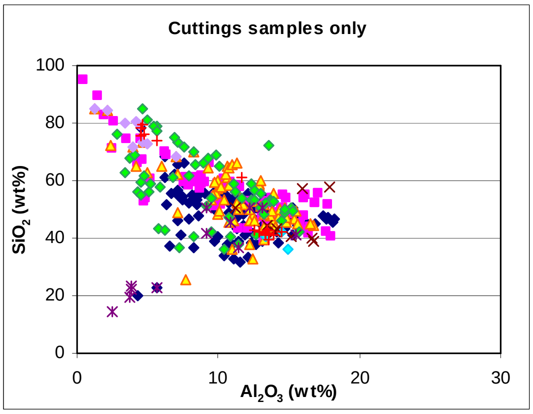
Cuttings samples only
SiO_2 (wt%)
Al_2O_3 (wt%)
0
20
40
60
80
100
0
10
20
30

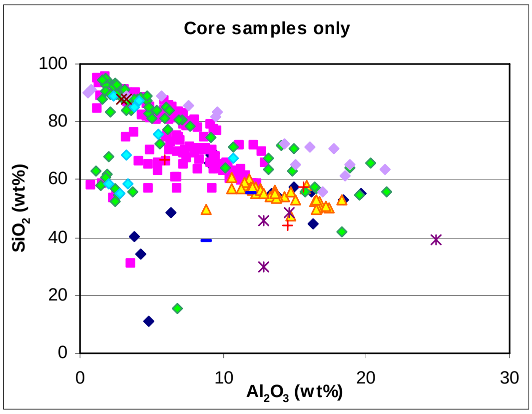
Core samples only
SiO_2 (wt%)
Al_2O_3 (wt%)
0
20
40
60
80
100
0
10
20
30

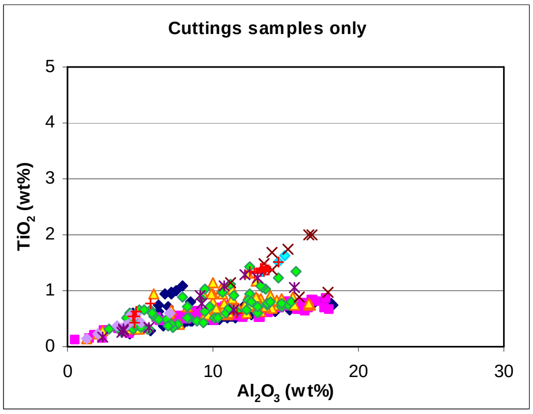
Cuttings samples only
TiO_2 (wt%)
Al_2O_3 (wt%)
0
1
2
3
4
5
0
10
20
30

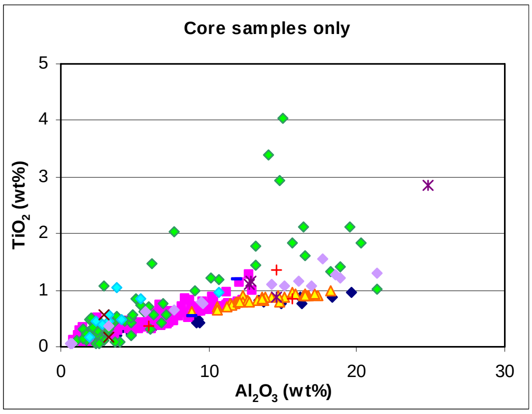
Core samples only
TiO_2 (wt%)
Al_2O_3 (wt%)
0
1
2
3
4
5
0
10
20
30

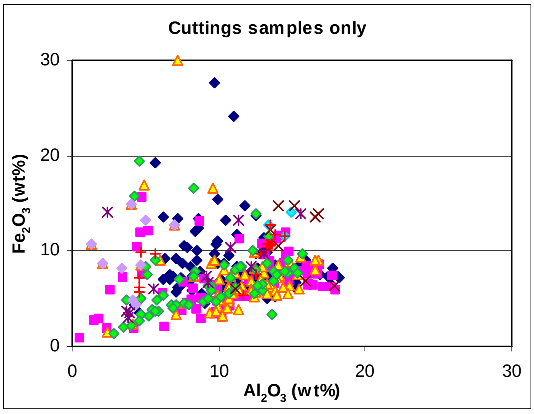
Cuttings samples only
Fe_2O_3 (wt%)
Al_2O_3 (wt%)
0
10
20
30
0
10
20
30

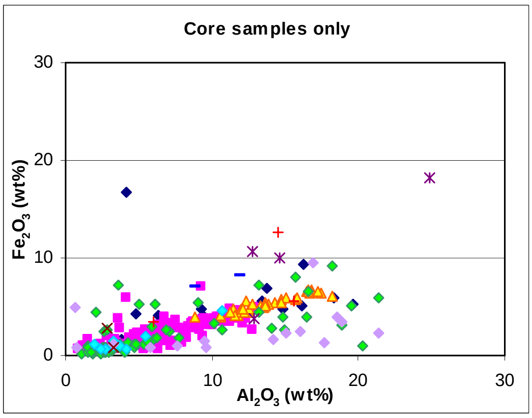
Core samples only
Fe_2O_3 (wt%)
Al_2O_3 (wt%)
0
10
20
30
0
10
20
30

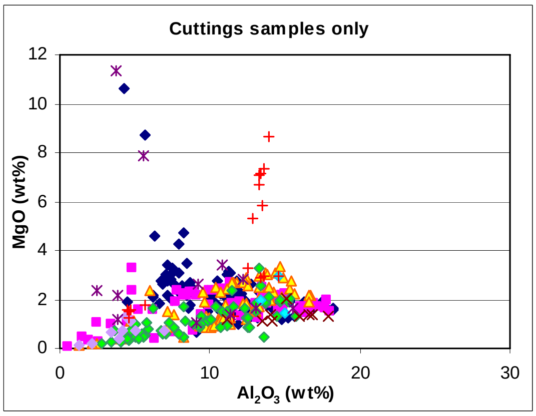
Cuttings samples only
MgO (wt%)
Al_2O_3 (wt%)
0
2
4
6
8
10
12
0
10
20
30

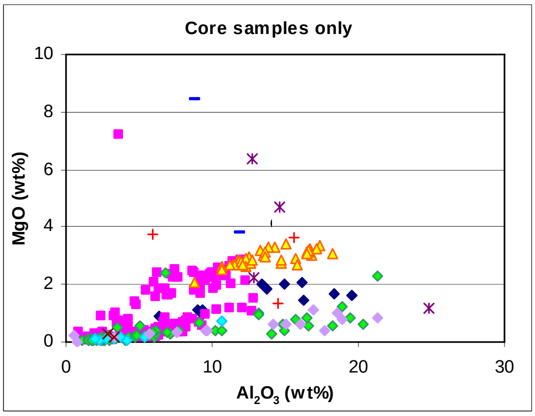
Core samples only
MgO (wt%)
Al_2O_3 (wt%)
0
2
4
6
8
10
0
10
20
30

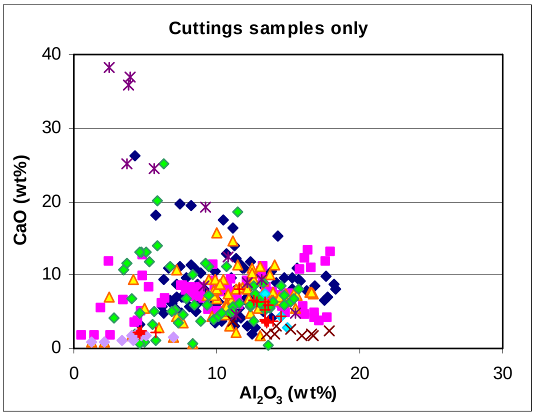
Cuttings samples only
CaO (wt%)
Al_2O_3 (wt%)
0
10
20
30
40
0
10
20
30

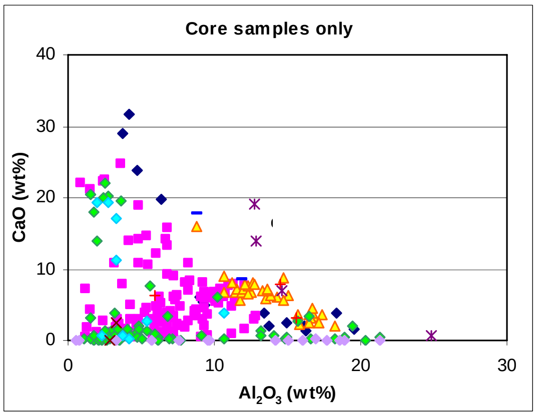
Core samples only
CaO (wt%)
Al_2O_3 (wt%)
0
10
20
30
40
0
10
20
30

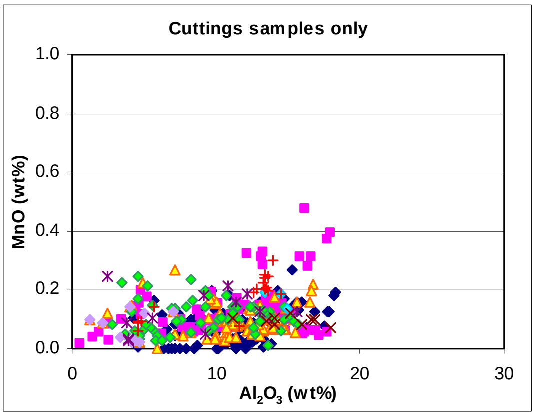
Cuttings samples only
MnO (wt%)
Al_2O_3 (wt%)
0.0
0.2
0.4
0.6
0.8
1.0
0
10
20
30

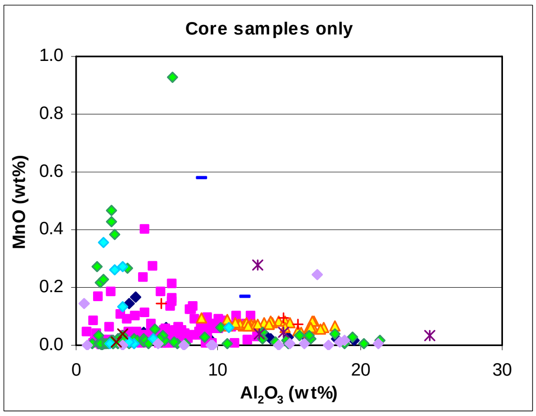
Core samples only
MnO (wt%)
Al_2O_3 (wt%)
0.0
0.2
0.4
0.6
0.8
1.0
0
10
20
30

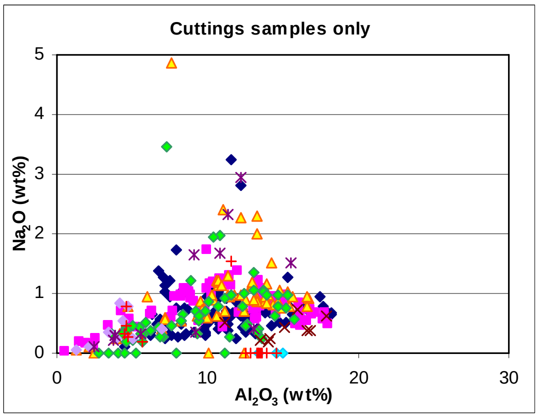
Cuttings samples only
Na_2O (wt%)
Al_2O_3 (wt%)

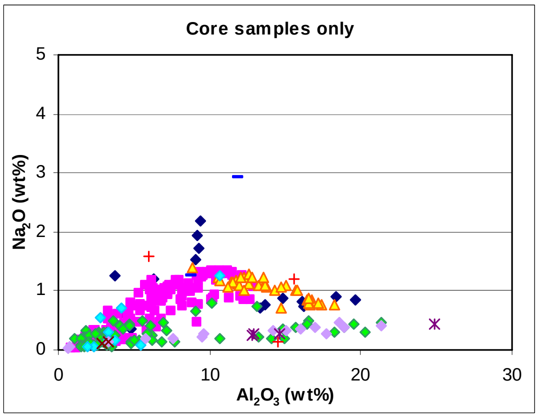
Core samples only
Na_2O (wt%)
Al_2O_3 (wt%)

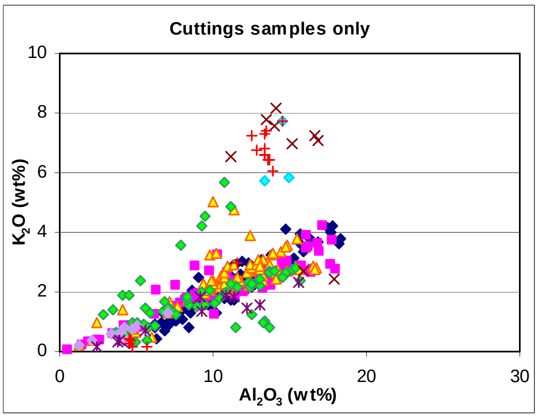
Cuttings samples only
K_2O (wt%)
Al_2O_3 (wt%)

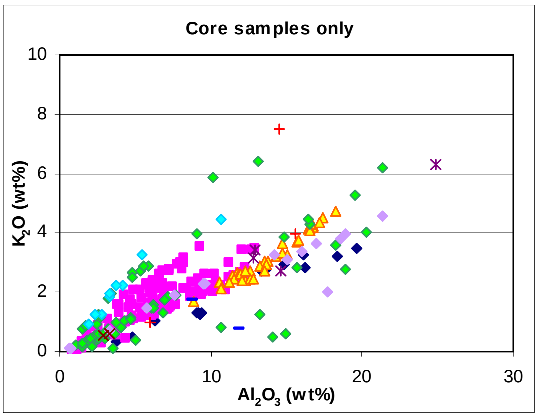
Core samples only
K_2O (wt%)
Al_2O_3 (wt%)

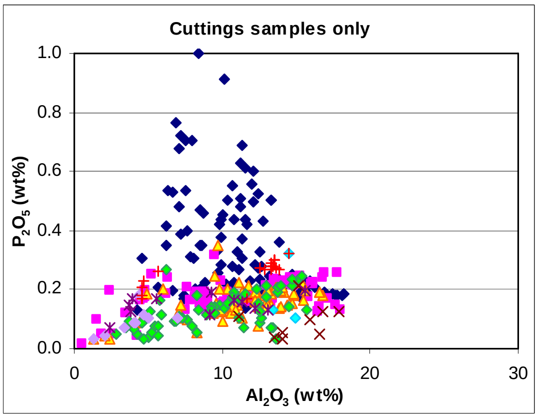
Cuttings samples only
P_2O_5 (wt%)
Al_2O_3 (wt%)

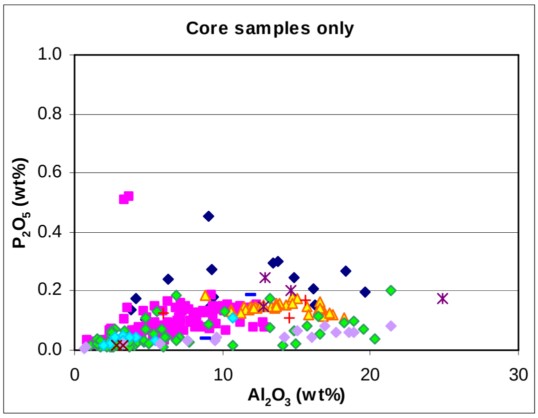
Core samples only
P_2O_5 (wt%)
Al_2O_3 (wt%)

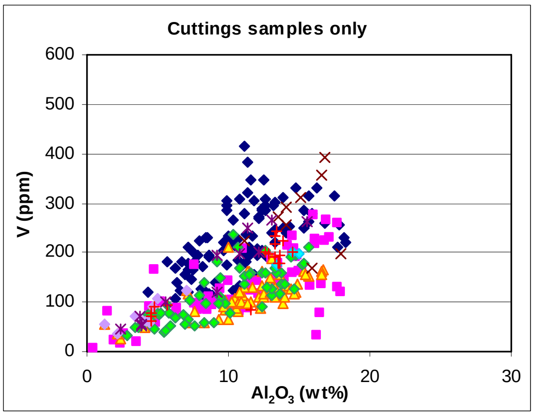
Cuttings samples only
V (ppm)
Al2O3 (wt%)

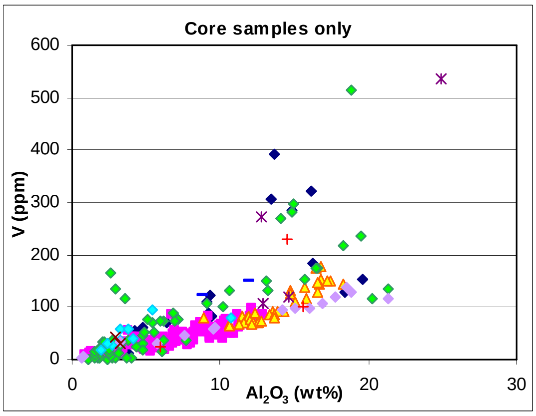
Core samples only
V (ppm)
Al2O3 (wt%)

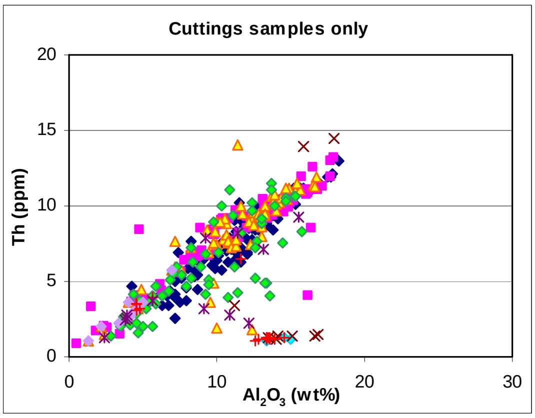
Cuttings samples only
Th (ppm)
Al2O3 (wt%)

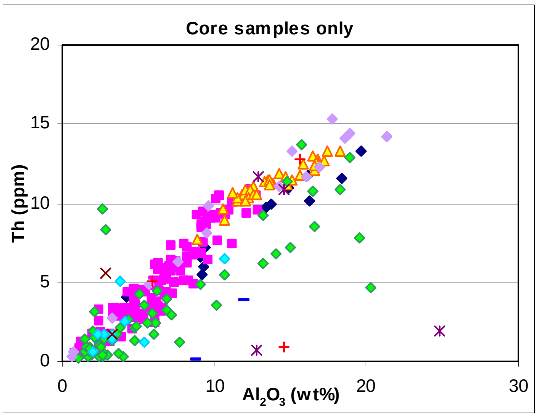
Core samples only
Th (ppm)
Al2O3 (wt%)

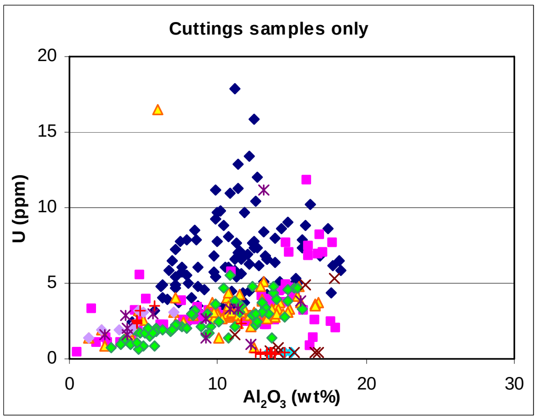
Cuttings samples only
U (ppm)
Al2O3 (wt%)

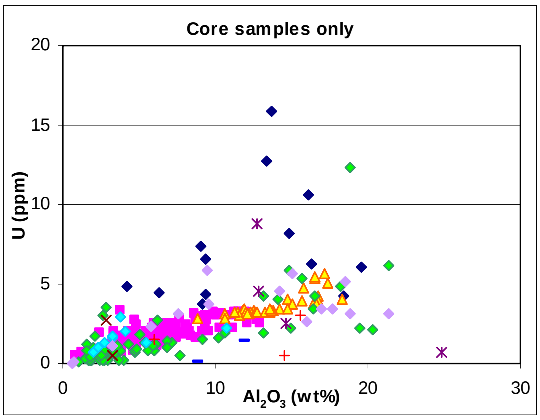
Core samples only
U (ppm)
Al2O3 (wt%)

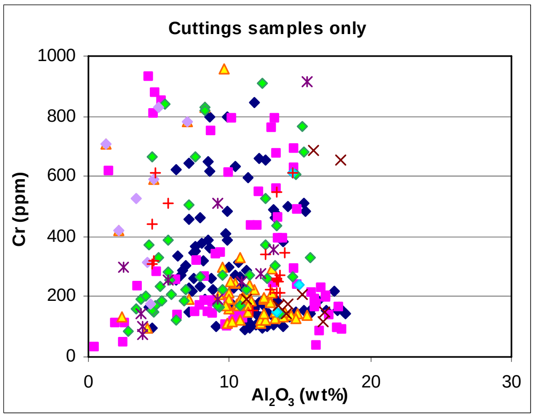
Cuttings samples only
Cr (ppm)
Al$_2$O$_3$ (wt%)

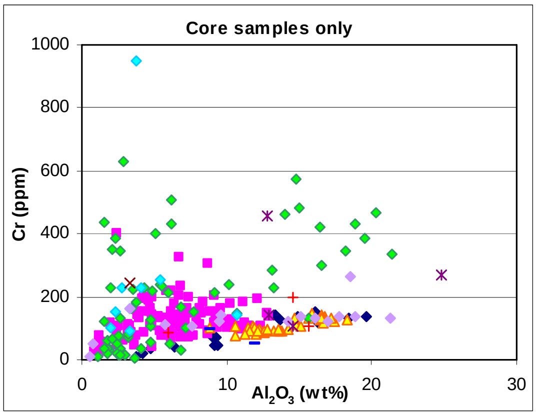
Core samples only
Cr (ppm)
Al$_2$O$_3$ (wt%)

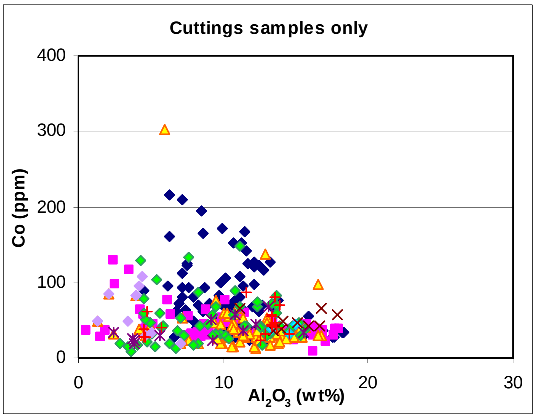
Cuttings samples only
Co (ppm)
Al$_2$O$_3$ (wt%)

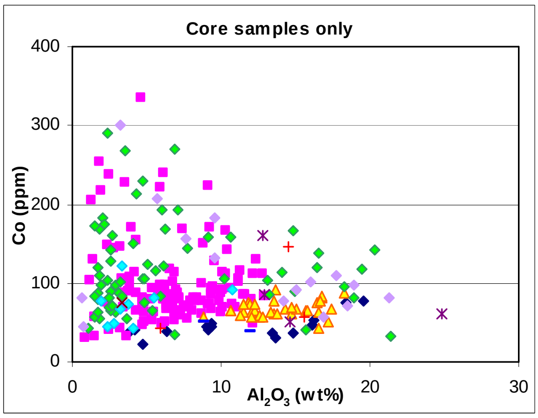
Core samples only
Co (ppm)
Al$_2$O$_3$ (wt%)

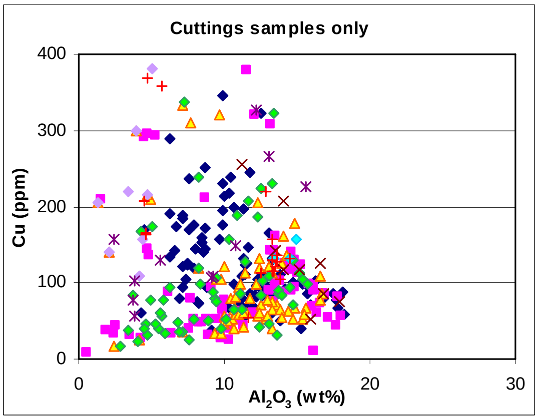
Cuttings samples only
Cu (ppm)
Al$_2$O$_3$ (wt%)

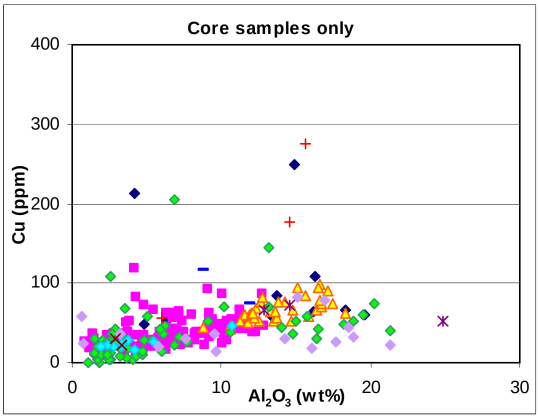
Core samples only
Cu (ppm)
Al$_2$O$_3$ (wt%)

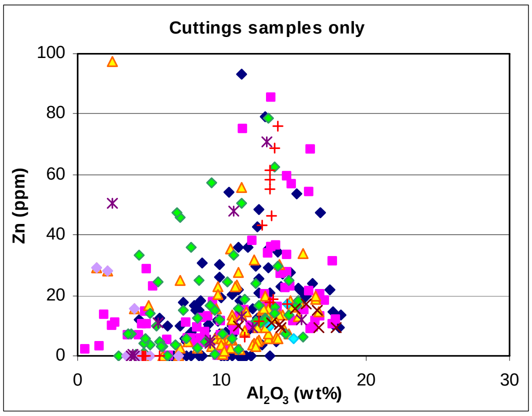
Cuttings samples only
Zn (ppm)
Al_2O_3 (wt%)

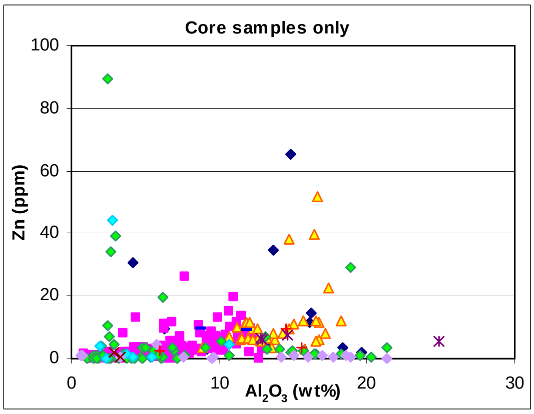
Core samples only
Zn (ppm)
Al_2O_3 (wt%)

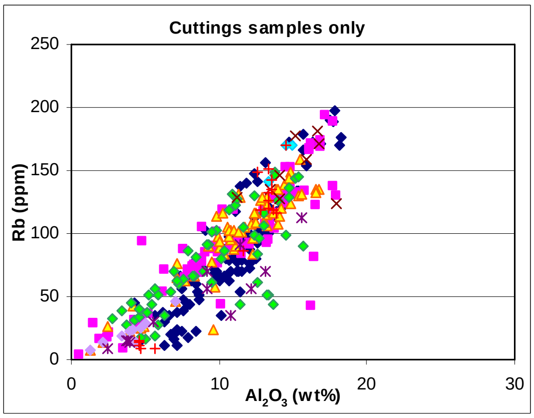
Cuttings samples only
Rb (ppm)
Al_2O_3 (wt%)

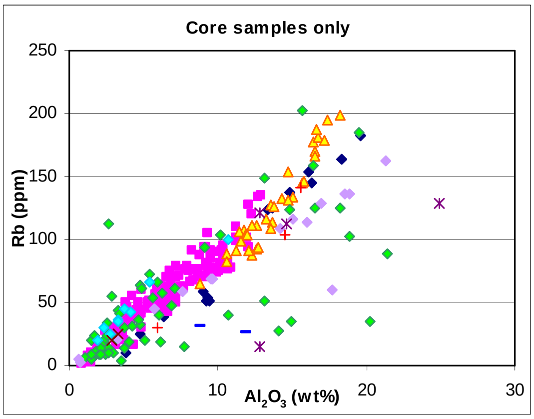
Core samples only
Rb (ppm)
Al_2O_3 (wt%)

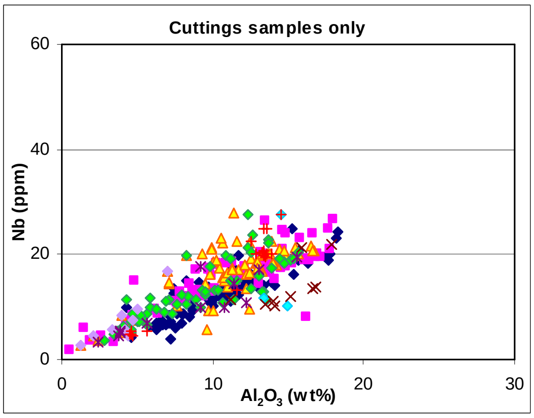
Cuttings samples only
Nb (ppm)
Al_2O_3 (wt%)

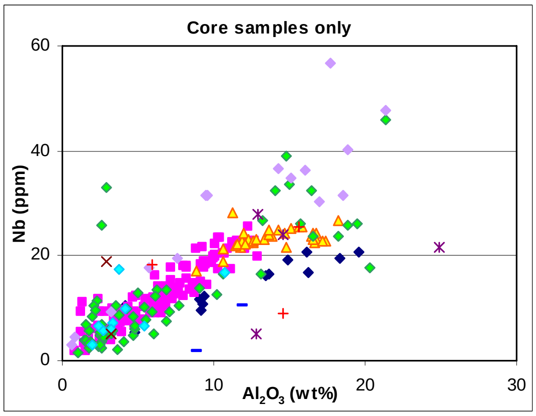
Core samples only
Nb (ppm)
Al_2O_3 (wt%)

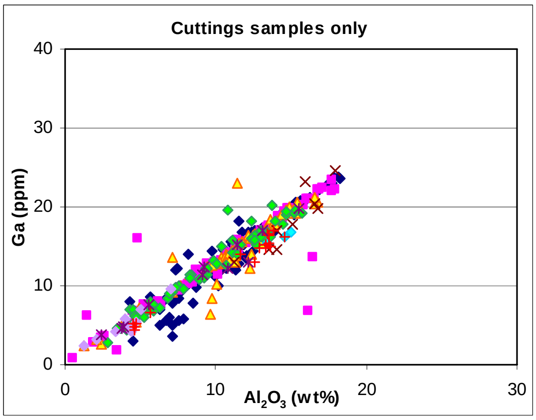
Cuttings samples only
Ga (ppm)
Al2O3 (wt%)
0
10
20
30
40

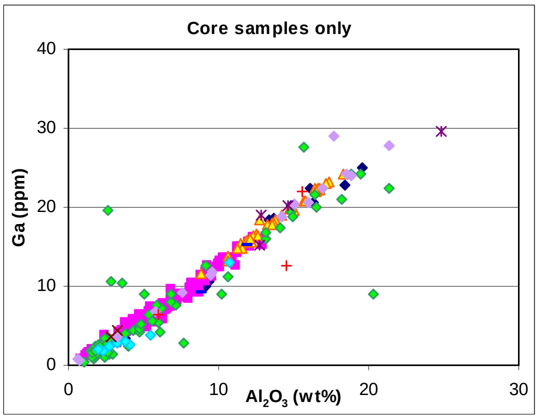
Core samples only
Ga (ppm)
Al2O3 (wt%)
0
10
20
30
40

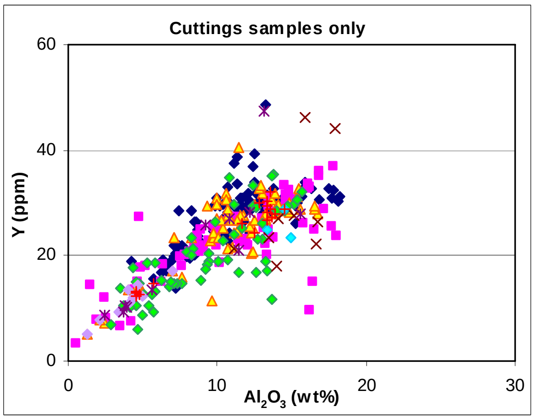
Cuttings samples only
Y (ppm)
Al2O3 (wt%)
0
10
20
30
40
60

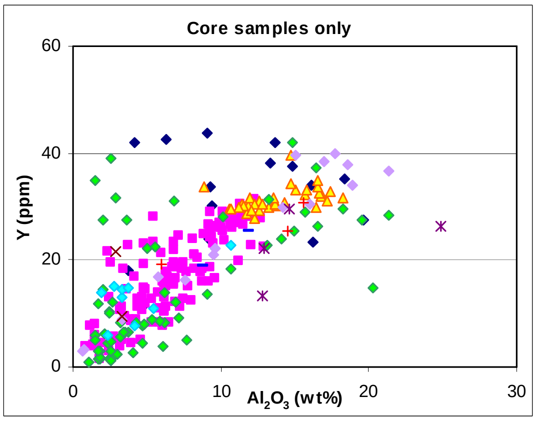
Core samples only
Y (ppm)
Al2O3 (wt%)
0
10
20
30
40
60

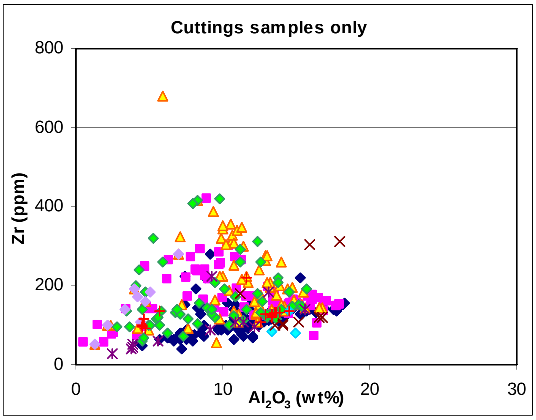
Cuttings samples only
Zr (ppm)
Al2O3 (wt%)
0
200
400
600
800
10
20
30

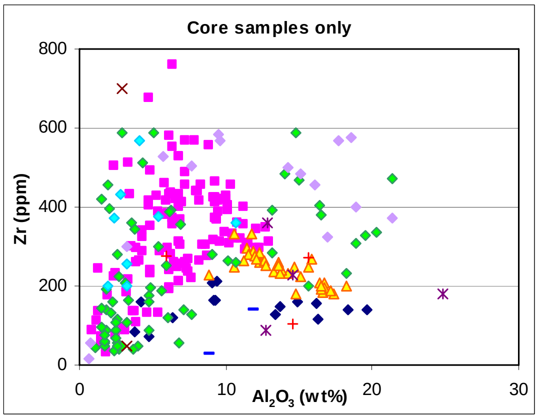
Core samples only
Zr (ppm)
Al2O3 (wt%)
0
200
400
600
800
10
20
30

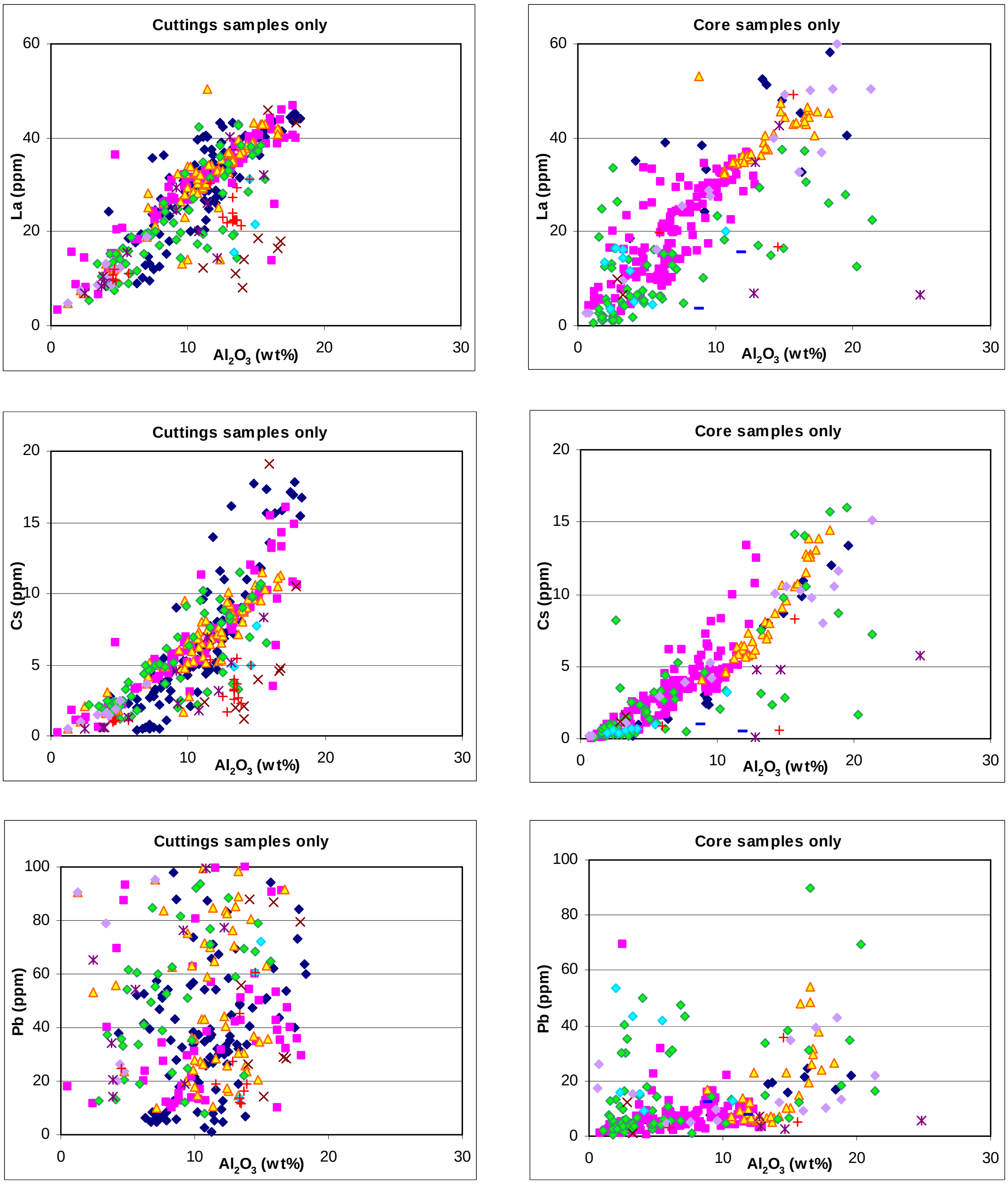

Cuttings samples only
La (ppm)
Al2O3 (wt%)
Core samples only
La (ppm)
Al2O3 (wt%)
Cuttings samples only
Cs (ppm)
Al2O3 (wt%)
Core samples only
Cs (ppm)
Al2O3 (wt%)
Cuttings samples only
Pb (ppm)
Al2O3 (wt%)
Core samples only
Pb (ppm)
Al2O3 (wt%)

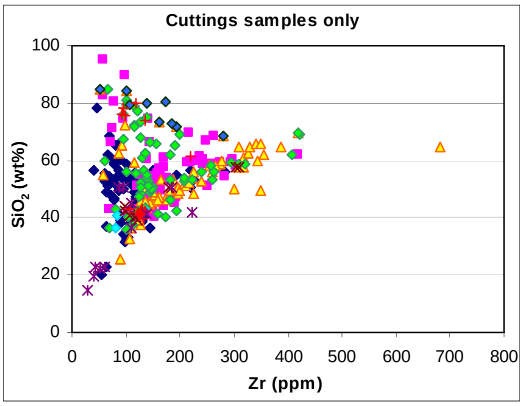
Cuttings samples only
SiO2 (wt%)
Zr (ppm)

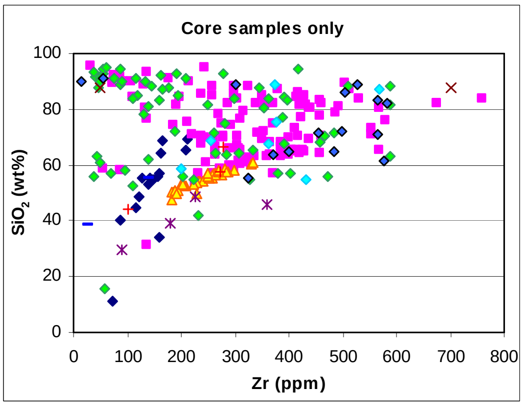
Core samples only
SiO2 (wt%)
Zr (ppm)

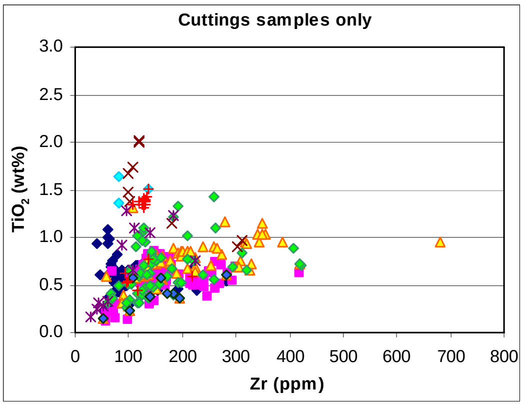
Cuttings samples only
TiO2 (wt%)
Zr (ppm)

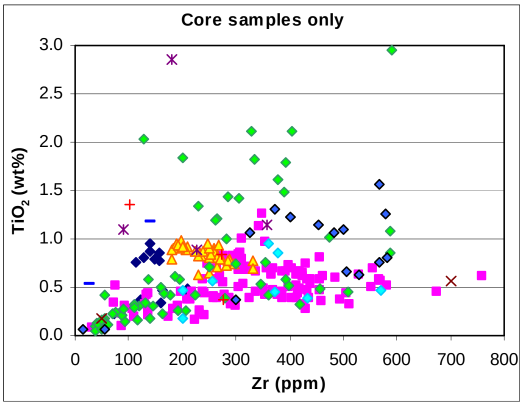
Core samples only
TiO2 (wt%)
Zr (ppm)

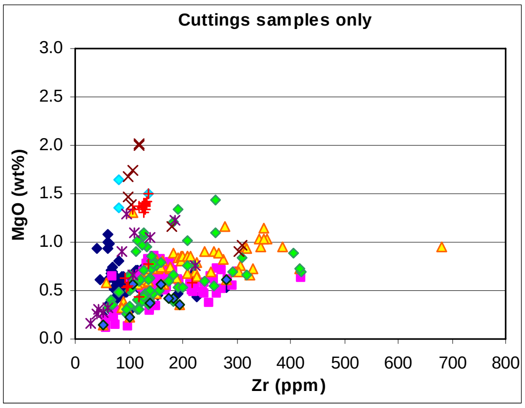
Cuttings samples only
MgO (wt%)
Zr (ppm)

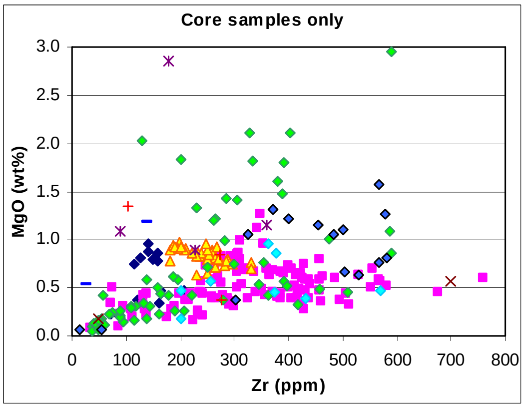
Core samples only
MgO (wt%)
Zr (ppm)

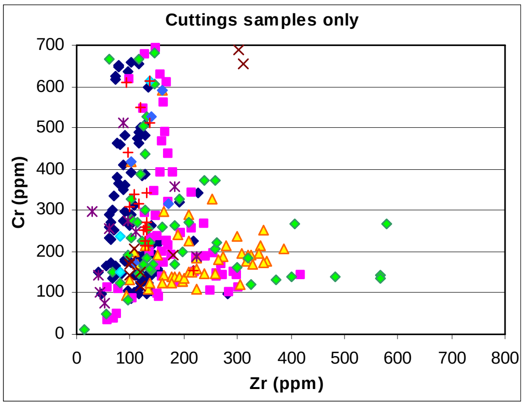
Cuttings samples only
Cr (ppm)
Zr (ppm)
0
100
200
300
400
500
600
700
800

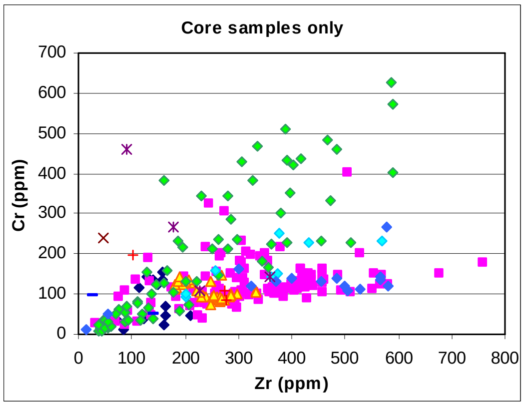
Core samples only
Cr (ppm)
Zr (ppm)
0
100
200
300
400
500
600
700
800

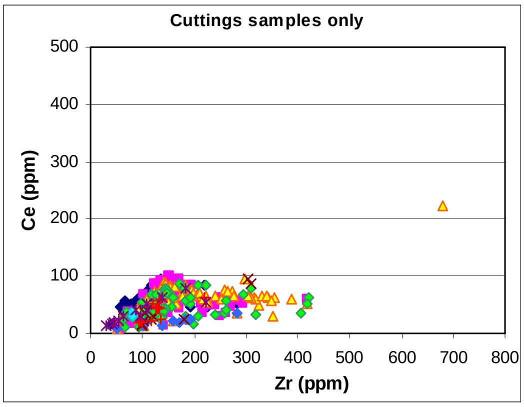
Cuttings samples only
Ce (ppm)
Zr (ppm)
0
100
200
300
400
500
600
700
800

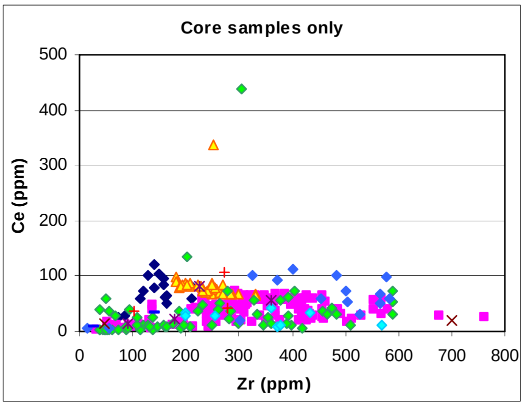
Core samples only
Ce (ppm)
Zr (ppm)
0
100
200
300
400
500
600
700
800

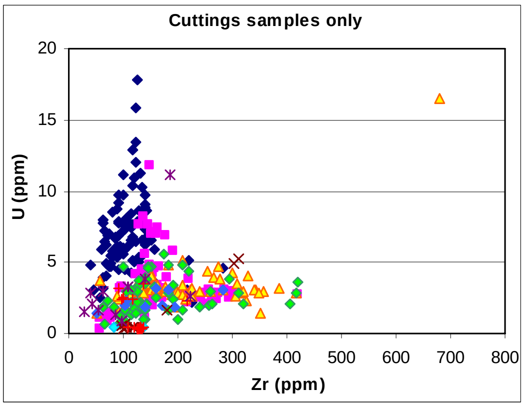
Cuttings samples only
U (ppm)
Zr (ppm)
0
5
10
15
20
100
200
300
400
500
600
700
800

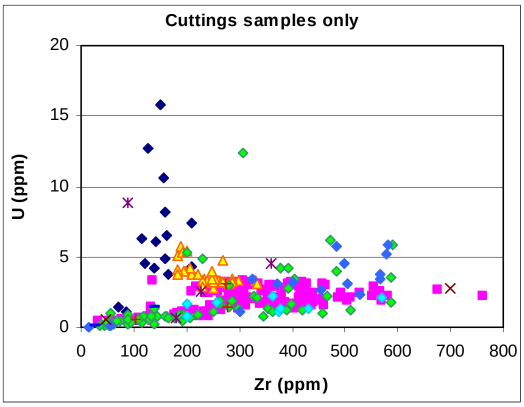
Cuttings samples only
U (ppm)
Zr (ppm)
0
5
10
15
20
100
200
300
400
500
600
700
800

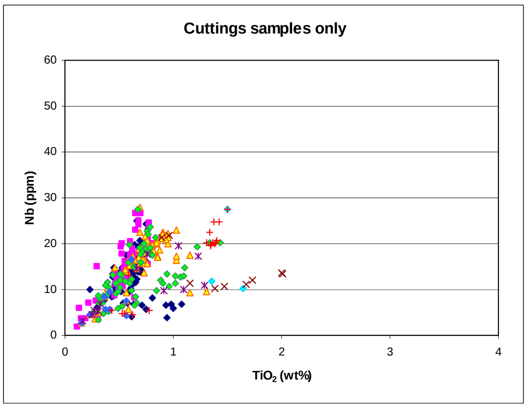
Cuttings samples only
Nb (ppm)
TiO_2 (wt%)

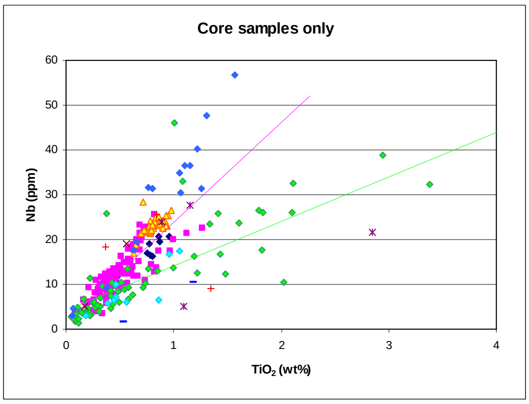
Core samples only
Nb (ppm)
TiO_2 (wt%)

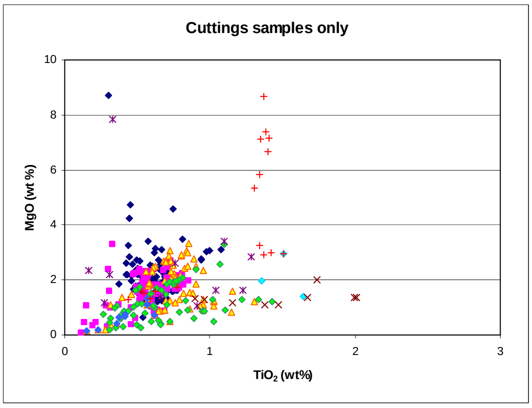
Cuttings samples only
MgO (wt %)
TiO_2 (wt%)

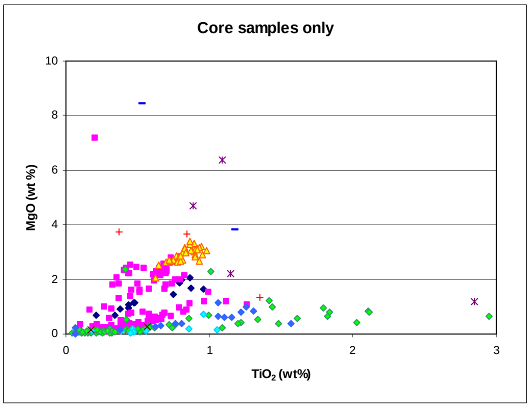
Core samples only
MgO (wt %)
TiO_2 (wt%)

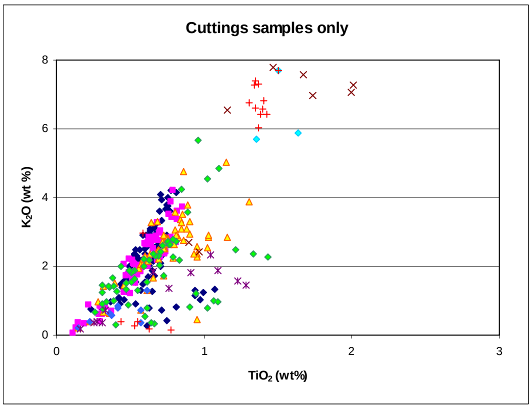
Cuttings samples only
K_2O (wt %)
TiO_2 (wt%)

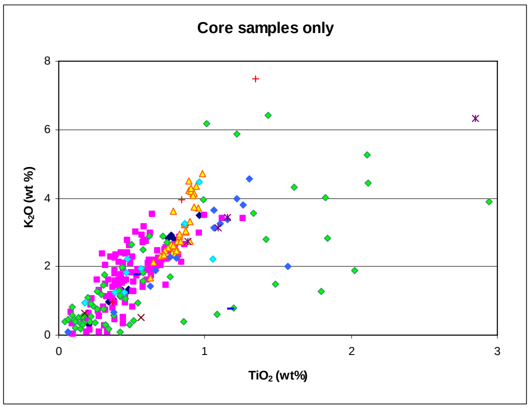
Core samples only
K_2O (wt %)
TiO_2 (wt%)

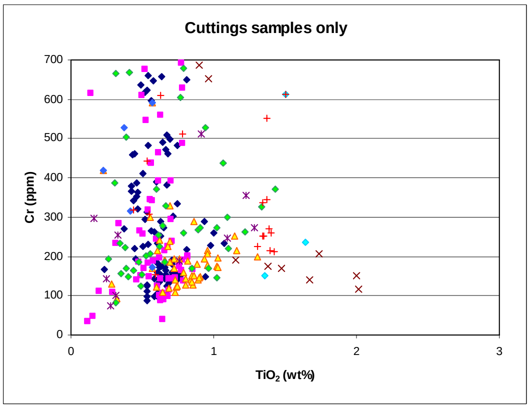
Cuttings samples only
Cr (ppm)
0
100
200
300
400
500
600
700
0
1
2
3
TiO2 (wt%)

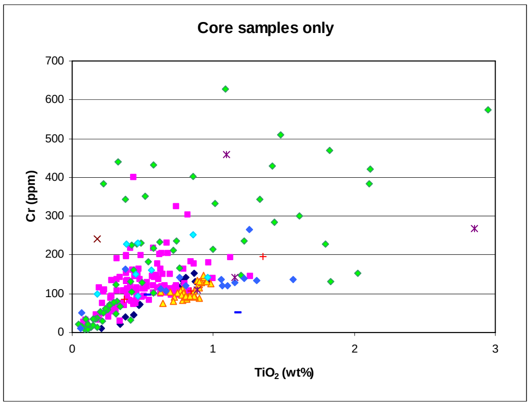
Core samples only
Cr (ppm)
0
100
200
300
400
500
600
700
0
1
2
3
TiO2 (wt%)

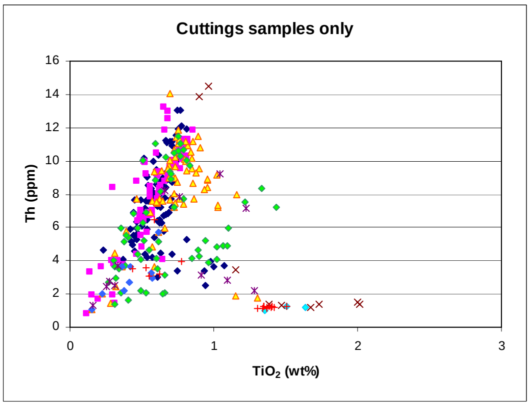
Cuttings samples only
Th (ppm)
0
2
4
6
8
10
12
14
16
0
1
2
3
TiO2 (wt%)

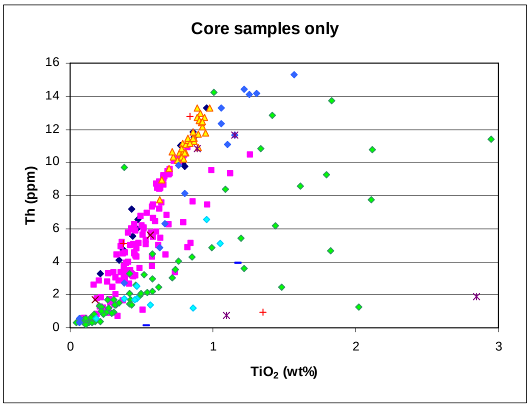
Core samples only
Th (ppm)
0
2
4
6
8
10
12
14
16
0
1
2
3
TiO2 (wt%)

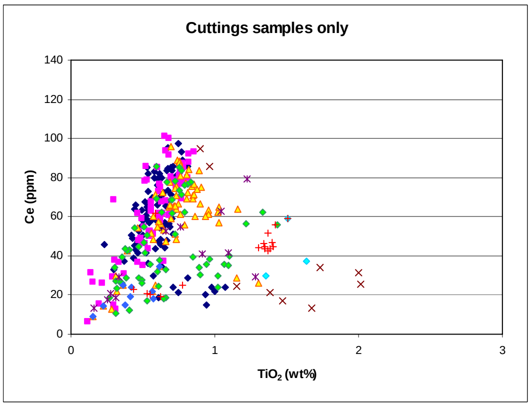
Cuttings samples only
Ce (ppm)
0
20
40
60
80
100
120
140
0
1
2
3
TiO2 (wt%)

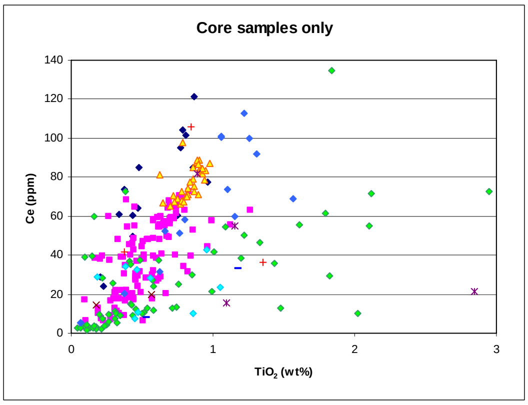
Core samples only
Ce (ppm)
0
20
40
60
80
100
120
140
0
1
2
3
TiO2 (wt%)

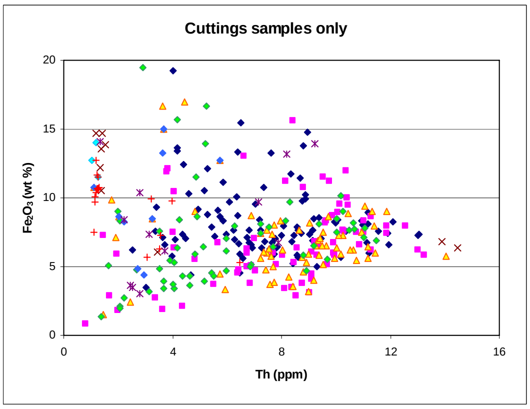
Cuttings samples only
Fe_2O_3 (wt %)
0 5 10 15 20
0 4 8 12 16
Th (ppm)

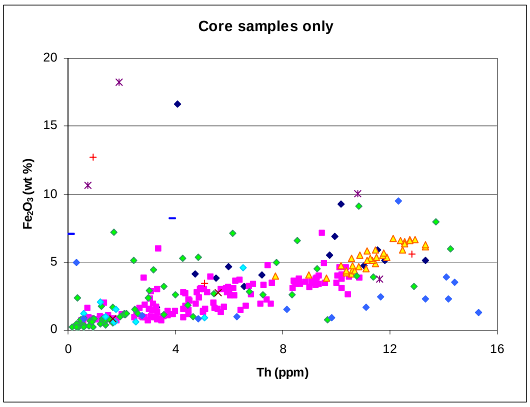
Core samples only
Fe_2O_3 (wt %)
0 5 10 15 20
0 4 8 12 16
Th (ppm)

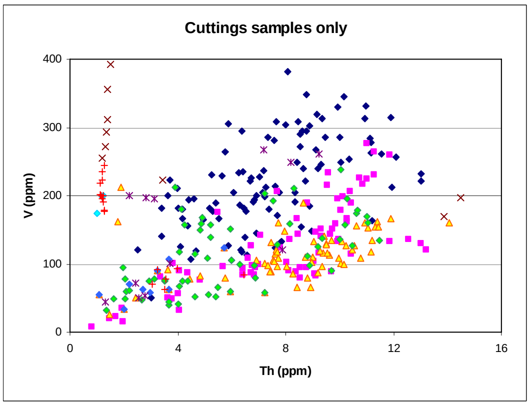
Cuttings samples only
V (ppm)
0 100 200 300 400
0 4 8 12 16
Th (ppm)

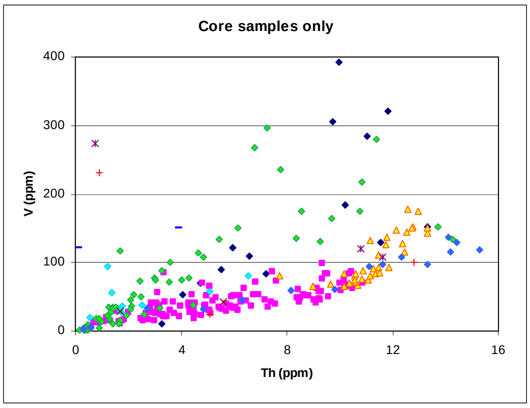
Core samples only
V (ppm)
0 100 200 300 400
0 4 8 12 16
Th (ppm)

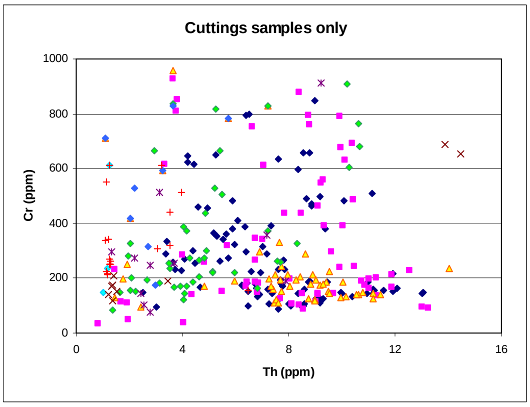
Cuttings samples only
Cr (ppm)
0 200 400 600 800 1000
0 4 8 12 16
Th (ppm)

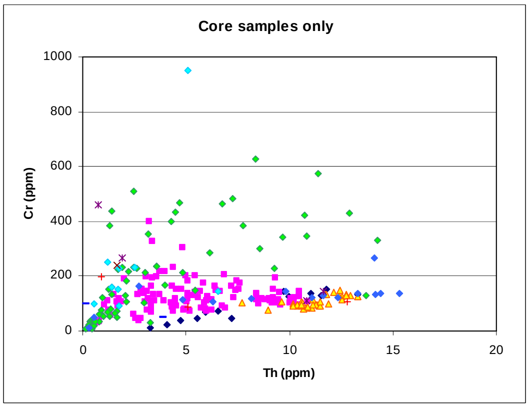
Core samples only
Cr (ppm)
0 200 400 600 800 1000
0 5 10 15 20
Th (ppm)

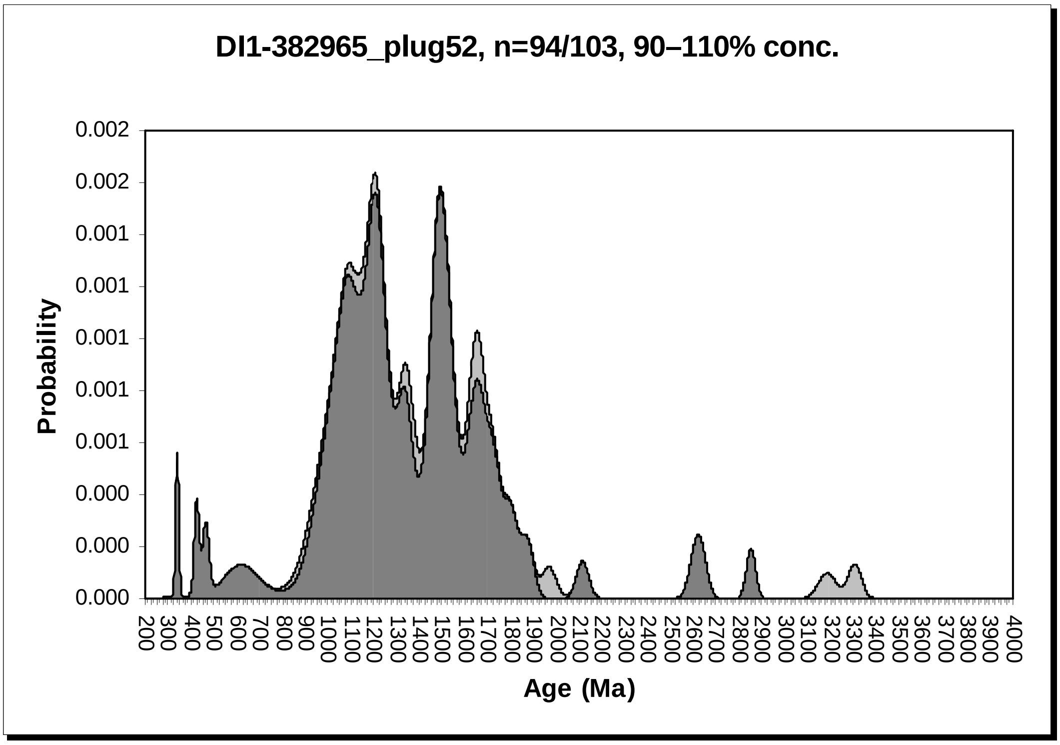
DI1-382965_plug52, n=94/103, 90–110% conc.
Probability
0.002
0.002
0.001
0.001
0.001
0.001
0.001
0.000
0.000
0.000
200
300
400
500
600
700
800
900
1000
1100
1200
1300
1400
1500
1600
1700
1800
1900
2000
2100
2200
2300
2400
2500
2600
2700
2800
2900
3000
3100
3200
3300
3400
3500
3600
3700
3800
3900
4000
Age (Ma)

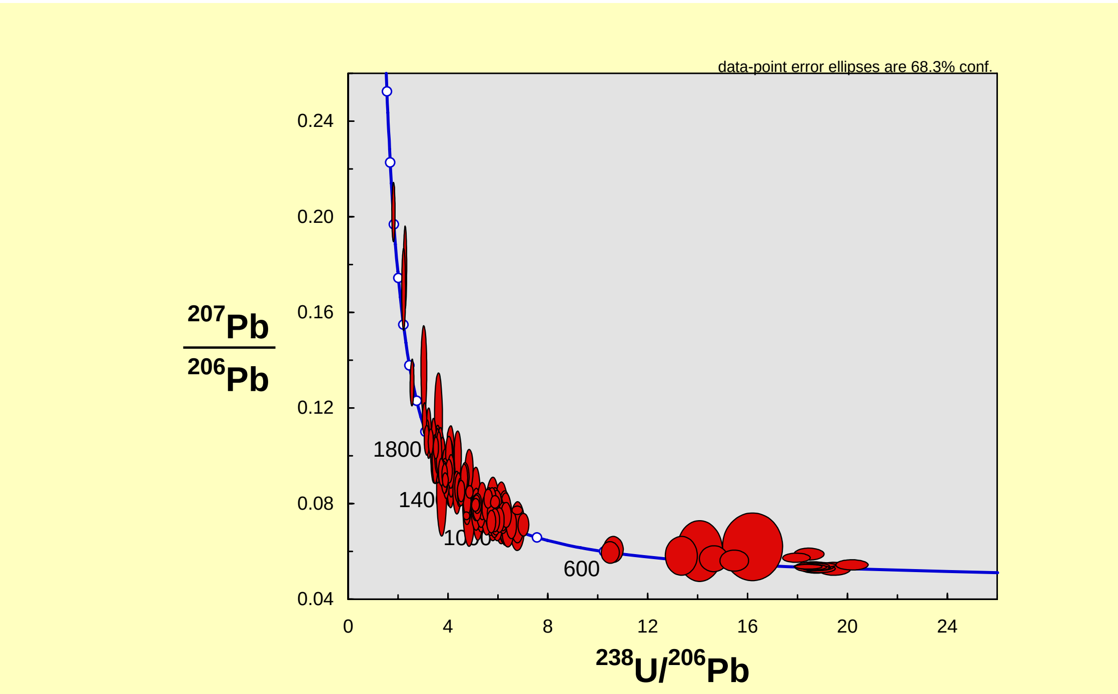
data-point error ellipses are 68.3% conf.
207Pb/206Pb
0.24
0.20
0.16
0.12
0.08
0.04
1800
140
10
600
0
4
8
12
16
20
24
238U/206Pb

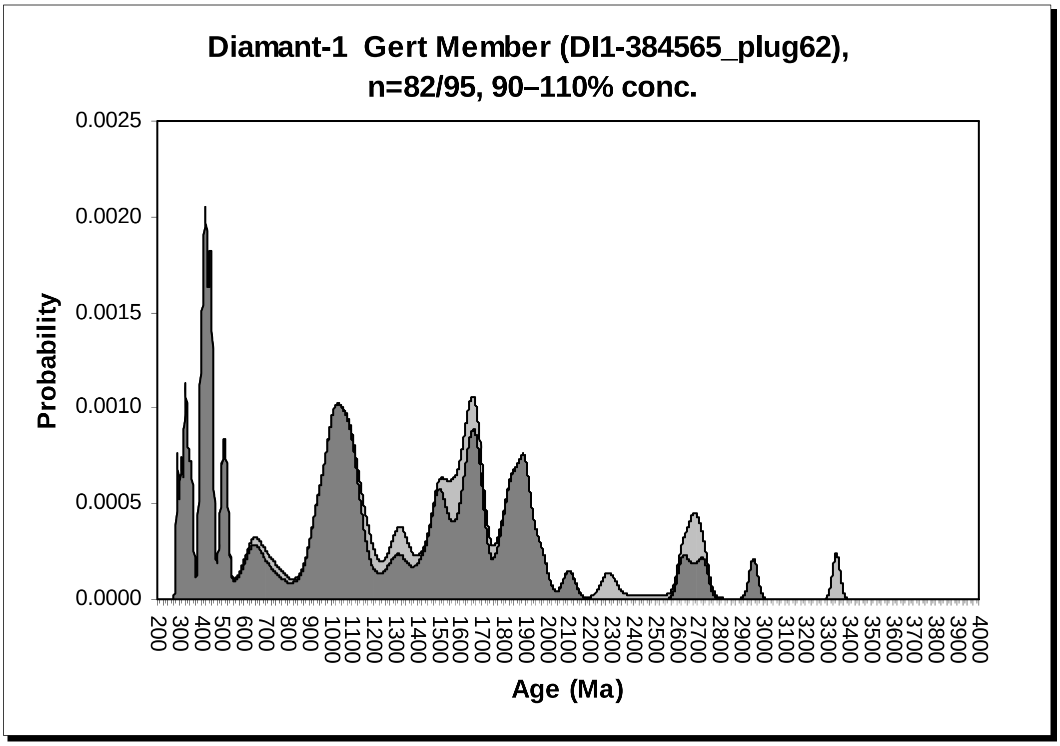
Diamant-1 Gert Member (DI1-384565_plug62),
n=82/95, 90–110% conc.
Probability
Age (Ma)
0.0025
0.0020
0.0015
0.0010
0.0005
0.0000
200
300
400
500
600
700
800
900
1000
1100
1200
1300
1400
1500
1600
1700
1800
1900
2000
2100
2200
2300
2400
2500
2600
2700
2800
2900
3000
3100
3200
3300
3400
3500
3600
3700
3800
3900
4000

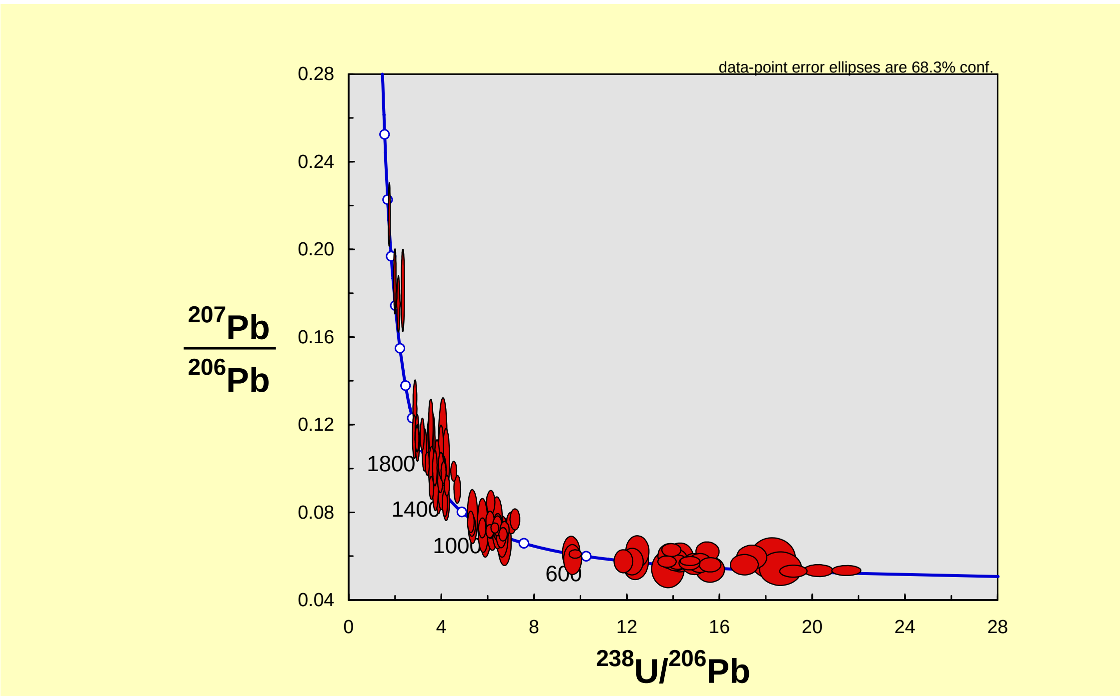
data-point error ellipses are 68.3% conf.
207Pb/206Pb
238U/206Pb
0.28
0.24
0.20
0.16
0.12
0.08
0.04
0
4
8
12
16
20
24
28
1800
1400
1000
600

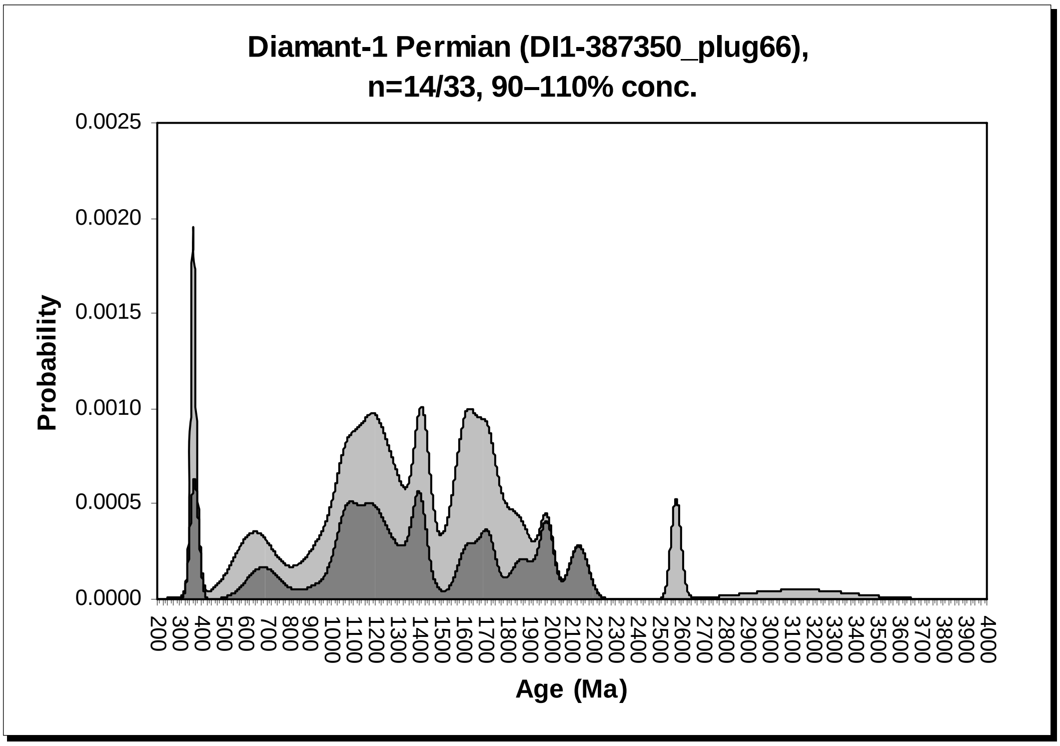
Diamant-1 Permian (DI1-387350_plug66),
n=14/33, 90–110% conc.
Probability
Age (Ma)

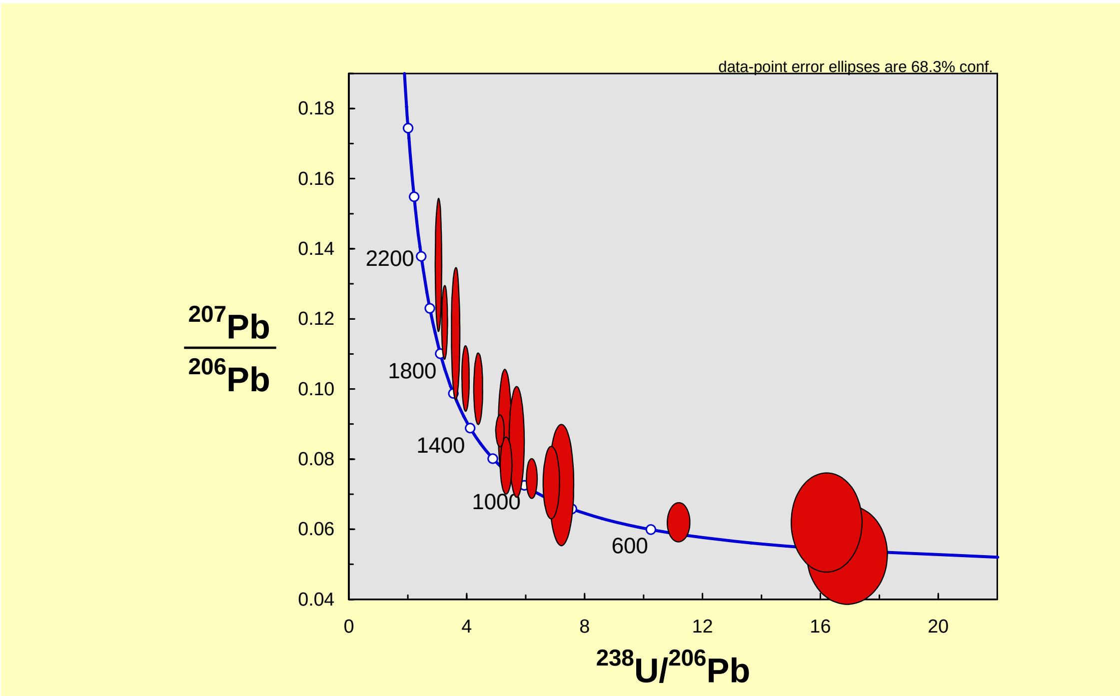
data-point error ellipses are 68.3% conf.
2200
1800
1400
1000
600
207Pb/206Pb
238U/206Pb

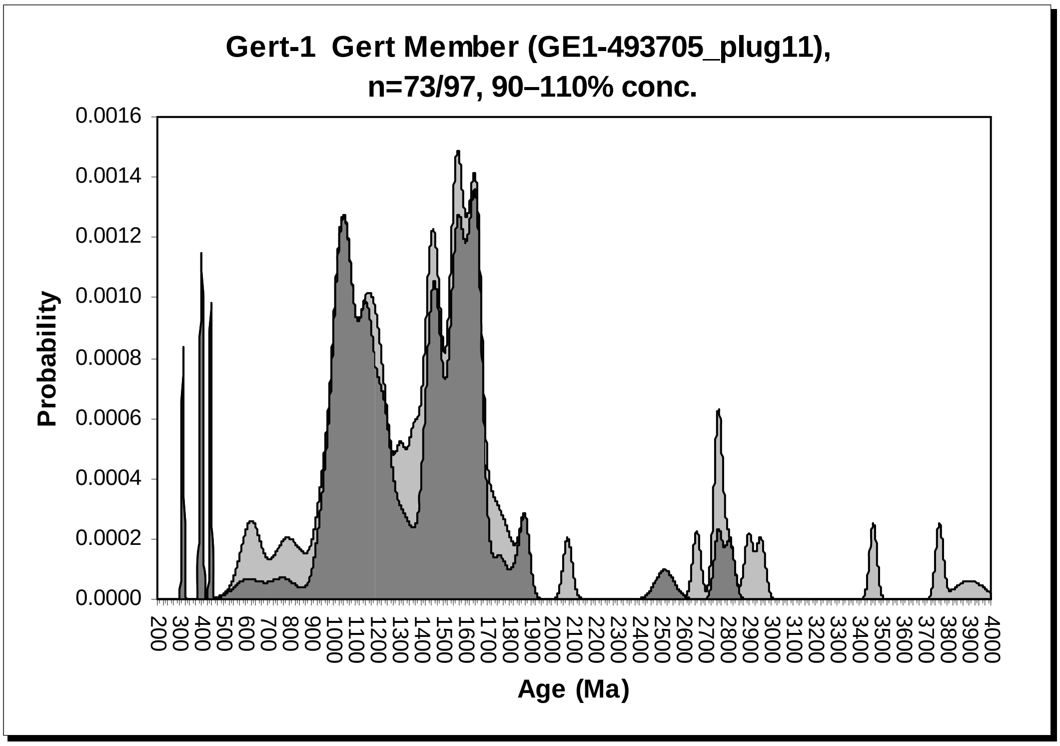
Gert-1 Gert Member (GE1-493705_plug11),
n=73/97, 90–110% conc.
Probability
0.0016
0.0014
0.0012
0.0010
0.0008
0.0006
0.0004
0.0002
0.0000
Age (Ma)

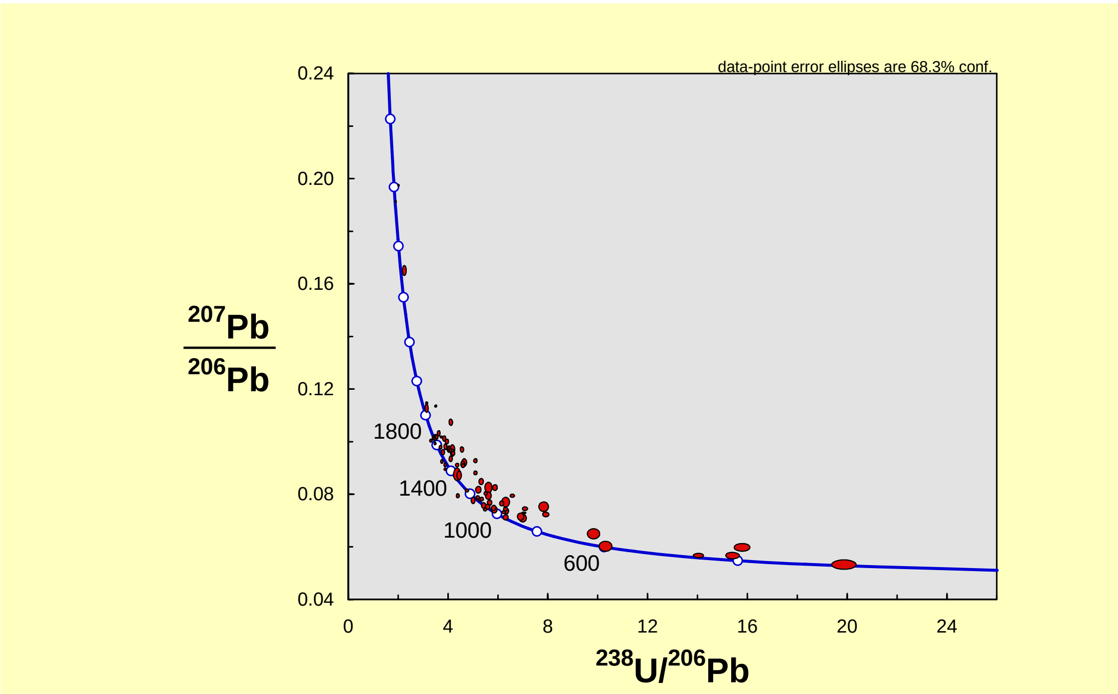
data-point error ellipses are 68.3% conf.
1800
1400
1000
600
207Pb/206Pb
238U/206Pb

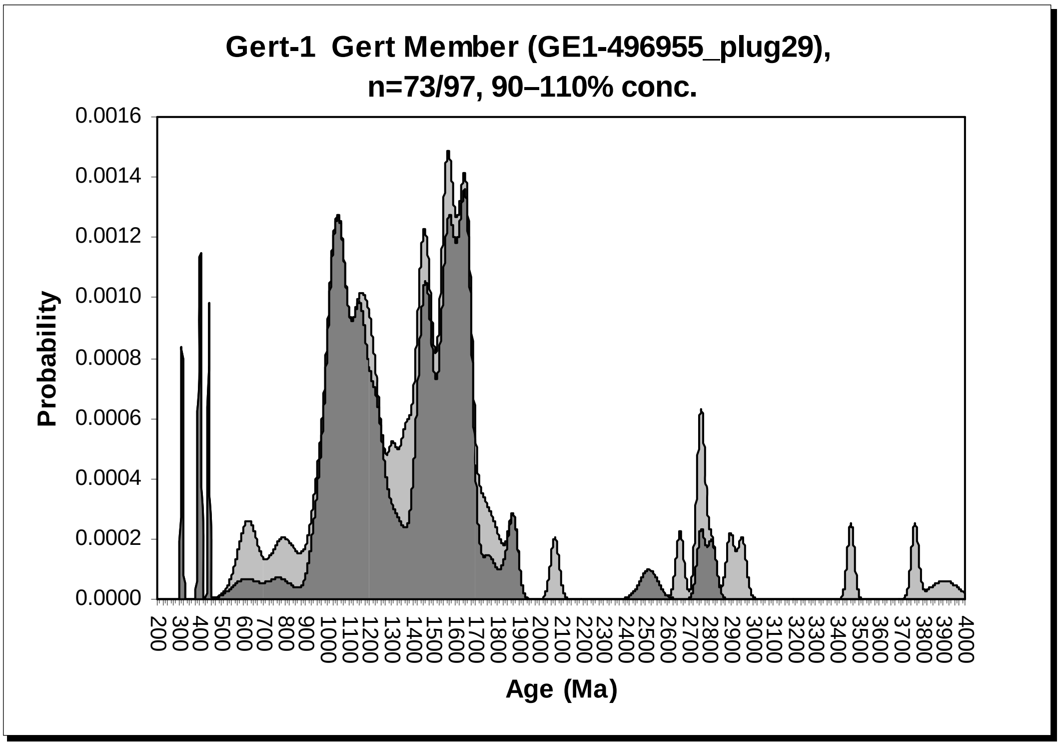

Gert-1 Gert Member (GE1-496955_plug29),
n=73/97, 90–110% conc.
Probability
Age (Ma)

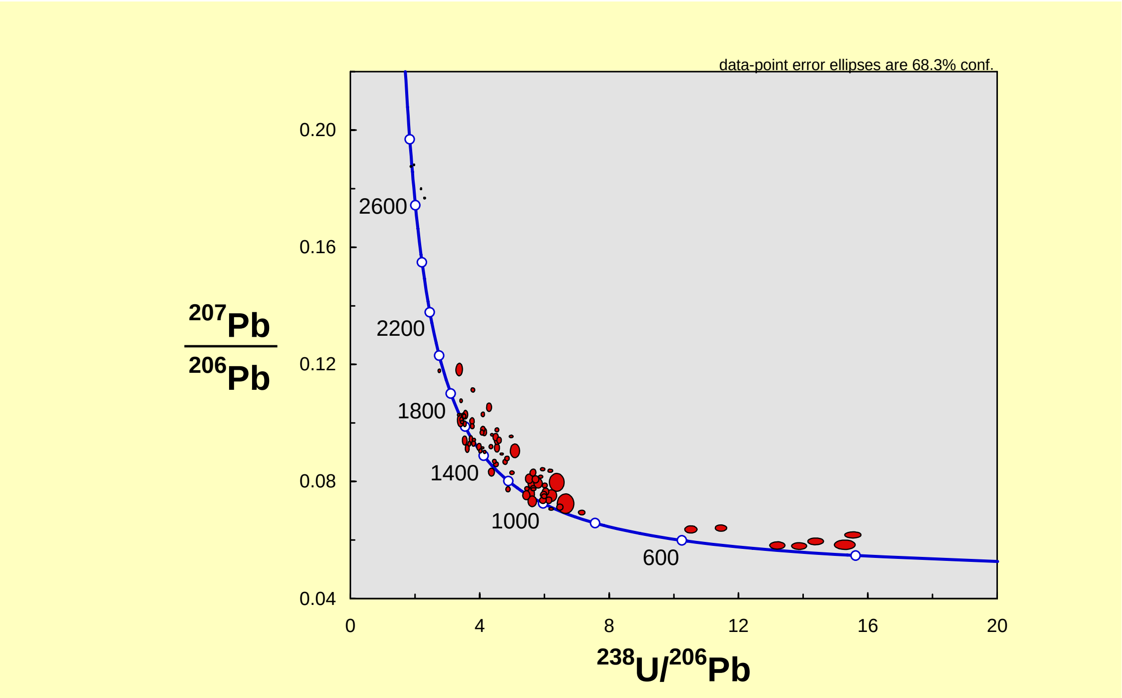

data-point error ellipses are 68.3% conf.
2600
2200
1800
1400
1000
600
207Pb/206Pb
238U/206Pb

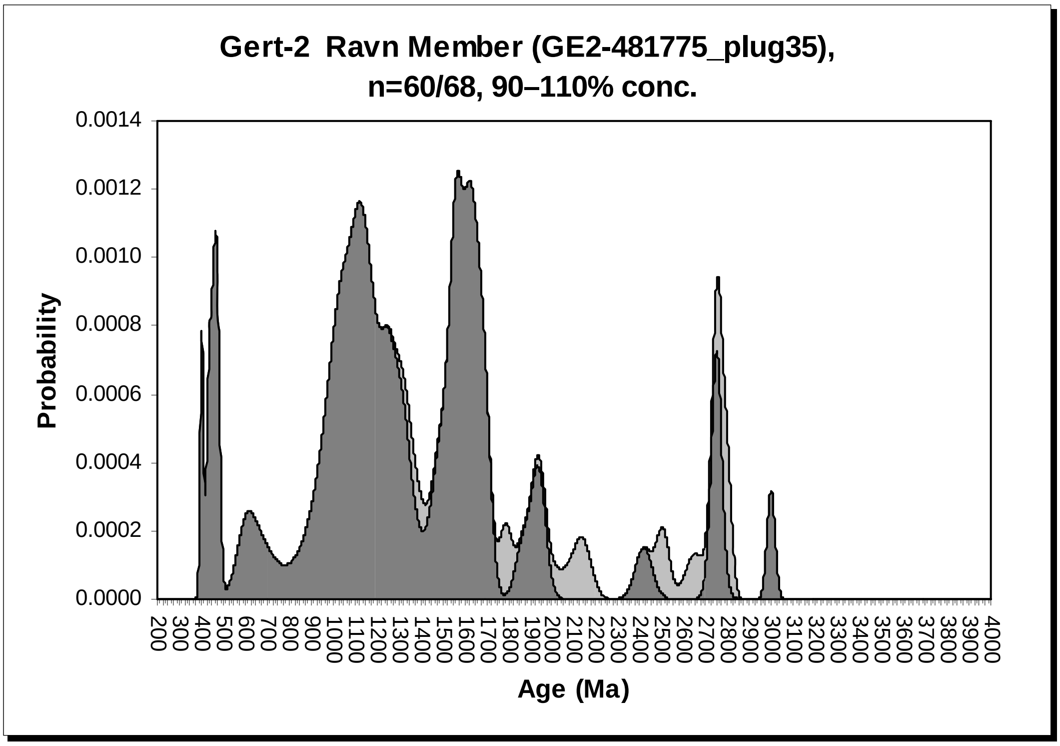
Gert-2 Ravn Member (GE2-481775_plug35),
n=60/68, 90–110% conc.
Probability
0.0014
0.0012
0.0010
0.0008
0.0006
0.0004
0.0002
0.0000
200 300 400 500 600 700 800 900 1000 1100 1200 1300 1400 1500 1600 1700 1800 1900 2000 2100 2200 2300 2400 2500 2600 2700 2800 2900 3000 3100 3200 3300 3400 3500 3600 3700 3800 3900 4000
Age (Ma)

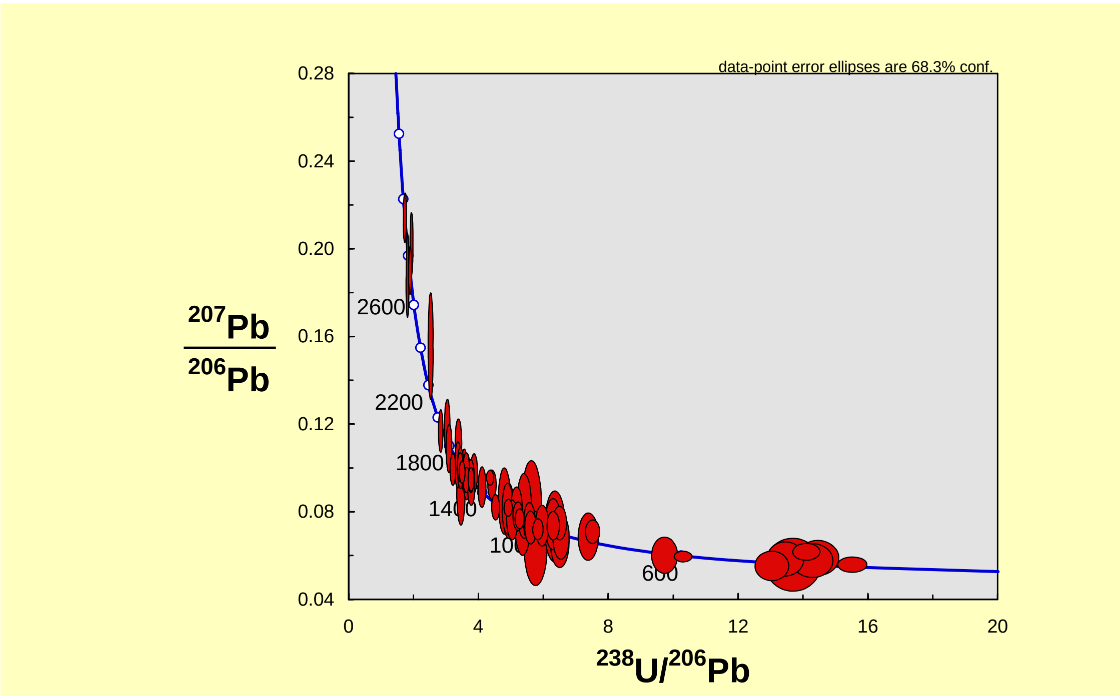
data-point error ellipses are 68.3% conf.
0.28
0.24
0.20
0.16
0.12
0.08
0.04
2600
2200
1800
600
$^{207}Pb/^{206}Pb$
0
4
8
12
16
20
$^{238}U/^{206}Pb$

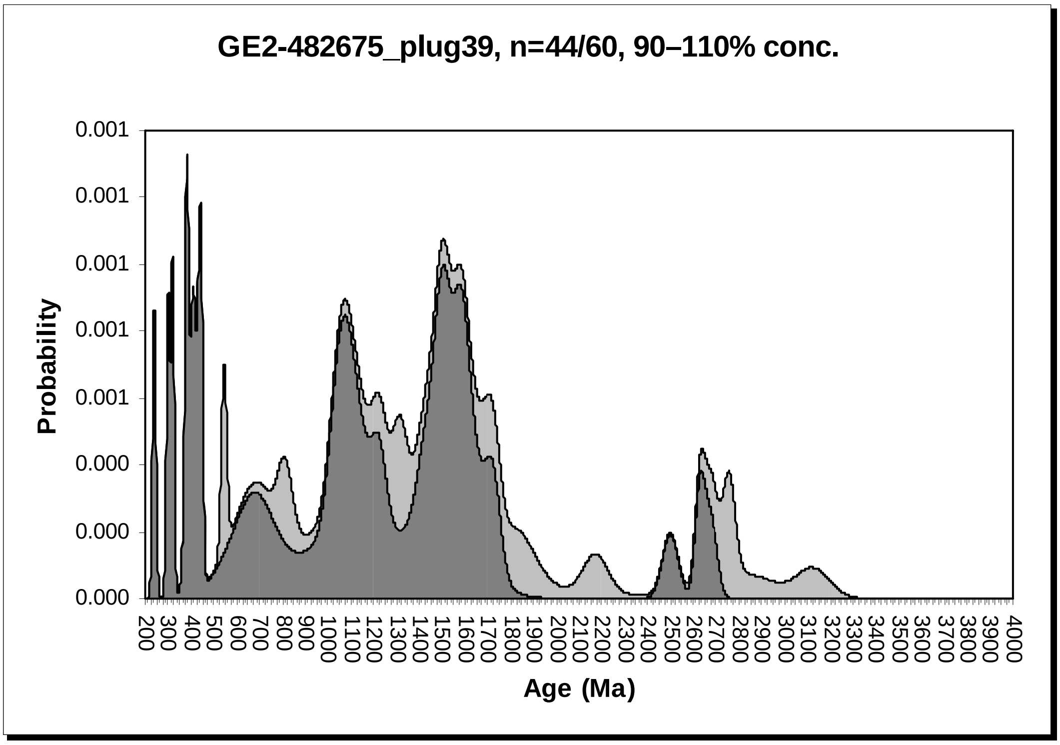
GE2-482675_plug39, n=44/60, 90–110% conc.
Probability
0.001
0.001
0.001
0.001
0.001
0.000
0.000
0.000
Age (Ma)
200
300
400
500
600
700
800
900
1000
1100
1200
1300
1400
1500
1600
1700
1800
1900
2000
2100
2200
2300
2400
2500
2600
2700
2800
2900
3000
3100
3200
3300
3400
3500
3600
3700
3800
3900
4000

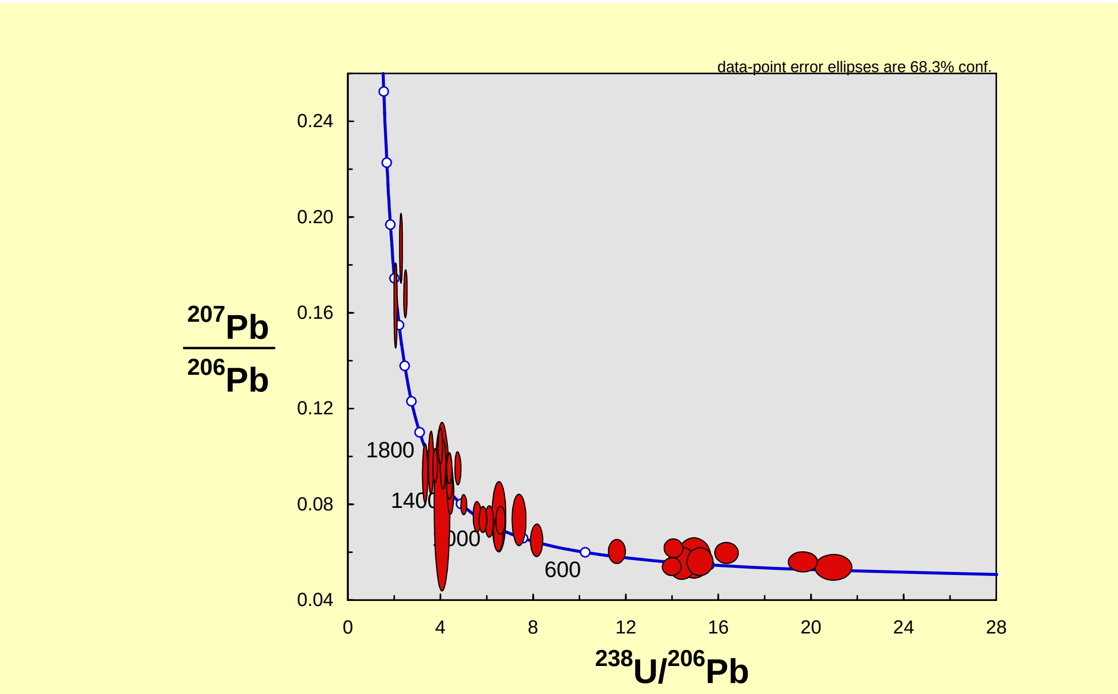
data-point error ellipses are 68.3% conf.
207Pb/206Pb
0.24
0.20
0.16
0.12
0.08
0.04
1800
1400
1000
600
0
4
8
12
16
20
24
28
238U/206Pb

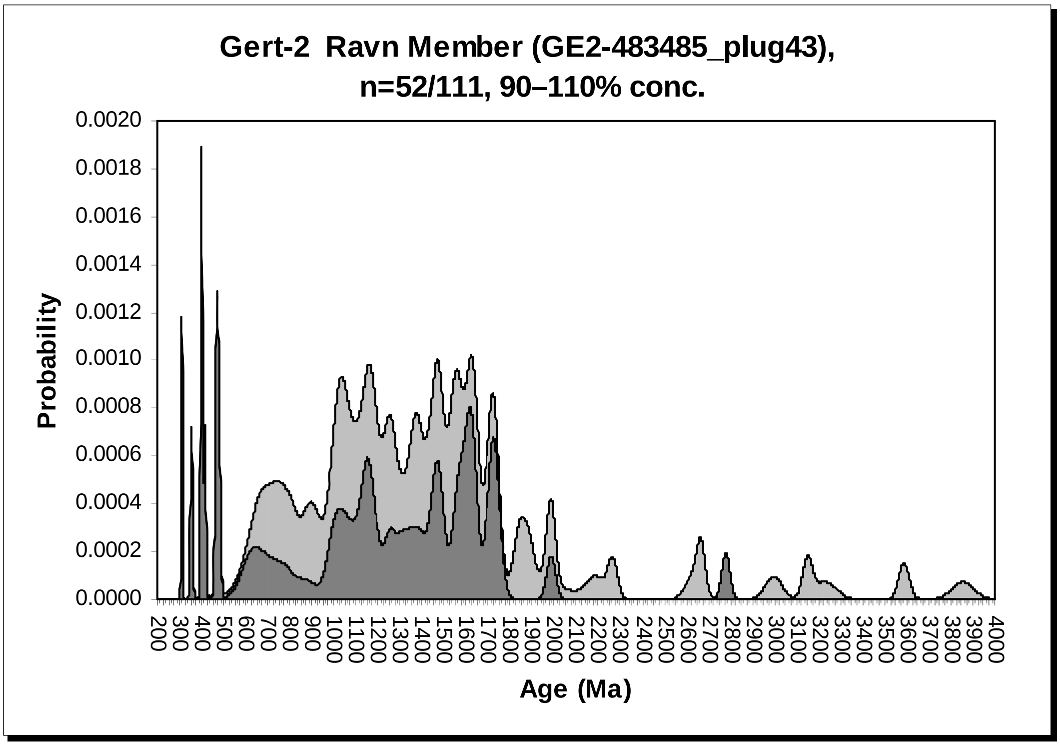
Gert-2 Ravn Member (GE2-483485_plug43),
n=52/111, 90–110% conc.
Probability
0.0020
0.0018
0.0016
0.0014
0.0012
0.0010
0.0008
0.0006
0.0004
0.0002
0.0000
200
300
400
500
600
700
800
900
1000
1100
1200
1300
1400
1500
1600
1700
1800
1900
2000
2100
2200
2300
2400
2500
2600
2700
2800
2900
3000
3100
3200
3300
3400
3500
3600
3700
3800
3900
4000
Age (Ma)

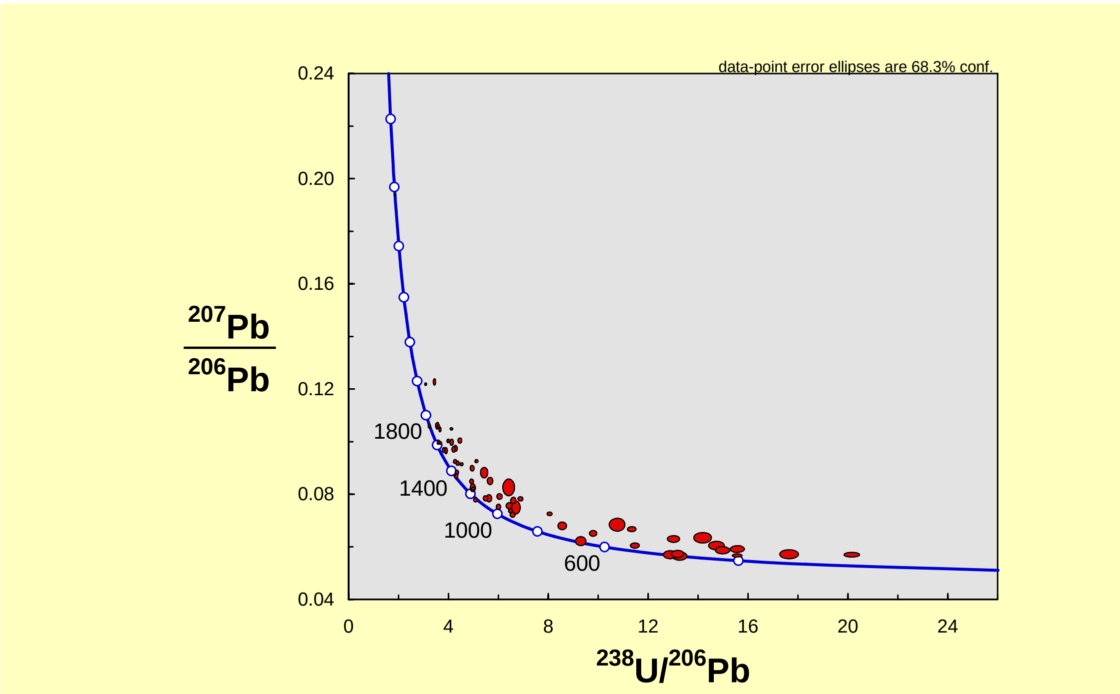
data-point error ellipses are 68.3% conf.
0.24
0.20
0.16
0.12
0.08
0.04
207Pb/206Pb
1800
1400
1000
600
0
4
8
12
16
20
24
238U/206Pb

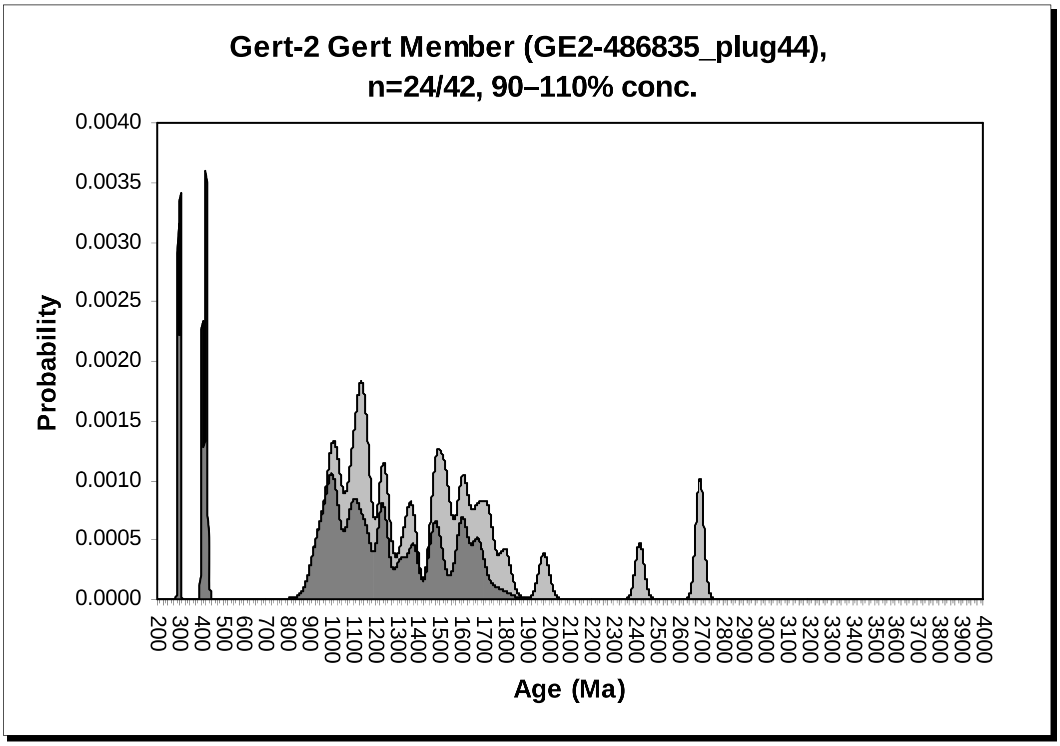
Gert-2 Gert Member (GE2-486835_plug44),
n=24/42, 90–110% conc.
Probability
0.0040
0.0035
0.0030
0.0025
0.0020
0.0015
0.0010
0.0005
0.0000
200
300
400
500
600
700
800
900
1000
1100
1200
1300
1400
1500
1600
1700
1800
1900
2000
2100
2200
2300
2400
2500
2600
2700
2800
2900
3000
3100
3200
3300
3400
3500
3600
3700
3800
3900
4000
Age (Ma)

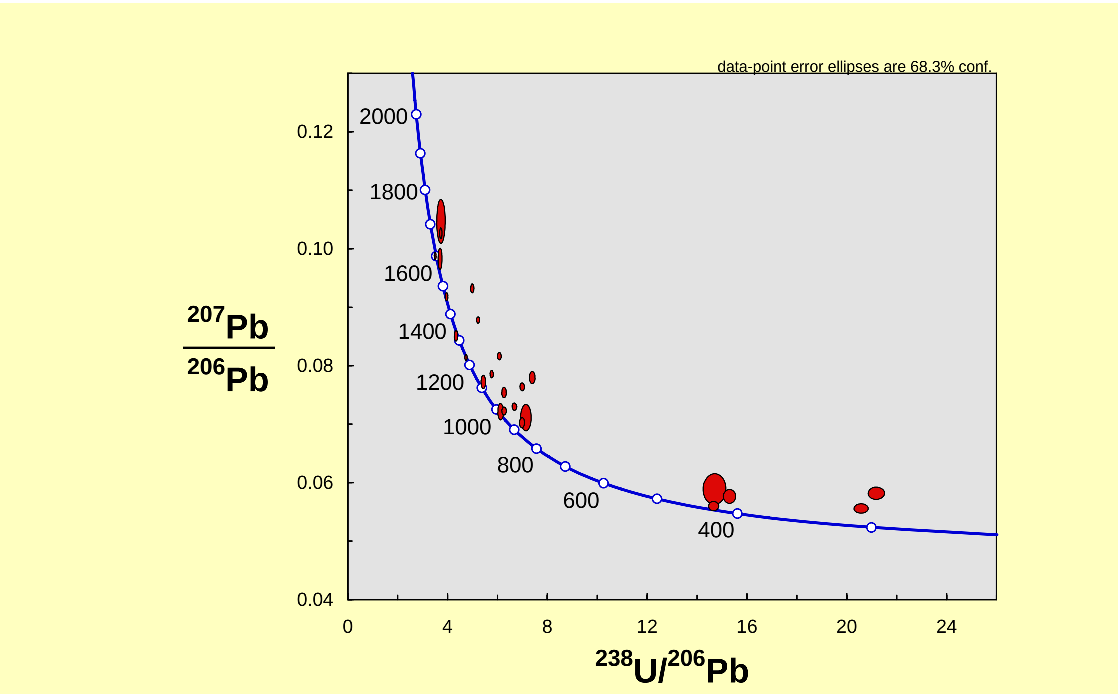
data-point error ellipses are 68.3% conf.
207Pb/206Pb
0.12
0.10
0.08
0.06
0.04
2000
1800
1600
1400
1200
1000
800
600
400
0
4
8
12
16
20
24
238U/206Pb

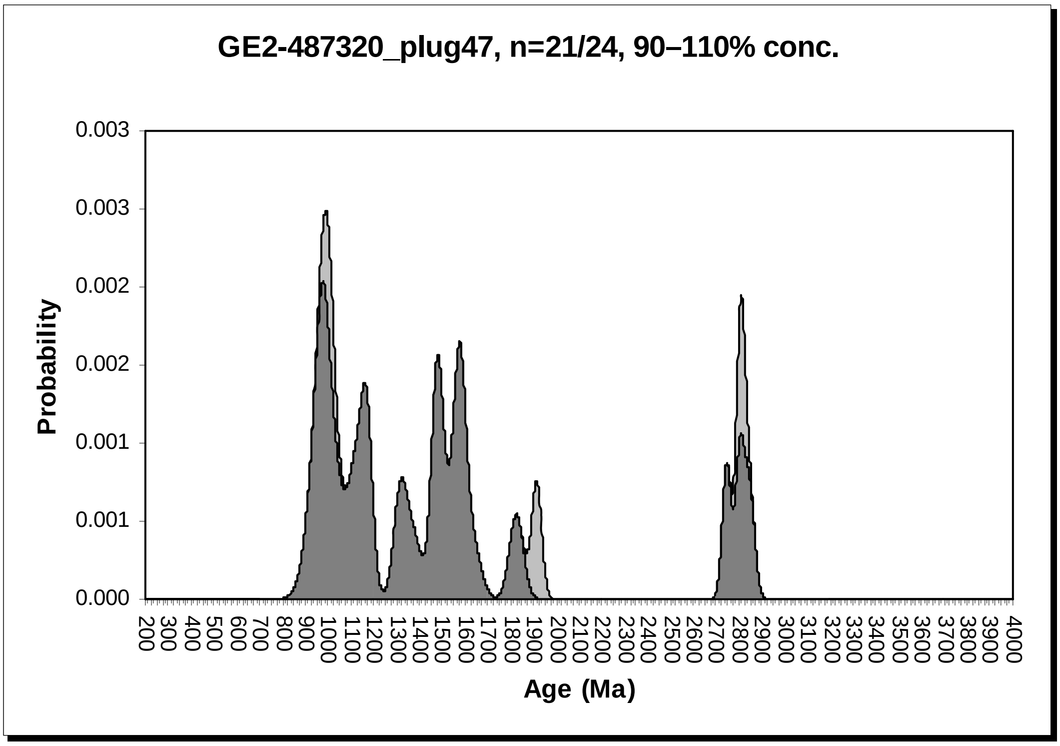
GE2-487320_plug47, n=21/24, 90–110% conc.
Probability
Age (Ma)
0.000
0.001
0.001
0.002
0.002
0.003
0.003

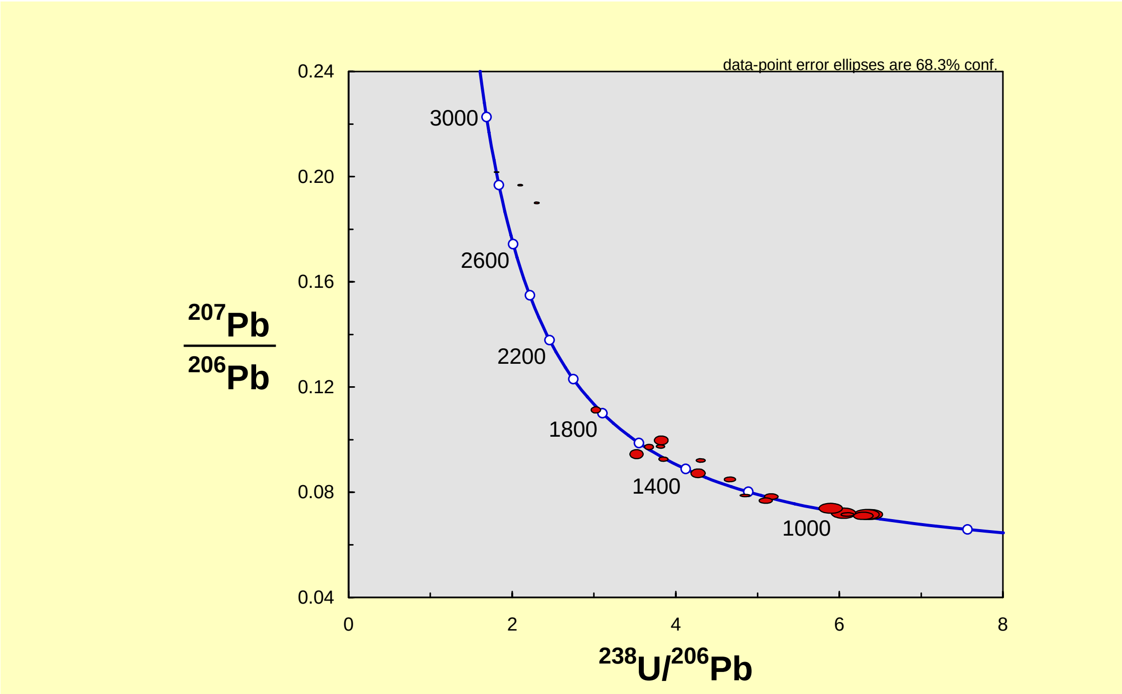
data-point error ellipses are 68.3% conf.
3000
2600
2200
1800
1400
1000
$^{207}Pb/^{206}Pb$
$^{238}U/^{206}Pb$

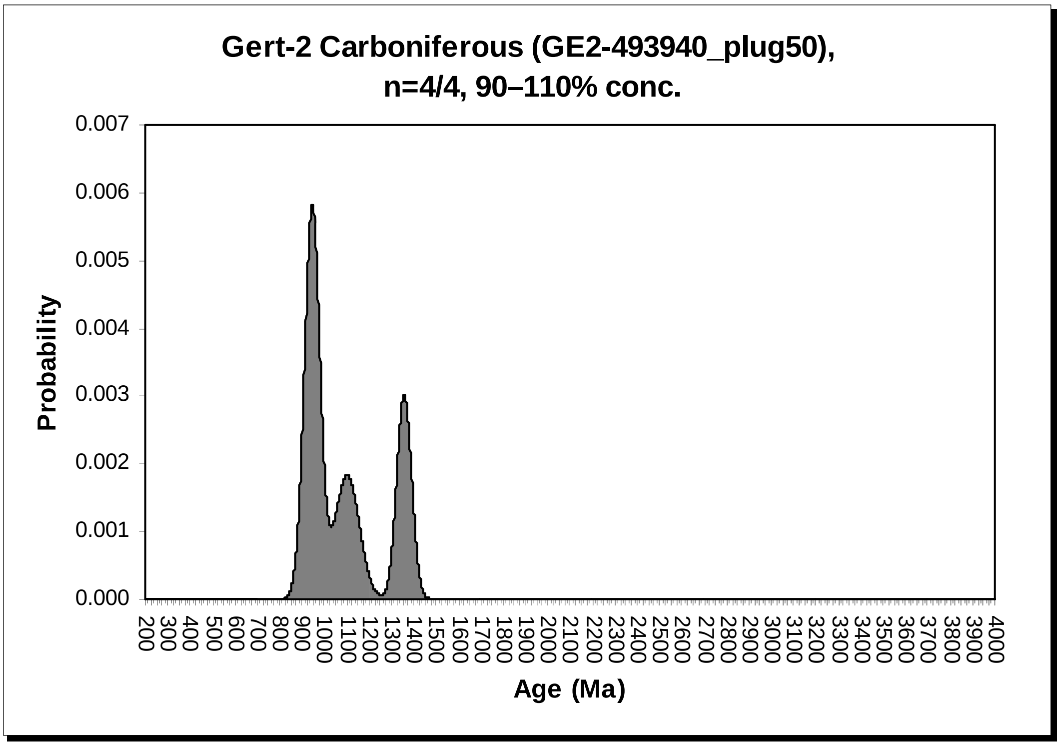
Gert-2 Carboniferous (GE2-493940_plug50),
n=4/4, 90–110% conc.
Probability
0.007
0.006
0.005
0.004
0.003
0.002
0.001
0.000
200 300 400 500 600 700 800 900 1000 1100 1200 1300 1400 1500 1600 1700 1800 1900 2000 2100 2200 2300 2400 2500 2600 2700 2800 2900 3000 3100 3200 3300 3400 3500 3600 3700 3800 3900 4000
Age (Ma)

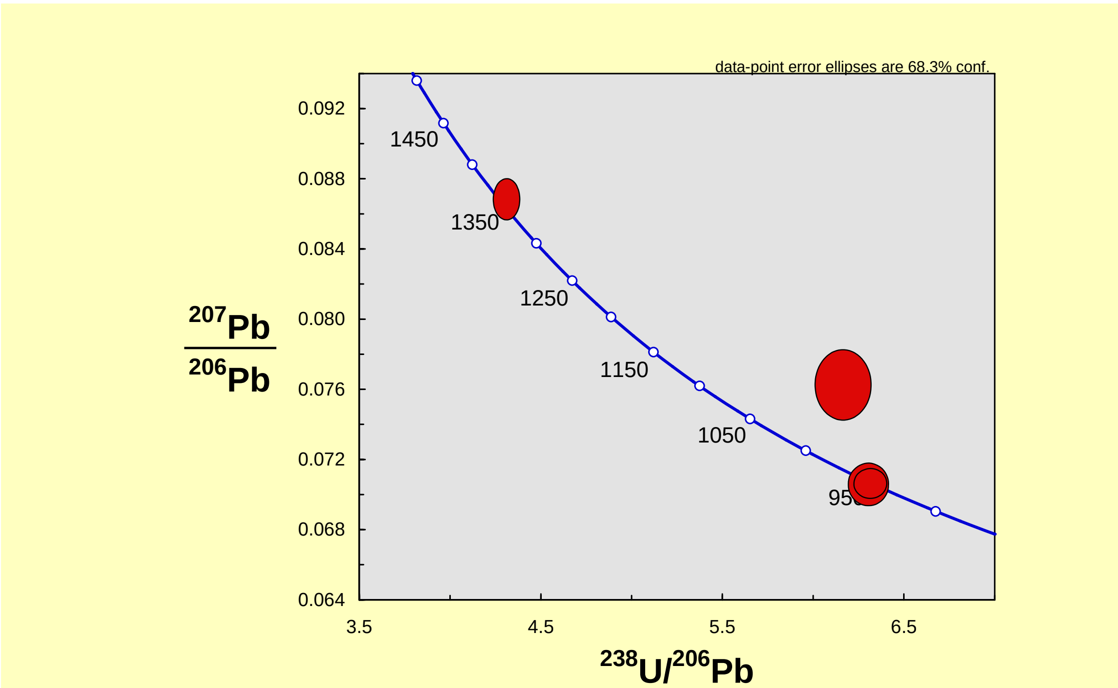
data-point error ellipses are 68.3% conf.
207Pb/206Pb
0.092
0.088
0.084
0.080
0.076
0.072
0.068
0.064
1450
1350
1250
1150
1050
3.5
4.5
5.5
6.5
238U/206Pb

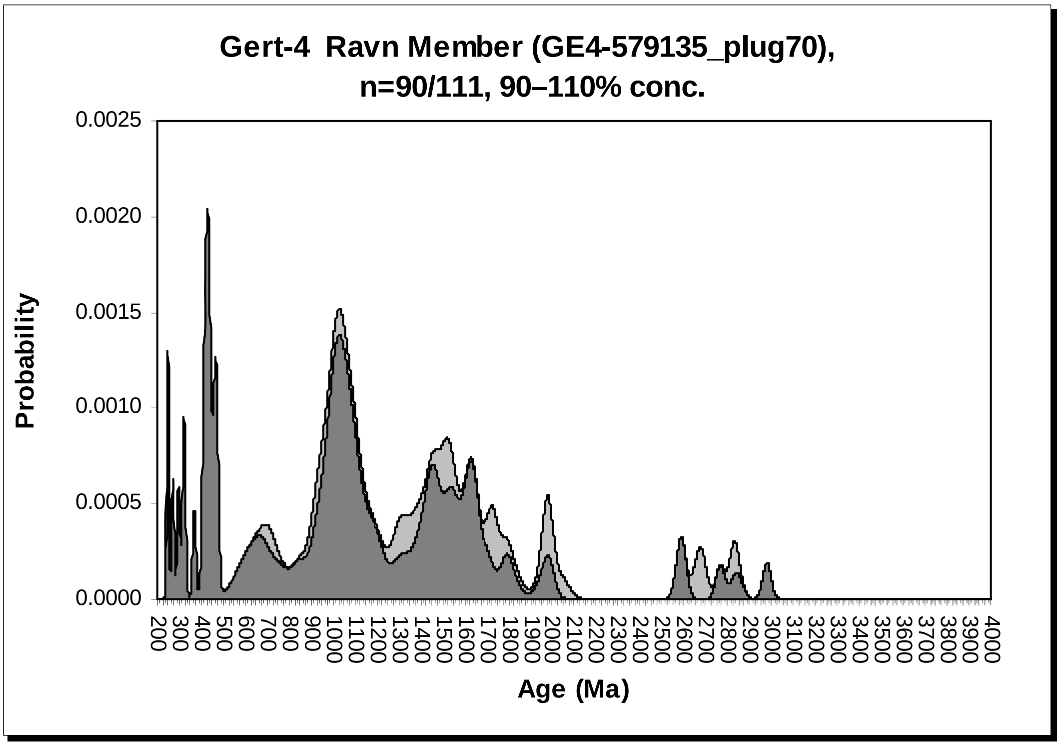
Gert-4 Ravn Member (GE4-579135_plug70),
n=90/111, 90–110% conc.
Probability
0.0025
0.0020
0.0015
0.0010
0.0005
0.0000
200
300
400
500
600
700
800
900
1000
1100
1200
1300
1400
1500
1600
1700
1800
1900
2000
2100
2200
2300
2400
2500
2600
2700
2800
2900
3000
3100
3200
3300
3400
3500
3600
3700
3800
3900
4000
Age (Ma)

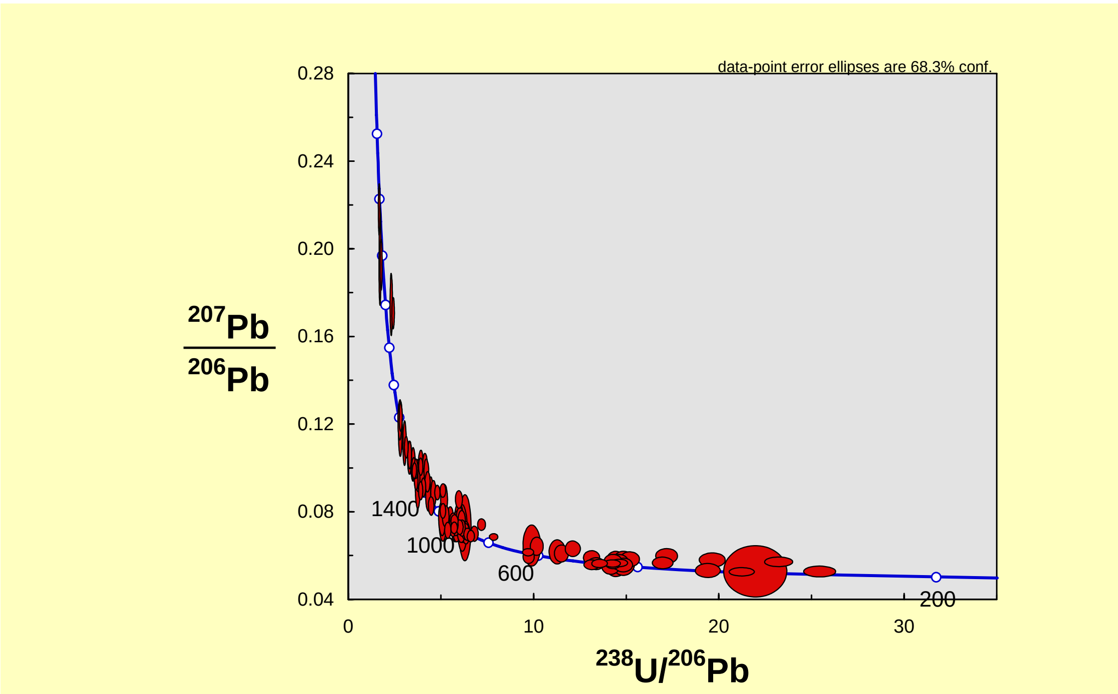
data-point error ellipses are 68.3% conf.
0.28
0.24
0.20
0.16
0.12
0.08
0.04
207Pb/206Pb
1400
1000
600
200
0
10
20
30
238U/206Pb

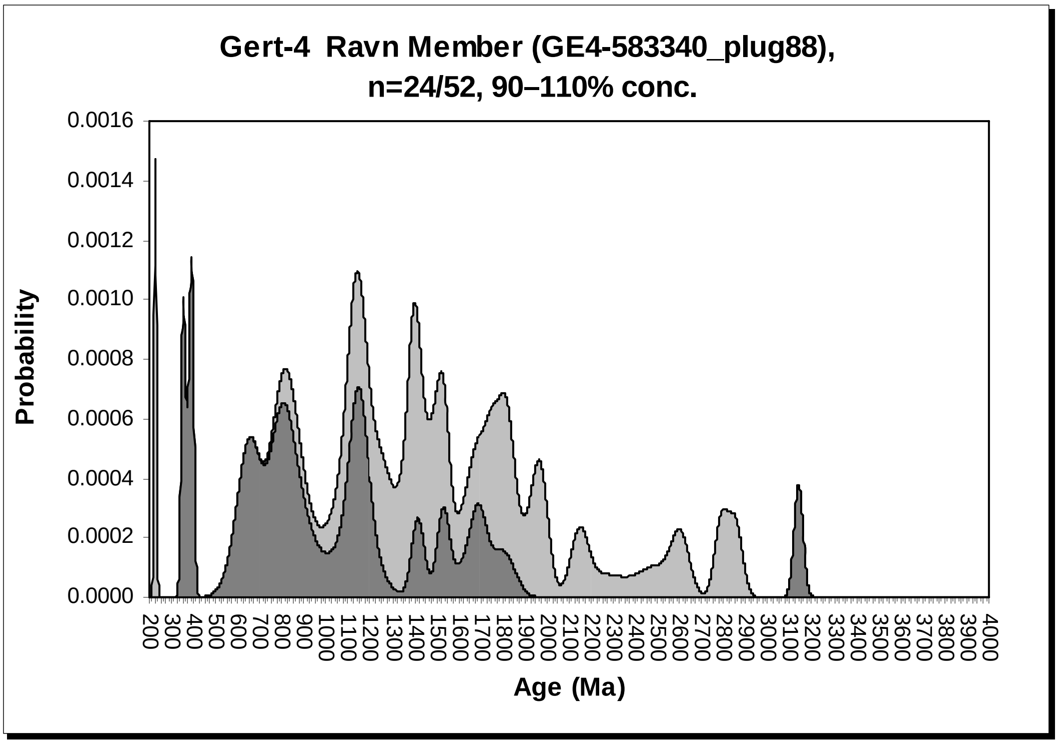

Gert-4 Ravn Member (GE4-583340_plug88), n=24/52, 90–110% conc.
Probability
Age (Ma)

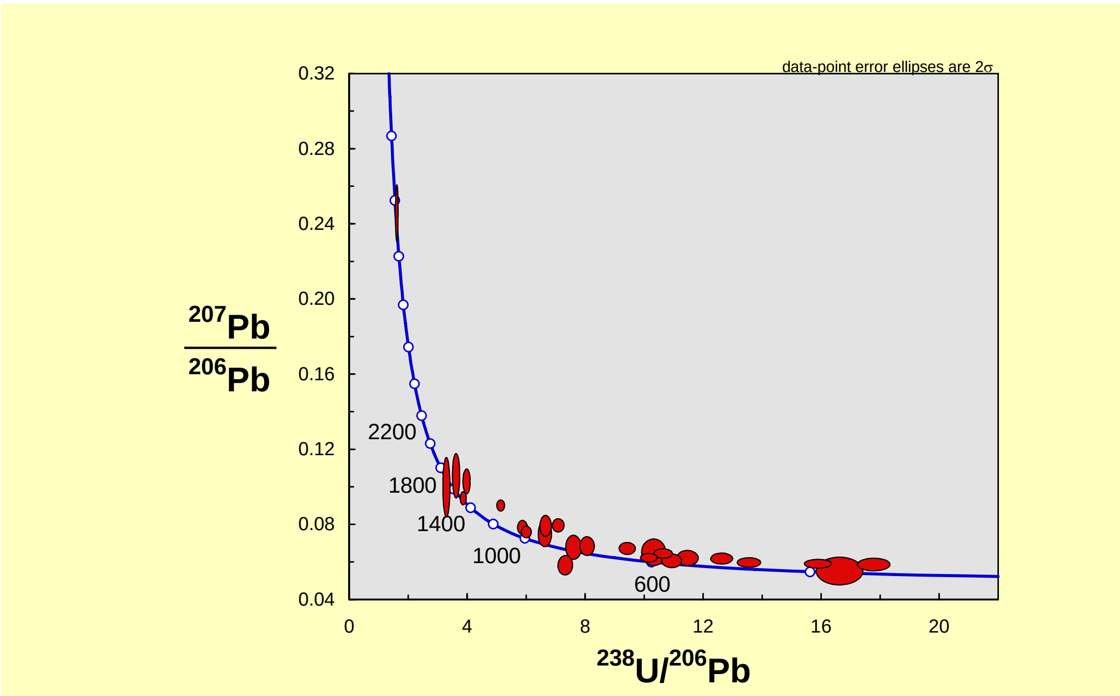

data-point error ellipses are 2σ
207Pb/206Pb
238U/206Pb
2200
1800
1400
1000
600

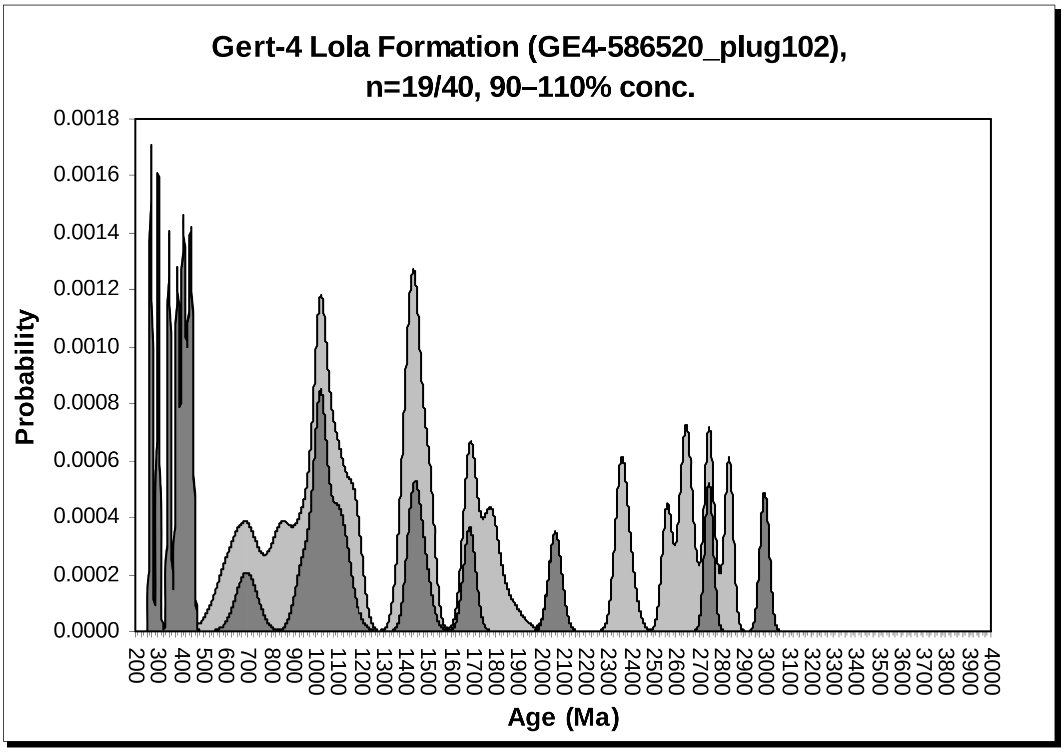
Gert-4 Lola Formation (GE4-586520_plug102),
n=19/40, 90–110% conc.
Probability
0.0018
0.0016
0.0014
0.0012
0.0010
0.0008
0.0006
0.0004
0.0002
0.0000
200
300
400
500
600
700
800
900
1000
1100
1200
1300
1400
1500
1600
1700
1800
1900
2000
2100
2200
2300
2400
2500
2600
2700
2800
2900
3000
3100
3200
3300
3400
3500
3600
3700
3800
3900
4000
Age (Ma)

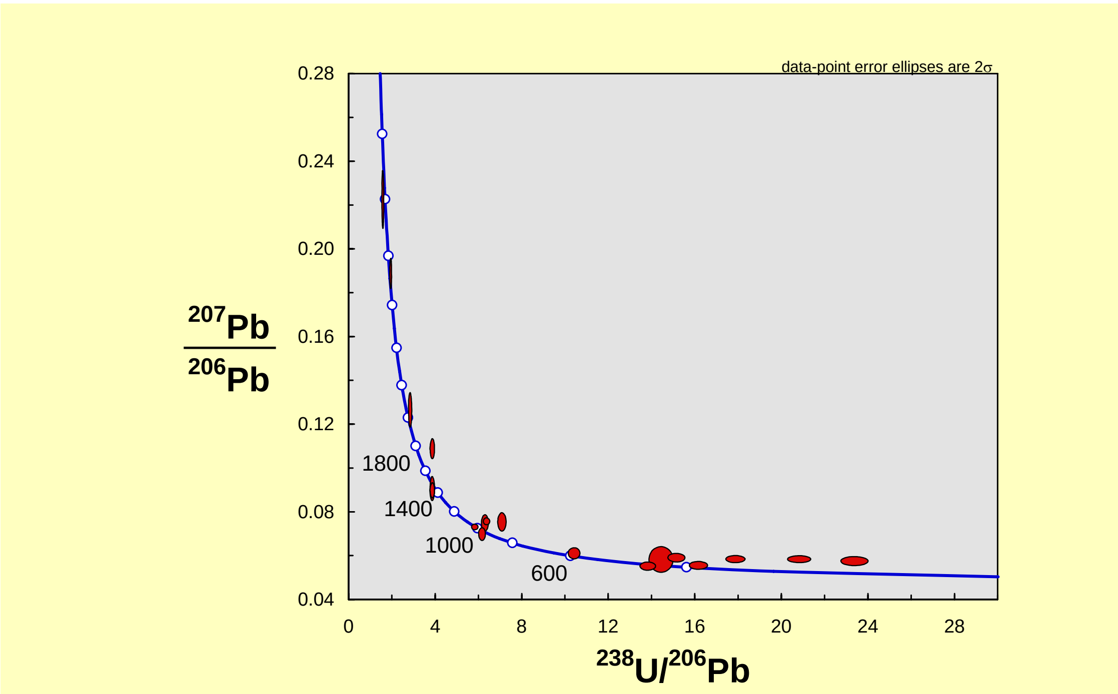
data-point error ellipses are 2σ
0.28
0.24
0.20
0.16
0.12
0.08
0.04
207Pb/206Pb
1800
1400
1000
600
0
4
8
12
16
20
24
28
238U/206Pb

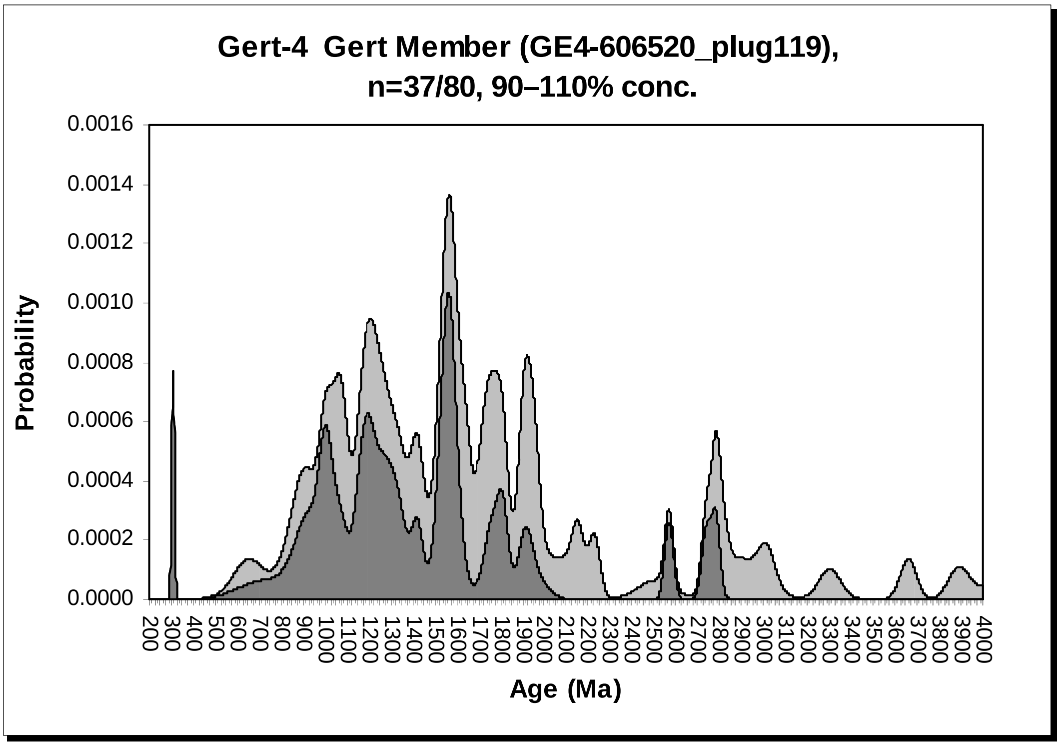
Gert-4 Gert Member (GE4-606520_plug119),
n=37/80, 90–110% conc.
Probability
0.0016
0.0014
0.0012
0.0010
0.0008
0.0006
0.0004
0.0002
0.0000
200 300 400 500 600 700 800 900 1000 1100 1200 1300 1400 1500 1600 1700 1800 1900 2000 2100 2200 2300 2400 2500 2600 2700 2800 2900 3000 3100 3200 3300 3400 3500 3600 3700 3800 3900 4000
Age (Ma)

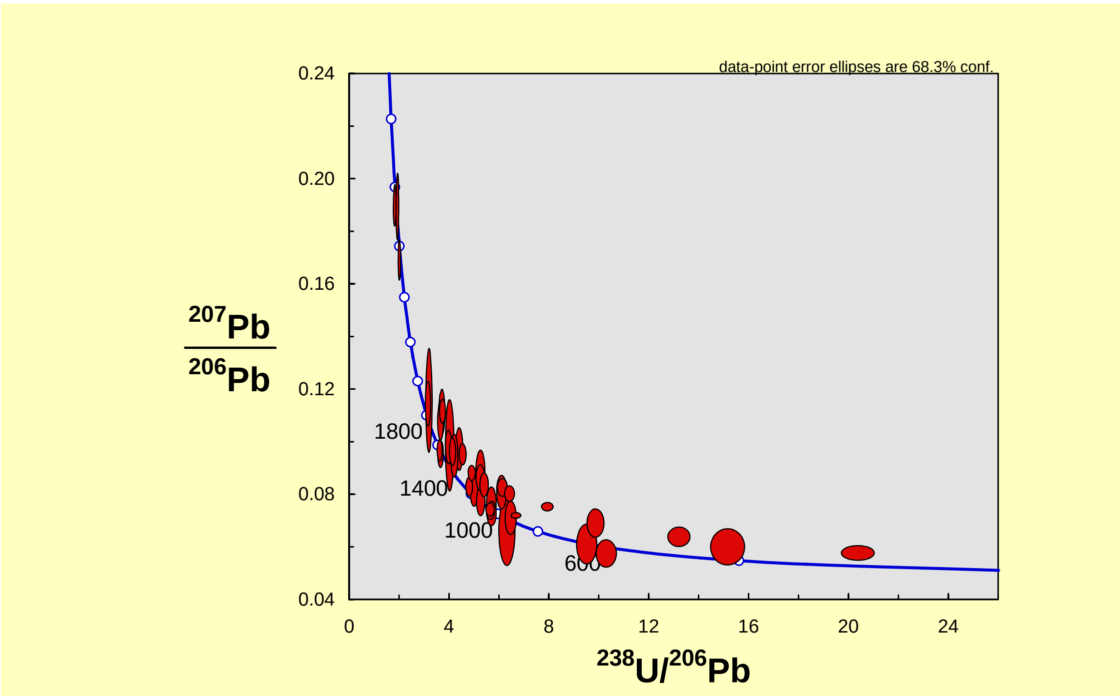
data-point error ellipses are 68.3% conf.
207Pb/206Pb
0.24
0.20
0.16
0.12
0.08
0.04
1800
1400
1000
600
0
4
8
12
16
20
24
238U/206Pb

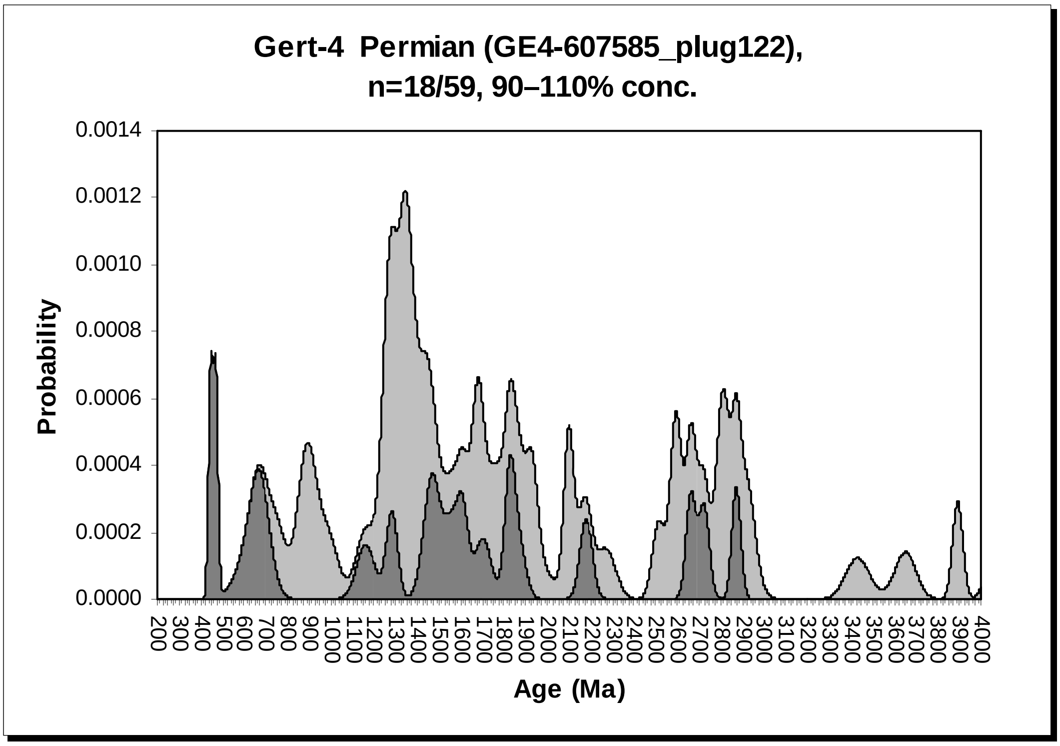

Gert-4 Permian (GE4-607585_plug122),
n=18/59, 90–110% conc.
Probability
Age (Ma)

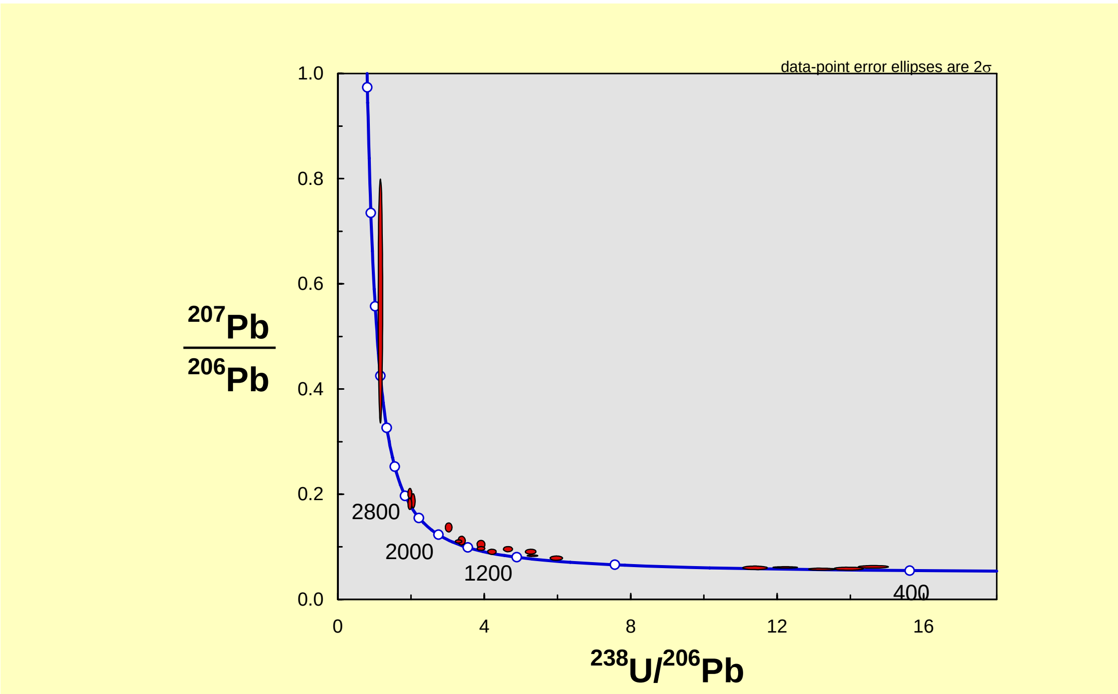

data-point error ellipses are 2σ
2800
2000
1200
400

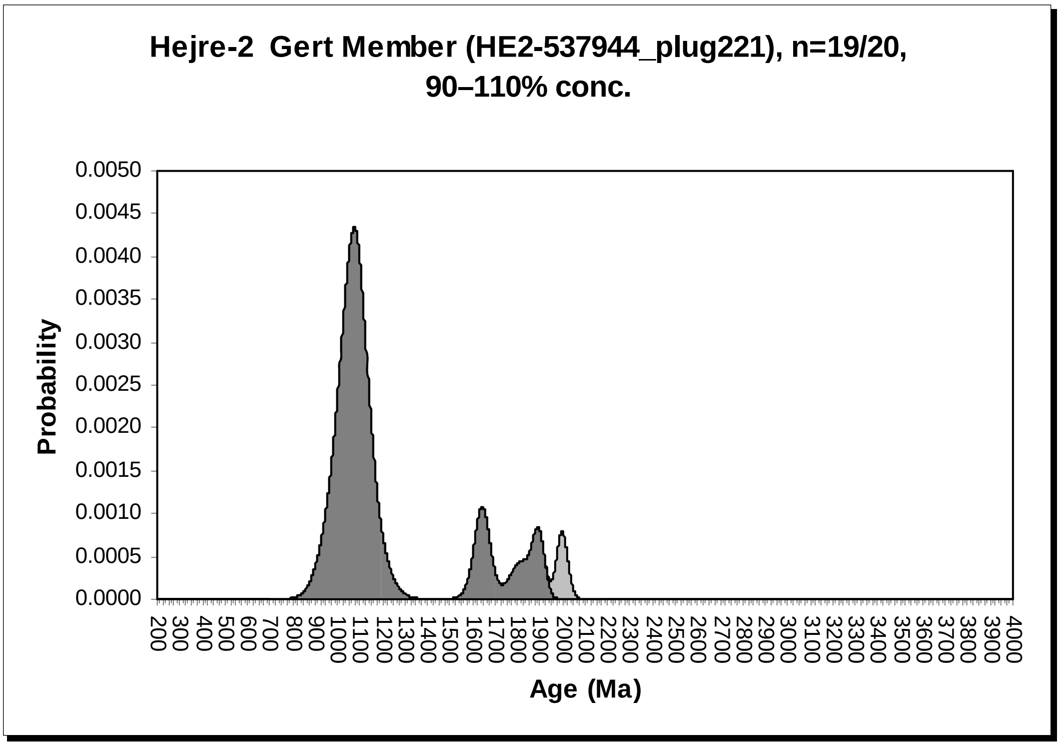
Hejre-2 Gert Member (HE2-537944_plug221), n=19/20,
90–110% conc.
Probability
0.0050
0.0045
0.0040
0.0035
0.0030
0.0025
0.0020
0.0015
0.0010
0.0005
0.0000
200 300 400 500 600 700 800 900 1000 1100 1200 1300 1400 1500 1600 1700 1800 1900 2000 2100 2200 2300 2400 2500 2600 2700 2800 2900 3000 3100 3200 3300 3400 3500 3600 3700 3800 3900 4000
Age (Ma)

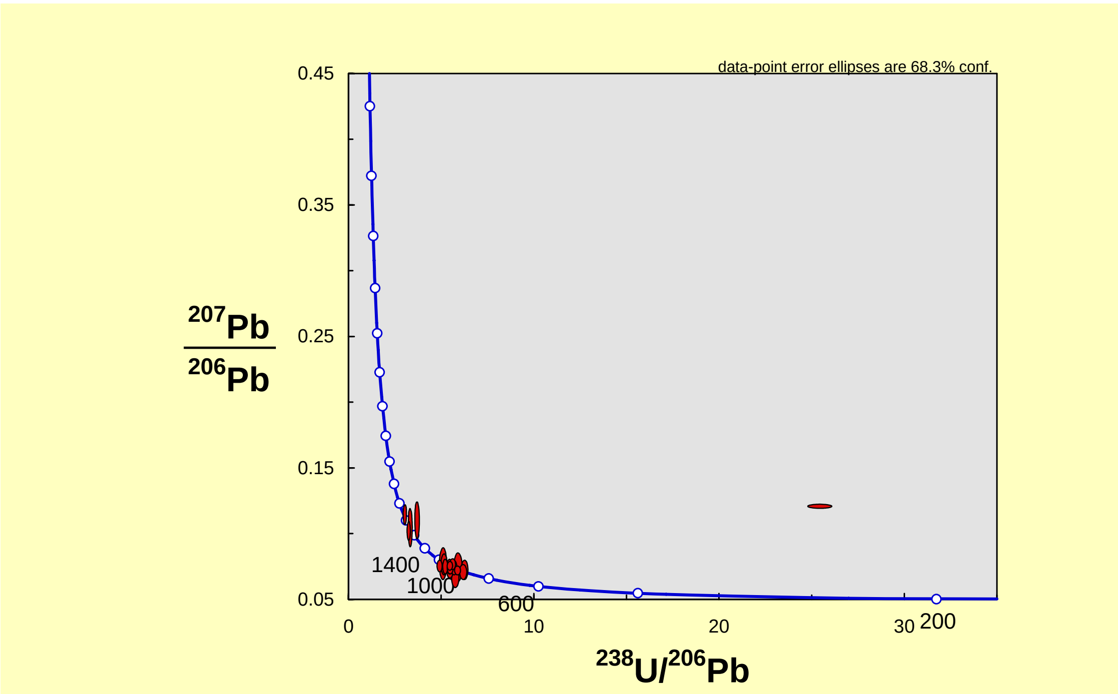
data-point error ellipses are 68.3% conf.
0.45
0.35
0.25
0.15
0.05
$^{207}Pb/^{206}Pb$
1400
1000
600
200
0
10
20
30
$^{238}U/^{206}Pb$

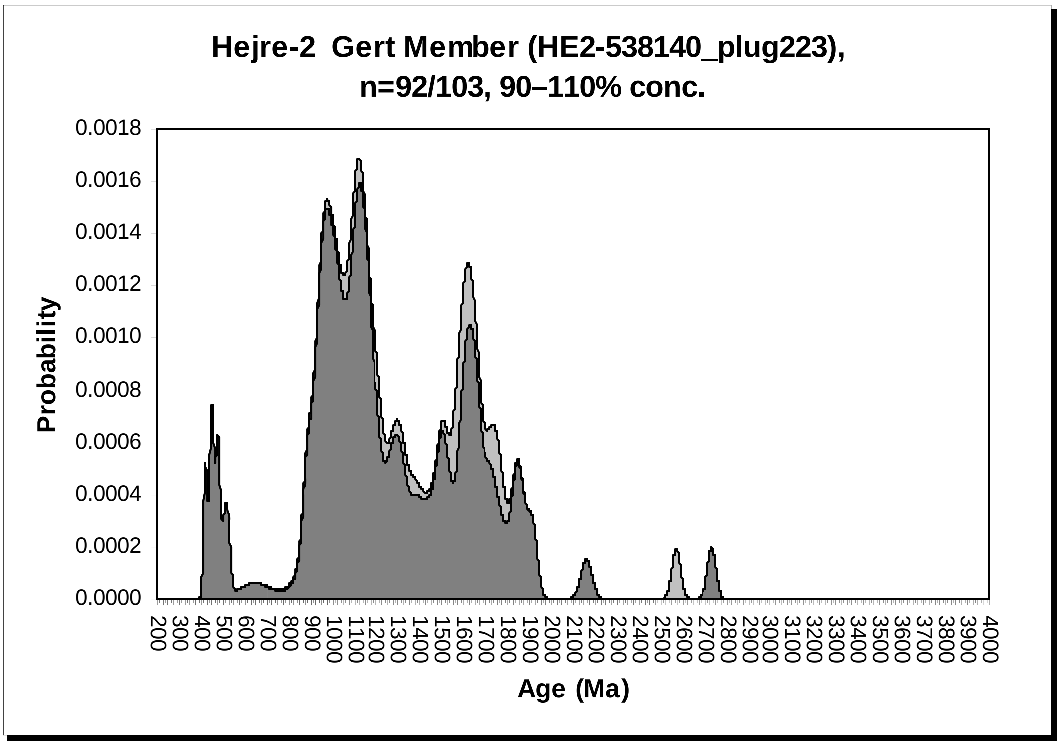
Hejre-2 Gert Member (HE2-538140_plug223),
n=92/103, 90–110% conc.
Probability
0.0018
0.0016
0.0014
0.0012
0.0010
0.0008
0.0006
0.0004
0.0002
0.0000
200
300
400
500
600
700
800
900
1000
1100
1200
1300
1400
1500
1600
1700
1800
1900
2000
2100
2200
2300
2400
2500
2600
2700
2800
2900
3000
3100
3200
3300
3400
3500
3600
3700
3800
3900
4000
Age (Ma)

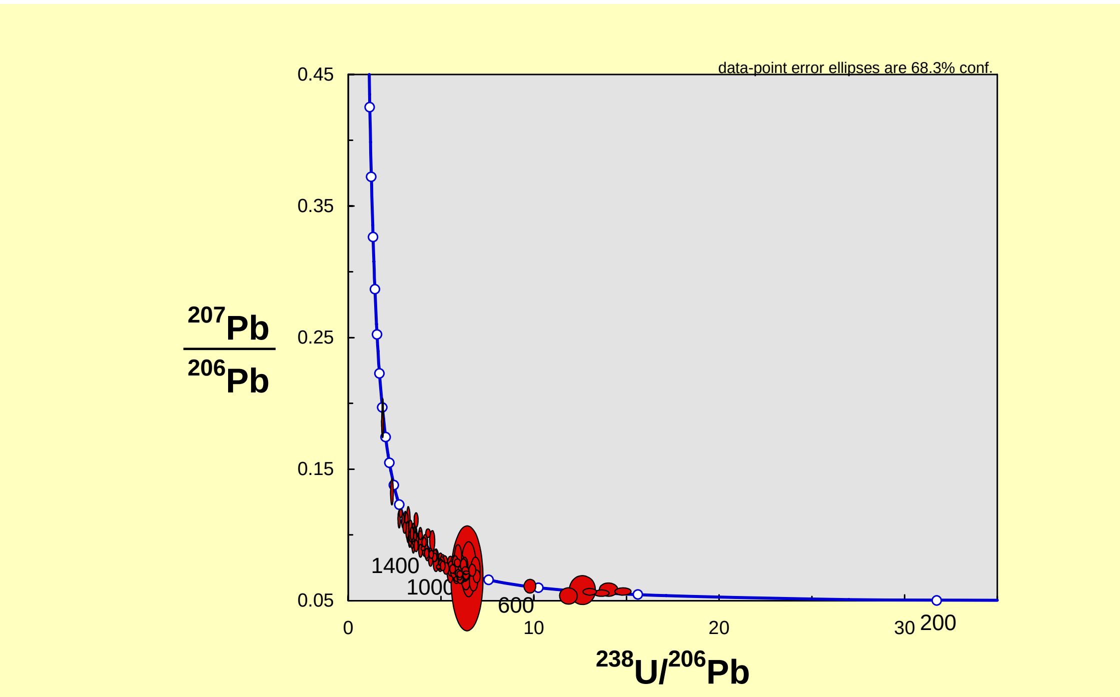
data-point error ellipses are 68.3% conf.
0.45
0.35
0.25
0.15
0.05
207Pb/206Pb
1400
1000
600
200
0
10
20
30
238U/206Pb

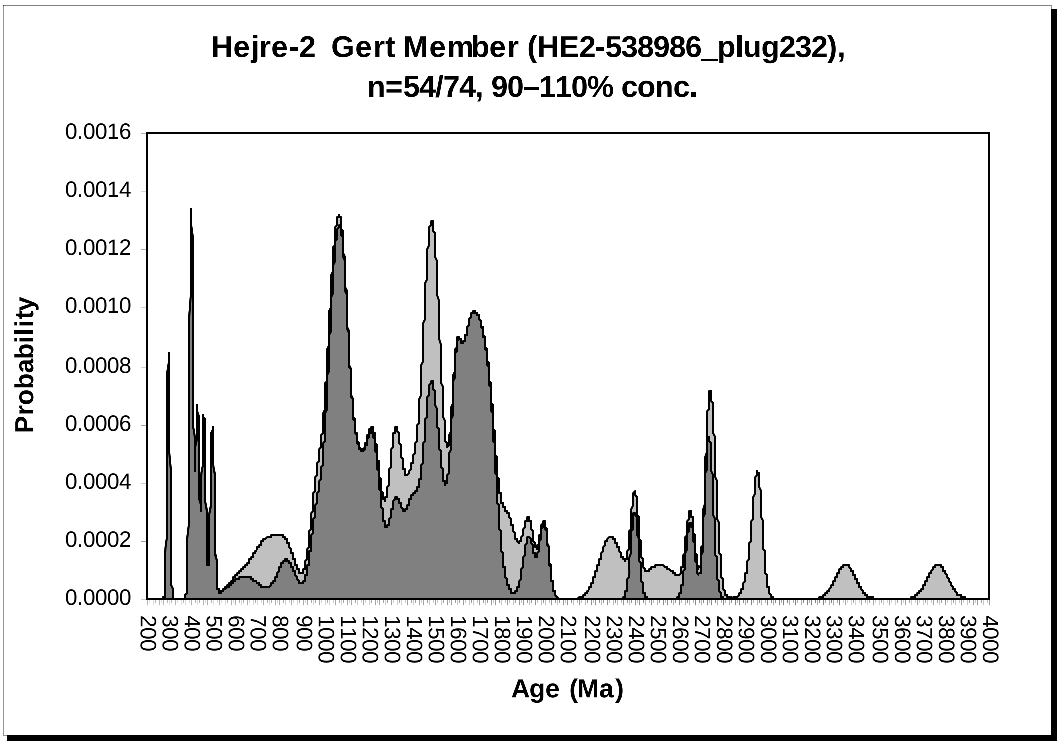
Hejre-2 Gert Member (HE2-538986_plug232),
n=54/74, 90–110% conc.
Probability
Age (Ma)

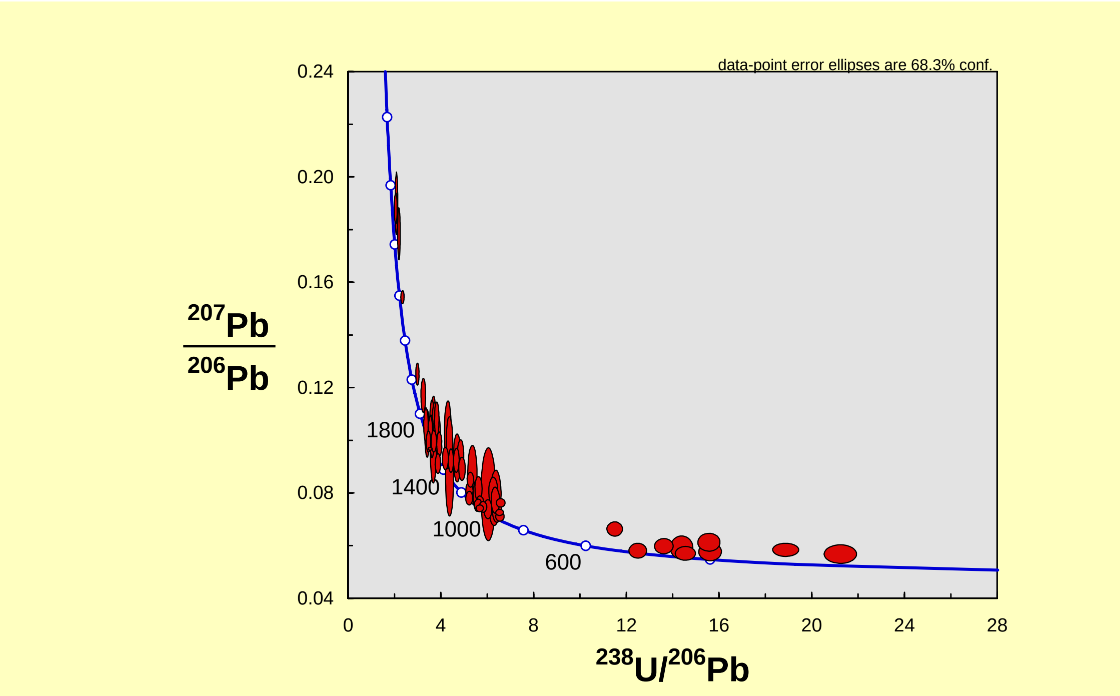
data-point error ellipses are 68.3% conf.
207Pb/206Pb
238U/206Pb
1800
1400
1000
600

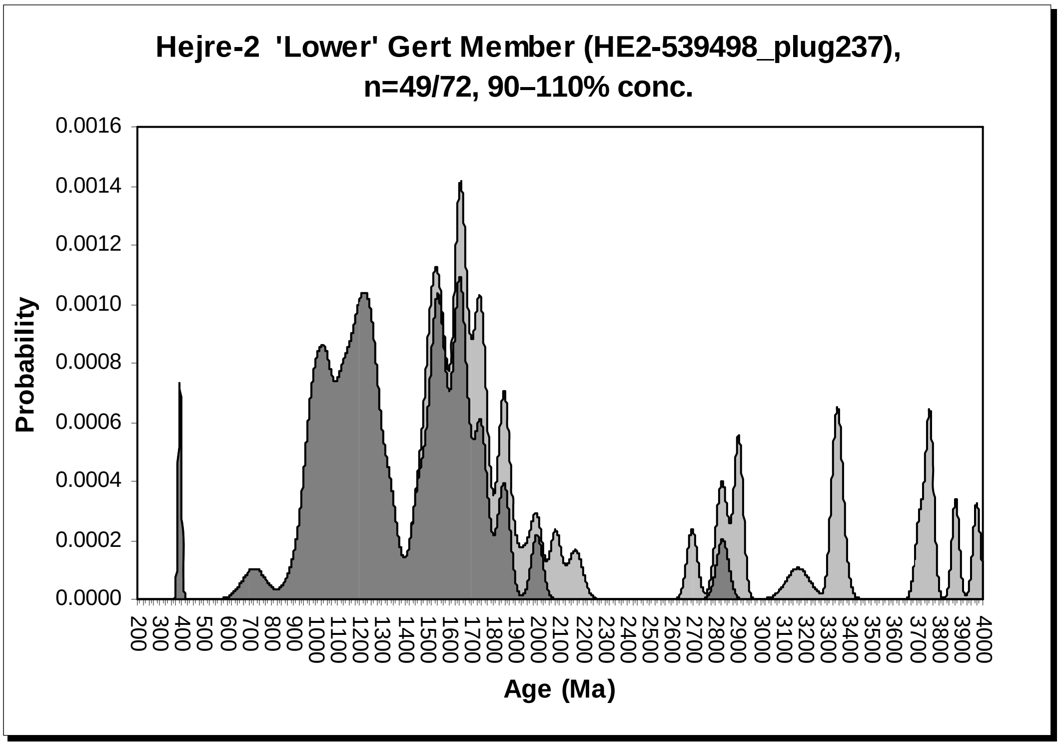

Hejre-2 'Lower' Gert Member (HE2-539498_plug237),
n=49/72, 90–110% conc.
Probability
Age (Ma)

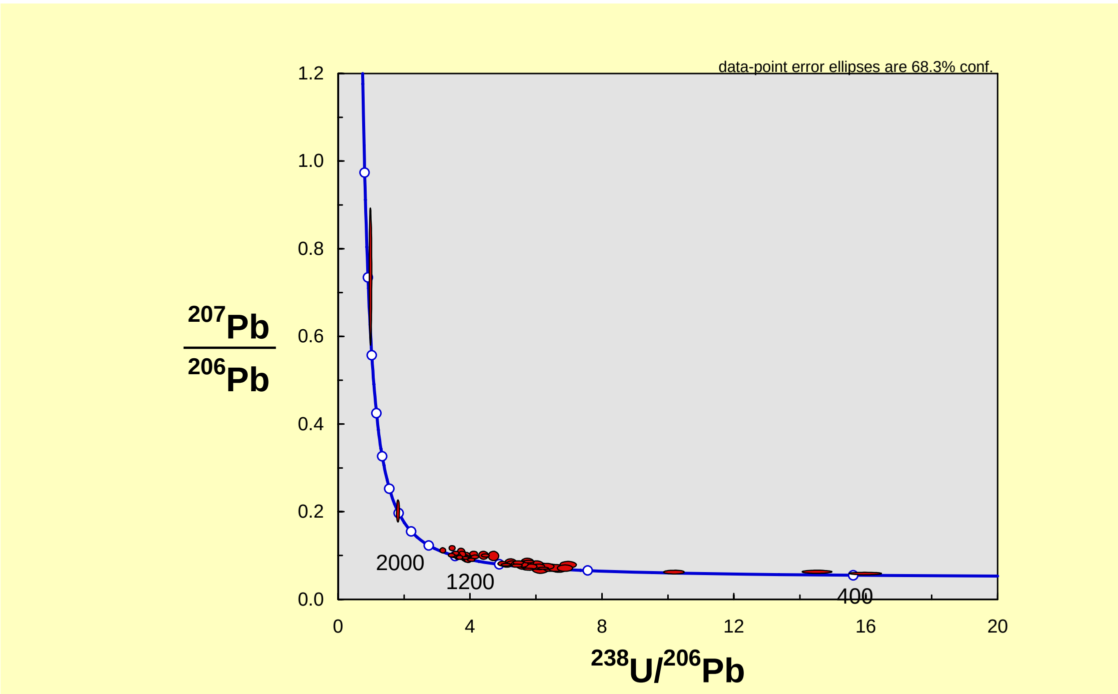

data-point error ellipses are 68.3% conf.
2000
1200
400
$^{207}Pb/^{206}Pb$
$^{238}U/^{206}Pb$

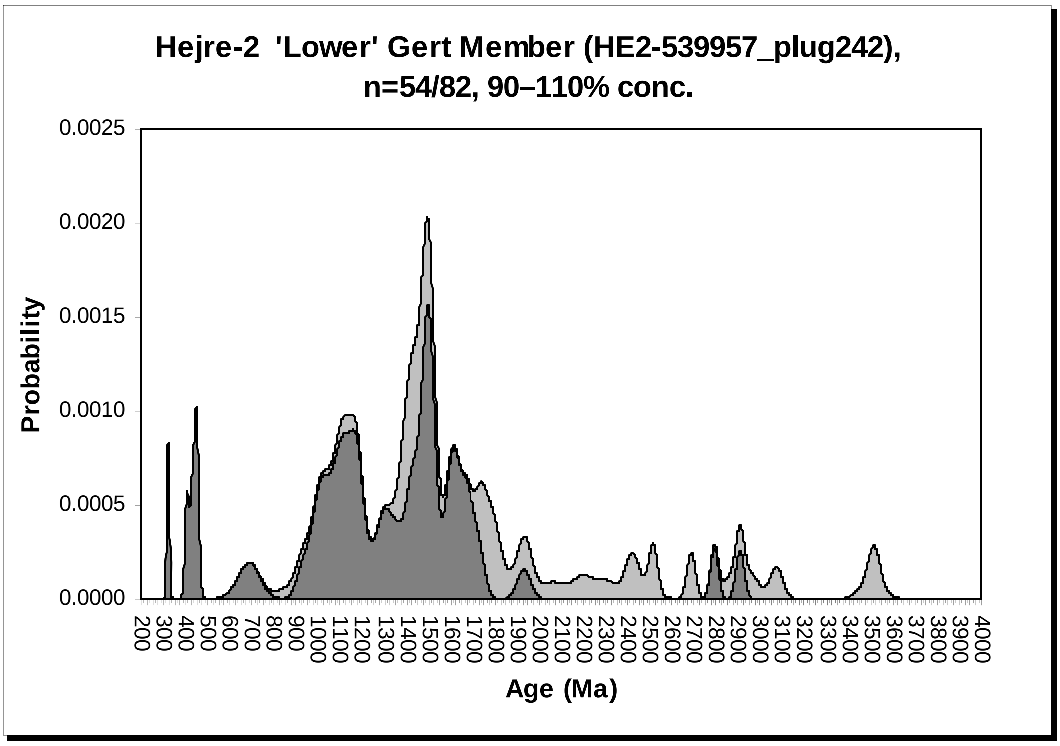

Hejre-2 'Lower' Gert Member (HE2-539957_plug242),
n=54/82, 90–110% conc.
Probability
0.0025
0.0020
0.0015
0.0010
0.0005
0.0000
200 300 400 500 600 700 800 900 1000 1100 1200 1300 1400 1500 1600 1700 1800 1900 2000 2100 2200 2300 2400 2500 2600 2700 2800 2900 3000 3100 3200 3300 3400 3500 3600 3700 3800 3900 4000
Age (Ma)

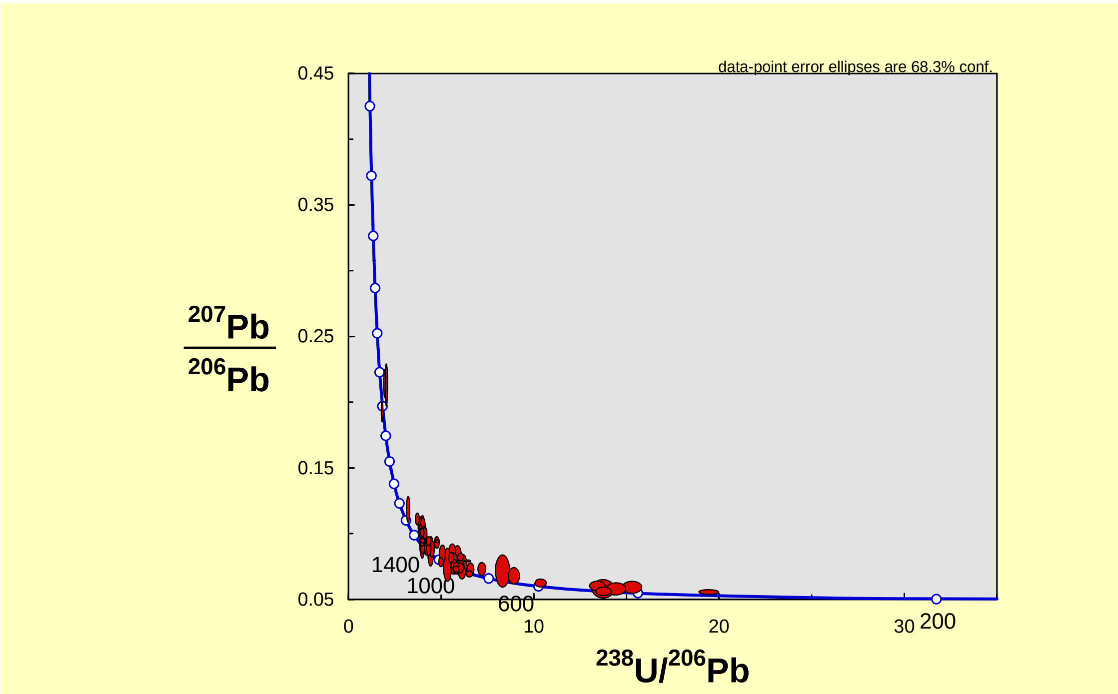

data-point error ellipses are 68.3% conf.
0.45
0.35
0.25
0.15
0.05
207Pb/206Pb
1400
1000
600
200
0
10
20
30
238U/206Pb

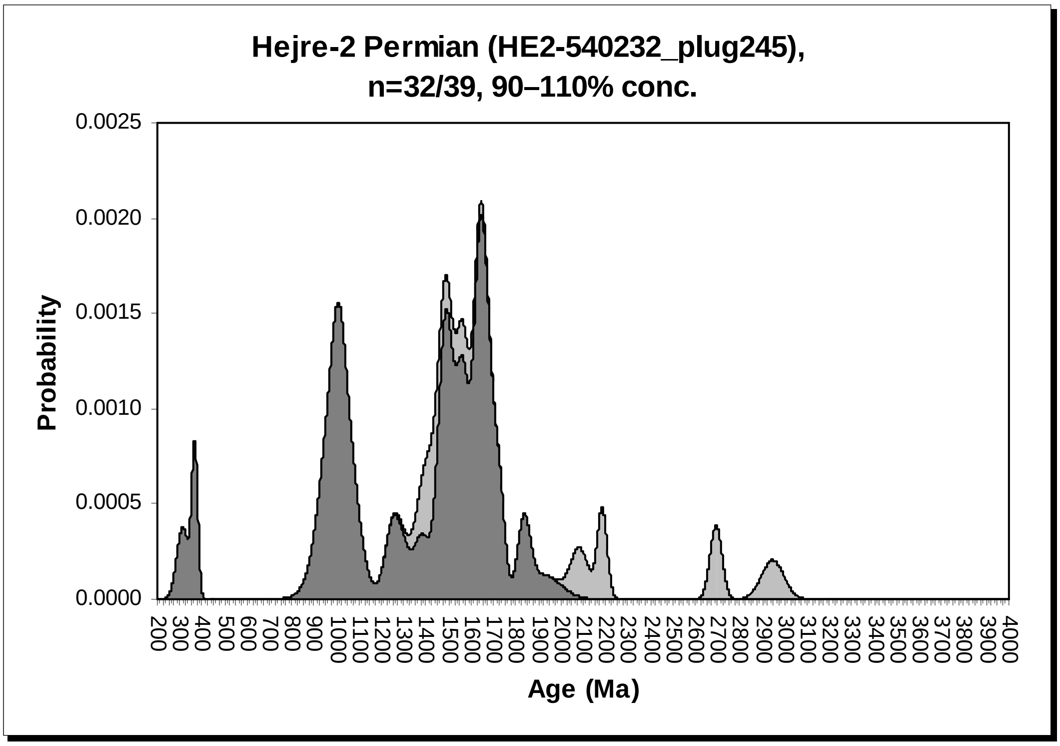
Hejre-2 Permian (HE2-540232_plug245),
n=32/39, 90–110% conc.
Probability
0.0025
0.0020
0.0015
0.0010
0.0005
0.0000
200 300 400 500 600 700 800 900 1000 1100 1200 1300 1400 1500 1600 1700 1800 1900 2000 2100 2200 2300 2400 2500 2600 2700 2800 2900 3000 3100 3200 3300 3400 3500 3600 3700 3800 3900 4000
Age (Ma)

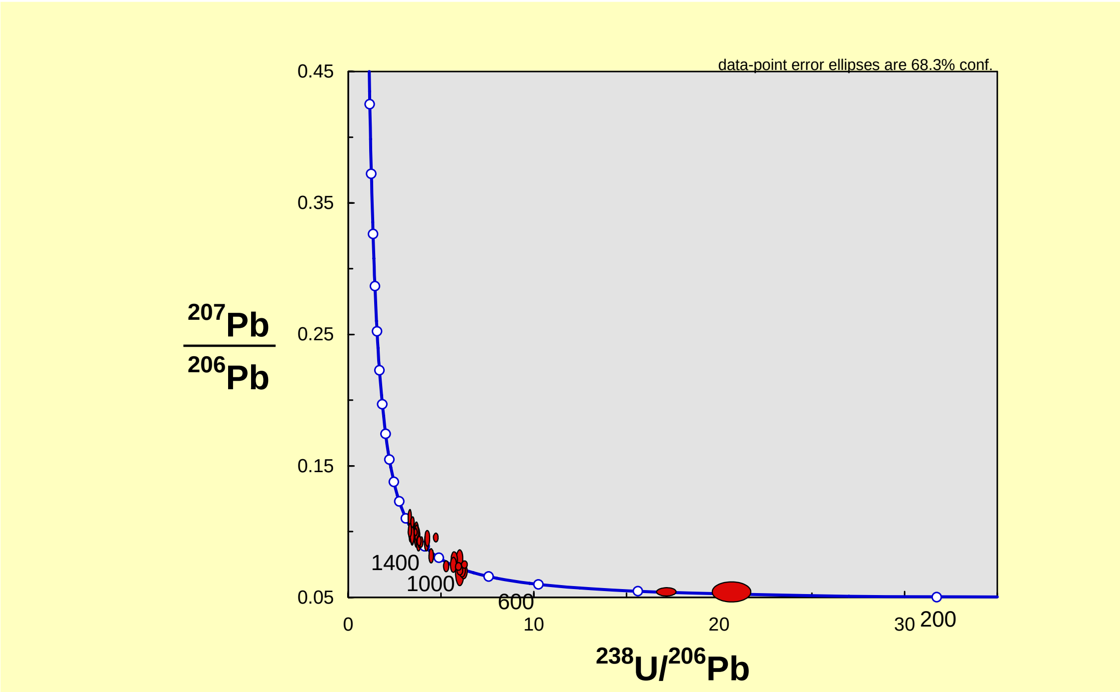
data-point error ellipses are 68.3% conf.
207Pb/206Pb
0.45
0.35
0.25
0.15
0.05
1400
1000
600
200
0
10
20
30
238U/206Pb

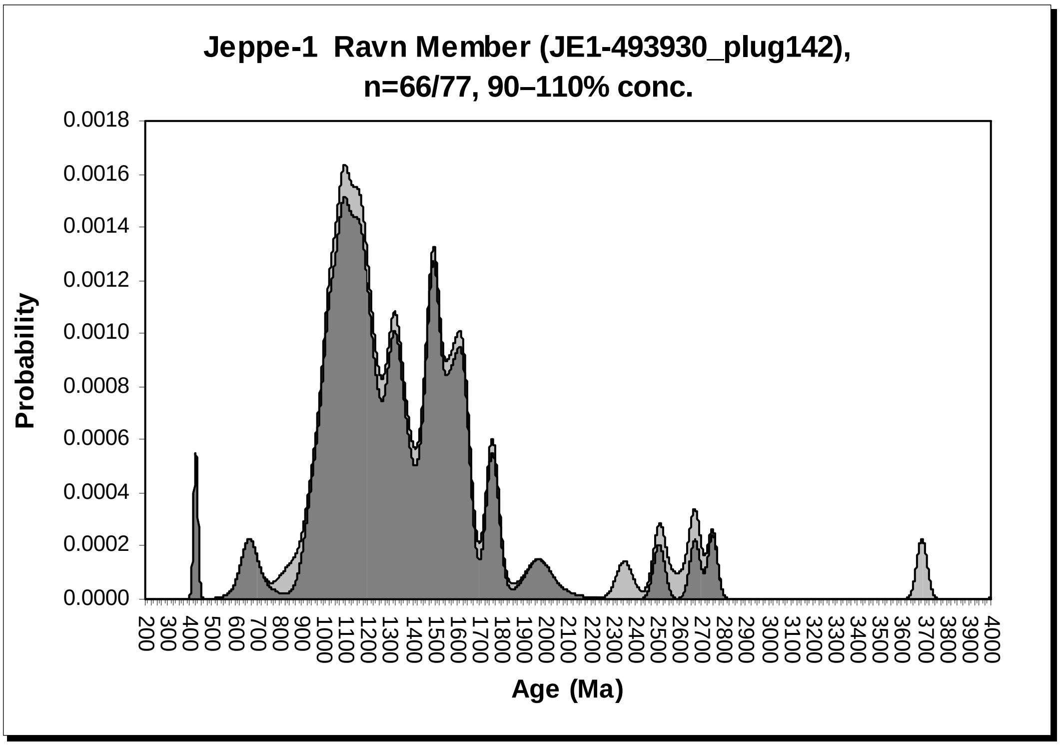
Jeppe-1 Ravn Member (JE1-493930_plug142),
n=66/77, 90–110% conc.
Probability
Age (Ma)

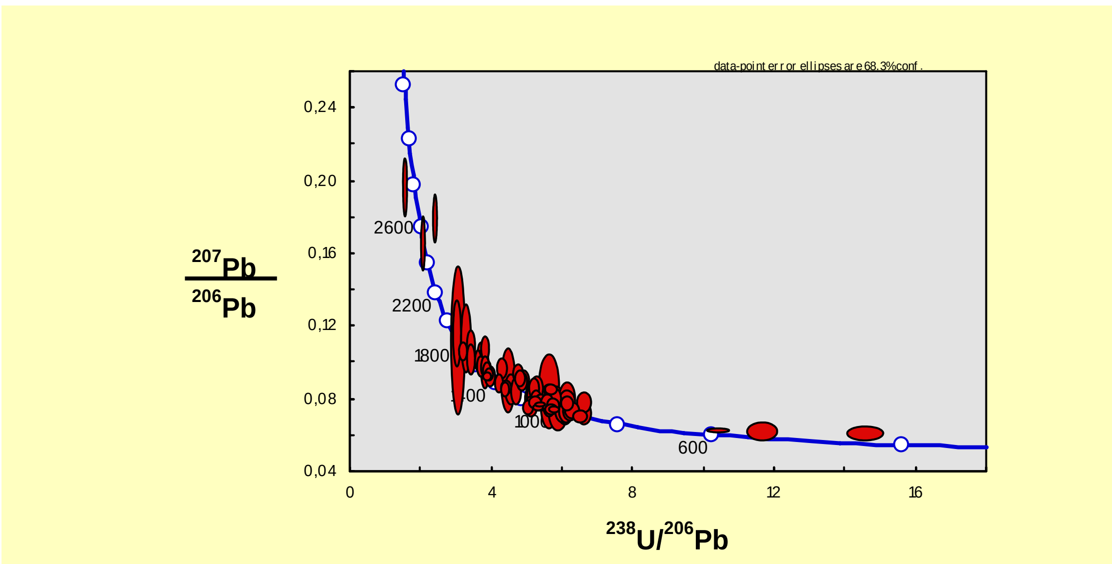
data-point error ellipses are 68.3% conf.
2600
2200
1800
600
^{207}Pb / ^{206}Pb
^{238}U/^{206}Pb

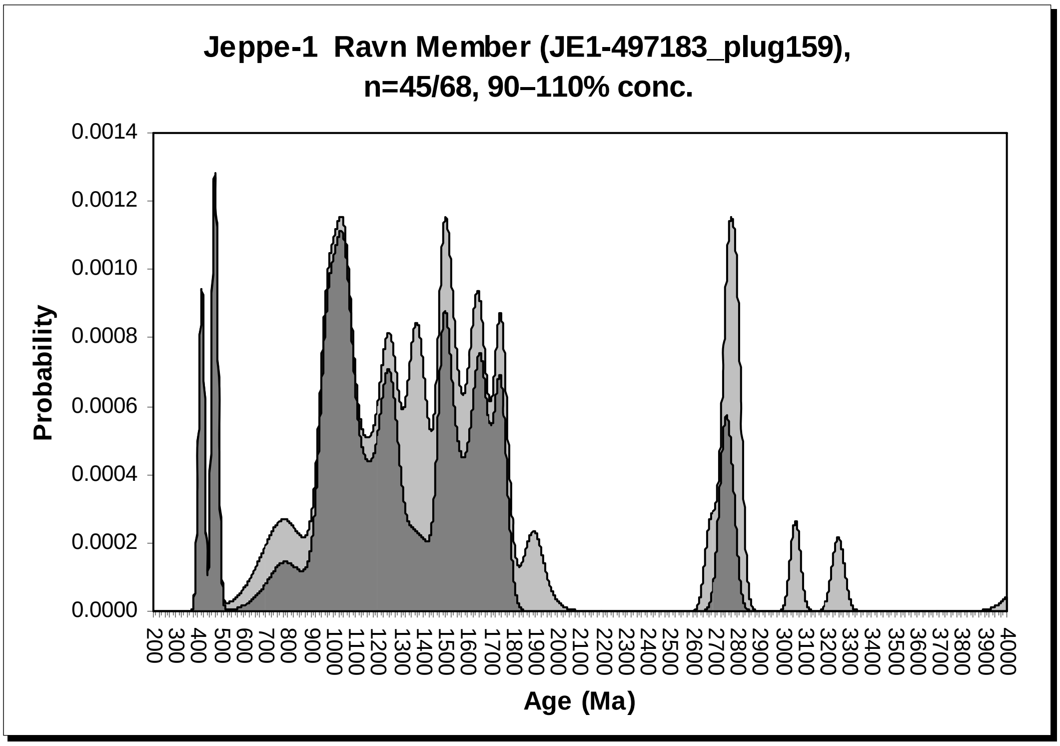

Jeppe-1 Ravn Member (JE1-497183_plug159),
n=45/68, 90–110% conc.
Probability
Age (Ma)

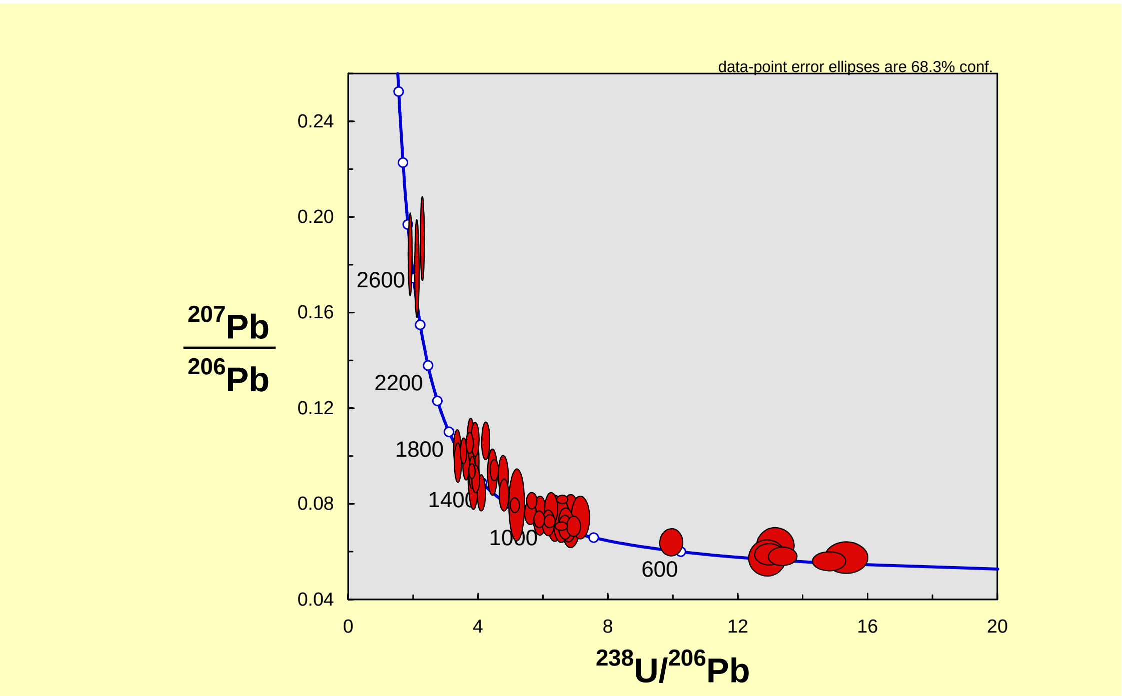

data-point error ellipses are 68.3% conf.
207Pb/206Pb
238U/206Pb
2600
2200
1800
1400
1000
600

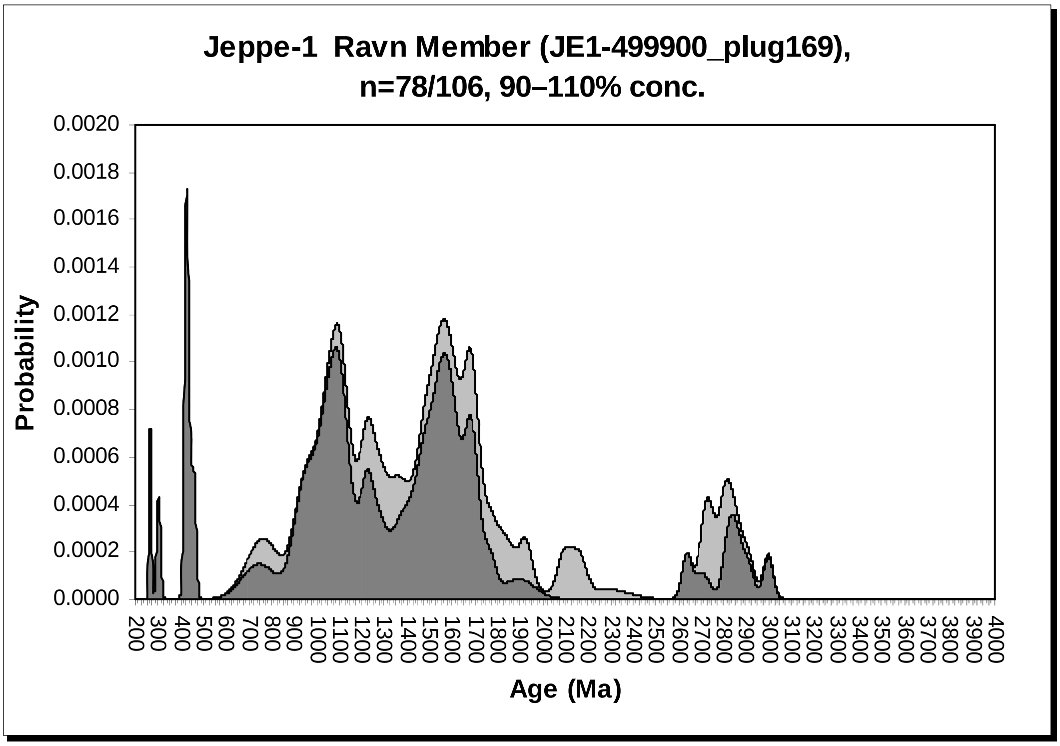
Jeppe-1 Ravn Member (JE1-499900_plug169),
n=78/106, 90–110% conc.
Probability
0.0020
0.0018
0.0016
0.0014
0.0012
0.0010
0.0008
0.0006
0.0004
0.0002
0.0000
200
300
400
500
600
700
800
900
1000
1100
1200
1300
1400
1500
1600
1700
1800
1900
2000
2100
2200
2300
2400
2500
2600
2700
2800
2900
3000
3100
3200
3300
3400
3500
3600
3700
3800
3900
4000
Age (Ma)

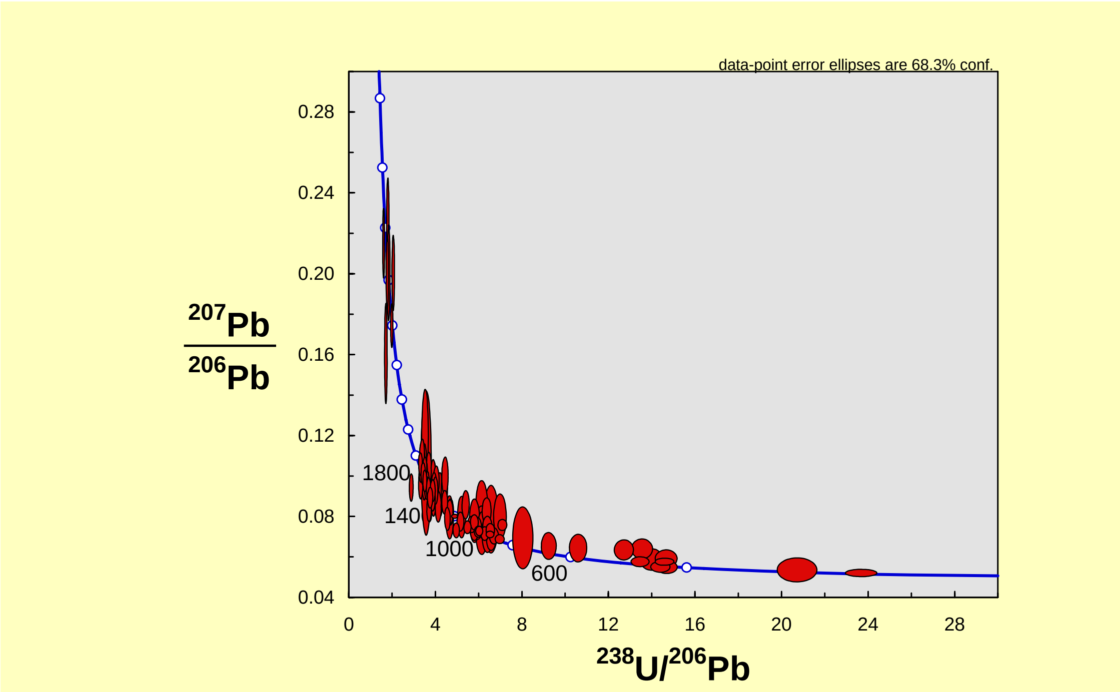
data-point error ellipses are 68.3% conf.
207Pb/206Pb
0.28
0.24
0.20
0.16
0.12
0.08
0.04
1800
1400
1000
600
0
4
8
12
16
20
24
28
238U/206Pb

Appendix 6. Garnet chemistry

Chemostratigraphy and mineral-chemical fingerprinting, Heno Formation, Danish North Sea

CCSEM results on heavy mineral concentrate:

Gert-1 Gert Member (GE1-496955)

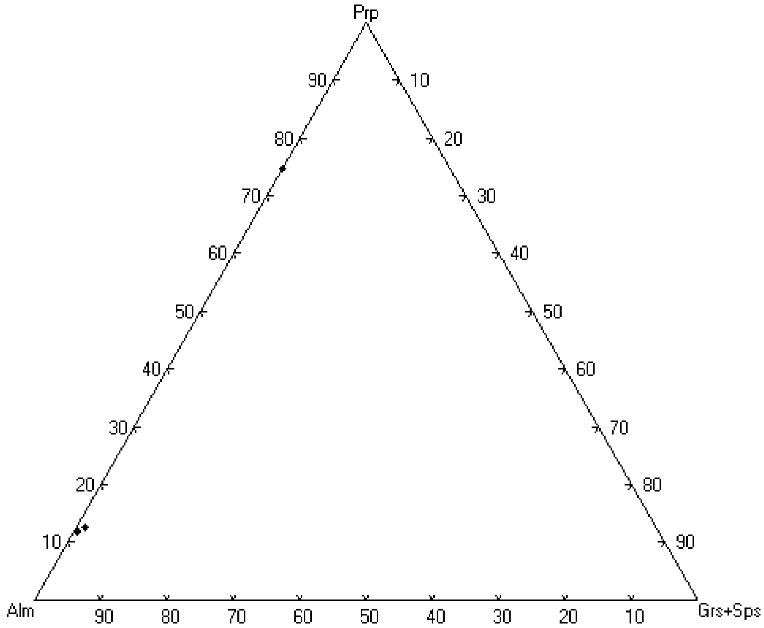

Gert-2 Ravn Member (GE2-483485)

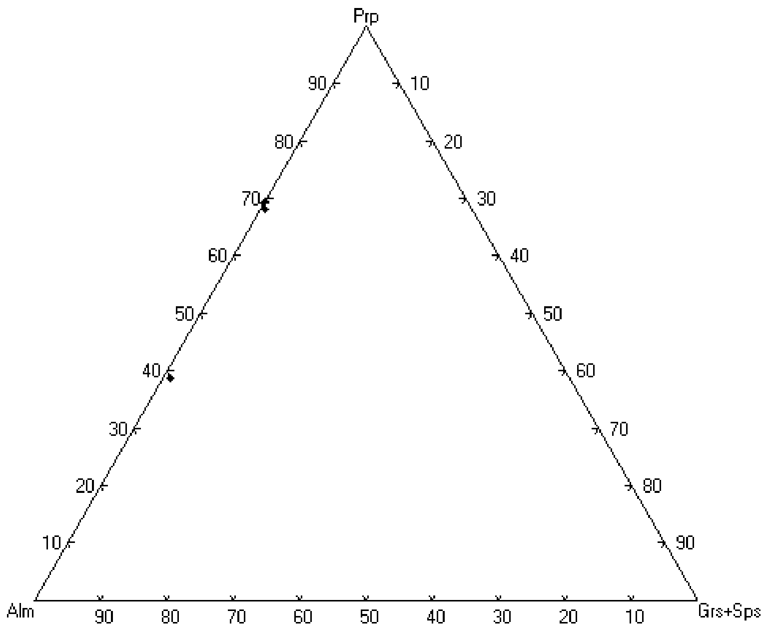

Gert-2 Gert Member (GE2-486835)

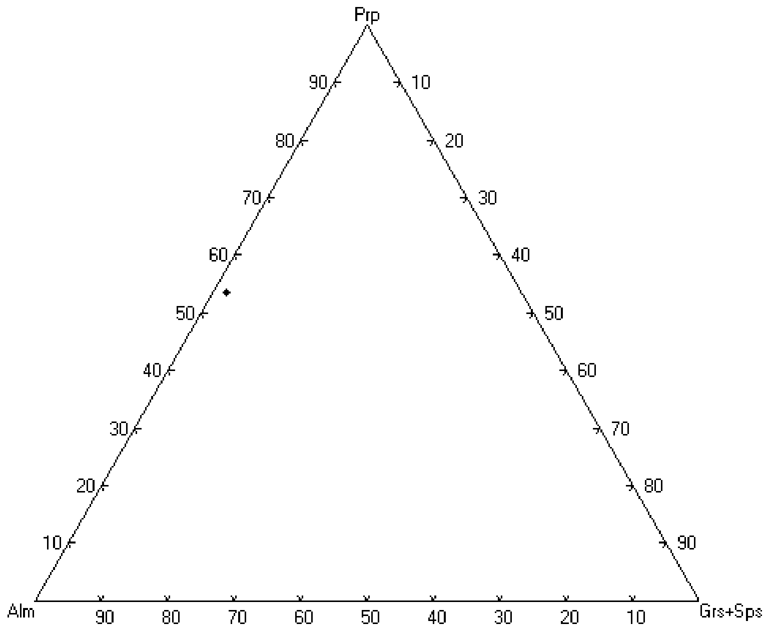

Gert-2 Carboniferous (GE2-493940)

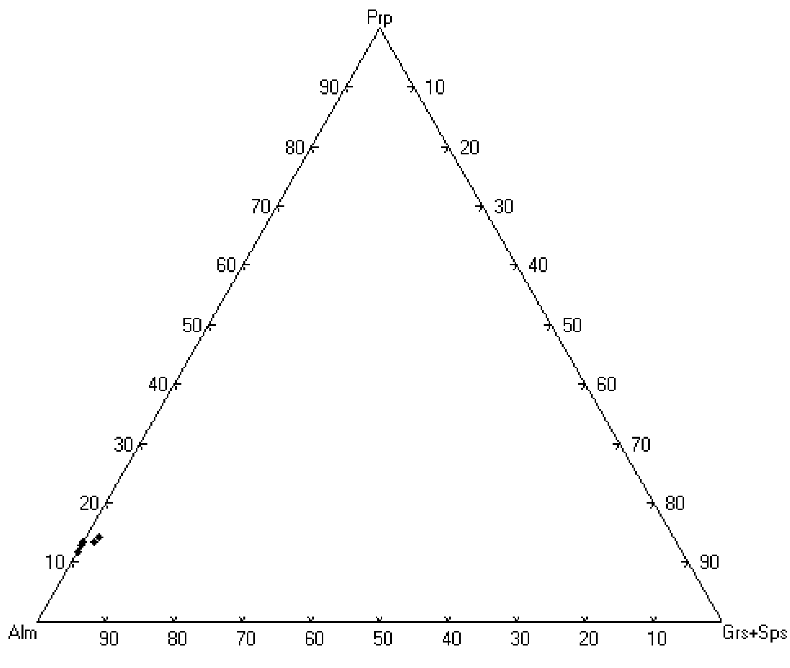

Gert-4 Gert Member (GE4-604450)

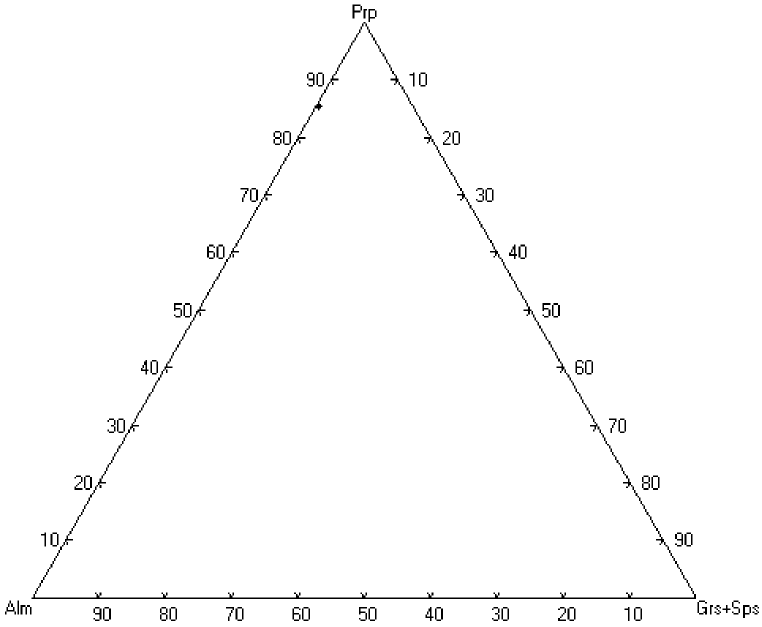

Jeppe-1 Ravn Member (JE1-493930)

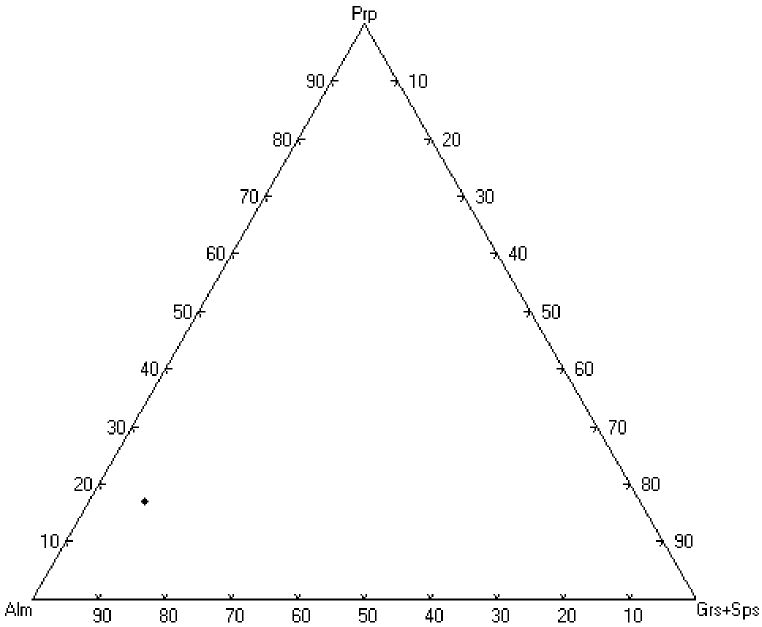

Jeppe-1 Ravn Member (JE1-499100)

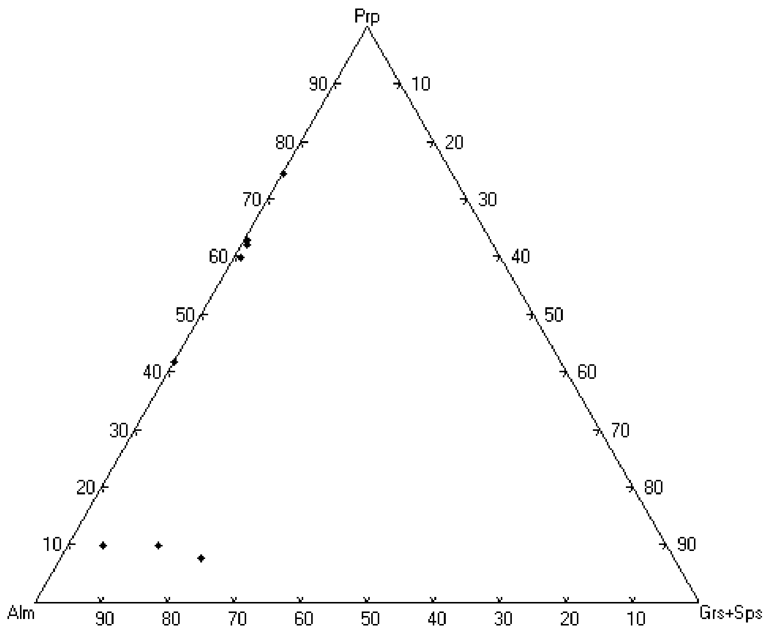

Diamant-1 Ravn Member (DI1-382965)

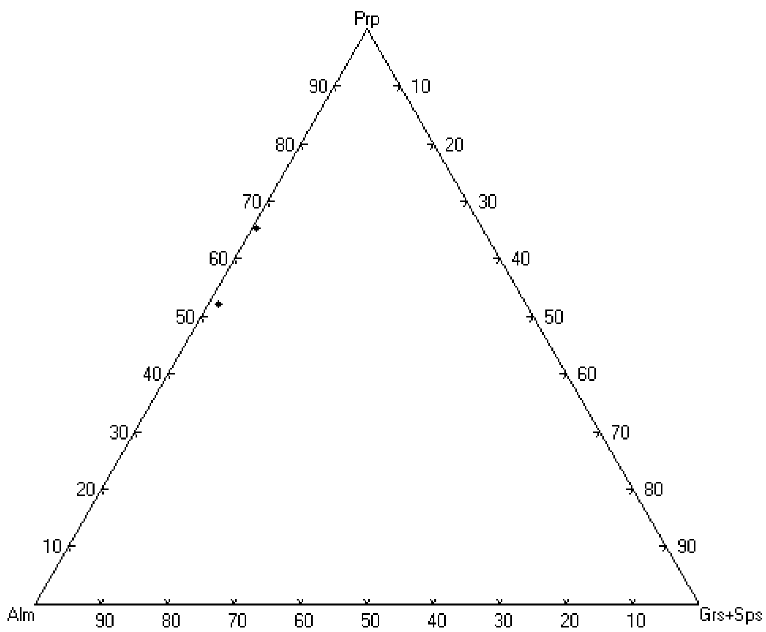

Diamant-1 Gert Member (DI1-384565)

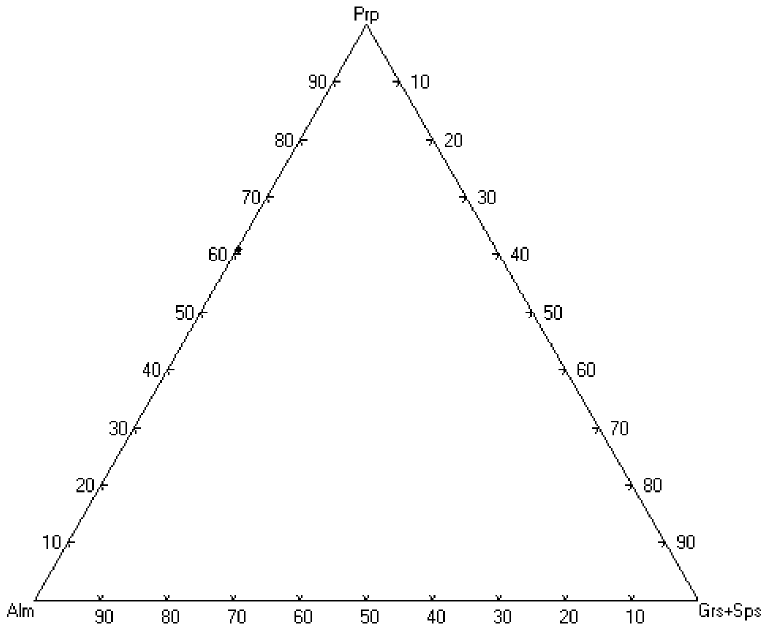

CCSEM on large thin sections:

Hejre-2 Lower Gert Member (HE2-539957)